Part II

Heat–moisture interactions in textile materials

7

Thermal conduction and moisture diffusion in fibrous materials

Z. SUN and N. PAN, University of California, USA

7.1 Introduction

7.1.1 Thermal conduction

Thermal transfer is a subject analyzing the energy change of a system. Of the three main physical mechanisms for heat transfer, i.e. conduction, convection and radiation, thermal convection refers to heat passing through the movement of *substances* and, if occurring, it occurs only at the surface of a normal solid material. The situation changes when we come to a fibrous material; as a multiphase system, all the thermal transfer processes become possible, depending on the construction and environmental conditions. Theoretically, thermal conduction always happens as long as a temperature gradient is present between a material system and the environment. When that temperature gradient is small, heat transfer via radiation can be ignored. Furthermore, if the fiber volume fraction is high enough, convection is suppressed by the tiny pores between fibers. Consequently, thermal conduction turns out to be the only or the most dominant heat transfer mechanism. Unlike many other porous media, since the pores in a fibrous material are virtually all interconnected, at low fiber volume fraction, heat loss due to convection can become dominant, as in the case of wearing a loosely knitted sweater on a windy day.

In the engineering field, because of such complexities, effective thermal resistance is usually adopted to characterize thermal properties of fibrous material systems by approximating a complex thermal process to an equivalent thermal conduction process in normal solids (Martin and Lamb, 1987; Satsumoto, Ishikawa *et al*., 1997; Jirsak, Gok *et al*., 1998). The other advantage in dealing with the thermal conduction problem is that the mathematical formulation of thermal conduction is better documented. The equations governing different initial and boundary conditions have been more widely explored and more analytical and numerical tools are thus made available for ready applications.

7.1.2 Similarity and difference between thermal conduction and moisture diffusion

There are many similarities between thermal conduction and moisture diffusion. Governing equations for both thermal conduction and moisture diffusion are in the same form. Thus, analysis methods and results would be analogous for both processes when system scale, material properties, and initial and boundary conditions are similar. A more detailed comparison of conduction and diffusion processes is available in the literatures (Crank, 1979; Bird, Stewart *et al.*, 2002). Macroscopic similarity between these two processes results from microscopic physical mechanisms. Both of the processes are governed by statistical behaviors of micro-particles' (atoms, molecules, electrons) random movement in the system. Thermal conduction deals with changes in system internal energy; heat flow is a result of a change of system internal energy due to spatial and temporal temperature differences. In this process, the change of system energy is achieved by changing vibration, collision and migration energy of the micro-particles. Moisture diffusion describes the migration of water molecules and/or the assembly of water molecules in the system. Thus, mass diffusivity of moisture in air is much larger than it is in fibers, whereas the thermal conductivity of fibers is larger than that of air. Furthermore, for most fibers, which are composed of polymers, anomalous mass diffusion processes are observed due to the effects of water molecules on large macromolecules. Although the governing equations for both processes are built on a requirement for balance, thermal conduction is based on energy conservation, and moisture diffusion requires mass conservation.

In this chapter, we focus mainly on continuum approaches to thermal conduction and moisture diffusion. This means the micro-level interactions will not be present in the formulations. The fibrous system will therefore be treated as a continuum or several continua, characterized by macroscopic material properties. Most analysis methods will be illustrated for thermal conduction; analogies, to moisture diffusion condition whenever they exist, will be mentioned. More detailed treatment of moisture diffusion, however, such as anomalous diffusion in polymers, are briefly reviewed in Section 7.8.

7.2 Thermal conduction analysis

Generally, the goal of thermal transfer analysis is to determine the temporal and spatial distributions of the scalar temperature field in a given system. To achieve this, the governing equation, and the initial and boundary conditions need to be formulated. Conceptually, detailed information about temperature and derived variables of the system, such as heat flow rate and heat flux through a given surface, will all be available from solutions of the governing

equations with auxiliary conditions. Although formulation of the governing equation for pure thermal conduction in a homogeneous system is rather simple, a good understanding of the procedure not only illustrates the basic idea about transport processes in general, but builds up fundamentals to extend the analysis of heterogeneous systems such as fibrous systems.

When dealing with a physical process in homogeneous and isotropic materials, it is implied that every differential part inside the system will contribute the same response to the process. Thus, the governing equation and bulk material properties can be derived based on one differential unit of the material. Consider an arbitrary volume V of a homogenous and isotropic material bounded by the surface A. The heat flow rate across the surface A, is given by

$$-\int_{A(t)} q \cdot n \mathrm{d}A \qquad [7.1]$$

where n denotes the unit outward directed normal to A. Assuming no bulk movement of the material, the transfer rate of thermal energy can be related to the change rate of the internal energy in the volume V,

$$\frac{\partial}{\partial t}\int_V \rho e \mathrm{d}V = -\int_A q \cdot n \mathrm{d}A + \int_V \Phi \mathrm{d}V \qquad [7.2]$$

where Φ is the heat generating rate inside volume V, including the adsorption heat, condensation latent heat and so on. Applying the divergence theorem, the surface integral can be changed into a volume integral, and Equation [7.2] becomes

$$\int_V \left[\rho \frac{\partial e}{\partial t} + \nabla \cdot q + \Phi\right] = 0 \qquad [7.3]$$

Since the volume V is chosen arbitrarily, the governing equation is thus given as

$$\rho \frac{\partial e}{\partial t} + \nabla \cdot q + \Phi = 0 \qquad [7.4]$$

However, as we have four unknown variables, e and q_i (i = 1, 2, 3), with only one equation now, additional equations have to be established.

First, the specific heat, i.e. heat capacity per unit mass, is introduced to describe the relationship between the system's internal energy and temperature change. The specific heat of a material at constant volume is defined as

$$C_v(T) = \left(\frac{\partial e}{\partial T}\right)_\rho \qquad [7.5]$$

The specific heat has dimensions of [energy][temperature]$^{-1}$[mass]$^{-1}$. Specific

heats for general fibers are listed in Table 7.1 (Morton and Hearle, 1993). The constitutive equation for heat flux is the well-known Fourier's Law. When in differential form,

$$q = -k\nabla T \qquad [7.6]$$

where another material property is introduced, the thermal conductivity, k, with dimensions $[\text{energy}][\text{time}]^{-1}[\text{temperature}]^{-1}[\text{length}]^{-1}$. Thermal conductivities of some polymer materials that are used as textile fibers are listed in Table 7.2 (Morton and Hearle, 1993; Warner, 1995).

Strictly, Fourier's Law is not a law of nature but an approximation, and potentially it may lead to the problem that heat excitations would be transferred with infinite speed (Ali and Zhang, 2005). However, Equation [7.6] does have some theoretical basis, and has been widely and successfully used in many science and engineering applications (Bird, Stewart *et al.*, 2002).

Table 7.1 Specific heats of general fibers

Fiber	Specific heat (J g^{-1} K^{-1})
Cotton	1.21
Rayon	1.26
Wool	1.36
Silk	1.38
Nylon 6	1.43
Polyester Terylene	1.34
Asbestos	1.05
Glass	0.80

Adapted from Morton and Hearle (1997)

Table 7.2 Thermal conductivity of polymer materials used in textile fibers

Material	Thermal conductivity (mW m^{-1} K^{-1})
Poly(vinyl chloride)	160
Cellulose acetate	230
Nylon	250
Polyester	140
Polyethylene	340
Polypropylene	120
Polytetrafluoroethylene	350
PET	140
Glycerol	290
Cotton (cellulose)	70
Cotton bats	60
Wool bats	54
Silk bats	50

Adapted from Morton and Hearle (1997)

With the relationships shown above, the governing equation for thermal transfer with temperature as the field variable is given by

$$\rho c_v \left(\frac{\partial T}{\partial t} \right) = \nabla \cdot (k \nabla T) + \Phi \qquad [7.7]$$

This equation is valid for constant volume processes. For constant pressure cases, however, a corresponding constant pressure specific heat, c_p, should be substituted. The difference between the two values is negligible for solids yet relatively larger for liquids and gases (Carslaw and Jaeger, 1986; Bird, Stewart *et al.*, 2002). Considering the processes in fibrous systems in which we are interested, the constant pressure form is obviously more appropriate. For given material properties, the classical three-dimensional conduction equation for constant pressure processes is obtained as

$$\frac{\partial T}{\partial t} = \alpha \nabla^2 T + \frac{\Phi}{\rho c_p} \qquad [7.8]$$

where α, called the thermal diffusivity, is a combined material property with the dimensions $[\text{length}]^2[\text{time}]^{-1}$. It is clear that thermal diffusivity has the same dimensions as mass diffusivity D. The dimensionless ratio between these two properties, called the Lewis number, indicates the relative ease of thermal conduction versus mass diffusion transport in a material. This governing partial differential equation shares the same form as the time-dependent diffusion equation when $\Phi = 0$. The corresponding steady-state equation is in the elliptical form. The properties of these equations have been well explored and can be found in books dealing with partial differential equations (Haberman,1987; Arfken and Weber, 2005).

In order to obtain the distribution of temperature field, the boundary conditions and initial condition are needed to determine the constants resulting from integration of the governing differential equations. The initial condition for transient thermal conduction is a given temperature distribution in the form of

$$T(x, 0) = f(x) \qquad [7.9]$$

where $f(x)$ is a known function whose domain coincides with the region the material occupied. A solution of the governing equation, $T(x, t)$ with $t > 0$, has to satisfy the initial condition $\lim_{t \to 0} T(x, t) \to f(x)$.

The boundary conditions describe the physical behavior at the surface of the material. They are determined from experiments at a given operation environment. Three kinds of boundary condition are often used to approximate real-world situations.

(i) Prescribed temperature
The prescribed temperature could be constant or a function of time,

position or both of them. This boundary condition is mostly well explored and is applicable to model conditions where material boundaries are in contact with a well-controlled thermal environment, such as a thermal guard plate.

(ii) Prescribed thermal flux across the boundary surface
This boundary condition implies $k\frac{\partial T}{\partial n} = g$ at the boundary surface, for $t > 0$. When the prescribed function g is equal to zero, it represents an insulated condition which is particularly important when fibrous materials are used for thermal insulation.

(iii) Linear thermal transfer at the boundary surface
This boundary condition assumes that thermal flux varies linearly with temperature difference between the boundary and the environment, given by

$$k\frac{\partial T}{\partial n} + h(T - T_{env}) = 0 \text{ for } t > 0 \qquad [7.10]$$

in which h is a positive measured variable called the surface heat transfer coefficient. This boundary condition is generally referred to as the 'Newton's law of cooling' and describes a material cooled by an external, well-stirred fluid. Also, it is applicable to black-body or near black-body radiation at boundaries where the temperature difference between the material and the environment is not too large.

There are still many other boundary conditions, including both linear and non-linear forms. Some of them are listed in Carslaw and Jaeger (1986). Choosing, or setting up, appropriate boundary conditions depends on one's understanding of the process and is critical for further analysis.

The thermal conduction governing equation with certain initial and boundary conditions can be solved by both analytical and numerical methods. General discussions about analytical methods and their results, such as separation variables, integral transformation and Green functions methods, are available in both applied mathematics and transport phenomena books (Carslaw and Jaeger, 1986; Haberman, 1987; Bird, Stewart *et al*., 2002; Arfken and Weber, 2005). Numerical methods for thermal conduction problems, such as finite difference and finite elements analysis, are also well developed (Shih, 1984; Minkowycz, 1988). These results are critical not only for thermal analysis but are also important for measurement of thermal conductivity. By carefully setting up experiments, a one-dimensional steady-state heat transfer solution has been applied widely to guide the static hot-plate thermal conductivity measurement (Satsumoto, Ishikawa *et al*., 1997; Jirsak, Gok *et al.*, 1998; Mohammadi, Banks-Lee *et al*., 2003). Transient thermal conduction results have also found their application in dynamic measurement of fabric thermal conductivities (Martin and Lamb, 1987; Jirsak, Gok *et al*., 1998). In order to

improve experimental design and data analysis, however, a deeper understanding of these theoretical results and their limitations are required.

In fibrous materials, anisotropic characteristics are of predominant importance. It is known that the longitudinal and lateral thermal conductivities of a single fiber are significantly different owing to its anisotropic nature (Woo, Shalev *et al.*, 1994a,b; Fu and Mai, 2003). Furthermore, this directional dependence of thermal conductivity is magnified in fiber assemblies due to asymmetry packing of fibers. In this context, we would like to review some fundamental characteristics of anisotropic thermal conductivity and its effects on the conduction process.

The generalization of Fourier's Law for anisotropic materials is given by

$$q = K \cdot \nabla T \qquad [7.11]$$

where k is the thermal conductivity tensor. In the Cartesian coordinate system, it is written in matrix form as

$$K = \begin{bmatrix} k_{xx} & k_{xy} & k_{xz} \\ k_{yx} & k_{yy} & k_{yz} \\ k_{zx} & k_{zy} & k_{zz} \end{bmatrix} \qquad [7.12]$$

Depending on the system symmetry, the conductivity matrix can be simplified. It has been proved that the thermal conductivity matrix is symmetrical, based on Onsager's principle of microscopic reversibility, i.e. $k_{rs} = k_{sr}$ for all r and s. The other important aspect for the thermal conductivity tensor is the transformation of the coordinate system. Assume that we try to consider a new Cartesian system x', y' and z', whose directional cosines relative to the old coordinate x, y, z system are (c_{11}, c_{21}, c_{31}), (c_{12}, c_{22}, c_{32}), (c_{13}, c_{23}, c_{33}) respectively. The components of conductivity tensor k'_{ik} in the new system are given by

$$k'_{ik} = \sum_{r=1}^{3} \sum_{s=1}^{3} c_{ri} c_{sk} k_{rs} \qquad [7.13]$$

These are just the transformation laws for a second-order tensor.

With the introduction of the thermal conductivity tensor, the governing equation for homogenous anisotropic materials without heat generation is given by

$$\rho c_p \frac{\partial T}{\partial t} = k_{xx} \frac{\partial^2 T}{\partial x^2} + k_{yy} \frac{\partial^2 T}{\partial y^2} + k_{zz} \frac{\partial^2 T}{\partial z^2} + (k_{xy} + k_{yx}) \frac{\partial^2 T}{\partial x \partial y}$$

$$(k_{xz} + k_{zx}) \frac{\partial^2 T}{\partial x \partial z} + (k_{yz} + k_{zy}) \frac{\partial^2 T}{\partial y \partial z} \qquad [7.14]$$

It can be shown that a transformation to a particular Cartesian system ξ, η, ζ leads to the simplified representation

$$\rho c_p \frac{\partial T}{\partial t} = k_1 \frac{\partial^2 T}{\partial \xi^2} + k_2 \frac{\partial^2 T}{\partial \eta^2} + k_3 \frac{\partial^2 T}{\partial \zeta^2} \quad [7.15]$$

These new axes are called the principal axes of thermal conductivity and k_1, k_2 and k_3 are the principal conductivities. The directions of the principal axes depend on the symmetry of the system in question. For an orthotropic system, which has different conductivities k_1, k_2 and k_3 in three mutually perpendicular directions, these directions coincide with the principal axes.

Different from isotropic materials, an important characteristic for heat conduction in anisotropic media is that the heat flux vector does not locate in the same direction as the temperature gradient. Thus, two thermal conductivities at a given point P in an anisotropic material are defined. k_m is defined as the conductivity in the direction of the flux vector at P, and satisfies

$$q_m = -k_m \frac{\partial T}{\partial m} \quad [7.16]$$

where q_m and $\frac{\partial T}{\partial m}$ are the flux and rate of change of temperature along the direction of flux vector at point P.

Similarly, the conductivity normal to the isothermals at P, k_n is defined by relating the heat flux and rates of temperature change in the direction normal to the isothermal at P,

$$f_n = -K_n \frac{\partial T}{\partial n} \quad [7.17]$$

Relationships between these conductivities with principal conductivities are also found. Assuming the flux vector has directional cosines (l, m, n) relative to the principal axes of the conductivity, the conductivity in direction m, k_m, is given by

$$\frac{1}{k_m} = \frac{l^2}{k_1} + \frac{m^2}{k_2} + \frac{n^2}{k_3} \quad [7.18]$$

whereas the conductivity normal to isothermal k_n, whose normal has direction cosines (l', m', n') relative to the principal axes, is given by

$$k_n = l'^2 k_1 + m'^2 k_2 + n'^2 k_3 \quad [7.19]$$

Depending on the measurement method, k_m or k_n will be measured (Carslaw and Jaeger, 1986).

For more discussion about the geometrical properties of thermal conductivities and their effects on the thermal conduction process, one can refer to the classic treatise by Carslaw and Jaeger (1986).

7.3 Effective thermal conductivity for fibrous materials

7.3.1 Introduction

Fibrous materials are widely used in various engineering fields, such as textile fabrics as reinforcements in fiber-reinforced composites, fibrous thermal insulators, and fibrous scaffold in tissue engineering, to just name a few (Tong and Tien, 1983; Tong, Yang *et al*., 1983; Christensen, 1991; Freed, Vunjaknovakovic *et al*., 1994). Also, most biological tissues, e.g. tendons, muscles, are intrinsically fibrous materials (Skalak and Chien, 1987). In these applications, fibrous materials are often referred to as assemblies of fibers. The behaviors of these fiber assembles are significantly different from those of single fibers.

Systems with fibers are generally heterogeneous. For example, textile fabrics are a mixture of fibers and air, and become a mixture of fibers and water when fully wetted. Fiber-reinforced composite materials are composed of a fiber assembly and matrix materials between fibers. Generally, we treat these mixtures as a whole, heterogeneous material system and analysis of the responses of these heterogeneous materials to external disturbances is our objective in research for engineering applications. Clearly, internal structure, properties of each component, and interactions among components, will determine the behaviors of the whole heterogeneous material. Ideally, a fully discrete analysis based on characterization of each fiber, interstitial materials and interface conditions will provide the most detailed information for the system. But the large number of fibers, often intricate internal structure, and complex interactions of components render the discrete analysis very expensive, if not impossible.

One way to overcome the difficulties in analysis of heterogeneous materials is to try to find a hypothetical homogeneous material equivalent to the original heterogeneous one (Bear and Bachmat, 1990; Christensen, 1991; Whitaker, 1999); the same external disturbances will lead to the same macro-responses. The properties of this equivalent homogeneous material are denoted as ‘effective material properties’. As soon as the effective material properties are determined, the analysis of a heterogeneous material can be reduced to that of a homogeneous one, a much easier case to tackle.

As in all mixed systems, some of the properties, such as the effective density and specific heat in the thermal conduction case, can easily be obtained by some form of averaging over the corresponding properties of each

component. However, there are other system properties, including the effective thermal conductivity, that depend not only on the properties of each component, but also on the way those components are assembled into the whole system, i.e. the internal structure and the interactions among the individual components. Sometimes, the effective thermal conductivity can be measured directly. But, there are often many difficulties and practical limitations in the experimental approach. For example, when testing a fibrous material, many issues have to be settled before the test can proceed, such as the time to reach a steady state, influence of other thermal transfer processes, effect of applied pressure, and so on. Also, the results only can be applied in certain environment ranges, and costs are often expensive. Thus, prediction effective thermal conductivity by setting up constitutive laws from component properties and structure is still very attractive.

The most important and difficult task in prediction is characterization of structure. The structure of fiber assemblies must be understood from several aspects. Basically, information about the structure of a single fiber is needed, including longitudinal and transverse length, and ratio between them, geometry of cross-sections, crimp of fibers, and so on. After that, distribution of fibers and connection between them are required information for the understanding of fiber assembly structures. Depending on applications, fibers may be woven into yarns and woven fabric forms or packed together into nonwoven form. In the modeling process, an appropriate mathematical description has to be introduced to account for different ways of assembling such as the geometrics of yarns for woven fabrics (Dasgupta and Agarwal, 1992; Ning and Chou, 1995a,b) and orientation functions for the random packing of fibers (Pan, 1993, 1994; Fu and Mai, 2003).

The structure of interstitial materials among fibers may also contribute to effective thermal conductivity. But no rules can be summarized unless the particular system is given. The simplest term accounting for interaction between the fiber assembly and other components is the volume fraction of each one. Further interaction characterization needs a knowledge of interface properties, such as contact resistance, continuity of thermal flux, and so on.

7.3.2 Prediction of the effective thermal conductivity (ETC)

Due to the importance of effective thermal conductivity, much work has been done in this field. Most of it has concerned research on porous media and composite materials. The first major contribution should be attributed to Maxwell (Bird, Stewart *et al.*, 2002), who predicted the effective thermal conductivity of composite materials with small volume fraction spherical inclusions. During analysis, only one inclusion sphere embedded in an infinite matrix was considered, with the assumption that the temperature field of a

sphere is unaffected by presence of other spheres. The result is represented by

$$\frac{k_{eff}}{k_1} = 1 + \frac{3\varepsilon}{\left(\frac{k_2 + 2k_1}{k_2 - k_1}\right) - \varepsilon} \qquad [7.20]$$

where, k_1 and k_2 are thermal conductivities of the matrix and inclusion spheres, respectively. ε is the volume fraction of spheres.

Generally, analysis for dilute particles tries to solve the problem

$$q = -k_1 \nabla T,\ \nabla \cdot q = \nabla^2 T = 0 \text{ in each phase} \qquad [7.21]$$

$$n \cdot k_1 \nabla T = n \cdot k_2 \nabla T \text{ on interface } A_{12}$$

With given particle geometry and boundary conditions, the solution can be found. And for isotropic materials the effective thermal conductivity is given by

$$k_{eff} = -\frac{\langle q \rangle}{\langle \nabla T \rangle} \qquad [7.22]$$

where $\langle\ \rangle$ denote the average over the whole domain.

For large particle concentrations, Rayleigh (Bird, Stewart *et al.*, 2002) provides the results with spherical inclusions located in a cubic lattice and square arrays of long cylinders. And Batchelor and Obrien (Batchelor and Obrien, 1977) applied ensemble average and field analysis to dealing with particles.

Prediction of the lower and upper bound of effective thermal conductivity is the other important category of prediction methods (Miller, 1969; Schulgasser, 1976; Vafai, 1980; Torquato and Lado, 1991). Miller (1969) used an *n*-point correlation function to characterize the structure of heterogeneous media. He showed that the simple law of mixtures will be achieved when one-point correlation is adopted, i.e. $k_{eff} = \varepsilon k_1 + (1 - \varepsilon)k_2$. In the same paper, three-point correlation is also used to predict boundries for effective transport properties of heterogeneous media with different geometrical inclusions. Torquato and Lado (1991) predicted the effective conductivity tensor boundaries for media, including oriented, possibly overlapping, spheroids, by noticing the scaling relation between the spheroid and the sphere systems. With incorporation of the probability occurrence of four different packing structures, Vafai (1980) predicted the boundaries for microsphere packing beds. The boundries for the transverse effective thermal conductivity of two-dimensional parallel fibers F_1, and three-dimensional dispersed fibrous materials F_2 are also found by Vafai (1980), given by

$$F_1(\varepsilon, \omega, H) \geq (k_{eff} / \sqrt{k_1 k_2}) \geq F_2(\varepsilon, \omega, H)$$

$$F_1(\varepsilon, \omega, H) = \frac{1 + \varepsilon(\omega - 1)}{\sqrt{\omega}} \times \left\{1 - \frac{\varepsilon(\omega - 1)^2(1 - \varepsilon)}{3[1 + \varepsilon(\omega - 1)][1 + \varepsilon(\omega - 1) + 3(\omega - 1)(1 - 2\varepsilon)H]}\right\}$$

$$F_2(\varepsilon, \omega, H) = \sqrt{\omega}\left\{\omega - \varepsilon(\omega - 1) - \frac{[4(\omega - 1)^2(1 - \varepsilon)\varepsilon]}{3[1 + \omega + 3(2\varepsilon - 1)(\omega - 1)H]}\right\}^{-1} \quad [7.23]$$

where k_1 is the larger of two component thermal conductivities, ε is the volume fraction of the component with property k_1, $\omega = k_1/k_2$, i.e. $\omega > 1$, and H is the cell geometry factors. H = 1/4 and 1/6 for two-dimensional parallel and three-dimensional dispersed fibers, respectively.

An equivalent inclusion method is applied by Hatta and Taya (1985) and by Ehen and Wang (1996) to predict effective thermal conductivity of a misoriented short-fiber composite. The basic idea is replacement of the inhomogeneity domain by a corresponding inclusion domain filled with a uniformly distributed doublet. Then, the relationship between different temperature gradients is given in index form,

$$k_m \delta_{ij}\left(\frac{\partial T^0}{\partial x_j} + \frac{\partial \tilde{T}}{\partial x_j} + \frac{\partial T^c}{\partial x_j} - \frac{\partial T^*}{\partial x_j}\right) = k^f_{ij}\left(\frac{\partial T^0}{\partial x_j} + \frac{\partial \tilde{T}}{\partial x_j} + \frac{\partial T^c}{\partial x_j}\right) \quad [7.24]$$

where k_m and k^f_{ij} are thermal conductivities of matrix and fibers, respectively. $\frac{\partial T^0}{\partial x_j}$ is the temperature gradient related to the far field applied heat flux; $\frac{\partial T^c}{\partial x_j}$ is the temperature gradient disturbed by the existence of the inhomogeneity; $\frac{\partial T^*}{\partial x_j}$ corresponds to the uniformly distributed doublet in the inclusion domain and $\frac{\partial \tilde{T}}{\partial x_j}$ is the temperature gradient related to interaction between inhomogeneities. By setting up a relationship between these temperature gradients and applying Fourier's law for each phase, the effective thermal conductivity of the composite material is given by the relationship,

$$k^{eff}_{ij}\left\langle\frac{\partial T^t}{\partial x_j}\right\rangle = k^m \delta_{ij}\left\langle\frac{\partial T^t}{\partial x_j}\right\rangle + \frac{1}{V_D}(k^f_{ij} - k^m_{ij}\delta_{ij})\int_\Omega \frac{\partial T^t}{\partial x_j} dV \quad [7.25]$$

where, $\frac{\partial T^t}{\partial x_j}$ is the total (actual) temperature gradient and is related to the temperature gradients mentioned above; Ω denotes the inhomogeneities domain and $\langle\ \rangle$ means averaging over the whole composite body. Integration in the above equation is performed by consideration of fiber orientation distribution. Hatta and Taya (1985) and Chen and Wang (1996) present the results for three-dimensional and two-dimensional misoriented short-fiber composites with uniform distribution and cosine-type distribution.

There are still more methods for predicting effective thermal conductivity of heterogeneous materials (Schulgasser, 1976; Nayak and Tien, 1978; Furmanski, 1992). We will review thermal resistance network models, the volume averaging method and the homogenization method in the following three sections. For more detailed information, please refer to the review for composite systems by Progelhof, Throne *et al.* (1976) and the review for porous media by Kaviany (1995).

7.4 Prediction of ETC by thermal resistance networks

The thermal resistance network method is based on the similarity between thermal conduction and electrical conduction. By parallel or serial connecting components of the system, a thermal resistance network is built up. This has been successful applied in many multiphase systems. Hsu has predicted the effective thermal conductivity of a packed particle bed by this method. With appropriate treatment of the thermal resistance network, the particle morphology, contacts between particles, and even the bi-porous structure of particles, can all be incorporated into the model and provide fairly good results (Hsu, Cheng *et al.*, 1994; Cheng and Hsu, 1999; Chen, Cheng *et al.*, 2000). Applications of this method to the fibrous system are also found in the literature; such materials as unidirectional fiber-reinforced composites (Springer and Tsai, 1967), fabric-reinforced composites (Dasgupta and Agarwal, 1992; Ning and Chou, 1995a,b; Dasgupta, Agarwal *et al.*, 1996), nonwoven textile fabrics (Woo, Shalev *et al.*, 1994a), and misaligned short-fiber-reinforced composites (Fu and Mai, 2003). In the next part, procedures and results from the application of the thermal resistance network method to the fibrous system will be carefully reviewed.

The simplest application of this method to the fibrous system, such as fiber-reinforced composite and textile fabrics, is prediction of the upper and lower bound of effective thermal conductivity by parallel and serial arrangement of each phase:

$$k_{eff,upper} = k_f V_f + k_m V_m,\ k_{eff,lower} = 1/(V_f/k_f + V_m/k_m) \qquad [7.26]$$

The bounds resulting from this prediction are generally too wide to apply.

The volume fraction alone is not enough to characterize the contributions of the fibers and the matrix and interactions between them. More geometrical description of each phase has to be introduced into the model to get reasonable results. This implies that the structure characterization should be emphasized during the modeling process.

As a first step for the thermal resistance network method, a unit cell is chosen from the system. The unit cell is the smallest repeating pattern of the fibrous system and represents all geometrical information at a microscopic level. The thermal resistance network is built up by dividing the unit cell into several components, which can be a single-phase material or a combination of multi-phase materials. Based on certain assumptions of the thermal conduction process and the structure of the unit cell, a thermal resistance network can be built up by serial or parallel connection of the unit cells. For a spatially periodic fibrous system, the effective thermal conductivity of the unit cell is just the bulk effective properties of the system. But, the arrangement of unit cells also contributes to system-level effective thermal conductivity when the system is built up by spatially distributed unit cells.

The other important point in application of the thermal resistance network model lies in the assumption of a thermal conduction process inside the unit cell. Due to the geometry of the fibers and the complex packing pattern, many fibrous materials are anisotropic, and effective thermal conductivity has to be predicted for a given direction. Generally, the temperature gradient is applied to the unit cell only along one direction. The surfaces of the unit cell parallel to the one-dimensional heat flux are assumed to be insulated surfaces (Springer and Tsai, 1967; Dasgupta and Agarwal, 1992; Ning and Chou, 1995b; Cheng and Hsu, 1999). By solving this one-dimensional steady-state thermal conduction problem, the effective thermal conductivity of the unit cell in the conduction direction is obtained. Though thermal conduction through the two phases' interface is a multidimensional process, a one-dimensional approximation is valid for most conditions because effective thermal conductivity is an averaged bulk property. Our review of the thermal resistance network method will start from a simple system – a unidirectional fiber-reinforced composite. Springer and Tsai (1967) analyzed composites with filaments arranged in the rectangular periodic array shown in Fig. 7.1. Filaments were uniform in shape and size, also symmetrical about the x- and y-axes. The unit cell was chosen straightforwardly as in Fig. 7.2. Due to the structural symmetry, only two effective thermal conductivities need to be evaluated. One was along the longitudinal direction of the fibers, $k_{eff.zz}$. The other was the transverse effective thermal conductivity $k_{eff,t}$. The longitudinal ETC, $k_{eff,zz}$ can be easily predicted by assuming a parallel arrangement of the matrix and the fibers. On the other hand, the transverse ETC $k_{eff,t}$ is predicted by applying the thermal resistance network model. With the assumption of one-dimensional thermal conduction, heat flows along the x-direction through

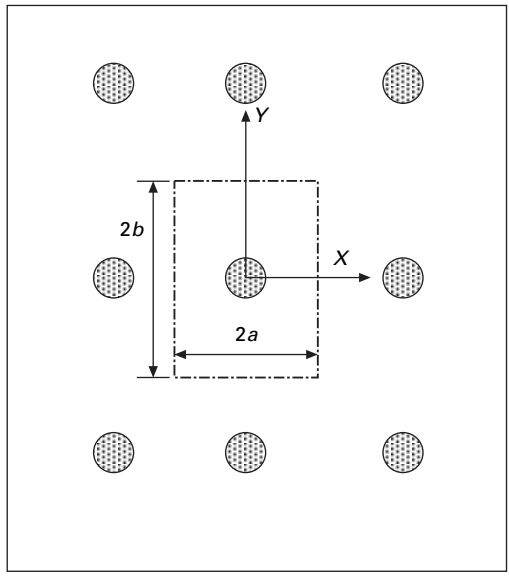

7.1 Structure of unidirectional fiber-reinforced composites with rectangular filaments arrangement. Adapted from Springer, G.S. and S.W. Tsai, 'Thermal conductivities of unidirectional materials'. *Journal of Composite Materials*, 1967. 1: pp. 166–173.

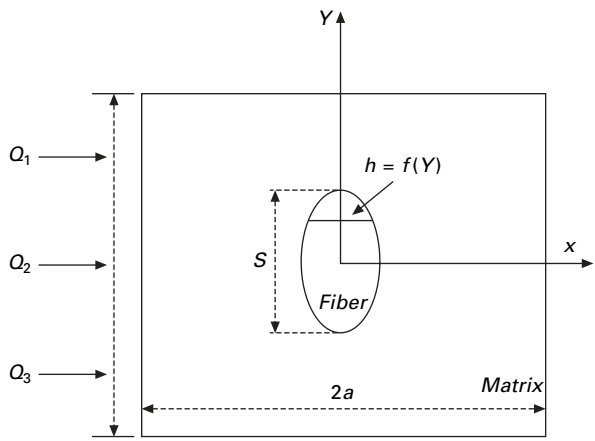

7.2 Unit cell used in effective thermal conductivity prediction. Adapted from Springer, G.S. and S.W. Tsai, 'Thermal conductivities of unidirectional materials'. *Journal of Composite Materials*, 1967. 1: pp. 166–173.

three parallel components. The thermal resistance of each component in the thermal resistance network is given by

$$R_i = \frac{l_i}{A_i k_i} \qquad [7.27]$$

where l_i is the component dimension along the conduction direction; A_i is the cross-sectional area orthogonal to the conduction direction; k_i is the thermal conductivity of the component. In the unit cell, three parallel components are easily identified, shown in Fig. 7.2. Components 1 and 3 are composed of purely matrix material and the thermal resistance of them is written by

$$\frac{1}{R_1} + \frac{1}{R_3} = \frac{(2b - s)wk_m}{2a} \qquad [7.28]$$

where w is the length in the z-direction, and is constant for a unidirectional system. The component 2 is a combination of matrix material and fiber, i.e. the interphase between the matrix and the fiber, whose thermal resistance R_2 may be calculated from the thermal resistance of an infinitely thin slice dy,

$$R_{2,dy} = \frac{1}{wdy}\left[\frac{2a - h(y)}{k_m} + \frac{h(y)}{k_f}\right] \qquad [7.29]$$

Three components are connected in parallel. The thermal effective conductivity of the unit cell is obtained from the relationship

$$\frac{1}{R} = \frac{2a}{2bwk_{eff}} = \frac{1}{R_1} + \frac{1}{R_2} + \frac{1}{R_3} \qquad [7.30]$$

$$\frac{k_{eff}}{k_m} = \left(1 - \frac{s}{2b}\right) + \frac{a}{b}\int_0^s \frac{dy}{(2a - h(y)) + h(y)(k_m/k_f)} \qquad [7.31]$$

The effects of structure are shown in two ways. Firstly, the geometry of the fibers is characterized by two variables: s, the maximum dimension of the fiber in the y direction; and $h(y)$, the width of the fiber at any given y. Both are shown in the equation. Then the rectangular packing pattern of unit cells exhibits its effect by parameters a and b. By choosing appropriate unit cells, other regular packing patterns can be handled in the way similar to the above derivation. Springer and Tsai (1967) predicted the effective thermal conductivity of square fibers and cylindrical fibers in a square packing pattern.

$$\frac{k_{eff,square}}{k_m} = (1 - \sqrt{V_f}) + \frac{1}{\sqrt{V_f} + B/2} \qquad [7.32]$$

$$\frac{k_{eff,cylinder}}{k_m} = (1 - 2\sqrt{V_f/\pi}) + \frac{1}{B}\left[\pi - \frac{4}{\sqrt{1 - (B^2 V_f/\pi)}} \tan^{-1} \frac{\sqrt{1 - (B^2 V_f/\pi)}}{1 + (B^2 V_f/\pi)}\right] \quad [7.33]$$

where

$$B = 2\left(\frac{k_m}{k_f} - 1\right)$$

These results were compared with numerical calculations from the shear loading analogy and experimental data (Springer and Tsai, 1967). Depending on the thermal conductivity ratio between the fibers and the matrix, the discrepancies between the two models and experiment data are different. But the difference is generally less than 10%. Considering the simple derivation procedure and resulting analytical equations, the thermal resistance network provides a reasonably accurate method for unidirectional composite analysis.

As shown in the above example, structure characterization determines effective thermal conductivity prediction. The importance of, and difficulties in, structure modeling are well illustrated in the following reviews of woven fabric composites (Dasgupta and Agarwal, 1992; Ning and Chou, 1995a,b 1998; Dasgupta, Agarwal *et al*., 1996).

7.5 Structure of plain weave woven fabric composites and the corresponding unit cell

In order to simplify structure characterization, Ning and Chou (1995a,b, 1998) idealized the unit cell by replacement of the yarn crimp with linear segments. Taking account of the symmetry of the unit cell, it is assumed that transverse thermal conductivity can be predicted by analysis on a quarter of the idealized unit cell. This implies that the interaction between the quarters of the unit cell is negligible. In order to predict transverse effective thermal conductivity, thermal conduction in the unit cell is assumed to be one-dimensional, and heat flow lines to be all parallel to the z-axis. The unit cell is partitioned into eleven components, with the characteristics that each component is composed of a single material. Taking advantage of this partition and simplified geometry, the thermal resistance of each component can be calculated in simple algebraic form. The effective thermal conductivity of the unit cell is obtained by constructing the thermal resistance network of each component. Based on a structure periodicity assumption, the effective thermal conductivity of the whole woven fabric composite is the same as a single unit cell.

$$k_{\text{eff}} = \frac{k_m}{\left(1 + \frac{g_w}{a_w}\right)\left(1 + \frac{g_f}{a_f}\right)}\left[\frac{g_w}{a_w}\frac{g_f}{a_f} + \frac{\frac{g_f}{a_f}}{\left(\frac{h_m}{h} + \frac{h_f}{h}\right) + \frac{k_m}{k_{w1}}\frac{h_w}{h}} + \right.$$

$$\left. \frac{1}{\frac{h_m}{h} + \left(\frac{k_m}{k_{w2}}\frac{h_w}{h} + \frac{k_m}{k_{f2}}\frac{h_f}{h}\right)} + \frac{\frac{g_w}{a_w}}{\left(\frac{h_m}{h} + \frac{h_f}{h}\right) + \frac{k_m}{k_{f1}}\frac{h_f}{h}}\right] \quad [7.34]$$

The parameters in the above equation can be classified into two categories: g_w, g_f, a_w, a_f, h_m, h_f, h are geometrical characteristics of the unit cell and are determined by the weave style. k_m, k_{d1}, k_{d2} ($d = w, f$) are the thermal conductivities of resin matrix and impregnated warp and fill yarns with mean fiber orientation angle $\overline{\theta_{di}}$ Taking into account the measurement of these parameters, two more steps are needed for prediction closure. Yarn thermal conductivity is predicted by assuming that yarns are unidirectional fiber-reinforced composites with certain fiber orientations. Hence, these parameters are predicted by

$$k_{di} = k_a \sin^2 \overline{\theta_{di}} + k_t \cos^2 \overline{\theta_{di}} \ (d = w, f \ i = 1, 2) \quad [7.35]$$

where k_a and k_t are the longitudinal and transverse thermal conductivity of the yarns without fiber orientation and are calculated from the fiber and resin thermal conductivity and fiber volume fraction in the yarn (Dasgupta and Agarwal, 1992; Ning and Chou, 1995a,b; Dasgupta, Agarwal *et al.*, 1996). $\overline{\theta_{di}}$ is the mean fiber orientation angle with respect to the x- or y-axis, and is measurable for given woven fabric composites.

Considering the geometrical characterization of the unit cell, the matrix volume fraction h_m is rather difficult to measure practically. The way to overcome this difficulty is by relating this parameter to the fiber volume fraction, h, in both composites and yarns.

$$\frac{h_m}{h} = 1 - \frac{V_f}{V_{fy}}\left(1 + \frac{g_f}{a_f}\right)\left(1 + \frac{g_w}{a_w}\right) + \frac{h_w}{h}\frac{g_f}{a_f} + \frac{h_f}{h}\frac{g_w}{a_w} \quad [7.36]$$

With these two additional equations, the transverse effective thermal conductivity of plain weave woven fabric composites can be predicted from all measurable parameters. The effects of volume fraction and weave style on effective thermal conductivity are discussed for yarn-balanced fabric composites and compared with other numerical and experimental results (Ning and Chou, 1995a). The consistency of these data implies that the

thermal resistance network method is robust and that the assumptions made during derivation are valid under pure thermal conduction. Using the same method and assumptions, Ning also successfully predicted the transverse effective thermal conductivities of twill weave, four-harness satin weave, and five- and eight-harness satin weave fabric composites. The results are documented in the literature in their general form (Ning and Chou, 1998).

Dasgupta and Agarwal (1992) and Dasgupta, Agarwal *et al*. (1996) also analyzed the woven fabric composites by a homogenization method and the thermal resistance network model. The unit cell used in this work is shown in Fig. 7.3. Instead of simplification by linear segment, vertical cross-sections and undulation of yarns are approximated by circular arcs in Dasgupta's work. The effective thermal conductivity of the unit cell has to be calculated from analysis of infinitesimal slices and numerical integration over the whole unit cell domain because of the complex structure of the unit cell. The other important point of this model is incorporation of correction for heat flow lines. Based on observation from the homogenization analysis, Dasgupta allowed the heat to flow preferably from transverse yarns to longitudinal yarns when the resin had high thermal resistance. In-plane and out-of-plane effective thermal conductivity of plain weave fabric composites are all predicted in numerical form based on the thermal resistance network method. Comparison of the homogenization method and experimental data shows good prediction ability for the model.

Nonwoven fabric is the other important category of fibrous materials. Fibers are spatially distributed and packed together to form a network structure. The thermal conductivity of a single fiber, fiber volume fraction and orientation of the fibers will determine effective thermal conductivity of nonwoven

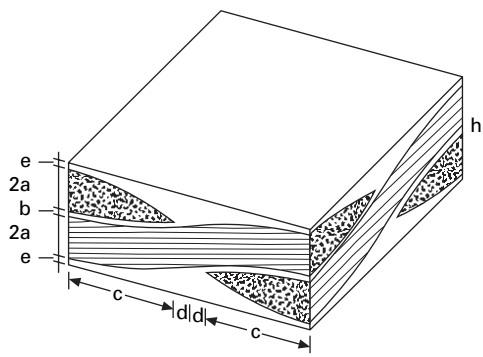

7.3 Unit cell of a balanced plain weave fabric-reinforced composites lamina. The warp yarn and fill yarns are assumed to be identical. Adapted from Dasgupta, A. and R.K. Agarwal, 'Orthotropic Thermal-Conductivity of Plain-weave Fabric Composites using a Homogenization Technique'. *Journal of Composite Materials*, 1992. 26(18): pp. 2736–2758.

fabric. Based on analysis of the unit cell, Woo, Shalev *et al.* (1994a) proposed a model in terms of measurable geometry parameters to predict out-of-plane effective thermal conductivity of nonwoven fabrics.

As shown in Fig. 7.4(a), the unit cell is chosen as two touching layers of fiber assembly. The number of fibers oriented along the *x*- and *y*-axes are *n* and *m*, respectively. Applying the thermal resistance network method, the effective thermal conductivity of this unit cell is given by

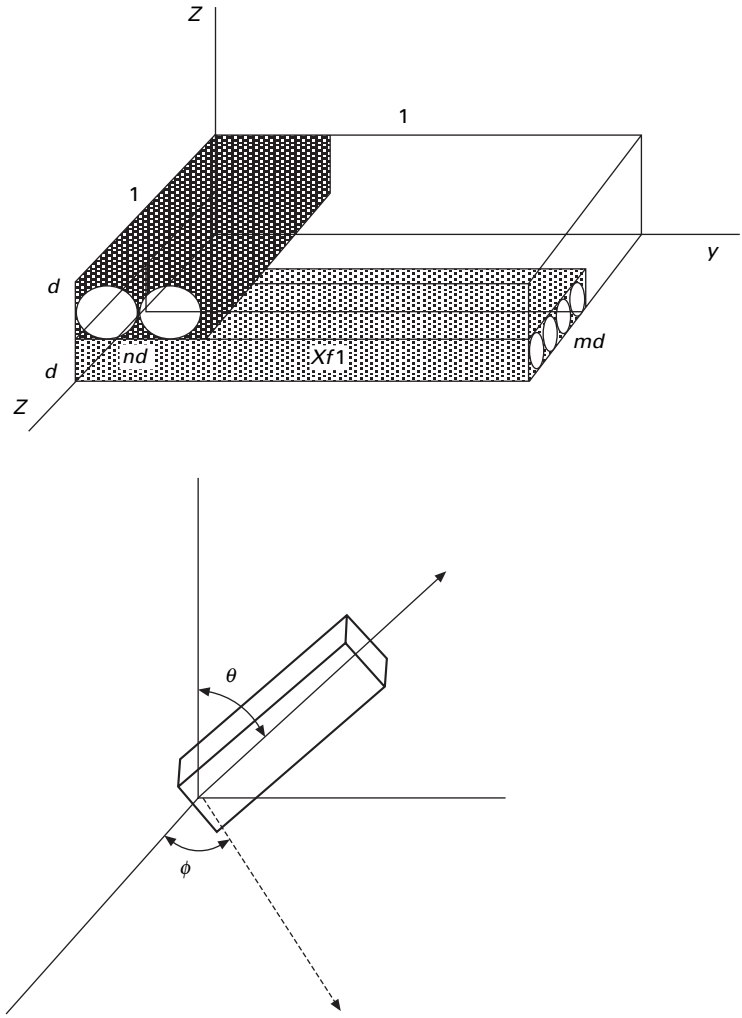

7.4 (a) Idealized unit cell structure of nonwoven fabrics. (b) Orientated unit cells simulating structure of real nonwoven fabrics. Adapted from Woo, S.S., I. Shalev, and R.L. Barker, 'Heat and Moisture Transfer Through Nonwoven Fabrics.1. Heat-Transfer'. *Textile Research Journal*, 1994. 64(3): pp. 149–162.

$$k_{eff,zz} = P_o k_a + \frac{(1 - P_o)^2}{\frac{V_f}{k_1} + (1 - P_o - V_f)/k_a} \quad [7.37]$$

$$k_{eff,xx} = (0.5 - V_{f1})k_a + V_{f1}k_2 + \frac{0.5}{2V_{f2}k_1 + \frac{(1 - 2V_{f2})}{k_a}} \quad [7.38]$$

$$k_{eff,yy} = (0.5 - V_{f2})k_a + V_{f2}k_2 + \frac{0.5}{2V_{f_1}k_1 + \frac{(1 - 2V_{f1})}{k_a}} \quad [7.39]$$

where V_{f1} and V_{f2} are the fiber volume fractions along the x- and y-directions; k_1 and k_2 are the longitudinal and transverse thermal conductivities of a single fiber; P_o is the optical porosity of the unit cell, which corresponds to the area fraction of through pores, given by

$$P_o = 1 - nd - md + ndmd = 1 - V_f + (8/\pi)^2 V_{f1} V_{f2} \quad (7.40)$$

The nonwoven structure cannot be reconstructed by simply periodic packing of the unit cell. Practically, the behavior of nonwoven fabrics will be better represented by the unit cell with a certain orientation, shown in Fig. 7.4(b). Because orientation distribution function is not introduced in Woo's model, the polar orientation angle θ and azimuthal orientation angle ϕ in the following discussion should be considered as average quantities. The out-of-plane effective thermal conductivity of nonwoven fabric is obtained by analysis of this oriented unit cell,

$$k_{eff,oz} = k_{eff,xx}(\cos^2 \phi \cos^2\theta) + k_{eff,yy}(\cos^2 \phi \sin^2\theta) + k_{eff,zz}(\sin^2 \theta) \quad [7.41]$$

The optical porosity depends on the thickness of the nonwoven fabric. Based on this observation, Woo assumed that unit cells are regularly packed along the fabric thickness direction for predicting whole fabric optical porosity

$$P_i = [1 - (8/\pi)V_{f1} - (8/\pi)V_{f2} + (8/\pi)^2 F_{f1} V_{f2}]^{L/(2d)} \quad [7.42]$$

With this correction, the out-of-plane effective thermal conductivity, i.e. $k_{eff,oz}$ is given by

$$\begin{aligned} k_{eff,oz} = {} & k_a\{\sin^2 \phi P_i - \cos^2\phi[\cos^2\theta\,(0.5 - V_{f1}) + \sin^2\theta\,(0.5 - V_{f2})]\} \\ & + k_2 \cos^2 \phi\,(\cos^2\theta V_{f1} + \sin^2\theta V_{f2} + 0.5 \cos^2 \phi\,\{\cos^2\theta/[2V_{f2} \\ & + /k_1 + (1 - 2V_{f2})/k_a]\} + \sin^2\theta/[2V_{f1}/k_1 + (1 - 2V_{f1})/k_a] \\ & + \sin^2 \phi\,(1 - P_1)^2/[F_f/k_1 + (1 - P_i - V_f)/k_a] \end{aligned} \quad [7.43]$$

This representation is rather clumsy and some parameters may not be

measurable. Woo simplifies the above equation by structuring special nonwoven fabrics in his research. For melt blow or spunbond nonwovens, the average polar orientation angle is approximately zero. Also, an easily measurable anisotropy factor is introduced to take account of the distribution of fibers inside the unit cell,

$$\alpha = V_{f1}/V_{f2} \qquad [7.44]$$

The resulting out-of-plane effective thermal conductivities are given in the form of measurable physical parameters,

$$\begin{aligned} k_{eff,oz} = {} & k_a \sin^2 \phi P_i + k_2 \cos^2 \phi \alpha V_f/(1+\alpha) + \sin^2 \phi (1-P_i)^2/ \\ & + [V_f/k_1 + (1-P_i-V_f)/k_a] + \cos^2 \phi (1+\alpha-\alpha V_f)^2/ \\ & + \{(1+\alpha)[V_f/k_1 + (1-V_f)(1+\alpha)/k_a]\} \end{aligned} \qquad [7.45]$$

and

$$P_i = [1 - (8/\pi)V_f + (8/\pi)^2 V_f^2 \alpha/(1+\alpha)^2]^{L/(2d)} \qquad [7.46]$$

In Woo's work, a series of measurements for different nonwoven fabrics have been made and have validated the prediction model (Woo, Shalev *et al.*, 1994a). It is seen from the above equation that the effective thermal conductivity of nonwoven fabrics is influenced by many physical characteristics, such as fiber volume fraction, anisotropic thermal conductivity of single fibers, orientation of fibers, and so on. The contribution of these effects can be obtained from parameter analysis and validated by experiments. However, the present model is simplified by considering the structure of specific systems. It is better to consider the prediction equation as a semi-experimental approach.

In some fibrous materials, such as short-fiber-reinforced composites and textile fiber assemblies, the structure of the system is best described using statistical distribution functions. Compared with mechanical property prediction, analyzing effective thermal conductivity based on a statistical approach is relatively rare (Hatta and Taya, 1985; Chen and Wang, 1996; Fu and Mai, 2003). Among them, Fu and Mai (2003) present a simple model to predict thermal conductivity of spatially distributed, short-fiber-reinforced composites.

Depending on the researchers, different statistical distribution functions have been employed to describe fiber distribution. Fu introduced two density functions to account for fiber length and orientation distributions.
Fiber length distribution:

$$f(L) = abL^{b-1} \exp(-aL^b) \quad \text{for} \quad L > 0 \qquad [7.47]$$

Fiber orientation distribution:

$$g(\theta, \phi) = g(\theta)\, g(\phi)/\sin\theta \qquad [7.48]$$

where

$$g(\theta) = (\sin\ \theta)^{2p-1}(\cos\ \theta)^{2q-1} / \int_{\theta_{\min}}^{\theta_{\max}} (\sin\theta)^{2p-1} d\theta \text{ for } 0 \le \theta_{\min} \le \theta \le \theta_{max} \le \frac{\pi}{2} \quad [7.49]$$

$g(\phi)$ is defined in a similar way to $g(\theta)$.

The parameters a, b, p, q are applied to represent the size and shape of the distribution density function and can be measured for given composites.

As Fig. 7.5 shows, Fu's model tries to predict effective thermal conductivity along direction 1. The laminate analogy approach (Agarwal, 1990) is employed to formulate the model. The original composite with distribution functions $f(L)$ and $g(\theta, \phi)$ is illustrated in Fig. 7.5(a). Because only the thermal conductivity in direction 1 is concerned, the original composite is first approximated as a hypothetical composite with orientation distribution $g(\theta, \phi) = 0$ as in Fig. 7.5(a). The next approximation step is treating the hypothetical composite as a combination of laminates as seen in Figs. 7.5(b) and 7.5(c). Shown in Fig. 7.5(d), the final 'equivalent' system is a series of lamina $L(L_j, \theta_j)$, $j = 1,2, \ldots, m$. Each lamina contains fibers with the same length L_j and orientation angle θ_j.

Based on this laminate analogy approach, the thermal conductivity of each laminate is predicted from the results of unidirectional fiber-reinforced composites with a certain orientation angle. The Halpin–Tsai equation (Agarwal, 1990) is applied in Fu's work.

$$k_1 = \frac{1 + 2\alpha\mu_1 V_f}{1 - \mu_1 V_f} k_m \quad \mu_1 = \frac{k_{f1}/k_m - 1}{k_{f1}/k_m + 2\alpha}$$

$$k_2 = \frac{1 + 2\mu_2 V_f}{1 - \mu_2 V_f} k_m \quad \mu_2 = \frac{k_{f2}/k_m - 1}{k_{f2}/k_m + 2} \quad [7.50]$$

where $\alpha = L/d_f$ is the aspect ratio of the fibers. Taking account of the orientation of the fibers, the thermal conductivity of each laminate is given by

$$k_{ij} = k_{1j} \cos^2\ \theta_j + k_2 \sin^2\ \theta_j \quad [7.51]$$

Assuming all laminates are connected in parallel with respect to direction 1, the effective thermal conductivity of the composite is predicted by integration with the distribution density functions,

$$k_{eff} = \sum_{j=1}^{M} k_{lj} h_j = \int_{L_{\min}}^{L_{\max}} \int_{\theta_{\min}}^{\theta_{\max}} (k_1 \cos^2\theta + k_2 \sin^2\theta) f(L) g(\theta) dL d\theta \quad [7.52]$$

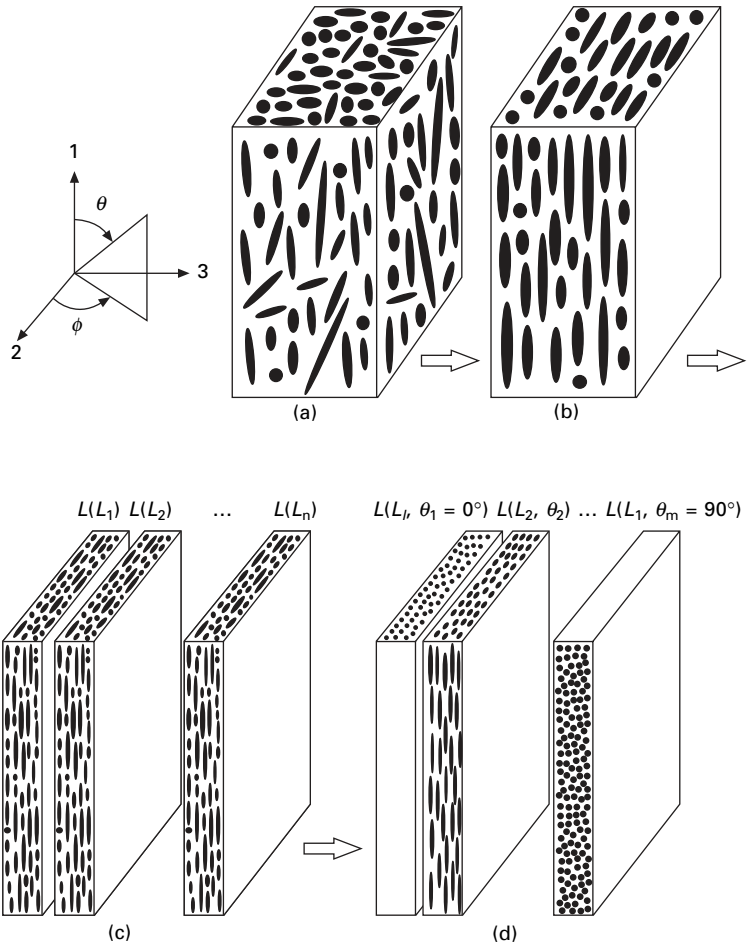

7.5 (a) Real misaligned short-fiber-reinforced composites with orientation distribution $g(\theta, \phi)$. (b) Hypothetical composite with orientation distribution $g(\theta, \phi = 0)$. (c) Hypothetical composite treated as combination of laminates $L(L_j)$, and each laminate contains fibers of same length L_j. (d) Each laminate is treated as a stacked sequence of lamina $L(L_j, \theta_j)$, and each laminae contains fibers with same length L_j and orientation angle θ_j. From Fu, S.Y. and Y.W. Mai, 'Thermal conductivity of misaligned short-fiber-reinforced polymer composites'. *Journal of Applied Polymer Science*, 2003. 88(6): pp. 1497–1505. Reproduced with permission.

Parameter analysis is performed by Fu to evaluate the effects of volume fraction, mean fiber length and mean fiber orientation angle on effective thermal conductivity. For uniform length short fibers, the thermal conductivity of two-dimensional and three-dimensional random fiber distributions is easily predicted by the simplified distribution functions.

$$k_{eff,2D} = \frac{1}{2}(k_1 + k_2) \quad [7.53]$$

$$k_{eff,3D} = \frac{1}{3}k_1 + \frac{2}{3}k_2 \quad [7.54]$$

Unfortunately, further discussion concerning distribution function effects is not available in current literature. Improvement of the present statistical model is still needed.

In this section, we have reviewed the prediction of the effective thermal conductivity of fibrous materials by the thermal resistance network method. With the assumption of a one-dimensional conduction process and easily built thermal circuits, this method provides a simple and efficient way for thermal conductivity prediction. Comparison with other methods and experimental data also shows that reasonable accuracy can be achieved with appropriate treatment of structures. The numerical, even analytical in some cases, results from this relatively simple method, are believed to be very useful for practical engineering and science applications.

7.6 Prediction of ETC by the volume averaging method

Fibrous materials are not only multiphase but also multiscale systems. With a glance at textile fabrics, several disparate length scales can be identified, such as the diameter of fibers, the length of fibers, the distance between fibers, the size of the whole fibrous system, and so on. Analysis of these multiscale systems may have special challenges due to interactions between different scales. Local volume averaging is a method to upscale the system from the microscale to the macroscale. It has been widely applied in the field of porous media. A well-known example is starting from the microscopic Navier–Stokes equation to arrive at the macroscopic Darcy's law for creeping flow through porous media (Whitaker, 1969, 1999; Kaviany, 1995).

The volume averaging method is well suited for multiphase systems, such as fibrous materials. Textile fibers can form network structures, even with a very low fiber volume fraction. A fiber assembly can be treated as a single continuum, which is called the solid phase in porous media study; the air or water inside the voids between the fibers is referred to as the fluid phase. The length scale, corresponding to the void in fibrous materials, should be the average distance between fibers. Based on basic geometrical fibrous characterization (Pan 1993, 1994), we can get this distance and relate it to the general geometry parameters of the textile fibrous system. Thus, treatment for general porous media may be applied to textile fabrics with appropriate adjustment. In this section, we will review the basic ideas of the local volume averaging method and its application to pure thermal conduction.

The first step for the application of the volume averaging method is finding an appropriate representative element volume (REV), also called averaging volume, schematically shown in Fig. 7.6. Generally, averaged properties, such as porosity, will depend on the chosen average volume. The representative element volume in porous media is identified as a volume range, in which averaging properties is independent of volume size, i.e. adding or subtracting pores and solids does not change the average value. Bachmat and Bear (1986; Bear and Bachmat, 1990; Bear, Buchlin *et al.*, 1991) provide detailed discussion about size of REV based on porous media structure and statistical concerns. Representative element volume size is also important for assumptions made during the volume averaging process and will be discussed in following parts.

Volume averaged variables are defined by integration of micro-scale variables over the whole REV. For any quantity ψ associated with the fluid, the volume averaged value for the centroid of REV is defined in two ways: superficial averaged ψ is

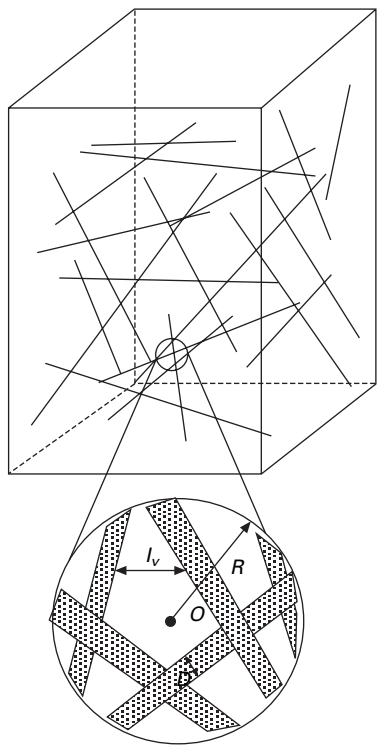

7.6 A typical representative element volume (REV) selected from fibrous materials.

$$\langle \psi \rangle = \frac{1}{V} \int_{V_f} \psi dV \qquad [7.55]$$

where $V = V_f + V_s$;
and intrinsic averaged ψ is

$$\langle \psi_f \rangle^f = \frac{1}{V_f} \int_{V_f} \psi dV. \qquad [7.56]$$

Generally, intrinsic averaged value is preferred because it is a better representation of properties in the fluid phase. The relationship between them is given by $\langle \psi \rangle = \varepsilon \langle \psi \rangle^f$ differing by the porosity ε. The same definitions and operations are also applicable for solid phase variables. Throughout the whole fibrous system, we can select REV and perform the volume averaging operation point by point. Thus, new variables over the whole fibrous system are defined. These variables from volume averaging methods have their thermodynamic significance; for instance, discussion about volume averaged temperature is available from Hager's work (Hager and Whitaker; 2002).

Now, one question may be raised – why volume averaged temperature is needed for thermal analysis of fibrous materials. The requirement for these averaged variables lies on two sides, the intrinsic multiscale properties of the fibrous system and the experimental measurement conditions. In previous sections, we discussed only the point temperature field in homogeneous and heterogeneous systems. But, point temperature is a microscale variable in a multiscale system. That means that the characteristic length of a point temperature in a fibrous system will be the size of fibers or the average distance between fibers. From the whole system point of view, i.e. fabrics, the point temperature fluctuates spatially with very high frequency. Detailed information about point temperature will not only depend on boundary conditions imposed on fabrics but also on short-length correlations between fibrous system structures. On the other hand, volume averaged temperature will provide much less frequent fluctuation over the whole fibrous domain by smoothing out fluctuations over the REV, schematically illustrated in Fig. 7.7. Hence, volume averaged temperature is characterized by macroscopic length and is appropriate for analyzing thermal response of whole fibrous materials to certain excitations.

The other reason to adopt volume averaged temperature lies in the measurement of temperature fields and setting up boundary conditions. In most scientific and engineering applications, instruments used to measurement temperature must have a measure window. Results from the instruments are volume averaged temperature over the measurement window (Bear and Bachmat, 1990; Bear, Buchlin *et al.*, 1991). Furthermore, boundary conditions in most scientific and engineering applications are not specified as point temperature. They are generally specified in macroscopic variables; for example,

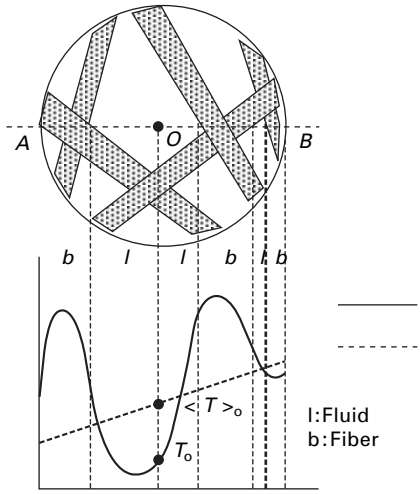

7.7 Schematic illustration of point temperature and volume averaged temperature fluctuation in the REV.

area average temperature and heat flux are specified in heat plate methods (Satsumoto, Ishikawa *et al*., 1997; Jirsak, Gok *et al*., 1998; Mohammadi, Banks-Lee *et al*., 2003). The advantage of applying volume averaging methods is gained by sacrifice of detailed microscopic information. This means that this method is not efficient in predicting behavior at pore and fiber scale. However, the thermal response of the fibrous system to macroscopic boundary and initial conditions are most attractive information for us. Thus, the volume averaging method is appropriate for this purpose.

The importance of volume averaging variables has been realized by textile scientists and applied to the analysis of heat and mass transfer through fabrics (Gibson and Charmchi, 1997; a,b; Fohr, Couton *et al*., 2002; de Souza and Whitaker, 2003). However, the ability of the volume averaging method to upscale the system and predict effective thermal conductivity of the system is rarely found in fibrous materials references. In this section, we will review procedures for the derivation of effective thermal conductivity by the volume averaging method. Following the methods developed by Whitaker (Whitaker, 1991, 1999; Quintard and Whitaker, 1993; Kaviany, 1995), the macroscopic governing equation and a closed solution for effective thermal conductivity will be obtained for the system with special structures.

In the following discussion, fibers are assumed to be interconnected to form a continuous phase, referred as the solid phase. Pores are assumed to be fully saturated by air or water, then denoted as the fluid phase. Thermal conduction is assumed to be the only dominant heat transfer process. Based on these assumptions, the point governing equation can be written for each phase as

$$(\rho c_p)_s \frac{\partial T_s}{\partial t} = \nabla \cdot (k_s \nabla T_s)$$

$$(\rho c_p)_f \frac{\partial T_f}{\partial t} = \nabla \cdot (k_f \nabla T_f)$$

$$T_f = T_s \text{ on } A_{fs}$$

$$-n_{fs} \cdot k_f \nabla T_f = -n_{fs} \cdot k_s \nabla T_s \text{ on } A_{fs} \quad [7.57]$$

in which the boundary conditions indicate that the temperature and the normal component of the heat flux are continuous at the fluid–solid surfaces. Thermal conductivity k_s for the fibrous phase should be treated as a lumped parameter, which includes bulk heat conductivity of single fibers and thermal contact resistance between fibers. It is clear from observation of these equations that two more boundary conditions at the fabric boundaries and one initial condition are needed to explicitly solve the point temperature field. However, this information is not generally available in the form of point temperature and is not important for derivation of effective thermal conductivity. It will not be shown in the following discussion.

Upscaling is achieved by performing volume averaging operations on the above point governing equations. Due to the similarity between solid and fluid phases, we will only discuss procedures for the fluid phase equation. The resulting volume averaged equation for the fluid phase is given by

$$\varepsilon(\rho c_p)_f \frac{\partial \langle T_f \rangle^f}{\partial t} = \langle \nabla \cdot (k \nabla T_f) \rangle \quad [7.58]$$

where $\langle\ \rangle$ denote superficial volume averaging.

In order to obtain the macroscopic governing equation, the right-hand side of the above equation must be related to the gradient of the volume averaging temperature. This step is done by application of the spatial averaging theorem, which has already been developed and well discussed by several researchers (Whitaker, 1969, 1999; Gray, 1993; Slattery, 1999).

$$\langle \nabla \psi \rangle = \nabla \langle \psi \rangle + \frac{1}{V} \int_{A_{sf}} n_{sf} \psi dA \quad [7.59]$$

$$\langle \nabla \cdot \psi \rangle = \nabla \langle \psi \rangle + \frac{1}{V} \int_{A_{sf}} n_{sf} \cdot \psi dA \quad [7.60]$$

After applying the averaging theorem twice to the volume averaged governing equation, the result is given by

$$\varepsilon(\rho c_p)_f \frac{\partial \langle T_f \rangle^f}{\partial t} = \nabla \cdot \left[k_f \left(\varepsilon \nabla \langle T_f \rangle^f + \langle T_f \rangle^f \nabla \varepsilon + \frac{1}{V} \int_{A_{fs}} n_{fs} T_f dA \right) \right] + \frac{1}{V} \int_{A_{fs}} n_{fs} \cdot k_f \nabla T_f dA \quad [7.61]$$

The last term in above equation corresponds to the interfacial heat flux at the fluid and solid interface and will be handled with the information from the solid phase. Now, the central problem turns out to be the integral of point temperature over the fluid–solid interface. As shown by Slattery (1999) and Whitaker (1999), this problem can solved by introducing spatial decomposition of point temperature as

$$T_f = \langle T_f \rangle^f + \tilde{T}_f \quad [7.62]$$

After substituting decomposition form into the governing equation, the integral term of the volume averaged temperature, $\frac{1}{V} \int_{A_{sf}} n_{sf} \langle T_f \rangle^f dA$, needs to be noticed. It is clear that this integral is evaluated from the volume averaged temperature other than the centroid of the REV. This is an indication of non-local transport phenomena. In order to get the local form-governing equation, Taylor expansion and order of magnitude analysis is applied. The result is given by

$$\frac{1}{V} \int_{A_{sf}} n_{sf} \langle T_f \rangle^f dA = -\langle T_f \rangle^f \nabla \varepsilon \quad [7.63]$$

with length scale constraints,

$$l_f << r_0 \quad r_0^2 << L_\varepsilon L_{T1} \quad [7.64]$$

where l_f is the characteristic length of the fluid phase, i.e. the average distance between fibers; r_0 is the size of REV and L_ε and L_{T1} are length scales resulting from the order of magnitude estimates,

$$\nabla \varepsilon_f = O\left(\frac{\nabla \varepsilon_f}{L_\varepsilon} \right), \nabla \nabla \langle T_f \rangle^f = O\left(\frac{\nabla \langle T_f \rangle^f}{L_{T1}} \right) \quad [7.65]$$

Depending on the process under analysis, the structure of the porous medium and the position inside the medium, these length scales may be different. As we mentioned above, these constraints also show the importance of choosing REV size. Identifying each length scale and validating constraints will be the task of scientists and engineers for the governing equation derivation.

With satisfaction of the above length scale constraints, the macroscopic governing equation for the fluid phase will be given by

$$\varepsilon(\rho c_p)_f \frac{\partial \langle T_f \rangle^f}{\partial t} = \nabla \cdot \left[k_f \left(\varepsilon \nabla \langle T_f \rangle^f + \frac{1}{V} \int_{A_{fs}} n_{fs} \tilde{T}_f dA \right) \right] + \frac{1}{V} \int_{A_{fs}} n_{fs} \cdot k_f \nabla T_f dA \quad [7.66]$$

Following the same procedures, the macroscopic governing equation for the solid phase can be written as

$$\varepsilon(\rho c_p)_s \frac{\partial \langle T_s \rangle^s}{\partial t} = \nabla \cdot \left[k_s \left(\varepsilon \nabla \langle T_s \rangle^s + \frac{1}{V} \int_{A_{fs}} n_{fs} \tilde{T}_s dA \right) \right] + \frac{1}{V} \int_{A_{sf}} n_{sf} \cdot k_s \nabla T_s dA \quad [7.67]$$

For a pure thermal conduction process, a local thermal equilibrium assumption is often made to further simplify derivation (Whitaker 1991, 1999; Kaviany, 1995). The essence of local thermal equilibrium is assuming that the local averaged temperature difference between two phases is negligible, i.e.

$$\langle T_f \rangle^f = \langle T_s \rangle^s \quad [7.68]$$

The constraints for the validity of this assumption were first given by Carbonell and Whitaker (1984) in the form of time scale and length scale constraints:

Time scale

$$\frac{\varepsilon(\rho c_p)_f l_f^2}{t} \left(\frac{1}{k_f} + \frac{1}{k_s} \right) << 1, \frac{(1-\varepsilon)(\rho c_p)_s l_s^2}{t} \left(\frac{1}{k_f} + \frac{1}{k_s} \right) << 1 \quad [7.69]$$

Length scale

$$\frac{\varepsilon k_f l_f}{A_0 L^2} \left(\frac{1}{k_f} + \frac{1}{k_s} \right) << 1, \frac{(1-\varepsilon) k_s l_s}{A_0 L^2} \left(\frac{1}{k_f} + \frac{1}{k_s} \right) << 1$$

It is clear that local thermal equilibrium assumptions will fail when very fast transients are analyzed. As also shown in other references (Whitaker, 1991; Quintard and Whitaker, 1993; Kaviany, 1995; Quintard, Kaviany *et al.*, 1997), local thermal equilibrium will not validate when significant heat generation exists in the solid or fluid phase, such as adsorption heat and condensation heat in fibrous systems. A two-equation model has to be applied under these conditions. More effective thermal conductivity, K_{fs} and K_{sf}, may be introduced to characterize heat flux in one phase generated by a temperature gradient in the other phase.

In a fibrous system without significant heat generation in each phase, and

pure thermal conduction analysis, governing equations for solid and fluid phases can be added together to get

$$[\varepsilon(\rho c_p)_f + (1-\varepsilon)(\rho c_p)_s]\frac{\partial\langle T\rangle}{\partial t} = \nabla\cdot\{[\varepsilon k_f + (1-\varepsilon)k_s]\nabla\langle T\rangle + \frac{k_f}{V}\int_{A_{fs}} n_{fs}\tilde{T}_f dA + \frac{k_f}{V}\int_{A_{sf}} n_{sf}\tilde{T}_s dA\Big\} \quad [7.70]$$

where $\langle T\rangle$ is volume average temperature and satisfies

$$\langle T\rangle = \varepsilon\langle T_f\rangle^f + (1-\varepsilon)\,\langle T_s\rangle^s$$

and with local thermal equilibrium assumption, $\langle T\rangle = \langle T_f\rangle^f = \langle T_s\rangle^s$.

The other advantage gained by adding the two equations together is the elimination of interfacial heat flux terms. This is the result of heat flux continuity boundary conditions at the solid–fluid interface. Interfacial boundary conditions for point variables will affect the macroscopic governing equations. This is a general characteristic of the multiphase, multiscale system because the macroscopic averaged equation need include not only information in each phase but also that at the interface.

At this point, one governing equation to describe the thermal conduction process through porous medium is obtained. It is only valid for fibrous materials with certain constraints satisfied. Comparing this result with the fundamental thermal conduction equation, it is appealing to write the right-hand side of Equation [7.70] in the form

$$\nabla\cdot\{[\varepsilon k_f + (1-\varepsilon)k_s]\,\nabla\langle T\rangle + \frac{k_f}{V}\int_{A_{fs}} n_{fs}\tilde{T}_f dA + \frac{k_f}{V}\int_{A_{sf}} n_{sf}\tilde{T}_s dA\Big\} = K_{eff}\cdot\nabla\langle T\rangle \quad [7.71]$$

The central problem turns out to be finding the relationship between spatial deviation temperature $\tilde{T}_f$, $\tilde{T}_s$, and volume average temperature $\langle T\rangle$. This is generally referred to as the closure problem.

The solution of the closure problem represents our understanding about transport processes, system structures and interactions between them. Several closure schemes have been proposed by different researchers (Quintard and Whitaker, 1993; Travkin and Catton, 1998; Hsu, 1999; Slattery, 1999; Whitaker, 1999). Slattery introduced a new variable named the thermal tortuosity vector to represent deviation temperature effects. Based on dimensional analysis, he set up correlations of that vector with experimental measured variables to close the problem. On the other hand, Whitaker built up the governing equations and boundary conditions for spatial deviation variables. With a certain assumption of spatial periodic structure of the system, the general formulation

is set and special closed solutions are obtained for the symmetrically structured unit cell. In the following parts, we will review the way that Whitaker's work can be applied.

The governing equations for spatial deviation temperature is obtained by subtracting the volume averaged macroscopic equation from the point governing equation. Through order of magnitude analysis and certain assumptions, a simplified result for $\tilde{T}_f$ is given by

$$(\rho c_p)_f \frac{\partial \tilde{T}_f}{\partial t} = \nabla \cdot (k_f \nabla \tilde{T}_f) - \frac{\varepsilon^{-1}}{V} \int_{A_{fs}} n_{fs} \cdot k_f \nabla \tilde{T}_f dA \qquad [7.72]$$

The further assumption is made that $\tilde{T}_f$ and $\tilde{T}_s$ have quasi-steady fields. Even when macroscopic heat conduction is unsteady, this assumption will be generally valid. This can be understood by considering the constraints for the quasi-steady assumption,

$$\frac{k_s t}{(\rho c_p)_s l_s^2} >> 1, \frac{k_f t}{(\rho c_p)_f l_f^2} >> 1 \qquad [7.73]$$

Taking account of the fact that the macroscopic length scale is several orders larger than the microscopic one, quasi-steady assumption will be validated except for very quick transients. With this assumption, there is no heat diffusion boundary layer inside the REV and governing equations are written as

$$\nabla \cdot (k_f \nabla T_f) = \frac{\varepsilon^{-1}}{V} \int_{A_{fs}} n_{fs} \cdot k_f \nabla \tilde{T}_f dA$$

$$\nabla \cdot (k_s \nabla T_s) = \frac{(1-\varepsilon)^{-1}}{V} \int_{A_{sf}} n_{sf} \cdot k_s \nabla \tilde{T}_s dA$$

$$\tilde{T}_f = \tilde{T}_s \text{ on } A_{fs}$$

$$-n_{fs} \cdot k_f \nabla T_f = -n_{fs} \cdot k_s \nabla T_s + n_{fs} \cdot (k_f - k_s) \nabla \langle T \rangle \text{ on } A_{fs} \qquad [7.74]$$

In order to solve the spatial deviation temperature through the whole domain, two more boundary conditions at the system boundary surfaces are needed. Obviously, this idea is not attractive. The difficulty is overcome by introducing assumptions about the system structure. A spatially periodic structure with a certain unit cell is concerned in the following analysis. The unit cell can be arbitrarily complex and contains all local geometric information of the system. But the size of a unit cell must never be larger than the averaging volume, i.e. REV. When we think about practical applications in textile fabrics, such a periodic structure assumption is rather accurate.

Since the system boundary conditions will affect the deviation temperature field over a distance only in the order of the microlength scale, no consequence

would be expected for prediction of bulk effective thermal conductivity. Thus, the periodicity boundary condition is added to the closure problem:

$$\tilde{T}_f(r + l_i) = \tilde{T}_f(r), \tilde{T}_s(r + l_i) = \tilde{T}_s(r), \quad i = 1,2,3 \qquad [7.75]$$

Based on the above discussion, the purpose of the closure problem is to try to set up a relationship between the spatial deviation temperature and the volume average temperature. A set of constitutive equations is proposed to take account of this consideration,

$$\tilde{T}_f = b_f \cdot \nabla\langle T\rangle + \psi_f, \quad \tilde{T}_s = b_s \cdot \nabla\langle T\rangle + \psi_s \qquad [7.76]$$

where b_f and b_s are referred as the closure variables. It also can be proved that ψ_f and ψ_s are constants, which have no contributions to effective thermal conductivity prediction. Thus, the problem becomes one of solving closure variables in periodic unit cells.

$$k_f \nabla^2 b_f = \frac{\varepsilon^{-1}}{V} \int_{A_{fs}} n_{fs} \cdot k_f \nabla \tilde{T}_f dA$$

$$k_s \nabla^2 b_s = \frac{(1-\varepsilon)^{-1}}{V} \int_{A_{sf}} n_{sf} \cdot k_s \nabla \tilde{T}_s dA$$

$$b_f = b_s \text{ on } A_{fs}$$

$$-n_{fs} \cdot k_f \nabla b_f = -n_{fs} \cdot k_s \nabla b_s + n_{fs} \cdot (k_f - k_s) \text{ on } A_{fs}$$

$$b_f(r + l_i) = b_f(r), \quad b_s(r + l_i) = b_s(r), \; i = 1,2,3 \qquad [7.77]$$

Depending on the structure of the unit cell, these equations can be solved analytically or numerically. The effective thermal conductivity of the whole material can be written in the form of closure variables:

$$K_{\text{eff}} = [\varepsilon k_f + (1-\varepsilon)k_s]I + \frac{(k_f - k_s)}{V} \int_{A_{fs}} n_{fs} b_f dA \qquad [7.78]$$

The closure problem has been solved by several researchers (Nozad, Carbonell *et al*., 1985; Kaviany, 1995; Whitaker, 1999) in some simple unit cells. The resulting effective thermal conductivity has been compared with other theories and experimental data. Fairly good consistency is seen when the unit cell represents the geometrical characteristics of the system.

As shown in the above discussion, the volume averaging method provides a more rigorous treatment for thermal conduction through the multiphase, multiscale system. However, special attention must be paid to required constraints during formulation in order to guarantee validation of the theory. Characterization of system structure is still needed to close the problem. As a powerful theoretical approach, more complex physical phenomena, such as adsorption, phase change, convection, can also be incorporated into the model

with appropriate treatments (Quintard and Whitaker, 1993; Quintard, Kaviany *et al*., 1997; Duval, Fichot *et al*., 2004). Thus, more physical insights into the complex system and physical phenomena within it would be gained. Application of the volume averaging method to predict the fibrous material's effective thermal conductivity has not been found in the current literature. However, since thermal conduction through either dry fabrics or water-saturated fabrics are special cases of the above formulations, simultaneous moisture and heat transfer and air convection through fabrics can also be incorporated into the model with the treatments similar to those in dry porous media (Whitaker, 1998). Better characterization of the structure of the fiber assembly and choosing suitable models with certain constraints are important for taking advantage of this powerful theoretical tool.

7.7 The homogenization method

The method of homogenization is another way to deal with multiscale or multi-component systems. It is a rigorous mathematical method and is mainly applied to periodic structures. Numerous successes have been reported in the prediction of permeability of porous media (Hornung, 1997), mechanical properties of composite materials (Sun, Di *et al*., 2003) and effective thermal conductivity of fibrous materials (Dasgupta and Agarwal, 1992; Dasgupta, Agarwal *et al*., 1996; Rikte, Andersson *et al*., 1999) using this technique.

When the homogenization scheme is applied, two length scales in the heterogeneous materials are identified as (i) a macroscale indicating the characteristic length of the whole material (ii) and a microscale representing the periodical length of the microstructure. It is clear that the coefficients of microscale governing the equations and the resulting solution will fluctuate very rapidly. Mathematically, the homogenization method uses asymptotic expansion and periodic assumption to approximate the original partial differential equations with the equations that have slowly varying coefficients. More detailed and general discussion is available in Bensoussan, Lions *et al*. (1978).

In the homogenization method, a small positive parameter ε is introduced to represent the ratio between the two length scales. All the variables in the heterogeneous media are considered to be related to ε. By letting $\varepsilon \to 0$, the system will be upscaled. There are many schemes that can be applied to homogenizing fundamental thermal conduction equations. In this section, we will follow the method that Hassani and Hinton (1998a) summarized to explain the basic ideas and procedures of homogenization methods.

The macroscale and microscale are represented as x and y, respectively. The relationship between them is $y = x/\varepsilon$, where ε is a parameter. The fundamental thermal conduction equations are written as

$$\begin{cases} q^{\varepsilon} = -K^{\varepsilon} \cdot \nabla T^{\varepsilon} \\ \nabla \cdot q^{\varepsilon} + \Phi^{\varepsilon} = 0 \end{cases} \quad [7.79]$$

The superscript in the above equations implies we are interested in the behaviors of a family of functions with ε as the parameter. Heat flux q^{ε} and temperature T^{ε} are treated as functions of both length scales x and y, whereas thermal conductivity K^{ε} and heat generating rate Φ^{ε} are both assumed to be macroscopically uniform and only vary in the small unit cell, i.e.

$$K^{\varepsilon}(x, y) = K(y) \quad \text{and} \quad \Phi^{\varepsilon}(x, y) = \Phi(y)$$

The asymptotic expansion is applied to the heat flux and temperature variables as

$$q^{\varepsilon} = q^{0}(x, y) + \varepsilon q^{1}(x, y) + \varepsilon^{2} q^{2}(x, y) + \ldots \quad [7.80]$$

$$T^{\varepsilon} = T^{0}(x, y) + \varepsilon T^{1}(x, y) + \varepsilon^{2} T^{2}(x, y) + \ldots \quad [7.81]$$

where, $q^{i}(x, y)$ and $T^{i}(x, y)$ are all periodic on y and the length of the period denoted as Y resulting from microscopic periodicity. By realizing x and y are two independent variables, the gradient operator in this two-scale problem is given by

$$\nabla = \nabla_{x} + \varepsilon \nabla_{y} \quad [7.82]$$

By substituting asymptotic expanded variables into the governing equations and collecting terms by power of ε, we will get

$$\varepsilon^{-1} K^{\varepsilon} \cdot \nabla_{y} T^{0} + \varepsilon^{0}(q^{0} + K^{\varepsilon} \cdot \nabla_{x} T^{0} + K^{\varepsilon} \cdot \nabla_{y} T^{1}) + \varepsilon(q^{1} + K^{\varepsilon} \cdot \nabla_{x} T^{1} + K^{\varepsilon} \cdot \nabla_{y} T^{2}) + \ldots = 0 \quad [7.83]$$

$$\varepsilon^{-1} \nabla_{y} q^{0} + \varepsilon^{0}(\nabla_{x} q^{0} + \nabla_{y} q^{1} + \Phi^{\varepsilon}) + \varepsilon(\nabla_{x} q^{1} + \nabla_{y} q^{2}) + \ldots = 0 \quad [7.84]$$

Because these equations need to hold for all ε values, a series of partial differential equations is given:

$$\begin{cases} \nabla_{y} T^{0} = 0 \\ q^{0} = -K^{\varepsilon} \cdot (\nabla_{x} T^{0} + \nabla_{y} T^{1}) \\ \ldots \end{cases} \quad [7.85]$$

$$\begin{cases} \nabla_{y} q^{0} = 0 \\ \nabla_{x} q^{0} + \nabla_{y} q^{1} + \Phi^{\varepsilon} = 0 \\ \ldots \end{cases} \quad [7.86]$$

It is clear from the above equations that q^{0} and T^{0} are functions of x only. They represent the macroscopic behavior of heat flux and temperature. By

relating them to each other, the macroscopic effective thermal conductivity will be obtained. The higher terms, q^i, T^i ($i \geq 1$) indicates the higher modes of perturbation for the heat flux and temperature at macroscale resulting from microscopic heterogeneities. When the macroscale is much larger than the microscale, i.e. ε is small enough, only contributions from q^1 and T^1 need to be considered.

Considering the equation for q^0, it is obvious that the inhomogeneous term $\nabla_y T^1$ needs to be evaluated at microscale. In Dasgupta's work (Dasgupta and Agarwal, 1992; Dasgupta, Agarwal *et al.*, 1996), this problem is handled by setting up appropriate boundary conditions for the unit cell discussed in earlier sections and solving the boundary value problem with a finite element method at unit cell scale. The resulting heat flux and temperature gradient are volume averaged to get effective thermal conductivity. A comparison of the results with the thermal resistor network model and experiments show good consistency.

On the other hand, Hassani and Hinton (1998a,b) introduced a new function χ to formulate the problems at microscale and macroscale. After volume averaging over the unit cell and applying y-periodic properties of q^1 and T^1, the following homogenized results are obtained in the index form,

$$\begin{cases} \overline{q}_i(x) = -k_{ij}^{eff} \dfrac{\partial \overline{T}(x)}{\partial x_j} \\ \dfrac{\partial \overline{q}_i}{\partial x_i} + \overline{\Phi} = 0 \end{cases} \qquad [7.87]$$

where

$$k_{ij}^{eff} = \frac{1}{|Y|}\left[\int_Y k(y)\left(\delta_{ij} + \frac{\partial \chi^j}{\partial y_i}\right)dy\right] \qquad [7.88]$$

where Y denotes the unit cell domain; $\overline{a}(x)$ implies the volume average of function $a(x, y)$ over the unit cell; the function χ is y-periodic and can be solved from the equation,

$$\frac{\partial}{\partial y_i}\left[k(y)\left(\delta_{ij} + \frac{\partial \chi^j}{\partial y_i}\right)\right] = 0 \text{ on } Y \qquad [7.89]$$

This equation can be solved analytically for the simple unit cell (Chang, 1982). When distribution of heterogeneity in the unit cell is complex, numerical methods, such as finite element analysis must be adopted. Depending on the specific system structure, different numerical schemes can be formulated (Dasgupta and Agarwal, 1992; Dasgupta, Agarwal *et al.*, 1996; Hassani and Hinton, 1998b; Rikte, Andersson *et al.*, 1999; Sun, Di *et al.*, 2003). As soon as the information about χ is obtained, the effective thermal conductivity of the whole heterogeneous material can easily be derived from the above equation.

7.8 Moisture diffusion

Moisture diffusion is the process during which water molecules migrate through given materials. When we are only interested in mono-component mass transfer, i.e. water, the diffusion process is quite similar to the thermal conduction process, as discussed in the introduction section. Consequently, for homogeneous materials, the results of certain thermal conduction problems can be readily transcribed into solutions of the corresponding mass diffusion process by changing parameters and variables (Crank, 1979).

For multi-component systems such as fibrous materials, the system diffusion behavior is determined by the resultant of each, often different, behaviour of the multi-components. For instance, in a fibrous material, moisture diffusivity in the solid fiber is much smaller that in air, and the system behavior is not equal to that of either fiber or air. Based on our knowledge, the effects of moisture diffusion on fiber-reinforced composites may be negligible in most ordinary science and engineering applications, because both fiber and matrix show very high resistance to moisture diffusion. Furthermore, we will focus on moisture vapor diffusion through textile fabrics in this section; the migration of liquid water in fabrics is determined by other mechanisms and will not be analyzed in the context of the diffusion process.

As discussed previously, textile fabrics are composed of fibers and air in voids. Under certain concentration gradients, the main contribution to moisture flux is from the diffusion process through the air voids. But, it has been shown that adsorption of moisture by fibers will also affect the response of fabrics to the moisture gradient (Wehner, Miller *et al*., 1988). It is hence desirable to discuss the diffusion process in non-hygroscopic and hygroscopic cases separately.

Non-hygroscopic fibers can be treated as an inert phase during the moisture diffusion process. That implies this mass transfer process can be approximated as one happening in a single-phase system such that a simple representation is widely applied for porous media with an inert solid phase (Bejan, 2004),

$$D_{eff} = \varepsilon D_a / \tau \qquad [7.90]$$

where D_a is the moisture diffusivity in bulk air; ε and τ are porosity and tortuosity, respectively. Intuitively, this simple equation is established by treating ε and τ as correction terms, accounting for reduced diffusion area and blockage of diffusion path. Tortuosity is a dimensionless parameter that characterizes the deviation of the diffusion path from a straight one. For a simple system, tortuosity can be calculated out. However, measurement is needed when the structure is complex.

Analogous to the analysis of two-phase thermal conduction analysis, the volume averaging method is applicable to such moisture diffusion problems (Whitaker, 1999) and, moreover, the predicted effective moisture diffusivity

depends only on the geometrical arrangement of fibers. With the assumption that moisture molecules will diffuse along the surface of any intervening fibers, Woo, Shalev *et al.* (1994b) thus predicted the moisture diffusivity in non-hygroscopic nonwoven fabrics as

$$D_{eff} = D_a P + D_a(1 - V_f - P)\,(1 - P)/(1 + sV_f - P) \qquad [7.91]$$

where P is the optical porosity corresponding to the air fraction and s is a fiber-shape factor introduced to characterize the tortuosity effects in nonwoven fabrics. Fairly good consistency of prediction results and experimental data implies that using both porosity and tortuosity is an acceptable approach in characterizing moisture diffusion through non-hygroscopic fibrous materials.

However, many commonly used fibers, e.g. cotton and wool, are hygroscopic and the responses of hygroscopic fabric under moisture gradients is much more complex due to interactions between moisture and fibers (Downes and Mackay, 1958; Nordon and David, 1967; Crank, 1979; Wehner, Miller *et al.*, 1988). After the initial wetting process, so that the system is in a steady state, fibers are saturated and diffusion through the air void becomes a dominating process, except that swollen fibers lead to a smaller free space. However, experiments have shown that moisture sorption by hygroscopic fibers has to be treated as a dynamic sink when transient behavior of fabrics is analyzed (Wehner, Miller *et al.*, 1988).

$$\varepsilon \frac{\partial C_a}{\partial t} = \frac{D_a \varepsilon}{\tau} \frac{\partial^2 C_a}{\partial x^2} - (1 - \varepsilon) \frac{\partial C_f}{\partial t} \qquad [7.92]$$

where C_a and C_f are moisture concentrations in both void space and fibers, respectively. Moisture concentration distribution in the system can be obtained with information of moisture sorption kinetics, i.e. $\partial C_f/\partial t$. Sorption kinetics are also described by a diffusion process as

$$\begin{cases} \dfrac{\partial C_f}{\partial t} = \dfrac{1}{r} \dfrac{\partial}{\partial r} \left(r D_f \dfrac{\partial C_f}{\partial r} \right) & \text{for cylindrical fibers} \\ C_{fs} = f(C_a, T) & \text{at fiber surface} \end{cases} \qquad [7.93]$$

This formulation is not contradicted by neglection of the fibres' contribution for moisture flux through fabrics. In the analysis of the flux along the moisture gradient, the time scale and the length scale for both diffusion in air and fibers are the same. Hence, fibers with very low diffusivity provide only negligible contribution to the macroscopic moisture flux. On the other hand, sorption of moisture by fibers takes place at all fiber surfaces contacting with moisture vapor. The small fiber diameter leads to a very high surface area and small length scale for moisture diffusion into the fiber. Interactions between these two scale diffusion processes cannot be neglected. A simple

estimation of the time scale for them would qualitatively illustrate this point. The characteristic time scale t_c for the diffusion process can be defined as (Crank, 1979; Wehner, Miller *et al.*, 1988),

$$t_c = \frac{l_c^2}{D} \qquad [7.94]$$

where D is a nominal diffusivity. Based on Wehner's work (Wehner, Miller *et al.*, 1988), characteristic length scales l_c for moisture diffusion through void and fiber are estimated as 10 cm and 20 μm, respectively. Diffusivity in bulk air is 0.25 cm^2/s, and is 10^{-8} cm^2/s inside the fiber! Thus, the characteristic time scales for these two diffusion processes are both 400 seconds. Depending on the length scales of the fabrics, larger differences may be observed but not by much. Moreover, this simple estimation illustrates that moisture diffusion through fibers must be treated as a part of the whole system dynamical process due to the small length scale of fibers; and the contribution of diffusion through fibers cannot be ignored when macroscopic transient diffusion behavior is analyzed. Competition between these two processes will continue until adsorbed water reaches the sorptive capacity of the fibers. As demonstrated by experiments (Downes and Mackay, 1958; Wehner, Miller *et al.*, 1988), moisture sorptive capacity, diffusivity and diameter of fibers will all affect the transient response of hygroscopic fabrics under moisture gradients.

In order to quantitatively characterize sorption behavior, moisture diffusion into fibers must be analyzed in detail. But, the diffusivity in glassy polymeric fibers, such as wools, is not constant or a simple function of moisture concentration. A two-stage sorption behavior has been observed during moisture ingress into wool fibers (Downes and Mackay, 1958; Nordon and David, 1967; Crank, 1979). It is characterized by an initial rapid uptake of moisture obeying Ficken diffusion, and followed by a much slow sorption to approach final equilibrium. Generally, this kind of process in glassy polymers is called 'non-Ficken' or 'anomalous' diffusion (Downes and Mackay, 1958; Crank, 1979) and dynamic change of glassy polymer structure with ingression of moisture molecules is considered to be responsible for this anomalous behavior. When moisture is absorbed by a glassy polymer, the swelling stresses will be relaxed with time by accumulated movement of polymer chains. As the rate of relaxation and moisture diffusion is comparable, uptake of moisture will rise and lead to the second and slower sorption stage. Quantitative two-stage sorption models based on stress relaxation and irreversible thermodynamics have been found in the literature for specific systems, but no general model is available to explain interactions between moisture diffusion and polymer structure change (Downes and Mackay, 1958; Crank, 1979). In practical applications, many researchers have characterized the two-stage sorption behavior by a complex diffusivity resulting from regression of experimental data (Nordon and David, 1967; Li and Holcombe, 1992; Li and Luo, 1999).

Generation of latent heat is another consequence of moisture sorption by fibers. The magnitude of sorption heat depends on the amount of moisture absorbed and will affect the temperature field of the fabrics. This is where moisture and heat transfer are coupled with each other. More detailed discussion about these coupling effects will be discussed in other chapters.

In this section, we have mainly reviewed the special parts of moisture diffusion through fibrous systems that may not be found in an equivalent thermal conduction process. Firstly, moisture diffusion through non-hygroscopic fabrics was explored, and the concept of tortuosity was introduced for prediction of effective moisture diffusivity. For hygroscopic fabrics, interactions between macroscopic diffusion through air voids and microscopic diffusion into fibers were emphasized, mainly because adsorption of moisture vapor by fibers is *not* negligible. Finally, two-stage fiber sorption behavior was illustrated using the anomalous diffusion behavior of glassy polymers.

7.9 Sensory contact thermal conduction of porous materials

We know that steel has a higher thermal conductivity than wood by touching both materials with our hands. This simple technique can be deceiving, however, when dealing with porous materials, for they are mixtures of solid materials and air, often with vastly different thermal conductivities. Sawdust feels much warmer than solid wood lumber, and this phenomenon is hard to explain without appreciating the role that air is playing. When dealing with the thermal conduction of fibrous materials, it is highly intuitive to think that the thermal conductivity of the fibers would play a critical role. In fact, the perceived warmth through contacting, results from our tactile sense and is a reflection of contact transient, is actually related to the so-called effusivity $\varepsilon = \sqrt{k\rho c_p}$ of the material, where k is the thermal conductivity (W/m K), ρ is the density (kg/m^3) and c_p is the specific heat capacity (J/kg K) of the material. A surface with a higher effusivity value feels cooler. In fact, effusivity deals with the heat exchange between substances through interfaces, whereas conductivity describes the ability of that substance to transfer heat.

Obviously, the narrow range of the thermal conductivities k of various textile fibers (0.1–0.3 W/m K) cannot account for the vast scope of the cooling sensation received by touching different fabrics. It is the material density ρ and the specific heat capacity c_p that are responsible. Since both are either determined by, or are heavily dependent upon, the structural details of the fabric, this explains why fabrics made of the same fiber often exhibit entirely different skin contact sensations.

7.10 Future research

In this chapter, we carefully reviewed thermal conduction and moisture diffusion through fibrous materials. Many methods and results have been developed and documented in the literature but there are still many questions to be answered.

In most methods, the periodic structure of fibrous materials is assumed. Practically, characterization of structure based on a statistical description is more attractive. Though much research work has been done in mechanical fields, further investigation concerning the application of statistical methods in transport through fibrous materials is warranted.

Fibrous materials are widely used in science and engineering fields mainly due to special mechanical properties conferred by the structure of fiber assemblies. Research in porous media has shown that structure change under certain mechanical loadings will lead to change of effective thermal conductivity (Chan and Tien, 1973; Bejan, 2004; Weidenfeld *et al*., 2004). Evaluation of coupling effects between mechanical and transport responses under given external conditions must be an interesting and challenging area for future research.

Effective material properties mainly represent statistical average behaviors of fibrous systems. Structure and responses in local space may be quite different from that of bulk materials. In certain environments, the local extreme values will determine the performance of a fibrous system (Ganapathy, Singh *et al*., 2005). Fully discrete simulation is needed to get a detailed description of the system. Due to the complex structures and interactions between them, more advanced computation techniques and algorisms are still under development and need more attention.

7.11 References

Agarwal, B. D. and Broutman L. J. (1990). *Analysis and Performance of Fiber Composites*. New York, John Wiley & Sons, Inc.

Ali, Y. M. and Zhang, L. C. (2005). 'Relativistic heat conduction.' *International Journal of Heat and Mass Transfer* **48**(12): 2397–2406.

Arfken, G. B. and Weber, H.-J. (2005). *Mathematical Methods for Physicists*. Burlington, MA, Elsevier Academic Press.

Bachmat, Y. and Bear, J. (1986). 'Macroscopic Modeling of Transport Phenomena in Porous Media.1. The Continuum Approach.' *Transport In Porous Media* **1**(3): 213–240.

Batchelor, G. K. and Obrien, R. W. (1977). 'Thermal or Electrical Conduction Through a Granular Material.' *Proceedings of the Royal Society of London Series-A Mathematical Physical And Engineering Sciences* **355**(1682): 313–333.

Bear, J. and Bachmat, Y. (1990). *Introduction to Modeling of Transport Phenomena in Porous Media.* Dordrecht; Boston, Kluwer Academic Publishers.

Bear, J. and Buchlin, J.-M. *et al.* (1991). *Modelling and Applications of Transport Phenomena in Porous Media.* Dordrecht; Boston, Kluwer Academic Publishers.

Bejan, A. (2004). *Porous and Complex Flow Structures in Modern Technologies.* New York, Springer.

Bensoussan, A. and Lions, J. L. *et al*. (1978). *Asymptotic Analysis for Periodic Structures.* Amsterdam; New York, North-Holland Pub. Co.; New York: distributors for the U.S.A., Elsevier North-Holland.

Bird, R. B. and Stewart, W. E. *et al*. (2002). *Transport Phenomena.* New York, J. Wiley.

Carbonell, R. G. and Whitaker, S. (1984). 'Heat and Mass Transfer in Porous Media.' *Fundamentals of Transport Phenomena in Porous Media*. Bear, J. and Corapcioglu, M. Y. (eds), Lecden and Boston, Martinus Nijhoff: 121–198.

Carslaw, H. S. and Jaeger, J. C. (1986). *Conduction of Heat in Solids.* Oxford; New York, Clarendon Press; Oxford University Press.

Chan, C. K. and Tien, C. L. (1973). 'Conductance of packed spheres in vacuum.' *Journal of Heat Transfer–Transactions of the Asme*: 302–308.

Chang, H. C. (1982). 'Multi-scale Analysis of Effective Transport in Periodic Heterogeneous Media.' *Chemical Engineering Communications* **15**(1–4): 83–91.

Chen, C. H. and Wang, Y. C. (1996). 'Effective thermal conductivity of misoriented short-fiber reinforced thermoplastics.' *Mechanics of Materials* **23**(3): 217–228.

Chen, Z. Q. and Cheng, P. *et al*. (2000). 'A theoretical and experimental study on stagnant thermal conductivity of bi-dispersed porous media.' *International Communications in Heat and Mass Transfer* **27**(5): 601–610.

Cheng, P. and Hsu, C. T. (1999). 'The effective stagnant thermal conductivity of porous media with periodic structures.' *Journal of Porous Media* **2**(1): 19–38.

Christensen, R. M. (1991). *Mechanics of Composite Materials.* Malabar, Fla., Krieger Pub. Co.

Crank, J. (1979). *The Mathematics of Diffusion*. Oxford, [Eng], Clarendon Press.

Dasgupta, A. and Agarwal, R. K. (1992). 'Orthotropic Thermal Conductivity of Plain-weave Fabric Composites Using a Homogenization Technique.' *Journal of Composite Materials* **26**(18): 2736–2758.

Dasgupta, A. and Agarwal, R. K. *et al*. (1996). 'Three-dimensional modeling of woven-fabric composites for effective thermo-mechanical and thermal properties.' *Composites Science and Technology* **56**(3): 209–223.

de Souza, A. A. U. and Whitaker, S. (2003). 'The modelling of a textile dyeing process utilizing the method of volume averaging.' *Brazilian Journal of Chemical Engineering* **20**(4): 445–453.

Downes, J. G. and Mackay, B. H. (1958). 'Sorption kinetics of water vapor in wool fibers.' *Journal of Polymer Science* **28**: 45–67.

Duval, F. and Fichot, F. *et al.* (2004). 'A local thermal non-equilibrium model for two-phase flows with phase-change in porous media.' *International Journal of Heat and Mass Transfer* **47**(3): 613–639.

Fohr, J. P. and Couton, D. *et al.* (2002). 'Dynamic heat and water transfer through layered fabrics.' *Textile Research Journal* **72**(1): 1–12.

Freed, L. E. and Vunjaknovakovic, G. *et al*. (1994). 'Biodegradable Polymer Scaffolds for Tissue Engineering.' *Bio-Technology* **12**(7): 689–693.

Fu, S. Y. and Mai, Y. W. (2003). 'Thermal conductivity of misaligned short-fiber-reinforced polymer composites.' *Journal of Applied Polymer Science* **88**(6): 1497–1505.

Furmanski, P. (1992). 'Effective Macroscopic Description for Heat Conduction in Heterogeneous Materials.' *International Journal of Heat and Mass Transfer* **35**(11): 3047–3058.

Ganapathy, D. and Singh, K. *et al*. (2005). 'An effective unit cell approach to compute the

thermal conductivity of composites with cylindrical particles.' *Journal of Heat Transfer-Transactions of the ASME* **127**(6): 553–559.

Gibson, P. and Charmchi, M. (1997a). 'The use of volume-averaging techniques to predict temperature transients due to water vapor sorption in hygroscopic porous polymer materials.' *Journal of Applied Polymer Science* **64**(3): 493–505.

Gibson, P. W. and Charmchi, M. (1997b). 'Modeling convection/diffusion processes in porous textiles with inclusion of humidity-dependent air permeability.' *International Communications in Heat and Mass Transfer* **24**(5): 709–724.

Gray, W. G. (1993). *Mathematical Tools for Changing Spatial scales in the Analysis of Physical Systems.* Boca Raton, CRC Press.

Haberman, R. (1987). *Elementary Applied Partial Differential Equations: With Fourier Series and Boundary Value Problems*. Englewood Cliffs, N.J., Prentice-Hall.

Hager, J. and Whitaker, S. (2002). 'The thermodynamic significance of the local volume averaged temperature.' *Transport in Porous Media* **46**(1): 19–35.

Hassani, B. and Hinton, E. (1998a). 'A review of homogenization and topology optimization I - Homogenization theory for media with periodic structure.' *Computers & Structures* **69**(6): 707–717.

Hassani, B. and Hinton, E. (1998b). 'A review of homogenization and topology optimization II - Analytical and numerical solution of homogenization equations.' *Computers & Structures* **69**(6): 719–738.

Hatta, H. and Taya, M. (1985). 'Effective Thermal Conductivity of a Misoriented Short-fiber Composite.' *Journal of Applied Physics* **58**(7): 2478–2486.

Hornung, U. (1997). *Homogenization and Porous Media*. New York, Springer.

Hsu, C. T. (1999). 'A closure model for transient heat conduction in porous media.' *Journal of Heat Transfer-Transactions of the ASME* **121**(3): 733–739.

Hsu, C. T. and Cheng, P. *et al*. (1994). 'Modified Zehner–Schlunder Models for Stagnant Thermal Conductivity of Porous Media.' *International Journal of Heat and Mass Transfer* **37**(17): 2751–2759.

Jirsak, O. and Gok, T. *et al*. (1998). 'Comparing dynamic and static methods for measuring thermal conductive properties of textiles.' *Textile Research Journal* **68**(1): 47–56.

Kaviany, M. (1995). *Principles of Heat Transfer in Porous Media.* New York, Springer-Verlag.

Li, Y. and Holcombe, B. V. (1992). 'A 2-Stage Sorption Model of the Coupled Diffusion of Moisture and Heat in Wool Fabrics.' *Textile Research Journal* **62**(4): 211–217.

Li, Y. and Luo, Z. (1999). 'An improved mathematical simulation of the coupled diffusion of moisture and heat in wool fabric.' *Textile Research Journal* **69**(10): 760–768.

Martin, J. R. and Lamb, G. E. R. (1987). 'Measurement of Thermal Conductivity of Nonwovens Using a Dynamic Method.' *Textile Research Journal* **57**(12): 721–727.

Miller, M. N. (1969). 'Bounds for effective electrical, thermal, and magnetic properties of heterogeneous materials.' *Journal of Mathematical Physics* **10**(11): 1988–2004.

Minkowycz, W. J. (1988). *Handbook of Numerical Heat Transfer.* New York, Wiley-Interscience.

Mohammadi, M. anf Banks-Lee, P. *et al*. (2003). 'Determining effective thermal conductivity of multilayered nonwoven fabrics.' *Textile Research Journal* **73**(9): 802–808.

Morton, W. E. and Hearle, J. W. S. (1993). *Physical Properties of Textile Fibres.* Manchester, The Textile Institute.

Nayak, A. L. and Tien, C. L. (1978). 'Statistical Thermodynamic Theory for Coordination Number Distribution and Effective Thermal Conductivity of Random Packed Beds.' *International Journal of Heat and Mass Transfer* **21**(6): 669–676.

Ning, Q. G. and Chou, T. W. (1995a). 'Closed-form solution of the transverse effective thermal conductivity of woven fabric composites.' *Journal of Composite Materials* **29**(17): 2280–2294.

Ning, Q. G. and Chou, T. W. (1995b). 'Closed-form Solutions of the Inplane Effective Thermal Conductivities of Woven Fabric Composites.' *Composites Science and Technology* **55**(1): 41–48.

Ning, Q. G. and Chou, T. W. (1998). 'A general analytical model for predicting the transverse effective thermal conductivities of woven fabric composites.' *Composites Part A-Applied Science and Manufacturing* **29**(3): 315–322.

Nordon, P. and David, H. G. (1967). 'Coupled diffusion of moisture and heat in hygroscopic textile materials.' *International Journal of Heat and Mass Transfer* **10**: 853–866.

Nozad, I. and Carbonell, R. G. *et al.* (1985). 'Heat Conduction in Multiphase Systems.1. Theory and Experiment for 2-Phase Systems.' *Chemical Engineering Science* **40**(5): 843–855.

Pan, N. (1993). 'A Modified Analysis of the Microstructural Characteristics of General Fiber Assemblies.' *Textile Research Journal* **63**(6): 336–345.

Pan, N. (1994). 'Analytical Characterization of The Anisotropy and Local Heterogeneity of Short-fiber Composites - Fiber Fraction as a Variable.' *Journal of Composite Materials* **28**(16): 1500–1531.

Progelhof, R. C. and Throne, J. L. *et al.* (1976). 'Methods For Predicting Thermal-Conductivity Of Composite Systems.' *Polymer Engineering and Science* **16**(9): 615–625.

Quintard, M. and Kaviany, M. *et al.* (1997). 'Two-medium treatment of heat transfer in porous media: Numerical results for effective properties.' *Advances in Water Resources* **20**(2–3): 77–94.

Quintard, M. and Whitaker, S. (1993). 'Transport in Ordered and Disordered Porous Media – Volume-averaged Equations, Closure Problems, and Comparison with Experiment.' *Chemical Engineering Science* **48**(14): 2537–2564.

Rikte, S. and Andersson, M. *et al.* (1999). 'Homogenization of woven materials.' *AEU-International Journal of Electronics and Communications* **53**(5): 261–271.

Satsumoto, Y. and Ishikawa, K. *et al.* (1997). 'Evaluating quasi-clothing heat transfer: A comparison of the vertical hot plate and the thermal manikin.' *Textile Research Journal* **67**(7): 503–510.

Schulgasser, K. (1976). 'Conductivity of Fiber Reinforced Materials.' *Journal of Mathematical Physics* **17**(3): 382–387.

Shih, T. M. (1984). *Numerical heat transfer.* Washington, D.C., Hemisphere Pub. Corp.

Skalak, R. and Chien, S. (1987). *Handbook of Bioengineering*. New York, McGraw-Hill.

Slattery, J. C. (1999). *Advanced Transport Phenomena.* New York, Cambridge University Press.

Springer, G. S. and Tsai, S. W. (1967). 'Thermal conductivities of unidirectional materials.' *Journal of Composite Materials* **1**: 166–173.

Sun, H. Y. and Di, S. L. *et al.* (2003). 'Micromechanics of braided composites via multivariable FEM.' *Computers & Structures* **81**(20): 2021–2027.

Tong, T. W. and Tien, C. L. (1983). 'Radiative Heat Transfer In Fibrous Insulations. 1. Analytical Study.' *Journal of Heat Transfer-Transactions of the ASME* **105**(1): 70–75.

Tong, T. W. and Yang, Q. S. *et al.* (1983). 'Radiative Heat Transfer In Fibrous Insulations. 2. Experimental-Study.' *Journal of Heat Transfer-Transactions of the ASME* **105**(1): 76–81.

Torquato, S. and Lado, F. (1991). 'Trapping Constant, Thermal-Conductivity, and the

Microstructure of Suspensions of Oriented Spheroids.' *Journal of Chemical Physics* **94**(6): 4453–4462.

Travkin, V. S. and Catton, I. (1998). 'Porous media transport descriptions – non-local, linear and non-linear against effective thermal/fluid properties.' *Advances in Colloid and Interface Science* **77**: 389–443.

Vafai, K. (1980). Some fundamental problems in heat and mass transfer through porous media, University of California, Berkeley, Dec. 1980**:** xi.

Warner, S. B. (1995). *Fiber Science.* Englewood Cliffs, NJ, Prentice Hall.

Wehner, J. A. and Miller, B. *et al.* (1988). 'Dynamics of Water-vapor Transmission Through Fabric Barriers.' *Textile Research Journal* **58**(10): 581–592.

Weidenfeld, G. and Weiss, Y. *et al*. (2004). 'A theoretical model for effective thermal conductivity (ETC) of particulate beds under compression.' *Granular Matter* **6**(2–3): 121–129.

Whitaker, S. (1969). 'Fluid motion in porous media.' *Industrial and Engineering Chemistry* **61**(12): 14–28.

Whitaker, S. (1991). 'Improved Constraints for the Principle of local Thermal Equilibrium.' *Industrial & Engineering Chemistry Research* **30**(5): 983–997.

Whitaker, S. (1998). 'Coupled Transport in Multiphase Systems: A Theory of Drying.' *Advances in Heat Transfer* **31**: 1–102.

Whitaker, S. (1999). *The Method of Volume Averaging*. Dordrecht; Boston, Kluwer Academic.

Woo, S. S. and Shalev, I. *et al.* (1994a). 'Heat and Moisture Transfer Through Nonwoven Fabrics. 1. Heat Transfer.' *Textile Research Journal* **64**(3): 149–162.

Woo, S. S. and Shalev, I. *et al*. (1994b). 'Heat and Moisture Transfer Through Nonwoven Fabrics. 2. Moisture Diffusivity.' *Textile Research Journal* **64**(4): 190–197.

8

Convection and ventilation in fabric layers

N. GHADDAR, American University of Beirut, Lebanon,
K. GHALI, Beirut Arab University, Lebanon, and
B. JONES, Kansas State University, USA

8.1 Introduction

The clothing system plays an important role in human thermal responses because it determines how much of the heat generated in the human body can be exchanged with the environment. The heat and moisture transport processes are not only of diffusion type but are also enhanced by the ventilating motion of air through the fabric, initiated by the relative motion of the human with respect to the environment. During body motion, the size of the air spacing between the skin and the fabric is continuously varying with time, depending on the level of activity and the location, thus inducing variable airflow through the fabric. This induced airflow ventilates the fabric and contributes to the augmentation of the rates of condensation and adsorption in the clothing system and to the amounts of heat and moisture loss from the body.

In this chapter, the relevant fabric properties and parameters during wind and body motion are first described, followed by methods by which ventilation rates can be estimated. Then mathematical modeling of the associated heat and moisture transport in the clothing systems of walking humans is presented. A description is also given of the means by which the fabric microscopic heat and mass internal transport coefficients and macroscopic heat and mass transport coefficients from the skin to the trapped air layer are determined.

8.1.1 Fabric structure and dry and evaporative resistances

Fabrics are highly porous materials consisting mainly of solid fiber and air void spaces. The porosity of most fabrics ranges from 50 to 95%, depending on the fiber fineness, the tightness of the twist in the yarns, and the yarn count (Morris, 1953). The dry resistance to heat transport of the fabric is dependent upon the amount of still air entrapped in the interstices between the fibers and yarns, since the conductivity of air is much lower than that of

fiber materials (Fourt and Hollies, 1971). The solid fibers arrangement and their volume in the fabric influence the fabric insulation more than the fiber itself (Rees, 1941). The fiber properties have little influence on fabric insulation since the volume percentage of the solid fiber is relatively small compared to the volume of the entrapped air. Any fabric characteristics that would increase the amount of still air in the fabric would also increase its dry resistance. Thermal resistance of the fabric is usually negatively correlated with fabric density. The dry heat resistance for indoor worn fabrics is reported by McCullough *et al.* (1985, 1989) as follows:

$$R_D = 0.015 \times e_f \qquad [8.1]$$

where R_D is the dry resistance of the fabric in $m^2 \cdot K/mm \cdot W$ and e_f is the fabric thickness in mm.

Similar to dry heat transfer, vapor transfer in fabrics depends on the physical properties of the entrapped air medium and on the arrangement of the solid fibers. The solid fibers not only absorb/desorb moisture but they also represent an obstacle for the vapor molecules on their way through the fabric. Therefore, the vapor resistance of fabrics is expected to be larger than that of an equally thick air layer and is expressed as an equivalent thickness of still air that would give the same resistance to vapor transfer as that of the actual fabric. This equivalent air thickness was found by McCullough *et al.* (1989) to increase linearly with the fabric thickness for low-density fabrics, and to some extent for dense fabric materials.

The dry and evaporative resistances are also related through the permeability index, i_m, which was first proposed by Woodcock (1962). The relationship is expressed by

$$i_m = (R_D/R_E)LR \qquad [8.2]$$

where R_E is the evaporative resistance of the fabric in $m^2 \cdot kPa/W$ and LR is the Lewis ratio, which equals approximately 16.65 K/kPa at typical indoor conditions.

8.1.2 Clothing ensemble and heat/moisture transport from a stationary human body

A clothing ensemble acts as a barrier to heat and moisture transfer from the skin because of the insulation provided by both the fabric material (dry and evaporative resistances) and the entrapped air between the different fabric layers and between the skin and the inner fabric layer. The clothing material affects the heat loss because of its thermal resistance property and because it acts as a barrier against thermal radiation and air currents in the environment. The fabric material will also affect the moisture transport, depending on its

weave construction, by acting as an obstacle to the moving water vapor particles.

The amount of entrapped air between different garment layers in an ensemble affects the insulation of the clothing ensemble. As the thickness of the trapped air layer increases in a still-air environment and a stationary human body, the insulation provided by the clothing will also increase. But once the trapped air layer thickness reaches 1.0 cm, the insulation provided by the trapped air layer will decrease because of the natural convective heat between the skin and the garment layer (Rees, 1941).

The thickness of the trapped air layer depends primarily on the looseness or tightness of the clothing ensemble. Loose-fitting clothing traps more air within the garment compared to tight clothing. In addition, the body posture will affect the trapped air layer thickness and thus its insulation. For example, when sitting, the clothing layers compress the enclosed air layer and the clothing ensemble insulation decreases. Havenith *et al*. (1990a) showed that thicker ensembles had a greater insulation reduction than thinner ones when a person is seated.

8.1.3 Clothing ensemble insulation during dynamic conditions

Increasing the speed of the external air will reduce the thickness of the boundary layer formed at the outer surface of the clothing ensemble and thus reduce the resistance to convective heat and mass transfer to the external air. External wind can also reduce the thickness of the trapped microclimate air layer by compressing the garment layers and thus decreasing its resistance. On the other hand, body motion will not only reduce the thickness of the outer boundary layer by creating convective currents at the outer surface of the clothing ensemble but it will also induce internal air current in garments. Harter *et al*. (1981) called this particular aspect in clothing comfort 'ventilation of the microclimate within clothing'. Lotens (1993) derived empirically the steady ventilation rate through apertures of clothing assemblies as a function of the air permeability of the fabric and the effective wind velocity. The work of Lotens also showed that, for a clothing ensemble that is made of impermeable fabric materials with closed apertures, the vapor resistance at the skin and in the microclimate decreases with walking speed and with wind speed.

When outside air penetrates the clothing, either via openings or through the fabric material constituting the clothing, the reduction in the insulation properties of the clothing is not only due to the increase in the circulation underneath the clothing or at the surface of the clothing, but is also due to the increase in the renewal rate in the micro-climate air layer between the skin and the inner fabric surface. In addition, when air passes through the pores of the fabric material, the insulating properties of the fabric will be reduced

because the air trapped in the fibers is no longer stationary, allowing for more convective heat and moisture exchange. Fabrics with large pores between fibers are generally more permeable to air and hence are more likely to undergo reduction in their thermal properties and to have greater internal convection when subjected to an increase in the wind speed or body motion. Hong (1992) reported dynamic insulation values at different walking speeds of selected indoor clothing ensembles using a movable thermal manikin. Reported experiments consider the case of a walking human wearing a long-sleeve sweat suit ensemble (50% cotton, 50% polyester) and another wearing a long-sleeve turtle neck cotton sweater and cotton jeans. The measured standing and dynamic insulation values of the two ensembles showed a drop in the dynamic insulation from standing insulation values by 25% and 37%, respectively.

Another aspect of clothing insulation under dynamic conditions is the periodic renewal of air in the fabric void space. Periodic movement of clothed limbs causes air adjacent to the skin to flow through the fabric void space to the environment and air from the environment to flow into the trapped layer between clothing and skin. The periodic air flow through the fabric swings between the environment temperature and the skin temperature and will not be in thermal equilibrium with the fabric yarn. Microscopic convection takes place in the void space to the fabric fiber and thus enhances further heat and moisture loss from the human body. Ghali *et al.* (2002a, 2002b) reported values for the microscopic internal transfer coefficients in a cotton fibrous medium, based on a three-node fabric model that has a void space node and divides the fabric yarn into an inner node and an outer node adjacent to the void space.

8.1.4 The microclimate skin-adjacent air layer

Movement and wind increases the convective currents within loose garments and may contribute to a cooling effect (Fanger, 1982). Loosely hanging clothing entraps more air and thus will experience a greater decrease in its insulation value in the presence of movement and wind compared to the tight fitting clothing. However, when ensembles are constructed with more layers, the difference in the insulation value between a loose- and tight-fitting garment will be smaller (Havenith *et al*., 1990b). In addition, when garment openings are added, more body heat and moisture exchange occurs with the environment. Nielsen *et. al* (1985) showed a 10% decrease in intrinsic clothing insulation with an open jacket as compared to a closed jacket during walking, with wind velocity of 1.1 m/s, and an 8% reduction during walking with no wind. Lotens and Havenith (1988) found that the vapor permeability of a rain suit increased significantly in the presence of openings.

The thermal and moisture resistance of the fabric is relatively independent

of permeability under still air conditions and no movement. With an increase in air velocity and movement, fabrics with high permeability will experience a higher reduction in their insulation value when compared to impermeable fabrics (Fonseca and Breckenridge, 1965). For example, manufactured fur, which is generally categorized as a highly permeable fabric, can be made more insulative by lining it with a fabric of low permeability.

The effect of body motion (such as walking at different speeds, stepping, and cycling) on clothing insulation has been studied by several researchers. Up to 50% of the microclimate volume can be exchanged with the outside air during each step (Vokac *et al*., 1973). Hong (1992) studied the insulation values of 24 different types of indoor clothing on a movable manikin. She found that the drop in the total insulation of the clothing ranged, depending of the type of ensemble, from about 24% to 51% due to walking at 90 steps/min, when compared with standing at zero wind. Ghaddar *et al*. (2003) showed that a 50% increase in periodic ventilation frequency of a fabric reduced its dynamic dry resistance by 23% and its evaporative insulation by 32%. When movement and wind were combined, the effect of movement was greater than the effect of wind alone (Havenith, 1990a; Lotens, 1993.

8.2 Estimation of ventilation rates

Ventilation rate is the rate of air exchange with the environment in the microclimate air layer between the skin and the clothing. The microclimate air renewal takes place through penetration of air through the outer clothing layer and through clothing apertures of the outer garment where the internal air layer is connected to the environment at the legs, sleeves, neck, or waist. The amount of ventilation depends on the wind and wearer motion. Few studies have examined the microclimate internal air layer ventilation and even fewer investigations have dealt with the mechanism of microclimate ventilation and its effect on thermal response of the human–clothing system. The complex pathways of the microclimate trapped air layer make it difficult to extend the use of available empirical ventilation data to different environments, clothing systems, and activity levels. Accurate estimation of ventilation rates is an essential part for reliable modeling of the heat and moisture transport processes of a walking, clothed human. Empirical correlations for the estimation of ventilation rates are presented, followed by a mathematical model derived from conservation principles for estimating microclimate ventilation rates.

8.2.1 Lotens's empirical model

The trace gas method is an effective experimental technique that has been used to measure microclimate ventilation. Lotens (1993) used the tracer gas

method to measure ventilation rates in tight- and loose-fitting ensembles of open and closed apertures at various wind speeds and activity rates. The tracer gas method involves injecting an inert gas (argon) at a fixed rate through a perforated tubing system over the skin. At steady periodic conditions, the gas concentrations and concentration gradient become stable. The total volume flow rate renewal is calculated from the trace gas injection volume flow rate Ψ_{tr} (m^3/s), and from the measured concentrations in the distribution system, the microclimate, and the environment as follows:

$$\frac{\dot{m}_{\text{vent}}}{\rho_a}[C_{\text{in}} - C_a] + \psi_{\text{tr}} = 0 \qquad [8.3]$$

where $\dot{m}_{\text{vent}}$ is the total ventilation rate in kg/s of clothed body surface, ρ_a is the air density (kg/m^3), ψ_{tr} is the trace gas volume flow rate, (m^3/s), C_{in} is the gas concentration in the distribution system (m^3 Ar /m^3 air), and C_a is the gas concentration in the microclimate measurement location, (m^3 Ar /m^3 air). If ventilation takes place only through the garment penetration, then the renewal mass flow rate of air through the fabric is given by

$$\dot{m}_a = \rho_a \frac{\psi_{\text{tr}}}{[C_a - C_\infty]} \qquad [8.4]$$

where $\dot{m}_a$ is the normal mass flow rate of air through the fabric in kg/s of clothed body surface, and C_∞ is the gas concentration in the environment, (m^3 Ar/m^3 air).

Lotens empirically derived mathematical correlations of ventilation rates to effective wind velocity and air permeability of the outer fabric. Lotens' (1993) correlation for ventilation through open apertures is given by

$$V_{\text{vent},a} = 1.44 \times 10^{-4} \upsilon_{\text{eff}} \qquad [8.5]$$

where $V_{\text{vent},a}$ is the ventilation rate through apertures in $m^3/s{\cdot}m^2$ of clothed body surface, υ_{eff} is the effective wind velocity (m/s). The correlation for ventilation rate through outer fabric is given by

$$V_{\text{vent},w} = 4.5 \times 10^{-5} (\upsilon_{\text{eff}} / 0.16)^{0.5+0.05\sqrt{\alpha}} \qquad [8.6]$$

where $V_{\text{vent},w}$ is the ventilation rate due to air penetration of outer fabric in $m^3/s{\cdot}m^2$ of clothed body surface, and α is the air permeability through the outer fabric in $l/m^2{\cdot}s$ at 200 Pa pressure difference. The effective wind velocity consisted of three parts,

$$\upsilon_{\text{eff}} = \upsilon_{\text{natl}} + \upsilon_{\text{wind}} + \upsilon_{\text{act}} \qquad [8.7]$$

where υ_{natl} is the wind velocity of natural convection (= 0.07 m/s for sitting and 0.11 m/s for standing), υ_{wind} is the external wind speed (m/s), and υ_{act} is the equivalent air velocity of motion (m/s). The equivalent air velocity v_{act} can be evaluated by the following expression for treadmill walking:

$$\upsilon_{act} = 0.67 \times \upsilon_{walk} \quad [8.8]$$

where υ_{walk} is the walking speed in m/s. The walking speed can be estimated using Hong's (1992) formula as follows:

$$\upsilon_{walk}(\text{mph}) = \frac{0.47}{1056 + F \times H - 0.114} \quad [8.9]$$

where F is the stride frequency in steps/min, and H is the height of the human subject in meters.

Lotens' (1993) ventilation model has limited use since it was derived from experimental considerations and was not based on first principles. The model does not take into consideration the change in volume of the microclimate air layer and the driving mechanism by which air flow is induced through outer fabric or clothing apertures.

8.2.2 Mathematical modelling of ventilation

The normal air flow through the fabric is driven by pressure differences and is dependent on the permeability of the fabric material. The permeability is affected by the type of yarn, tightness of the twist in the yarn, count of yarn and fabric structure. In general, the fabric permeability is experimentally determined under a pressure difference of 0.1245 kPa. To get the airflow passing through the fabric at other pressure differentials, the amount of airflow is assumed to be proportional to the pressure differentials. At constant fabric permeability, the airflow rate through the fabric between the trapped air in the layer adjacent to the skin and the environment is then represented by

$$\dot{m}_{ay} = \frac{\alpha \rho_a}{\Delta P_m}(P_a - P_\infty) \quad [8.10]$$

where $\dot{m}_{ay}$ is the normal flow rate through fabric, α is the fabric air permeability in $m^3/m^2 \cdot s$, $\Delta P_m = 0.1245$ kPa from standard tests on the fabric's air permeability [ASTM D737-75, 1983], P_a is the air pressure in the microclimate trapped air layer between the human skin and the fabric (kPa), and P_∞ is the outside environment air pressure (kPa).

Li (1997) used the induced air flow through the fabric given in equation [8.10] to study the impact of the normal passing flow on the heat and mass transport by diffusion at the fabric (thermal equilibrium) and ultimately at the skin in a multi-layer clothing system. Ghali *et al*. (2002c) developed a periodic ventilation model valid for normal airflow through the fabric. The microclimate air pressure is governed by the periodic movement of the fabric boundary, which changes the size of the microclimate spacing between the skin and the fabric, thus inducing variable airflow in and out of the fabric. The 1-D model of Ghali *et al*. (2002c) assumed sinusoidal fabric motion as an approximate model of the periodic change of air spacing layer thickness

for a walking person. Human gait analysis shows repeated periodic pattern of limb motion that can be approximated by a sinusoid (Lamoreux, 1971). The normal periodic ventilation model is not applicable for clothed parts of the body with open apertures at the sleeve, waist, or neck or for loose garment fitting around slender body parts. The presence of open apertures induces air flow parallel to the fabric surface during walking. For loosely fitted clothing, airflow takes place in the angular direction in the microclimate air layer due to gap height asymmetry between the cylindrical shaped body parts and the clothing.

Li (1997) developed a 2-D model for parallel planar air flow between the fabric layers using a locally fully developed laminar Poiseuille flow to relate the parallel air flow to the driving pressure difference induced by open apertures in clothed segments. The pressure drop at the opening is calculated by applying Bernoulli's equation from P_∞ in the far environment to the opening. The air mass flow rate per unit area in the parallel direction is given by

$$\dot{m}_{ax} = -\rho_a \frac{Y^2}{12\mu} \frac{\partial P_a}{\partial x} \text{ kg/(s·m}^2\text{)} \qquad [8.11]$$

Where Y is the gap height (m), μ is the viscosity of air, and x is the coordinate of the parallel direction (m). Ghali *et al*. (2004) integrated Li's (1997) 2-D parallel flow model with their 1-D periodic normal ventilation model of the fabric. The reported reduction in sensible and latent heat loss of the Poiseuille flow model of Ghali *et al*. (2004) due to an open aperture did not agree well with the published empirical results of Lotens (1993). Both Li and Ghali *et al*. models neglected the fluid inertia associated with the flow modulation and reversal during the flow cycle in the parallel direction and hence limited the Poiseuille model applicability to low Womersley number ($W_o = (Y/2)\sqrt{\omega/2\nu}$ where ω is the ventilation circular frequency, Y is the air layer thickness, and ν is the air kinematic viscosity. Ghaddar *et al*. (2005a) assumed the microclimate parallel flow to be locally governed by Womersley's solution of time–periodic flow in a plane channel (Womersley, 1957). The Ghaddar *et al*. model agreed well with the empirical ventilation results of Lotens. Ghaddar *et al*. (2005b) extended the model to 3-D to predict ventilation flow rates in the radial, angular, and axial directions, induced by periodic motion of an inner cylinder, representing the body part with respect to a surrounding outer clothing cylinder, for closed and open aperture clothing systems. The model predictions of the time-averaged ventilation rates were validated by experiments using the tracer gas method. The 3-D cylinder periodic ventilation model of the microclimate will be discussed at length since it is the first comprehensive dynamic model of microclimate periodic ventilation.

8.2.3 Microclimate air layer periodic ventilation model

Air mass balance

The formulation of the periodic ventilation model of Ghaddar *et al.* (2005b) addresses the radial (normal) air flow through the outer fabric boundary; and the modeling of the internal air layer motion in the axial direction due to the presence of an open aperture and in the angular direction due to asymmetry in microclimate thickness during the walking cycle. Figure 8.1 depicts the schematic of the physical domain of the microclimate air-layer-fabric system considered by Ghaddar *et al*. (2005b) where an enclosed air layer annulus of

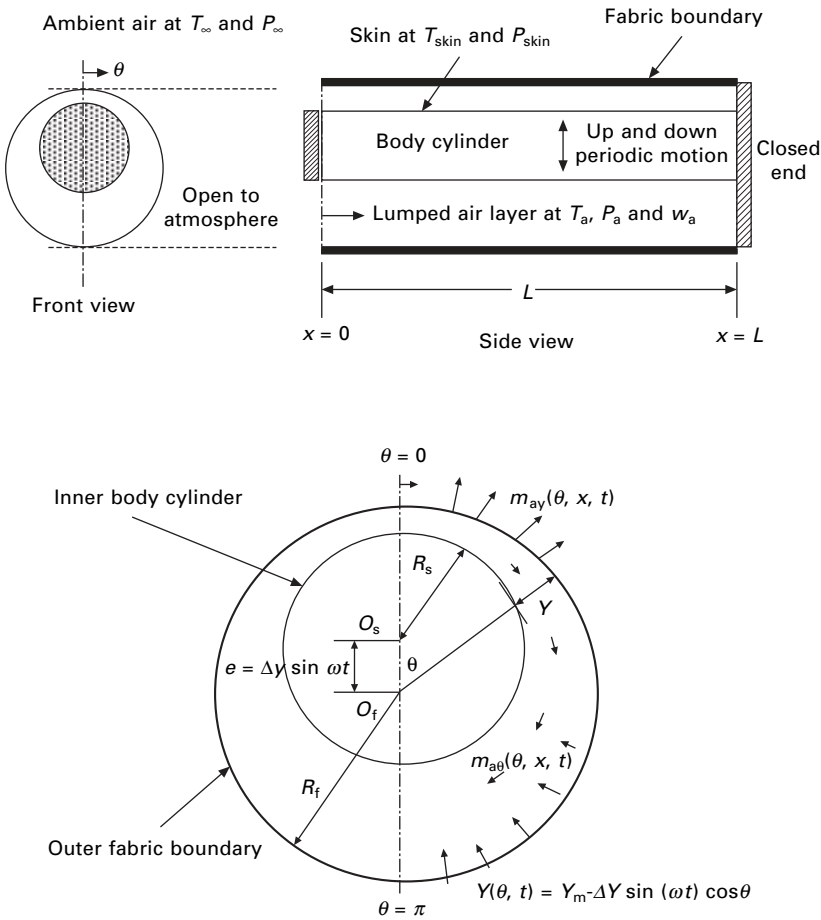

8.1 Schematic of the physical domain of the fabric–air layer–skin system and the fabric model.

thickness Y and length L separates the fabric boundary and the human skin. The physical domain of the air-layer-fabric system represents a situation where the skin boundary is a cylindrical impermeable surface of radius R_s covered with an outer clothing cylindrical boundary of radius R_f. One end of the domain at $x = 0$ is open to the atmosphere (loose clothing, openings at the sleeves end or around the neck) and the other end at $x = L$ is closed (no air flow escapes from the annulus). The skin boundary moves in a sinusoidal up-and-down motion at an angular frequency ω that induces air movement through the porous fabric. The flow of air is axial through the clothing openings (sleeves, skirts, neck), radial (normal to the fabric) through the clothing void spaces, and angular around the body segments. The fabric thickness is e_f. The frequency of the oscillating motion of the fabric is generally proportional to the activity level of the walking human. The microclimate air layer is formulated as an incompressible lumped layer.

The angular airflow is governed by a pressure differential, due to variation of the microclimate air gap length $Y(\theta, t)$ that drives the flow in θ-direction. The flow takes place in the narrow gap between the eccentric cylinders during the motion cycle. A dimensionless amplitude parameter ζ is defined by

$$\varsigma = \frac{\Delta Y}{Y_m} \qquad [8.12a]$$

The eccentricity e_c of the cylinders is time-dependent and is expressed in terms of oscillation frequency ω and amplitude ΔY as

$$e_c = \Delta Y \sin(\omega t) \quad (\zeta < 1, \text{ no skin–fabric contact}) \qquad [8.12b]$$

Some elementary geometry shows that the width of the gap Y between the two circular cylinders can be approximated by

$$Y(\theta, t) = Y_m[1 - \zeta \sin(\omega t)\cos(\theta)]$$

$$(\zeta < 1, \text{ no skin–fabric contact}) \qquad [8.12c]$$

where Y_m is the mean spacing between the human segment cylinder and the fabric outer cylinder ($Y_m = R_f - R_s$). No skin–fabric contact is present during the period of motion when the amplitude ratio is less than unity ($\zeta < 1$). Contact can locally be present when the amplitude ratio is greater than or equal to unity ($\zeta \geq 1$). The solution presented in this section covers only the case when the amplitude ratio is less than unity.

The general air layer mass balance performed on an element of height Y, thickness $R_f d\theta$, and depth dx is given by

$$\frac{\partial(\rho_a Y)}{\partial t} = \dot{m}_{ay} - \frac{\partial(Y\dot{m}_{ax})}{\partial x} - \frac{\partial(Y\dot{m}_{a\theta})}{R_f \partial\theta} \qquad [8.13]$$

where $\dot{m}_{ax}$ is the mass flux in the axial direction in kg/m^2·s, $\dot{m}_{a\theta}$ is the mass

flux in the angular direction, and $\dot{m}_{ay}$ is the radial air flow rate. The boundary conditions for the air flow are

$$\dot{m}_{ax}(x = 0, \theta) = C_D\left[\frac{2\rho_a}{|P_o - P_\infty|}\right]^{\frac{1}{2}}[P_\infty - P_o] \quad [8.14a]$$

$$\dot{m}_{ax}(x = L, \theta) = 0 \quad [8.14b]$$

$$\dot{m}_{a\theta}(x, \theta = 0) = 0 \quad [8.14c]$$

$$\dot{m}_{a\theta}(x, \theta = \pi) = 0 \quad [8.14d]$$

where Equation [8.14b] is derived from the pressure drop at the opening by applying Bernoulli's equation from a state at P_∞ in the far environment ($x \to -\infty$) to a state at P_o and flow rate $\dot{m}_{ax}(x = 0, \theta)$ at the opening, and C_D is the discharge loss coefficient at the aperture of the domain dependent on the discharge area ratio of the aperture to the internal air annulus *area*.

Womersley flow model in axial and angular directions

The flow in the x-direction, driven by the time-periodic pressure gradient, is treated as locally governed by Womersley time-periodic laminar channel base flow (Womersley, 1957). The channel is assumed of sufficient length for the flow to be fully developed and the slope $\partial Y/(R_f \partial\theta)$ is small to permit quasi-parallel flow in the angular direction within the annulus. With these assumptions, the governing momentum equations in the axial and angular directions respectively become

$$\frac{\partial u_x}{\partial t} = -\frac{1}{\rho_a}\frac{\partial P}{\partial x} + \nu\frac{\partial^2 u_x}{\partial y^2} \quad \text{and} \quad u_x\left(\pm\frac{Y}{2}, t\right) = 0 \quad [8.15a]$$

$$\frac{\partial u_\theta}{\partial t} = -\frac{1}{\rho_a R_f}\frac{\partial P}{\partial \theta} + \nu\frac{\partial^2 u_\theta}{\partial y^2} \quad \text{and} \quad u_\theta\left(\pm\frac{Y}{2}, \theta, t\right) = 0 \quad [8.15b]$$

where $u_x(y, t)$ and $u_\theta\ (y, t)$ are the plane channel angular velocities for x- and θ-directions, and ν is the kinametic viscosity of air in m^2/s. The driving pressure in the air layer is oscillating with the same frequency as the inner cylinder motion but with a phase difference of $(\pi/2)$. At the minimum spacing position $Y_{\min} = Y_m - \Delta Y$ and the maximum spacing position $Y_{\max} = Y_m + \Delta Y$, the pressure in the air layer equalizes with P_∞ before the radial flow changes direction. The driving pressure gradients in the axial and angular directions are given by

$$-\frac{1}{\rho_a}\frac{\partial P}{\partial x} = \Lambda_x \sin\left(\omega t + \frac{\pi}{2}\right) = \Lambda_x \cos(\omega t) \quad [8.16a]$$

$$-\frac{1}{\rho_a R_f}\frac{\partial P}{\partial \theta} = \Lambda_\theta \sin\left(\omega t + \frac{\pi}{2}\right) = \Lambda_\theta \cos(\omega t) \qquad [8.16b]$$

where Λ_x and Λ_θ are the pressure gradient amplitude parameters (Pa·m^2/kg) in the axial and the angular directions, respectively. Assuming a frequency-separable transient solution, Equations [8.16a] and [8.16b] are written for an oscillating laminar flow in a channel in x- and θ-directions as follows:

$$\frac{\partial u_x}{\partial t} = \Lambda_x \cos(\omega t) + \nu \frac{\partial^2 u_x}{\partial y^2}, \qquad [8.17a]$$

$$\frac{\partial u_\theta}{\partial t} = \Lambda_\theta \cos(\omega t) + \nu \frac{\partial^2 u_\theta}{\partial y^2}, \qquad [8.17b]$$

The dimensionless axial velocity $u'_x(y, t) = u_x(y, t)/(\Lambda_x/\omega)$ and the dimensionless angular velocity $u'_\theta(x, t) = u_\theta(y, t)/(\Lambda_\theta/\omega)$ are found analytically as a function of y, time t, and the physical parameters ω and ν (Straatman *et al.*, 2002). By prescribing a flow condition such as pressure or flow rate in either direction at the same ventilation frequency ω, the values of Λ_x and Λ_θ can be determined for any given channel height Y. The mass flow rate per unit area is then calculated as a function of time at position x as follows:

$$\dot{m}'_{ax}(t) = \dot{m}_{ax} Y = \rho_a \frac{Y \Lambda_x}{2\omega} \Phi(t) \quad (\text{kg/s} \cdot \text{m}) \qquad [8.18a]$$

where Φ is the dimensionless flow rate for a unit pressure gradient parameter Λ_x, given by

$$\Phi(t) = \int_{-1}^{1} u'_x(y', t)\, dy' \qquad [8.18b]$$

where $y' = 2y/Y$. Similarly, the angular mass flow rate at any local angular position θ is found by integrating u_θ over the layer spacing Y as

$$\dot{m}'_{a\theta} = \dot{m}_{a\theta}(t) Y = \rho_a \frac{Y \Lambda_\theta}{2\omega} \Phi(t) \quad (\text{kg/s·m}) \qquad [8.18c]$$

The air mass flow rate per unit depth $\dot{m}'_{ax}(t)$ is related to the pressure in the channel through Equation [8.16] and the pressure at the opening through Equation [8.14a]. The flow rate per unit width in the angular direction has been related to the angular pressure gradient by combining the standard lubrication theory in fluid dynamics (Acheson, 1990) and the Womersley flow in a channel. Since the mass flow rate is modeled as a function of pressure differences in r-, θ-, and x-directions, the mass balance of the air layer would result in the following pressure equation:

$$\rho_a \frac{\partial Y}{\partial t} = -\frac{\alpha \rho_a}{\Delta P_m}(P_a - P_\infty) + \frac{\rho_a \Phi(t)}{2\omega}\left[\frac{\partial(Y\Lambda_x)}{\partial x} + \frac{\partial(Y\Lambda_\theta)}{R_f \partial\theta}\right] \quad [8.19]$$

Equations [8.16] and [8.19] were solved numerically by Ghaddar *et al*. (2005b) for $P_a(x, \theta, t)$, Λ_x and Λ_θ at any discrete location within the air layer as a function of time while satisfying the imposed boundary conditions given in Equations [20.14a–d]. The angular–space–time-averaged value of the mass flow rate in the radial direction can be integrated over half the period of motion at any axial position as

$$\overline{\dot{m}_{ay}} = \frac{2}{\tau\pi}\int_0^{\tau/2}\int_{-\pi/2}^{\pi/2} \dot{m}_{ay} R d\theta dt \quad \text{kg/s·m}^2 \quad [8.20a]$$

where τ is the period of oscillation. The net flow in one period is zero. The net ventilation rate inflow or outflow to the microclimate air layer through the open aperture during half the period of motion is defined by

$$\dot{m}_o = \frac{2}{\tau\pi}\int_0^{\tau/2}\int_{-\pi/2}^{\pi/2} \dot{m}_o d\theta dt \ \text{kg/ s·m}^2 \quad [8.20b]$$

where $\dot{m}_o$ is net flow rate through the open aperture.

Ghaddar *et al.* (2005b) conducted experiments using the tracer gas method to measure time- and space-averaged air ventilation rates induced by inner cylinder periodic motion within a fabric cylindrical sleeve at spacing amplitude ratio with respect to the mean spacing of $\zeta = 0.8$ for both closed and open aperture cases. The predicted ventilation flow rates by the cylinder model of Ghaddar *et al*. (2005b) agreed well with their experimental measurements of total renewal rates for closed and open apertures. The agreement improved at higher frequencies of ventilation.

8.3 Heat and moisture transport modeling in clothing by ventilation

Ventilation can have a dominant effect on the thermal insulation of clothing and the heat and moisture transport from the human body to the environment. There have been many models simulating these transport processes to predict sensible and latent heat loss from the skin. Most of these models started from energy and mass balances at thermodynamic equilibrium and used the empirical ventilation relationships developed by Lotens (1993). Lotens calculated the sensible heat transport by air ventilation as

$$Q_s = C_p \dot{m}_{\text{vent}} \Delta T \quad [8.21a]$$

where Q_s is the sensible heat loss by ventilation, W/m^2, and C_p is the specific heat capacity of air, J/kg·K and ΔT is the temperature difference between

the locations where ventilation occurs. The latent heat transport of the ventilation is

$$Q_L = \dot{m}_{\text{vent}} h_{fg} \qquad [8.21b]$$

where Q_L is the latent heat loss by ventilation, W/m^2 and h_{fg} is the heat of evaporation of water, kJ/kg.

The work of Lotens (1993) assumed that the microclimate trapped air layers have the same average thickness in clothing ensembles, which is not true in dynamic situations, and that ventilation will mostly affect the clothing outer layer. The clothing model of Lotens consisted of four layers: a homogenous undergarment clothing layer, a trapped air layer, an outer garment and an adjacent external air layer. The trapped air layer was assumed to consist of two adjacent air layers to the clothing and free moving air in-between. The heat and vapor transmission that takes place by ventilation through apertures and by penetration of air through the outer material reduces clothing insulation. Motion affects internal convection coefficients in the trapped layer and the adjacent external air layer. The combined effect is already included in the effective wind speed (see Equation [8.7]). However, it is difficult to understand how ventilation can be incorporated into the dynamic clothing models if ventilation values are derived empirically for specific clothing ensembles and limited dynamic conditions. Lotens (1993) used the four-layer ventilation model to calculate the dry and heat loss from the human body by diffusion and ventilation. He approximated the human body by a vertical cylinder. The body is split in four parts: nude parts and clothed parts with and without additional radiation. He calculated the total heat transfer from the body, taking into account the clothing surface area. The model was tested by experiments on subjects with four types of clothing material, with the subjects participating in three activities: standing in still air (ST), standing in wind at 1 m/s (STW), and walking at 4 km/hour in quiet air (W). The reported measured average sensible heat flow in the absorbing garment was 52 W/m^2, 57 W/m^2 and 104 W/m^2 for activities of (ST), (STW) and (W), respectively. The average latent heat loss measured in walking condition was reported at 24 W/m^2 compared to 9 W/m^2 for standing in still air. For a highly permeable fabric, the dry heat loss was 105 W/m^2 for walking conditions at metabolic rate of 148 W/m^2 compared to 33 W/m^2 during standing at an average metabolic rate of 60 W/m^2. The dry heat loss predictions of the Lotens model, compared to the experiments, were at rms error of 10 to 12 W/m^2. The measured apparent intrinsic insulation in Lotens' experiment decreased by 46% from 0.16 in the standing activity to 0.085 m^{2}K/W in the walking activity.

Ventilation affects both microscopic convection within the fabric and internal convection coefficients between the human skin and the microclimate trapped air layer between the fabric and the skin. It is of interest to develop a thermal

model of the microclimate air layer from first principles which can capture the physics of the flow and thermal transport and can be easily integrated with clothing ventilation models. The model of Ghaddar *et al.* (2005b) of heat and moisture transport by ventilation is derived from first principles and is flexible enough to be applied to a wide variety of problems. In this section, Ghaddar's heat and moisture transport model of the microclimate heat layer will be described, followed by the associated fabric ventilation model of Ghali *et al.* (2002b), together with reported data on the fabric microscopic internal transport coefficients and the internal and external convection coefficients of adjacent air layers.

8.3.1 Microclimate air layer mass and heat balances without fabric skin contact

The interaction of the fabric and the microclimate layer during periodic motion is mainly due to the periodic renewal of the air in the void space of the porous fabric. Ghaddar *et al*. (2005b) derived the mass and heat balances in the microclimate air layer, as it interacts with the skin and the trapped air in the fabric void space. Their derivation assumes that, during the oscillation cycle, the air from the environment will pass through the fabric void at $\dot{m}_{ay}$ (calculated from Equation [8.10]) into the air layer when the pressure in the air layer $P_a < P_\infty$ and the air in the air layer will pass at $\dot{m}_{ay}$ through the fabric void space to the environment when $P_a \geq \mathrm{P}_\infty$. The airflow into the air spacing layer coming from the air void node of the fabric will have the same humidity ratio as the air in the void space of the fabric, while the airflow out of the air layer into the fabric void will carry the same humidity as the air layer. The water vapor mass balance for the air spacing layer is given by

$$\frac{\partial(\rho_a Y w_a)}{\partial t} = h_{m(\text{skin-air})}[P_{sk} - P_a] - \dot{m}_{ay} w_p - \frac{\partial(Y \dot{m}_{ax} w_a)}{\partial x}$$

$$- \frac{\partial(Y \dot{m}_{a\theta} w_a)}{R_f \partial\theta} + D\frac{\rho_a (w_{\text{void}} - w_a)}{e_f/2} + \frac{D}{R_f^2}\frac{\partial}{\partial\theta}\left(Y\frac{\partial w_a}{\partial\theta}\right)$$

$$+ DY\frac{\partial^2 w_a}{\partial x^2} + h_{m(o-\text{air})}[P_o - P_a]$$

$$\text{where} \quad w_p = \begin{cases} w_{\text{void}} & P_a(x,\theta,t) < P_\infty \\ w_a & P_a(x,\theta,t) \geq P_\infty \end{cases} \qquad [8.22]$$

where $h_{m(\text{skin-air})}$ is the mass transfer coefficient between the skin and the air layer, $h_{m(o\text{-air})}$ is the mass transport coefficient from the fabric to air, P_a is the water vapor pressure in the air layer, w_a is the humidity ratio of the air layer, P_{sk} is the vapor pressure at the skin solid boundary, w_{void} is the humidity ratio

of the air void, e_f is the fabric thickness, and D is the diffusion coefficient of water vapor into air. The terms on the right-hand side of Equations [8.22a] and [8.22b] are explained as follows: the first term represents the mass transfer from the skin to the trapped air layer where the mass transfer coefficient at the skin to the air layer is obtained from published experimental values of Ghaddar *et al*. (2003, 2005b); the second term is the convective mass flow coming through the fabric voids; the third and fourth terms represent the net flux in the axial and angular directions; the fifth term is the water vapor diffusion term from the air layer to the air in the fabric void due to the difference in water vapor concentration; the sixth and seventh terms represent vapor diffusion in angular and axial directions; and the final term is the mass transfer from the air layer to the fabric in the axial direction. The final term is significant only in the vicinity of the opening.

The energy balance of the air spacing of the fabric of Ghaddar *at al*. (2005b) expresses the rate of change of the air–vapor mixture energy in the air-layer in terms of: (i) the external work done by the environment on the air layer, (ii) the evaporative heat transfer from the moist skin, (iii) the dry convective heat transfer from the skin, (iv) the heat flow to or from the air layer associated with $\dot{m}_{ay}$, $\dot{m}_{a\theta}$,, and $\dot{m}_{ax}$, (v) the heat diffusion from void air of the thin fabric to the air layer, and (vi) the angular conduction and water vapor diffusion in the air layer. The energy balance of the air layer is given by

$$\begin{aligned}\frac{\partial}{\partial t}[\rho_a Y(C_v T_a + w_a h_{fg})] + P_a\frac{\partial Y}{\partial t} &= h_{m(\text{skin–air})}h_{fg}[P_{sk} - P_a] \\ &+ h_{c(\text{skin–air})}[T_{sk} - T_a] - \dot{m}_{ay}H_p - \frac{\partial Y[\dot{m}_{ax}(C_p T_a + w_a h_{fg})]}{\partial x} \\ &- \frac{\partial[Y\dot{m}_{a\theta}(C_p T_a + w_a h_{fg})]}{R_f \partial\theta} + \frac{Dh_{fg}}{R_f^2}\frac{\partial}{\partial\theta}\left(Y\frac{\partial w_a}{\partial\theta}\right) \\ &+ Dh_{fg}Y\frac{\partial^2 w_a}{\partial x^2} + h_{m(o–\text{air})}h_{fg}[P_o - P_a] + \frac{k_a}{R_f^2}\frac{\partial}{\partial\theta}\left(Y\frac{\partial T}{\partial\theta}\right) \\ &+ k_a Y\frac{\partial^2 T_a}{\partial x^2} + h_{c(o–\text{air})}[T_o - T_a] + k_a\frac{(T_{\text{void}} - T_a)}{e_f/2} \\ &+ Dh_{fg}\frac{\rho_a(w_{\text{void}} - w_a)}{e_f/2}\end{aligned} \quad [8.23a]$$

where H_p is the enthalpy of airflow into or from the air layer, defined by

$$H_p = \begin{cases} C_p T_{\text{void}} + w_{\text{void}} h_{fg} & P_a(x, \theta, t) < P_\infty \\ C_p T_a + w_a h_{fg} & P_a(x, \theta, t) \geq P_\infty \end{cases} \quad [8.23b]$$

where $h_{c(o\text{-air})}$ is the convection coefficient from the fabric to air, $h_{m(o\text{-air})}$ is the mass transport coefficient from the fabric to air, k_a is the thermal conductivity of air. Since the fabric void thickness is very small, conduction of heat from the fabric void air to the trapped air layer is represented by the law of the wall as given in the last two terms of Equation [8.23a]. The inner cylinder skin condition can be specified at either constant skin temperature and humidity ratio (P_{sk} and T_{sk} are known), or constant flux condition at the surface. The closed boundary at $x = L$ is assumed adiabatic, while the open boundary exchanges heat by conduction and convection to air at T_∞.

The solution of the mass and heat transport in the microclimate lumped air layer at T_a and w_a is coupled to the ventilated fabric through the fabric void space air conditions at T_{void} and w_{void} and to the human skin conditions through the transport coefficients from the skin, which has known temperature T_{sk} and vapor pressure P_{sk}. In highly permeable porous fabric, the air temperature and humidity in the void space are not equal to the fabric temperature and humidity due to the ventilation effect. An appropriate fabric model that takes into consideration the internal transport coefficients between the air in the void space and the fabric solid yarn should be used for accurate prediction of the ventilation effect on thermal response of the clothed human body system. In the next section (8.3.2), a discussion of known fabric models, and the reasons for adopting Ghali *et al*. (2002a and 2002b) three-node fabric adsorption model to integrate with the microclimate ventilation model are presented.

8.3.2 The fabric three-node ventilation model

Traditionally, ventilation models of heat and mass transfer through clothing layers assumed instantaneous equilibrium between the local relative humidity of the diffusing moisture and the regain of the fiber, and ignored the effect of ventilation on the heat and moisture exchange between the microclimate of the clothing and the ambient air. Jones *et al*. (1990) described a model of the transient response of clothing systems, which took into account the sorption behavior of fibers but assumed local thermal equilibrium with the surrounding air. However, the hypothesis of local equilibrium was shown to be invalid during periods of rapid transient heating or cooling in porous media as reported by Minkowycz *et al*. (1999). Their results show that local thermal equilibrium is not valid if the ratio of the Sparrow number to the Peclet number is small for 1-D flow in a porous layer. In the absence of local thermal equilibrium, the solid and fluid should be treated as two different constituents as reported in the works of Vafai and Sozen (1990), Amiri and Vafai (1994, 1998), Kuzentsov (1993, 1997, 1998), and Lee and Vafai (1999). Under vigorous movement of a relatively thin porous textile material, air will pass quickly between the fibers, invalidating the local thermal equilibrium

assumption. Ghali *et al*. (2002a) studied the effect of ventilation on heat and mass transport through fibrous material by developing a fabric two-node absorption model (aided by experimental results on moisture regain of ventilated fabric) to determine the transport coefficients within a cotton fibrous medium. Their model was further developed and experimentally verified to predict temporal variations in temperature and moisture content of the air within the fiber in a multilayer three-node model (Ghali *et al*. 2002b). The analysis presented here of airflow through the fabric is based on Ghali *et al*. (2002b) while using a lumped layer of two fabric nodes and an air void node to represent the fibrous medium. The model is simple and is applicable to highly permeable, thin fabrics. Lumped parameters have commonly been used in models of thin permeable fabrics (Farnworth, 1986; Jones and Ogawa, (1993).

The three-node model lumps the fabric into an outer node, an inner node, and an air void node. The fabric outer node represents the exposed surface of the yarns, which is in direct contact with the penetrating air in the void space (air void node) between the yarns. The fabric inner node represents the inner portion of the 'solid' yarn, which is surrounded by the fabric outer node. The outer node exchanges heat and moisture transfer with the flowing air in the air void node and with the inner node, while the inner node exchanges heat and moisture by diffusion only with the outer node. The air flowing through the fabric void spaces does not spend sufficient time to be in thermal equilibrium with the fabric inner and outer nodes. The moisture uptake in the fabric occurs first by the convection effect from the air in the void node to the yarn surface (outer node), followed by sorption/diffusion to the yarn interior (inner node). The fabric model is best represented by a flow of air around cylinders in cross flow, where the air voids are connected between the cylinders (yarns) as shown in Fig. 8.2. The fabric is represented by a large number of these three-node modules in cross flow, depending on the fabric effective porosity. The fabric area is $L \times W$ and the fabric thickness is e_f. The airflow is assumed normal to the fabric plane.

Effective heat and mass transfer coefficients, reported by Ghali *et al.* (2002a, 2002b), H_{co} and H_{mo} for the outer node of the fabric, and the heat and mass diffusion coefficients H_{ci} and H_{mi} for the inner nodes of the fabric, are used in the model in normalized form as follows:

$$H'_{mo} = H_{mo}\frac{A_o}{A_f},\ H'_{co} = H_{co}\frac{A_o}{A_f},\ H'_{mi} = H_{mi}\frac{A_i}{A_f},\ H'_{ci} = H_{ci}\frac{A_i}{A_f} \qquad [8.24]$$

where A_f is the overall fabric surface area, A_o is the outer-node surface area exposed to air flow and A_i is the inner node area in contact with the outer node.

The time-dependent mass and energy balances were derived by Ghali *et al*. (2002a) for the outer and inner nodes of the fabric yarn and for the air

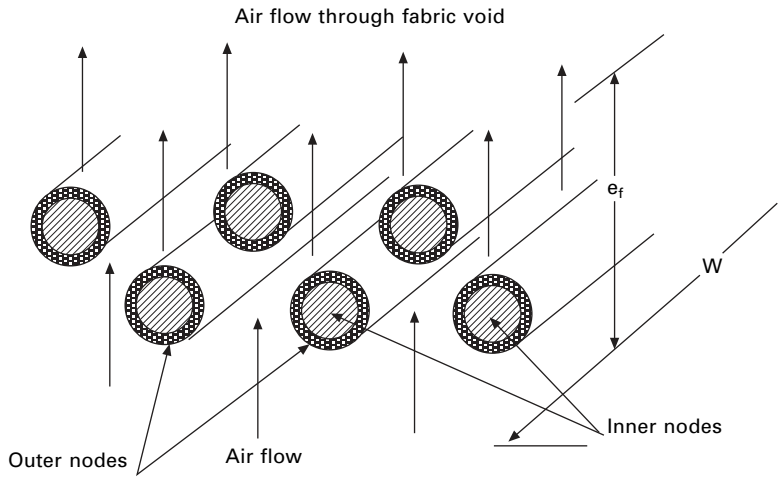

8.2 Schematic of the three-node fabric model of Ghali *et al.* (2002b).

void node in terms of the heat and mass transport coefficients between the penetrating air and the outer node and between inner and outer node. In the derivation of the water vapor mass balances in the fabric and void space nodes, the water vapor is assumed dilute compared with the air, and the bulk velocity of the mixture is very close to the velocity of the air. This assumption simplifies the mass balances by ignoring the effect of counter transfer of the air and assuming constant total pressure of the system. According to *ASHRAE Handbook of Fundamentals* (ASHRAE, 1997), no appreciable error is introduced when diffusion of a dilute gas through an air layer is carried out. The derivation included a term to correct for bulk motion of the fluid and its value is typically between 1.00 and 1.05 for conditions of the ventilating air. The water vapor mass balance in the air void node is given in Equations [8.25a] and [8.25b] when air flow enters the fabric void from the environment space to the microclimate layer ($P_a < P_\infty$) and when air flow enters the fabric void space from the microclimate layer to the environment ($P_a > P_\infty$), respectively, as

$$\frac{\partial}{\partial t}(\rho_a e_f w_{\text{void}} \varepsilon_f) = \dot{m}_{ay}[w_p - w_{\text{void}}] + H'_{mo}[P_o - P_a]$$

$$+ D\frac{\rho_a (w_a - w_{\text{void}})}{e_f/2} + D\frac{\rho_a (w_\infty - w_{\text{void}})}{e_f/2} + \frac{De_f}{R_f^2}\frac{\partial^2 w_{\text{void}}}{\partial \theta^2}$$

$$+ De_f \frac{\partial^2 w_{\text{void}}}{\partial x^2} \qquad [8.25a]$$

where $$w_p = \begin{cases} w_\infty & P_a(x, \theta, t) < P_\infty \\ w_a & P_a(x, \theta, t) \geq P_\infty \end{cases} \qquad [8.25b]$$

where ε_f is the fiber porosity. The last two terms in the equations are the mass diffusion terms within the fabric in angular and axial directions. The outer fiber node and the inner fiber node mass balances are expressed in terms of the fabric regain in Equations [8.26] and [8.27], respectively:

$$\frac{dR_o}{dt} = \frac{1}{\rho\gamma e_f}[H'_{mo}(P_{\text{void}} - P_o) + H'_{mi}(P_i - P_o)] \quad [8.26]$$

$$\frac{dR_i}{dt} = \frac{H'_{mi}}{\rho(1-\gamma)t_f}[P_o - P_i] \quad [8.27]$$

where R_o is the regain of the outer node (the mass of moisture adsorbed by the fiber outer node divided by the dry mass of the fiber outer node), R_i is the regain of the inner node, and H'_{mo} and H'_{mi} are the mass transfer coefficients between the outer node and the penetrating air and the outer node and the inner node, respectively. The parameter γ is the fraction of mass that is in the outer node and it depends on the fabric type and the fabric porosity. The total fabric regain R (kg of adsorbed H_2O/kg dry fiber) is given by

$$R = \gamma R_o + (1-\gamma)R_i \quad [8.28]$$

In the model of Ghali *et al.* (2002a), the value of γ is equal to 0.6.

The energy balance for the air vapor mixture in the air void node is given by

$$\begin{aligned}
&\varepsilon_f \frac{\partial}{\partial t}[\rho_a e_f (C_v T_{\text{void}} + h_{fg} w_{\text{void}})] = -\dot{m}_{ay}[H_e] \\
&+ \dot{m}_{ay}[C_p T_{\text{void}} + w_{\text{void}} h_{fg}] + H'_{co}[T_o - T_{\text{void}}] + k_a \frac{T_a - T_{\text{void}}}{e_f/2} \\
&+ k_a \frac{T_\infty - T_{\text{void}}}{e_f/2} + Dh_{fg} \frac{\rho_a (w_a - w_{\text{void}})}{e_f/2} + Dh_{fg} \frac{\rho_a (w_\infty - w_{\text{void}})}{e_f/2} \\
&+ \frac{Dh_{fg} e_f}{R_f^2} \frac{\partial^2 w_{\text{void}}}{\partial\theta^2} + Dh_{fg} e_f \frac{\partial^2 w_{\text{void}}}{\partial x^2} + \frac{k_a e_f}{R_f^2} \frac{\partial^2 T_{\text{void}}}{\partial\theta^2} \\
&+ k_a e_f \frac{\partial^2 T_{\text{void}}}{\partial x^2}
\end{aligned} \quad [8.29a]$$

and H_e is given by

$$H_e = \begin{cases} C_p T_\infty + w_\infty h_{fg} & \text{for} \quad P_a(x,\theta,t) < P_\infty \\ C_p T_a + w_a h_{fg} & \text{for} \quad P_a(x,\theta,t) \geq P_\infty \end{cases} \quad [8.29b]$$

The heat transfer coefficient between the outer node and the penetrating air in the voids is H'_{co}, and k_a is the thermal conductivity of air. The last four terms of the energy balance are heat diffusion terms in axial and angular

directions. These terms are negligible when only normal flow through the fabric is present.

The energy balance on the outer nodes gives

$$\rho_f (1 - \gamma)\left[C_f \frac{dT_o}{dt} - h_{ad} \frac{dR_o}{dt} \right] = \frac{H'_{co}}{e_f}[T_{void} - T_o] - \frac{H'_{ci}}{e_f}[T_o - T_i] + \frac{h_r}{2e_f}(T_{skin} - T_o) + \frac{h_r}{2e_f}(T_\infty - T_o) \quad [8.30]$$

where H'_{ci} is the heat diffusion coefficient between the outer node and the inner node, h_r is the linearized radiative heat exchange coefficient, and h_{ad} is the enthalpy of the water adsorption state. The density of the adsorbed phase of water is similar to that of liquid water. The high density results in the enthalpy and internal energy of the adsorbed phases being very nearly the same. Therefore, the internal energy, u_{ad}, can be replaced with the enthalpy of the adsorbed water. Data on h_{ad}, as a function of relative humidity, is obtained from the work of Morton and Hearle (1975).

The energy balance on the inner node gives

$$\rho_f \gamma\left[C_f \frac{dT_i}{dt} - h_{ad} \frac{dR_i}{dt} \right] = \frac{H'_{ci}}{e_f}[T_o - T_i] \quad [8.31]$$

The above coupled differential Equations [8.25] to [8.31] describe the time-dependent convective mass and heat transfer from the skin–adjacent air layer through the fabric, induced by the sinusoidal motion of the fabric. To solve the equations for the fabric transient thermal response, the fabric void microscopic transport coefficients, namely H'_{mo}, H'_{co}, and the inner node diffusion coefficients H'_{mi}, and H'_{ci}, and the internal convection coefficients from the skin to the air layer $h_{m(\text{skin-}a)}$ and $h_{c(\text{skin-}a)}$ must be known.

Microscopic fabric heat and mass transport coefficients Ghali *et al*. (2002c) ventilation model does not assume local thermal equilibrium in the fiber. The fabric microscopic transport coefficients H'_{mo} and H'_{co} were empirically derived by Ghali *et al*. (2002a) for cotton fabric and were found to increase linearly with the air normal mass flow rate through the fabric. Ghali *et al.* (2002a) experiments were conducted inside environmentally controlled chambers to measure the transient moisture uptake of untreated dry cotton fabric samples subjected to airflow driven through the fiber by a bulk pressure gradient generated by humid air at an elevated velocity impinging normal to the fabric. The untreated cotton chosen by Ghali *et al*. (2002a) was representative of a most commonly worn fabric. The ranges of flow rates per unit area and ventilation frequencies considered by the reported study were 0.0077 to 0.045 kg/m^2·s and 25 to 35 rpm, respectively. Human gait analysis (Lamoreux, 1971) shows that a walking speed of 0.9 m/s corresponds to 70

steps/min or 35 rpm ventilation frequency. Ghaddar *et al*. (2005a) calculated the minimum normal flow rate through the fabric ventilation three-node model that could reproduce the fabric total regain and temperature obtained by considering only diffusion transport based on fabric dry and evaporative resistances. The diffusion transport model produces the lowest regain that can physically take place in the fabric. At the mass flow rate of 0.0077 kg/m^2·s, Ghaddar *et al*. (2005b) found that the fabric regain predicted by the three-node fabric model is the same as the regain predicted by the diffusion model. The effective microscopic heat and mass transfer coefficients between the airflow in the fabric void and the outer node for cotton fabric are given by Ghaddar *et al*. (2005b):

$$H'_{co} = 495.72\dot{m}_a - 1.85693 \quad \text{W/m}^2\text{·K},\ \dot{m}_{ay} > 0.00777\ \text{kg/m}^2\text{·s} \qquad [8.32a]$$

$$H'_{co} = 2.0 \quad \text{W/m}^2\text{·K},\ \dot{m}_{ay} \le 0.00777\ \text{kg/m}^2\text{·s} \qquad [8.32b]$$

$$H'_{mo} = 3.408 \times 10^{-3}\dot{m}_a - 1.2766 \times 10^{-5}\ \text{kg/m}^2\text{·kPa·s},\ \dot{m}_{ay} > 0.00777\ \text{kg/m}^2\text{·s} \qquad [8.32c]$$

$$H'_{mo} = 1.3714 \times 10^{-5} \quad \text{kg/m}^2\text{·kPa·s},\quad \dot{m}_{ay} \le 0.00777\ \text{kg/m}^2\text{·s} \qquad [8.32d]$$

The inner node transport coefficients to be used in the fabric model are as reported by Ghali *et al*. (2002a) at H'_{ci} =1.574 W/m^2·K, and $H'_{mi} = 7.58 \times 10^{-6}$ kg/m^2·kPa·s.

Internal convection coefficients from the skin to the microclimate air layer Several researchers have empirically estimated the internal convection coefficients between the skin and the trapped air layer under dynamic conditions initiated by motion. Lotens (1993) reported internal mass transport coefficients in two-layer clothing at the skin to the clothing layer, for various garments and apertures. Havenith *et al*. (1990a) reported data for a clothing ensemble of cotton/polyester workpants, polo shirt, sweater, socks, and running shoes. Their data on dynamic clothing insulation of skin surface air layer were based on measurements of dry heat loss where the subject skin was wrapped tightly with a thin, water-vapor impermeable, synthetic foil. Danielsson (1993) reported internal forced convection coefficients for various parts of the body for a loose-fitting ensemble at walking speeds of 0.9, 1.4 and 1.9 m/s. Ghaddar *et al*. (2003, 2005b) experimental data on the convective transport coefficients from the skin to the internal air layer were based on the evaporative heat loss and the moisture adsorption in the clothing due only to normal ventilation action of the fabric for both planar and cylindrical geometry of the fabric boundary under periodic ventilation. The dry convective heat transport coefficient from the skin to the lumped air layer $h_{c(\text{skin-air})}$ was found from the Lewis relation for air–water vapor mixtures (ASHRAE, 1997). Ghaddar *et al*. (2003) experimental findings of convection coefficients are within 8%

of the findings of Danielsson, at a walking speed of 0.9 m/s, for the trunk and the arm parts of the body. The mean transport coefficients for a cylindrical geometry are 29% lower than the planar normal periodic flow coefficients reported by Ghaddar *et al*. (2005b). This is expected due to the reduced normal ventilation rate and increased angular motion parallel to the inner surface within the microclimate air layer annulus of the cylindrical geometry. Table 8.1 presents a summary of transport coefficients reported by various researchers for closed aperture high air permeable cotton clothing at various walking speeds, external winds, or frequencies.

When internal ventilation convection coefficients are known at the skin, then the steady periodic time-averaged sensible and latent heat losses per unit area from the skin can be calculated, respectively, as

$$Q_S = h_{c\,(\text{skin-air})}\left\{\frac{1}{\tau}\int_t^{t+\tau}(T_{sk} - T_a)dt\right\} + h_r\frac{1}{\tau}\int_t^{t+\tau}(T_{sk} - T_o)dt \qquad [8.33a]$$

$$Q_L = h_{fg}h_{m(\text{skin–air})}\left\{\frac{1}{\tau}\int_t^{t+\tau}(P_{sk} - P_a)dt\right\} \qquad [8.33b]$$

In addition, the average overall dry resistance of clothing, I_T (*clo*) and evaporative resistance R_E can be determined from the Jones and McCullough (1985) definition of

$$I_T = \frac{(T_{sk} - T_\infty)C_l}{Q_S} \qquad [8.34a]$$

$$R_E = \frac{(P_{sk} - P_\infty)}{Q_L} \qquad [8.34b]$$

where C_l is the unit conversion constant = 6.45 cloW/m^2 °C, and the *clo* value is a standard unit for comparing clothing insulation.

External convection coefficients Many researchers have estimated the heat transfer coefficient at the external exposed surface of clothing subject to elevated air velocities (Nishi and Gagge, 1970; Kerslake, 1972; Fonseca and Breckenridge, 1965; Danielsson, 1993). They suggested formulae for calculating the average convective coefficients from the human body for a range of speeds and body postures in the form of

$$h_{c\,(o\text{–air})} = a \cdot \upsilon_{\text{eff}}^{b} \qquad [8.35a]$$

where υ_{eff} is the effective wind velocity in m/s, b is a constant whose value is close to 0.5, and a is a constant evaluated from the characteristic diameter of the whole body, given by Danielsson (1993) as

$$a = 4.8 \times d^{-0.33} \qquad [8.35b]$$

Table 8.1 Internal mean heat and mass transfer film coefficients to the air layer as reported by Lotens (1993), Havenith *et al.* (1990a, 1990b), Danielsson (1993), and Ghaddar *et al.* (2004, 2005b) for highly permeable cotton fabric

Lotens' Data (1993)			Havenith *et al.* (1990a and 1990b), Ensemble A.			
Walking speed (m/s)	Wind speed (m/s)	$h_{m(\text{skin-fabric})}$ (kg/s·m^2·kPa)	Walking speed (m/s)	Wind speed (m/s)	$h_{c(\text{skin-a})}$ (W/m^2·K)	$h_{m(\text{skin-a})}$ (kg/s·m^2·kPa)
0.2	0	7.96×10^{-5}	0.3	0	10.093	6.943×10^{-5}
	0.694	10.69×10^{-5}		0.7	16.39	11.0×10^{-5}
	1.388	12.79×10^{-5}		4.0	31.25	21.9×10^{-5}
0.7	0	9.07×10^{-5}	0.9	0	10.31	7.09×10^{-5}
	0.694	12.68×10^{-5}		0.7	14.925	10.09×10^{-5}
	1.388	13.24×10^{-5}		4.0	38.26	26.3×10^{-5}
Measured heat transport coefficient from the skin to the air layer, Danielsson (1993)						
Walking speed (m/s)			0.9	1.4	1.9	
$h_{c(\text{skin-air})}$ (W/m^{-2}·K): [Leg]			13.7	17.4	19.0	
$h_{c(\text{skin-air})}$ (W/m^{-2}·K): [Trunk]			10.2	13.0	15.1	
$h_{c(\text{skin-air})}$ (W/m^{-2}·K): [Arm]			11.3	15.0	17.2	
Transport coefficient for planner oscillating fabric over planner wet skin, Ghaddar *et al.* (2003)						
f (rpm)			27	37	54	
$h_{m(\text{skin-air})}$ (kg/s·m^2·kPa)			8.0×10^{-5}	8.16×10^{-5}	9.216×10^{-5}	
$h_{c(\text{skin-air})}$ (W/m^2·K)			11.6	11.9	13.265	
Internal transport coefficient for cylindrical fabric and skin geometry, Ghaddar *et al.* (2005b)						
f (rpm)			60	80		
$h_{m(\text{skin-air})}$ (kg/s·m^2·kPa)			6.4×10^{-5}	7.54×10^{-5}		
$h_{c(\text{skin-air})}$ (W/m^2·K)			9.4	11.05		

where d is 0.16 m. Fonseca and Breckenridge (1965) reported that wind increases the heat transfer coefficient of outer clothing ensembles linearly with the square root of the velocity. Their correlation is given by

$$h_{c\,(\text{fabric}-\infty)} = a_1 + b_1\sqrt{\upsilon_{\text{eff}}} \qquad [8.36]$$

where a_1 is due to effective radiation and natural convection and the second term is due to forced convection.

8.3.3 Model extension for fabric–skin contact

The formulation of the periodic microclimate ventilation problem was solved using the 3-D cylinder model of Ghaddar *et al*. (2005b) for closed and open apertures at amplitudes of periodic motion that are greater than the mean spacing of that between the clothing and the skin ($\Delta Y < Y_m$), where the amplitude ratio is smaller than unity ($\zeta < 1$). For amplitude ratios greater or equal to unity ($\Delta Y \geq Y_m$ and $\zeta \geq 1$), the inner cylinder touches the fabric cylinder. Ghaddar *et al.* (2005c) suggested additional modifications on the ventilation model to include the region of contact shown in Fig. 8.3.

Ghaddar *et al*.'s (2005c) model assumed that, when the fabric cylinder is in contact with the solid cylinder (skin) at the top ($\theta = 0°$) or the bottom ($\theta = 180°$), both the fabric and the skin remain in touch at zero velocity for an interval of time until the reversal in motion takes place. The contact is not a point contact and is represented by a length of contact of the fabric spanning about 10° around the cylinder surface at ($\theta = 0°$) or ($\theta = 180°$) due to flattening that takes place in the fabric at the contact area as observed in the experiments.

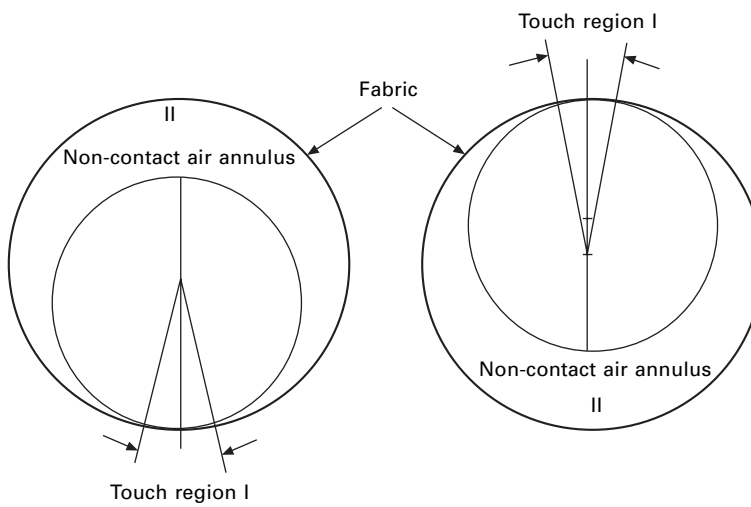

8.3 Fabric–skin contact of Ghaddar *et al*. (2005c) model.

The dimensionless air layer thickness Y' is defined as

$$Y' = \frac{Y(t)}{Y_m} = (1 - \zeta \sin(\omega t)) \qquad [8.37]$$

If $Y' < 0$, then Y' is taken as zero. During the touch period, Y' is frozen to the value of Y' at the time when touch starts in the motion cycle. The modeling of heat and moisture transport covers two regions during contact. The first region is the fabric–skin contact and the second region is a non-contact air layer region that separates the fabric from the skin as shown in Fig. 8.3. During skin fabric contact, the heat and mass transport problem in the fabric of region I is solved as a transient diffusion problem of a thin fabric with one surface suddenly exposed to a step change in temperature. The contact takes place at the skin with both the fabric outer node and the air void temperatures at a lower temperature than the skin surface. The weighted fabric temperature is defined as

$$T_f = \frac{(1 - \varepsilon_f)\rho_s C_s[\gamma T_o + (1 - \gamma)T_i] + \varepsilon_f \rho_a C_a T_v}{(1 - \varepsilon_f)\rho_s C_s + \varepsilon_f \rho_a C_a} \qquad [8.38]$$

where ε_f is the fabric porosity, γ is the mass fraction of the fabric in the outer node, T_i is the fabric inner node temperature, T_o is the fabric outer node temperature, R_i is the fabric inner node regain, and R_o is the fabric outer node regain. The lumping of the fabric inner, outer, and void nodes into one fabric node has permitted the use of the experimentally established properties of the fabric dry and evaporative resistances to estimate the heat and moisture diffusion during the touch period (Jones and McCullough, 1985; McCullough, 1989). The mass and energy balances of the lumped fabric in the contact region yields

$$\frac{\partial R}{\partial t} = \frac{1}{\rho_f e_f} * \left(\frac{(P_{sk} - P_f)}{\frac{R_E}{2} * h_{fg}} + \frac{(P_\infty - P_f)}{\frac{R_E}{2} * h_{fg} + \frac{1}{h_{m(f-\infty)}}} + D_a \left(\frac{1}{R_f^2} \frac{\partial^2 R}{\partial \theta^2} + \frac{\partial^2 R}{\partial x^2} \right) \right) \qquad [8.39a]$$

$$\frac{\partial T_f}{\partial t} = \frac{\partial R}{\partial t} * \frac{h_{ad}}{C_{pf}} + \frac{1}{\rho_f e_f C_{pf}} * \left(\frac{(T_{sk} - T_f)}{\frac{R_D}{2}} + \frac{(T_{\text{atm}} - T_{\text{fabric}})}{\frac{R_D}{2} + \frac{1}{h_r + h_{c(f-\infty)}}} + k_a \left(\frac{1}{R_f^2} \frac{\partial^2 T_f}{\partial \theta^2} + \frac{\partial^2 T_f}{\partial x^2} \right) \right) \qquad [8.39b]$$

where R is the fabric regain (kg of H_2O/kg of fabric), R_D is the fabric dry resistance which is equal to 0.029 m^2·K/W for cotton fabric, R_E *i*s the fabric evaporative resistance equal to 0.0055 m^2·kPa/W for cotton fabric, $h_{c(f\text{-}\infty)}$ and $h_{m(f\text{-}\infty)}$ are the external heat and mass transfer coefficients with the environment, respectively. When the fabric departs from the skin boundary after contact, the fabric inner node, outer node and void space will be in thermal equilibrium at T_f and R.

In the non-contact microclimate air layer region II, the mass and energy balances are given by

Mass balance

$$\frac{\partial}{\partial t}(\rho_a Y w_a) = h_{m(\text{skin–air})}[P_{sk} - P_a] + h_{m(o\text{–air})}[P_o - P_a] + \frac{D}{R_f^2}\frac{\partial}{\partial \theta}\left(Y\frac{\partial w_a}{\partial \theta}\right) + DY\frac{\partial^2 w_a}{\partial x^2} \quad [8.40]$$

Energy balance

$$\begin{aligned}\frac{\partial}{\partial t}[\rho_a Y(C_a T_a + h_{fg} w_a)] &= h_{c(\text{skin–air})}(T_{sk} - T_a) \\ &+ h_{c(o\text{–air})}(T_o - T_a) + H_{m(\text{skin–air})}h_{fg}(P_{sk} - P_a) \\ &+ h_{m(o\text{–air})}h_{fg}(P_o - P_a) + k_a\frac{T_{\text{void}} - T_a}{e_f/2} + Dh_{fg}\frac{P_{\text{void}} - P_a}{e_f/2} \\ &+ \frac{k_a}{R_f^2}\frac{\partial}{\partial \theta}\left(Y\frac{\partial T_a}{\partial \theta}\right) + h_{fg}\frac{D}{R_f^2}\frac{\partial}{\partial \theta}\left(Y\frac{\partial w_a}{\partial \theta}\right) \\ &+ k_a Y\frac{\partial^2 T_a}{\partial x^2} + h_{fg}DY\frac{\partial^2 w_a}{\partial x^2}\end{aligned} \quad [8.41]$$

The terms that appear in the energy balance include convective energy transport to the fabric outer node by conduction and moisture adsorption and conduction and mass diffusion terms in angular and axial directions to both the air layer and the fabric void space. The energy balances on the outer nodes and inner nodes of the fabric remain as previously described. The heat and moisture transfer are assumed to occur by diffusion through the void space air at the node in the fabric where the interface between the contact region and non-contact region occurs. The instantaneous sensible heat loss Q_s and latent heat loss Q_L from the skin during the contact interval are given, respectively, in the touch and the non-touch regions by

$$\textit{Contact region: } Q_s = \frac{T_{sk} - T_f}{R_D/2} \quad [8.42a]$$

$$Q_l = \frac{P_{sk} - P_f}{R_E h_{fg}/2} h_{fg} \quad [8.42b]$$

Non-contact air layer region: $Q_s = h_{c(\text{skin–air})}(T_{sk} - T_a) + h_r(T_{sk} - T_o)$ [8.43a]

$$Q_L = h_{m(\text{skin–air})} h_{fg}(P_{sk} - P_a) \quad [8.43b]$$

The contact model assumes that no wicking is present in the fabric.

8.4 Heat and moisture transport results of the periodic ventilation model

Ghaddar *et al*. (2005) presented results on heat and moisture transport using their 2-D radial and angular flow ventilation model for closed apertures at ambient conditions of 25 °C and 50% RH and at an inner cylinder isothermal skin condition of 35 °C and 100% relative humidity. Simulations were performed for a domain mean spacing Y_m = 26 mm at different frequencies and amplitude ratios for R_f = 6.5 cm and R_s = 3.9 cm. Their numerical simulation results of the model predicted for closed and open aperture the transient steady periodic mass flow rates in the radial and angular directions, the fabric regain, the internal air layer temperature and humidity ratio, the fabric temperature, the skin surface temperature, in addition to the sensible and latent heat losses from the skin.

For a closed aperture cylinder model, Fig. 8.4a,b shows the Ghaddar *et al*. (2005) ventilation model predictions as a function of the amplitude ratio ζ of (a) the time–space-averaged total air flow renewal (kg/m^2) in the microclimate, (b) the time–space-averaged sensible and latent heat loss in W/m^2 at f = 25, 40 and 60 rpm. The air renewal in the microclimate increases with increase of the ventilation frequency and the corresponding sensible and latent heat losses increase with increase in the ventilation frequency. However, at fixed ventilation frequency, the air renewal rate and the total heat loss variation with the amplitude ratio are affected by the fabric–skin contact occurrence during the cycle. The maximum sensible heat loss occurs at ζ = 1 and decreases very slightly with increased contact period within the studied range.

Introducing an aperture induces air renewal in the axial direction through the opening. Figure 8.5 presents (a) the total ventilation rate versus the amplitude ratio at different frequencies of motion; and (b) the time and θ-space-averaged radial flow rate variation in the axial direction at different amplitude ratios for f = 25, 40, and 60 rpm at ζ = 0.8 and ζ = 1.4. The air renewal through the opening increased with amplitude ratio up to ζ = 1, when fabric–skin periodic contact takes place, and then the change in the opening ventilation rate is negligible for ζ >1 (see Fig. 8.5a). At the opening (x = 0), the radial ventilation rate approaches zero and a high gradient of radial flow rate occurs within the first 10% of the opening even when contact

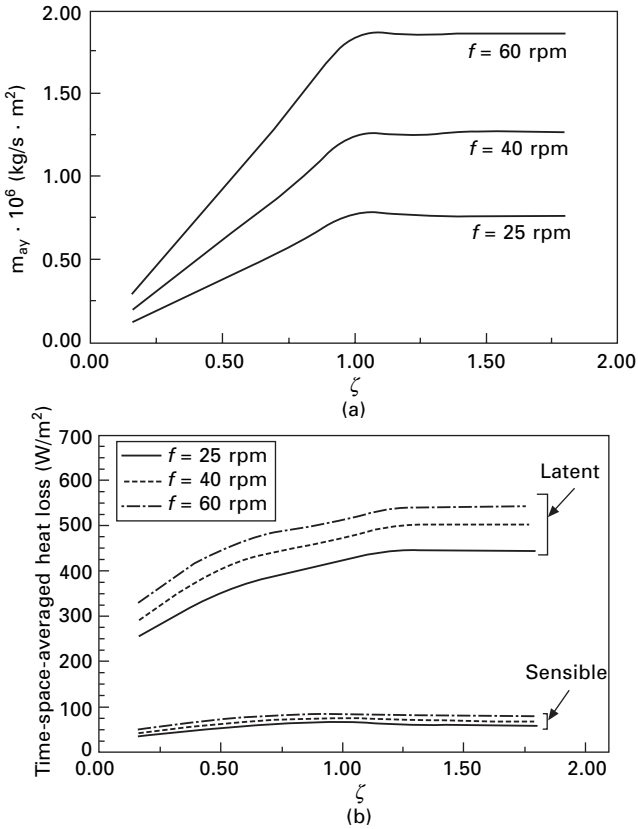

8.4 Ventilation model predictions for a closed aperture as a function of the amplitude ratio ζ of (a) the time–space-averaged total ventilation rate in the microclimate, (b) the time–space-averaged sensible and latent heat loss in W/m^2 at f = 25, 40 and 60 rpm.

is present for $\zeta > 1$. For most of the domain interior, negligible axial flow exists and the radial flow rate is constant. Figure 8.6 shows the variation of the steady periodic time and angular-space-averaged (a) sensible and (b) latent heat loss as a function of the axial position x for the ventilation frequencies of 25, 40, and 60 rpm at $\zeta = 0.8$ and $\zeta = 1.4$. The maximum latent and sensible heat loss takes place at the opening and the enhancement of the local sensible heat loss at the open aperture compared to the closed end is 27.6%, 17.5%, and 15.1% at f = 25, 40, and 60 rpm, respectively. The local latent heat loss at the opening increases by 17.4%, 12.7%, and 11.6% at f = 25, 40, and 60 rpm, respectively when compared with latent loss at the closed end.

The time- and space-averaged sensible and latent heat losses of the open and closed aperture systems reported in Ghaddar *et al.*'s (2005b,c) work are

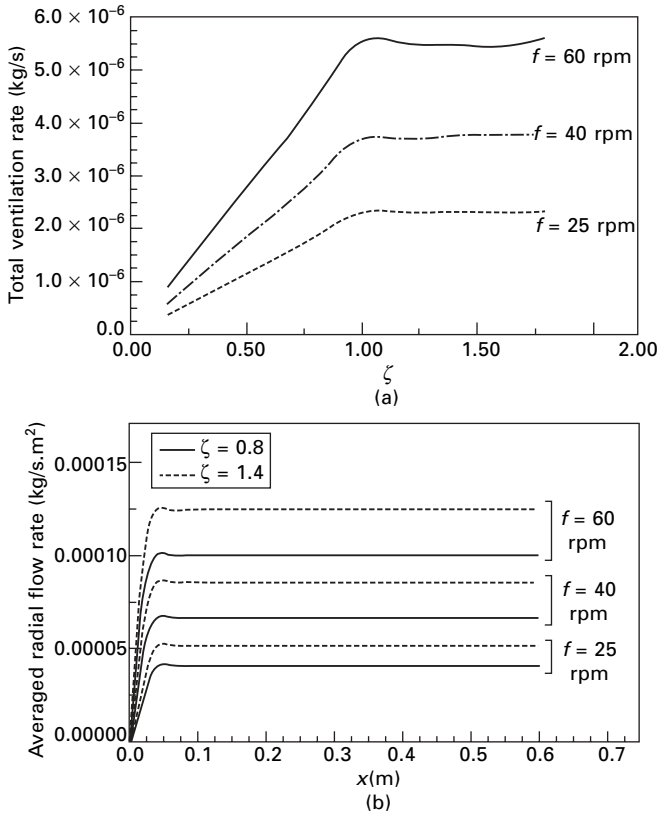

8.5 Plot of (a) the total ventilation rate versus the amplitude ratio at different frequencies of motion; and (b) the time and θ-space-averaged radial flow rate variation in the axial direction at different amplitude ratios for f =25, 40, and 60 rpm at ζ = 0.8 and ζ = 1.4.

summarized in Table 8.2 at $\zeta = 1.4$ and $\zeta = 0.8$ for a domain of length 0.6 m. The presence of the opening has minimal effect on the overall-time and space-averaged heat loss due to the limited size of the region near the opening where substantial axial flow renewal occurs. For an open aperture system at $\zeta = 1.4$, the overall total heat loss is slightly higher than for closed apertures, giving an increase of 4.4%, 2.8%, and 2.2% at f = 25, 40, and 60 rpm, respectively. Comparing the total heat loss for an open aperture system when no fabric–skin contact is present ($\zeta = 0.8$) to the case when periodic contact occurs (ζ =1.4), it is found that the contact increases the heat loss by 9.6%, 8.6%, and 8.5% at f = 25, 40, and 60 rpm, respectively. At higher frequencies, the effect of the opening on the heat loss is reduced.

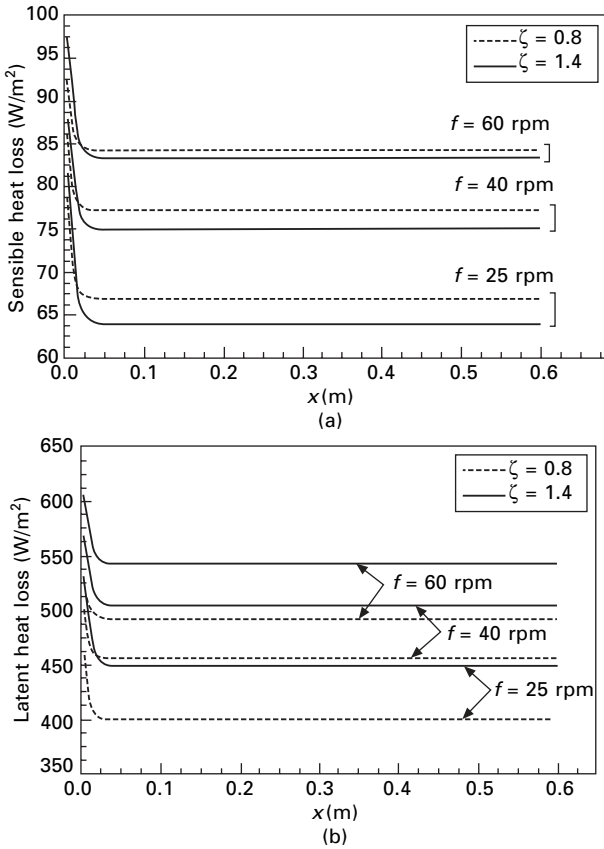

8.6 The variation of the steady periodic time and angular-space-averaged (a) sensible and latent heat loss as a function of the axial position x for the ventilation frequencies of 25, 40, and 60 rpm at $\zeta = 0.8$ and $\zeta = 1.4$.

8.5 Extension of model to real limb motion

The presented model approach for clothing ventilation systems is fundamental in its consideration of the periodic nature of air motion in the trapped layer between skin and fabric from first principles that capture all the physical parameters of the system. The ventilation model of Ghali *et al*. (2002c) and Ghaddar *et al*. (2005b) provides an effective and fast method of providing a solution of ventilation rates at low computational cost. This makes the model attractive for integration with human body thermal models to better predict human response under dynamic conditions. The 3-D motion within the air layer and its interaction with the ambient air through the fabric and the aperture is a complex basic problem. The use of Womersley flow in the axial and angular directions has reduced the complexity of the solution and predicts

Table 8.2 The time–space-averaged sensible and latent heat losses for closed and open aperture systems for $\zeta = 1.4$ and $\zeta = 0.8$

	Sensible heat loss W/m^2		Latent heat loss W/m^2	
Frequency (rpm)	Closed apertures (2-D flow)	Open aperture at $x = 0$ (3-D flow)	Closed apertures (2-D flow)	Open aperture at $x = 0$ (3-D flow)
		$\zeta = 1.4$		
25	61.4	64.2	448.16	450.14
40	72.9	75.04	503.77	505.06
60	81.5	83.31	541.46	543.03
		$\zeta = 0.8$		
25	63.08	67.3	401.1	401.97
40	73.4	77.3	451.1	457.004
60	81.81	84.36	492.25	492.79

realistic mass flow rates through the apertures. In long domains, the effect of the aperture is localized. The model is not computationally exhaustive since two independent 1-D ventilation models in the polar and axial directions are used in addition to a lumped model of the air layer in the radial direction.

The 3-D dynamic ventilation model of the fluctuating airflow in the variable size layer between the fabric and skin can easily be improved to account for rotational (tilting) inner limb motion with respect to the joint within the outer clothing, and the non-uniformity of the inner cylinder. The extension of the model considers variation in the air layer size in the axial direction as well as the angular direction. It should also consider the change in the external pressure around the cylinder due to the combined motion of the fabric and arm. The clothing ventilation model presented in this chapter is flexible, can be used for different conditions and different clothing materials (provided that their physical microscopic properties are known), and can be easily combined with multi-segmented human body models.

8.6 Nomenclature

A_f area of the fabric (m^2)
A_i inner node area in contact with the outer node (m^2)
A_o outer-node exposed surface area to air flow (m^2)
C_a gas concentration in the microclimate measurement location, (m^3 Ar /m^3 air)
C_f fiber specific heat (J/kg K)
C_{in} gas concentration in the distribution system (m^3 Ar /m^3 air)
C_p specific heat of air at constant pressure (J/kg·K)
C_v specific heat of air at constant volume (J/kg·K)
D water vapor diffusion coefficient in air (m^2/s)

e_f fabric thickness (m)
f frequency of oscillation of the inner cylinder in revolution per minute (rpm)
F stride frequency (steps/min)
H height of the human subject (m)
h_{ad} heat of adsorption (J/kg)
H'_{ci} normalized conduction heat transfer coefficient between inner node and outer node (W/m^2·K)
H'_{co} normalized convection heat transfer coefficient between outer node and air flowing through fabric (W/m^2·K)
$h_{c(f-\infty)}$ heat transport coefficient from the fabric to the environment (W/m^2·K).
$h_{c(o\text{-air})}$ heat transport coefficient from the fabric to the trapped air layer (W/m^2·K).
$h_{c(\text{skin-air})}$ heat transport coefficient from the skin to the trapped air layer (W/m^2·K).
h_{fg} heat of vaporization of water (J/kg)
H'_{mi} normalized diffusion mass transfer coefficient between inner node and outer node (kg/m^2·kPa·s)
H'_{mo} normalized mass transport coefficient between outer node and air void in the fabric (kg/m^2·kPa·s)
$h_{m(f-\infty)}$ mass transfer coefficient between the fabric and the environment (kg/m^2·kPa·s)
$h_{m(o\text{-air})}$ mass transfer coefficient between the fabric and the air (kg/m^2·kPa·s)
$h_{m(\text{skin-air})}$ mass transfer coefficient between the skin and the air layer (kg/m^2·kPa·s)
i_m permeability index
k_a thermal conductivity of air (W/m·K)
L fabric length in x-direction (m)
LR Lewis relation, 16.65 K/kPa
$\dot{m}_{ay}$ mass flow rate of air in y-direction (kg/m^2·s)
$\dot{m}_{ax}$ mass flow rate of air in x-direction (kg/m^2·s)
$\dot{m}_{a\theta}$ mass flow rate of air in θ-direction (kg/m^2·s)
$\dot{m}_o$ net flow rate through the open aperture (kg/s)
$\dot{m}_{\text{vent}}$ total ventilation rate (kg/s per m^2 of clothed body surface)
P_a air vapor pressure (kPa)
P_i vapor pressure of water vapor adsorbed in inner node (kPa)
P_o vapor pressure of water vapor adsorbed in outer node (kPa)
P_{sk} vapor pressure of water vapor at the skin (kPa)
P_∞ atmospheric pressure (kPa)
Q heat loss (W/m^2)
R total regain in fabric (kg of adsorbed H_2O/kg fiber)

R_D	fabric dry resistance (m^2·K/W unless specified in the equation per mm of thickness)
R_E	fabric evaporative resistance (m^2·kPa/W)
R_f	fabric cylinder radius (m)
R_s	inner cylinder radius (m)
rpm	revolutions per minute
t	time (s)
T	temperature (°C)
$V_{\text{vent,a}}$	ventilation rate through apertures in $m^3/s \cdot m^2$ of clothed body surface
V_{vent}	ventilation rate through outer fabric in $m^3/s \cdot m^2$ of clothed body surface.
w	humidity ratio (kg of water/kg of air)
Y	instantaneous air layer thickness (m)
Y_m	mean air layer thickness (m)

Greek symbols

ε	fabric emissivity
ρ	density of fabric (kg/m^3)
Φ	periodic dimensionless flow rate parameter in x-direction
ω	angular frequency (rad/s)
Λ_x	pressure gradient parameter in x-direction (Pa·m^2/kg)
Λ_θ	pressure gradient parameter in θ-direction (Pa·m^2/kg)
α	fabric air permeability (m^3/m^2·s)
γ	fraction of mass that is in the outer node
ν	kinematic air viscosity (m^2/s)
υ_{act}	equivalent air velocity of motion
υ_{eff}	effective wind velocity (m/s)
υ_{natl}	wind velocity of natural convection, 0.07 m/s for sitting and 0.11 m/s for standing
υ_{walk}	walking speed (m/s)
υ_{wind}	external wind speed (m/s)
τ	period of the oscillatory motion (s)
θ	angular coordinate
ζ	amplitude ratio
Ψ_{tr}	trace gas mass flux, (m^3/s)

Subscripts

a	conditions of air in the spacing between skin and fabric
i	inner node
o	outer node
L	latent
s	sensible
sk	conditions at the skin surface

void local air inside the void
∞ environment condition.

8.7 References

Acheson D J (1990), *Elementary Fluid Dynamics* (4th edn), Clarendon Press, New York.

Amiri A and Vafai K (1994), 'Analysis of dispersion effects and non-thermal equilibrium, non-Darcian, variable porosity incompressible flow through porous media', *Int. J. Heat Mass Transfer*, **37**, 939–954.

Amiri A and Vafai K (1998), 'Transient analysis of incompressible flow through a packed bed', *Int. J. Heat Mass Transfer, 41*, 4259–4279.

ASHRAE (1997), *ASHRAE Handbook of Fundamentals,* Atlanta, American Society of Heating, Refrigerating and Air-conditioning Engineers, Chapter 5.

ASTM, American Society for Testing and Materials (1983), ASTM D737–75, Standard Test Method for Air Permeability of Textile Fabrics, (IBR) approved 1983.

Danielsson U (1993), *Convection coefficients in clothing air layers*, Doctoral Thesis, The Royal Institute of Technology, Stockholm, Sweden.

Fanger P O (1982), *Thermal comfort analysis and applications in engineering*, New York, McGraw Hill, pp. 156–198.

Farnworth B (1986), 'A numerical model of combined diffusion of heat and water vapor through clothing', *Textile Res J*, **56**, 653–655.

Fonseca G F and Breckenridge J R (1965), 'Wind penetration through fabric systems: Part I', *Textile Res J*, 35, 95–103.

Fourt L and Hollies N (1971). *Clothing: Comfort and Function*, Dekker.

Ghaddar N, Ghali K and Harathani J (2005a), 'Modulated air layer heat and moisture transport by ventilation and diffusion from clothing with open aperture', *ASME Heat Trans J*, **127**, 287–297.

Ghaddar N, Ghali K and Jaroudi E (2005c) 'Heat and moisture transport through the micro-climate air annulus of the clothing–skin system under periodic motion', *Proceedings of the ASME 2005 Summer Heat Transfer Conference*, HT2005-72006, 17–22 July 2005, San Francisco.

Ghaddar N, Ghali K and Jones B (2003), 'Integrated human-clothing system model for estimating the effect of walking on clothing insulation', *Int J Thermal Sci*, **42** (6), 605–619.

Ghaddar N, Ghali K, Harathani J and Jaroudi E (2005b), 'Ventilation rates of micro-climate air annulus of the clothing–skin system under periodic motion', In*t J Heat Mass Trans*, **48** (15), 3151–3166.

Ghali K, Ghaddar N and Harathani J (2004), 'Two-dimensional clothing ventilation model for a walking human', Proc of the First Int Conf on Thermal Eng: Theory a*nd Applications*, ICEA-TF1-03, Beirut-Lebanon, May 31–June 4, 2004.

Ghali K, Ghaddar N and Jones B (2002a), 'Empirical evaluation of convective heat and moisture transport coefficients in porous cotton medium'; *ASME Trans*, *Heat Trans J*, **124** (3), 530–537.

Ghali K, Ghaddar N and Jones B (2002b), 'Multi-layer three-node model of convective transport within cotton fibrous medium', *J Porous Media*, **5** (1), 17–31.

Ghali K, Ghaddar N and Jones B (2002c), 'Modeling of heat and moisture transport by periodic ventilation of thin cotton fibrous media', *Int J Heat Mass Trans*, **45** (18), 3703–3714.

Harter K L, Spivak S L and Vigo T L (1981), 'Applications of the trace gas technique in clothing comfort', *Textile Res J*, **51**, 345–355.

Havenith G, Heus R and Lotens W A (1990a), 'Resultant clothing insulation: a function of body movement, posture, wind clothing fit and ensemble thickness', *Ergonomics*, **33** (1), 67–84.

Havenith G, Heus R and Lotens W A (1990b), 'Clothing ventilation, vapour resistance and permeability index: changes due to posture, movement, and wind', *Ergonomics*, **33** (8), 989–1005.

Hong S (1992), *A database for determining the effect of walking on clothing insulation*. Ph.D. Thesis, Kansas State University, Manhattan, Kansas.

Jones B W and McCullough E A (1985), 'Computer modeling for estimation of clothing insulation', *Proceedings CLIMA 2000, World Congress on Heating, Ventilating, and Air Conditioning*, Copenhagen, Denmark, **4**, 1–5.

Jones B W and Ogawa Y (1993), 'Transient interaction between the human and the thermal environment', *ASHRAE Trans,* **98** (1), 189–195.

Jones B W, Ito M and McCullough E A (1990), 'Transient thermal response systems', *Proceedings International Conference on Environmental* Ergonomics, Austin, TX, 66–67.

Kerslake D McK (1972), The stress of hot environments, Cambridge: Cambridge University Press.

Kuznetsov A V (1993), 'An investigation of a wave temperature difference between solid and fluid phases in porous packed bed', *Int. J. Heat Mass Transfer*, **37**, 3030–3033.

Kuznetsov A V (1997), 'A perturbation solution for heating a rectangular sensible heat storage packed bed with a constant temperature at the walls', *Int. J Heat Mass Transfer*, **40**, 1001–1006.

Kuznetsov A V (1998), 'Thermal non-equilibrium forced convection in porous media', Chapter in '*Transport Phenomena in Porous Media*', D.B. Ingham and I. Pope (Editors), Elsevier, Oxford, 103–129.

Lamoreux L W (1971), 'Kinematic measurements in the study of human walking', *Bulletin Prosthetics Res*, 3–86.

Lee DY and Vafai K (1999), 'Analysis characterization and conceptual assessment of solid and fluid temperature differentials in porous media', *Int. J. Heat Mass Transfer,* **42**, 423–435.

Li Y (1997), Computer modeling for clothing systems, M.S. Thesis, Kansas State University, Manhattan, Kansas.

Lotens W (1993), *Heat transfer from humans wearing clothing*, Doctoral Thesis, TNO Institute for Perception, Soesterberg, The Netherlands.

Lotens W and Havenith G (1988), 'Ventilation of rain water determined by a trace gas method', *Environmental Ergonomics* eds (Mekjavic I B, Bannister B W, Morrison J B) Taylor and Francis, London, 162–176.

McCullough E A, Jones B W and Huck J (1985), 'A comprehensive data base for estimating clothing insulation', *ASHRAE Trans*, **91**, 29–47.

McCullough E A, Jones B W and Tamura T (1989), 'A data base for determining the evaporative resistance of clothing, *ASHRAE Trans,* 95 (2), 316–328.

Mincowycz W J, Haji-Shikh A and Vafai K (1999), 'On departure from local thermal equilibrium in porous media due to a rapidly changing heat source: The Sparrow number', *Int J Heat Mass Trans*, **42**, 3373–3385.

Morris G J (1953), 'Thermal properties of textile materials' *J Textile Inst*, **44**, 449–476.

Morton W E and Hearle J W (1975), *Physical Properties of Textile Fibers*. Heinemann, London.

Nielsen R, Olesen B W and Fanger P O (1985), 'Effect of physical activity and air velocity on the thermal insulation of clothing', *Ergonomics,* **28**, 1617–1632.

Nishi Y and Gagge A P (1970), 'Moisture permeation of clothing – A factor governing thermal equilibrium and comfort', *ASHRAE Trans*, **75**, 137–145.

Rees W H (1941), The transmission of heat through textile fabrics, *J Textile Inst*, 32, 149–165.

Straatman A G, Khayat R E, Haj-Qasem E and Steinman D E (2002), 'On the hydrodynamic stability of pulsatile flow in a plane channel', *Phys Fluids*, **14** (6), 1938–1944.

Vafai K and Sozen M (1990), 'Analysis of energy and momentum transport for fluid flow through a porous bed', *ASME J Heat Transfer*, **112**, 690–699.

Vokac Z, Kopke V and Kuel P (1973), 'Assessment and analysis of the bellow ventilation of clothing', *Text Res J*, 42, 474–482.

Womersley J R (1957), 'An elastic tube theory of pulse transmission and oscillatory flow in mammalian arteries', Aeronautical Research Laboratory, *WADC Technical Report TR*, pp. 56–614.

Woodcock A (1962), 'Moisture Transfer in Textile Systems, Part I', *Textile Res J*, **32**, 628–633.

9

Multiphase flow through porous media

P. GIBSON, U.S. Army Soldier Systems Center, USA

9.1 Introduction

Two decades ago, Whitaker presented a comprehensive theory for mass and energy transport through porous media.[1] This model, with some modifications, is also applicable to fibrous materials. Whitaker modeled the solid portion of the solid matrix as a rigid inert material which participates in the transport process only through its thermal properties. In hygroscopic fibrous materials the diffusion of water into the solid is a significant part of the total transport process. The inclusion of the extra transport terms into and out of the solid fibers necessitates extensive modifications of Whitaker's original derivations.

9.2 Mass and energy transport equations

A typical control volume containing hygroscopic fibers is shown in Fig. 9.1.

A typical porous textile material may be described as a mixture of a solid phase, a liquid phase, and a gaseous phase. The solid phase, σ, consists of the

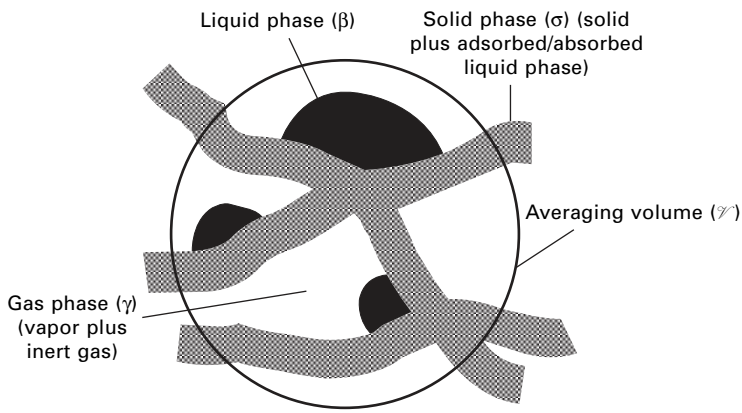

9.1 Representative volume containing fibers, liquid, and gas phases.

solid material (usually a polymer, e.g. wool or cotton) plus any bound water absorbed in the solid matrix. Hence, the solid phase density is dependent on the amount of water contained in the solid phase.

The liquid phase β, consists of the free liquid water which may exist within the porous medium. The liquid phase is a pure component, and its density is assumed to be constant.

The gaseous phase, γ, consists of water vapor plus the non-condensable gas (e.g. air). The gas phase density is a function of temperature, pressure, and vapor concentration.

The general conservation equations are as follows:

Continuity equation:

$$\frac{\partial \rho}{\partial t} + \nabla \cdot (\rho \vec{v}) = 0 \qquad [9.1]$$

Linear momentum equation:

$$\rho \frac{D\vec{v}}{Dt} = \rho \vec{g} + \nabla \cdot \mathsf{T} \qquad [9.2]$$

Energy equation:

$$\rho \frac{Dh}{Dt} = -\nabla \cdot \vec{q} + \frac{Dp}{Dt} + \nabla \vec{v} : \tau + \Phi \qquad [9.3]$$

In keeping with Whitaker's derivation, we will neglect the viscous stress tensor (T).

9.2.1 Point equations

σ-phase – solid

The solid σ-phase is a mixture of the dry solid (polymer) and any liquid or vapor that has dissolved into it or been adsorbed onto its surface. This may also result in a volume change for the solid phase (swelling). Swelling causes a small velocity due to displacement, and it can be accounted for by using the continuity equation:

$$\frac{\partial \rho_\sigma}{\partial t} + \nabla \cdot (\rho_\sigma \vec{v}_\sigma) = 0 \qquad [9.4]$$

and for the two components of liquid (1) and solid (2), the species continuity equation is:

$$\frac{\partial \rho_j}{\partial t} + \nabla \cdot (\rho_j \vec{v}_j) = 0, \quad j = 1, 2, \ldots \qquad [9.5]$$

The σ-phase density is not constant, since it includes the density of the true solid volume fraction plus the density of the liquid volume fraction contained within the solid phase. The species densities are calculated on the basis of the total phase volume. Hence, for the two species system:

$$\rho = \frac{m_1 + m_2}{V_\sigma} = \frac{m_1}{V_\sigma} + \frac{m_2}{V_\sigma} = \rho_1 + \rho_2 \qquad [9.6]$$

It is assumed that the dry density of the solid and the density of the liquid are constant. They are denoted as ρ_S and ρ_L, respectively.

The solid phase can further be divided into the fraction taken up by the liquid, and the fraction taken up by the solid:

$$\varepsilon_{\sigma L} = \frac{\text{Volume of liquid}}{\text{Total } \sigma \text{ phase volume}} \qquad [9.7]$$

The relations between the species densities and the solid and liquid densities are:

$$\rho_\sigma = \varepsilon_{\sigma L}\rho_L + (1 - \varepsilon_{\sigma L})\rho_S = \rho_1 + \rho_2 \qquad [9.8]$$

$$\rho_1 = \varepsilon_{\sigma L}\rho_L \qquad [9.9]$$

$$\rho_2 = (1 - \varepsilon_{\sigma L})\rho_S \qquad [9.10]$$

The density and velocity of the mixture, in terms of the species densities, are given as:

$$\rho_\sigma = \rho_1 + \rho_2 \qquad [9.11]$$

$$\rho_\sigma \vec{v}_\sigma = \rho_1 \vec{v}_1 + \rho_2 \vec{v}_2 \qquad [9.12]$$

or

$$\rho_\sigma = \varepsilon_{\sigma L}\rho_L + (1 - \varepsilon_{\sigma L})\rho_S \qquad [9.13]$$

$$\rho_\sigma \vec{v}_\sigma = \varepsilon_{\sigma L}\rho_L \vec{v}_1 + (1 - \varepsilon_{\sigma L})\rho_S \vec{v}_2 \qquad [9.14]$$

The species velocity is written in terms of the mass average velocity and the diffusion velocity as:

$$\vec{v}_i = \vec{v}_\sigma + \vec{u}_i \qquad [9.15]$$

and therefore, the continuity equation becomes:

$$\frac{\partial \rho_i}{\partial t} + \nabla \cdot (\rho_i \vec{v}_\sigma) = -\nabla \cdot (\rho_i \vec{u}_i), \quad i = 1, 2, 3, \ldots \qquad [9.16]$$

The diffusion flux may be written in terms of a diffusion coefficient as:

$$\rho_i \vec{u}_i = -\rho_\sigma \mathrm{D}_\sigma \nabla\left(\frac{\rho_i}{\rho_\sigma}\right) \qquad [9.17]$$

Hence, the continuity equation may be represented as:

$$\frac{\partial \rho_i}{\partial t} + \nabla \cdot (\rho_i \vec{v}_\sigma) = \nabla \cdot \left\{ \rho_\sigma \mathrm{D}_\sigma \nabla \left(\frac{\rho_i}{\rho_\sigma} \right) \right\}, i = 1, 2, 3, \ldots \quad [9.18]$$

For the purposes of comparing this model to other models developed for heat and mass transfer through porous materials, it will be convenient to rewrite these equations in terms of concentrations of water (component 1) in the solid (component 2).

The concentration of water in the solid (C_s) is defined as:

$$C_s = \frac{\text{Mass of water}}{\text{Mass of the solid phase}} = \frac{m_1}{m_1 + m_2} = \frac{\rho_1}{\rho_\sigma} \quad [9.19]$$

Since liquid water (l) is the only material crossing into or out of the solid phase, it is the most logical basis for the continuity equation:

$$\frac{\partial \rho_1}{\partial t} + \nabla \cdot (\rho_1 \vec{v}_\sigma) = \nabla \cdot \left\{ \rho_\sigma \mathrm{D}_\sigma \nabla \left(\frac{\rho_1}{\rho_\sigma} \right) \right\} \quad [9.20]$$

Depending on the treatment of the solid velocity, one can rewrite this equation a couple of ways. If solid velocity is included, then the continuity equation can be rewritten as:

$$\rho_L \left[\frac{\partial \varepsilon_{\sigma L}}{\partial t} + \nabla \cdot (\varepsilon_{\sigma L} \vec{v}_\sigma) \right] = \nabla \cdot \{ \rho_\sigma \mathrm{D}_{L\sigma} \nabla (C_s) \} \quad [9.21]$$

or

$$\frac{\partial \varepsilon_{\sigma L}}{\partial t} + \nabla \cdot (\varepsilon_{\sigma L} \vec{v}_\sigma)$$

$$= \left(1 - \frac{\rho_S}{\rho_L} \right) \nabla \cdot [\varepsilon_{\sigma L} \mathrm{D}_{L\sigma} \nabla (C_s)] + \frac{\rho_S}{\rho_L} \{ \nabla \cdot [\mathrm{D}_{L\sigma} \nabla (C_s)] \} \quad [9.22]$$

where

$$\rho_1 = \varepsilon_{\sigma L} \rho_L \text{ and } \rho_\sigma = \varepsilon_{\sigma L} \rho_L + (1 + \varepsilon_{\sigma L}) \rho_S \quad [9.23]$$

If solid velocity is neglected, the continuity equation becomes:

$$\frac{\partial \varepsilon_{\sigma L}}{\partial t} = \left(1 - \frac{\rho_S}{\rho_L} \right) \nabla \cdot [\varepsilon_{\sigma L} \mathrm{D}_{L\sigma} \nabla (C_s)] + \frac{\rho_S}{\rho_L} \{ \nabla \cdot [\mathrm{D}_{L\sigma} \nabla (C_s)] \} \quad [9.24]$$

Momentum balance is expressed as:

$$\rho_\sigma \frac{D\vec{v}_\sigma}{Dt} = \rho_\sigma \vec{g} + \nabla \cdot \mathsf{T}_\sigma \Rightarrow \rho_\sigma \left\{ \frac{\partial \vec{v}_\sigma}{\partial t} + (\vec{v}_\sigma \cdot \nabla)\vec{v}_\sigma \right\}$$

$$= \rho_\sigma \vec{g} + \nabla \cdot \mathsf{T}_\sigma \qquad [9.25]$$

Jomaa and Puiggali neglected the convection term,[2] and hence:

$$\rho_\sigma \frac{\partial \vec{v}_\sigma}{\partial t} = \rho_\sigma \vec{g} + \nabla \cdot \mathsf{T}_\sigma \qquad [9.26]$$

There are two ways to address the mass average solid phase velocity. If the thickness of the material under investigation does not change, then the total volume remains constant, and the change in volume of the solid is directly related either to the change in volume of the liquid phase or the change in volume of the gas phase. Another approach is to let the total volume of the material change with time. As the material dries out, and the total mass changes, the thickness of the material will decrease with time, proportional to the water loss. This total volume change with time can be translated into the solid phase velocity. The two situations are illustrated in Fig. 9.2 for a matrix of solid fibers undergoing shrinkage due to water loss.

Initially, the assumption is that the shrinkage behavior is like the first case shown in Fig. 9.2. This means that mass average velocity must be included in the derivations, and that the total material volume (or thickness in one dimension) no longer remains constant.

Jomaa and Puiggali also give an equation for the solid velocity,[2] in terms of the intrinsic phase average (discussed later) as:

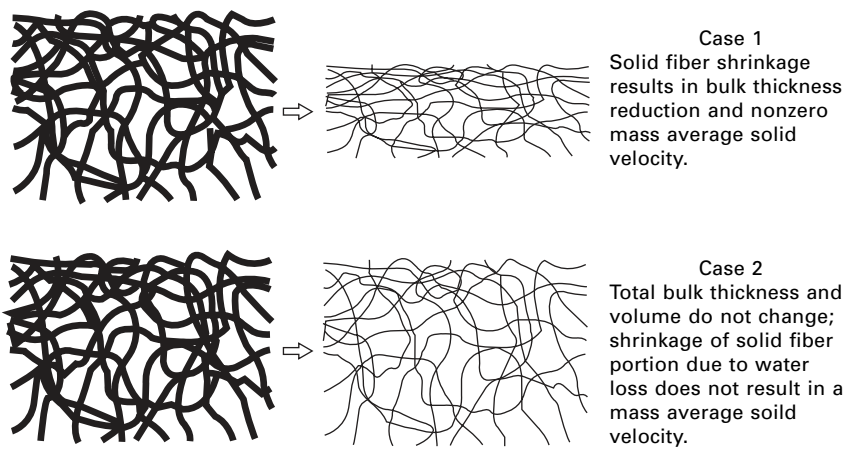

9.2 Two methods of accounting for shrinkage/swelling due to water uptake by a porous solid.

$$\langle v_\sigma \rangle^\sigma = \frac{1}{\langle \rho \rangle^\sigma \xi^{n-1}} \int_0^\xi \frac{\partial}{\partial t} \langle \rho_\sigma \rangle d\xi \qquad [9.27]$$

where ξ is the generalized space coordinate, with the origin at the center of symmetry, and n depends on the geometry ($n = 1$ – plane, $n = 2$ – cylinder, $n = 3$ – sphere) according to the paper by Crapiste *et al.*[3]

The thermal energy equation is:

$$\rho_\sigma \frac{Dh_\sigma}{Dt} = -\nabla \cdot \vec{q}_\sigma + \frac{Dp}{Dt} + \nabla \vec{v}_\sigma : \tau + \Phi_\sigma \qquad [9.28]$$

Some simplifying assumptions can be made at this point by neglecting several effects. For relatively slow flow through porous materials, one can neglect the reversible and irreversible work terms in the thermal energy equation, along with the source term, and expand the material derivative as:

$$\rho_\sigma \frac{Dh_\sigma}{Dt} = \rho_\sigma \left(\frac{\partial h_\sigma}{\partial t} + \vec{v}_\sigma \cdot \nabla h_\sigma \right) = -\nabla \cdot \vec{q}_\sigma \qquad [9.29]$$

It will be assumed that enthalpy is independent of pressure, and is only a function of temperature, and that heat capacity is constant for all the phases. We can replace the enthalpy by: $h = c_p T$ + constant, in the σ-, β-, and γ-phases

The thermal energy equation can be represented as:

$$\rho_\sigma \frac{\partial \{(c_p)_\sigma T_\sigma\}}{\partial t} + \rho_\sigma [\vec{v}_\sigma \cdot \nabla \{(c_p)_\sigma T_\sigma\}] = -\nabla \cdot \vec{q}_\sigma \qquad [9.30]$$

or

$$\rho_\sigma (c_p)_\sigma \left\{ \frac{\partial T_\sigma}{\partial t} + \vec{v}_\sigma \cdot \nabla T_\sigma \right\} = -\nabla \cdot \vec{q}_\sigma \qquad [9.31]$$

Application of Fourier's law yields

$$\rho_\sigma (c_p)_\sigma \left\{ \frac{\partial T_\sigma}{\partial t} + \vec{v}_\sigma \cdot \nabla T_\sigma \right\} = k_\sigma \nabla^2 T_\sigma \qquad [9.32]$$

or, for a multi-component mixture:

$$\rho_\sigma (c_p)_\sigma \left\{ \frac{\partial T_\sigma}{\partial t} + \vec{v}_\sigma \cdot \nabla T_\sigma \right\} = k_\sigma \nabla^2 T - \nabla \cdot \left(\sum_{j=1}^{j=N} \rho_j \bar{u}_j \bar{h}_j \right) \qquad [9.33]$$

where $(c_p)_\sigma = \sum_{j=1}^{j=N} \frac{\rho_j}{\rho_\sigma} (\bar{c}_p)_j$

and the partial mass heat capacity and enthalpies $(\bar{c}_p)_j$, $\bar{h}_j$ are given by the partial molar enthalpy and the partial molar heat capacity divided by the molecular weight of that component.

β-phase – liquid

The continuity equation for the liquid phase is:

$$\frac{\partial \rho_\beta}{\partial t} + \nabla \cdot (\rho_\beta \vec{v}_\beta) = 0 \qquad [9.34]$$

For the thermal energy equation, as was done earlier, compressional work and viscous dissipation are neglected:

$$\frac{Dp}{Dt} = \nabla \vec{v}_\beta : \tau_\beta = \Phi_\beta = 0 \qquad [9.35]$$

This reduces the thermal energy equation to:

$$\rho_\beta \left(\frac{\partial h_\beta}{\partial t} + \vec{v}_\beta \cdot \nabla h_\beta \right) = -\nabla \cdot \vec{q}_\beta \qquad [9.36]$$

Assuming enthalpy only depends on temperature, the thermal energy equation for the liquid phase is:

$$\rho_\beta (c_p)_\beta \left(\frac{\partial T_\beta}{\partial t} + \vec{v}_\beta \cdot \nabla T_\beta \right) = k_\beta \nabla^2 T_\beta \qquad [9.37]$$

The liquid momentum equation will be discussed later in terms of a permeability coefficient which depends on the level of liquid saturation in the porous solid.

γ-phase – gas

The gas phase consists of vapor and an inert component (air). Following the assumptions made by Whitaker[1] for this phase, the equations are as follows: Continuity equation:

$$\frac{\partial \rho_\gamma}{\partial t} + \nabla \cdot (\rho_\gamma \vec{v}_\gamma) = 0 \qquad [9.38]$$

and for the two components of vapor (1) + inert component (2), the species continuity equation is:

$$\frac{\partial \rho_i}{\partial t} + \nabla \cdot (\rho_i \vec{v}_i) = 0, \quad i = 1, 2, ... \qquad [9.39]$$

The density and velocity of the mixture are given as:

$$\rho_\gamma = \rho_1 + \rho_2 \qquad [9.40]$$

$$\rho_\gamma \vec{v}_\gamma = \rho_1 \vec{v}_1 + \rho_2 \vec{v}_2 \qquad [9.41]$$

The species velocity is written in terms of the mass average velocity and the diffusion velocity as:

$$\vec{v}_i = \vec{v}_\gamma + \vec{u}_i \qquad [9.42]$$

Then the continuity equation becomes:

$$\frac{\partial \rho_i}{\partial t} + \nabla \cdot (\rho_i \vec{v}_\gamma) = -\nabla \cdot (\rho_i \vec{u}_i), \quad i = 1, 2, 3, ... \qquad [9.43]$$

The diffusion flux may be written in terms of a diffusion coefficient as:

$$\rho_i \vec{u}_i = -\rho_\gamma D \nabla \left(\frac{\rho_i}{\rho_\gamma} \right) \qquad [9.44]$$

and the continuity equation may be represented as:

$$\frac{\partial \rho_i}{\partial t} + \nabla \cdot (\rho_i \vec{v}_\gamma) = \nabla \cdot \left\{ \rho_\gamma D \nabla \left(\frac{\rho_i}{\rho_\gamma} \right) \right\}, \quad i = 1, 2, 3, ... \qquad [9.45]$$

Due to incompressibility, the time-dependent term may be omitted. However, the vapor portion may change with time due to condensation, evaporation, or sorption/desorption. Thus, for the vapor component of the gas phase (component 1):

$$\frac{\partial \rho_1}{\partial t} + \nabla \cdot (\rho_1 \vec{v}_\gamma) = \nabla \cdot \left\{ \rho_\gamma D \nabla \left(\frac{\rho_1}{\rho_\gamma} \right) \right\} \qquad [9.46]$$

If gas phase convection is neglected (gas is stagnant in the pore spaces), the continuity equation becomes:

$$\frac{\partial \rho_1}{\partial t} = \nabla \cdot \left\{ \rho_\gamma D \nabla \left(\frac{\rho_1}{\rho_r} \right) \right\} \qquad [9.47]$$

The thermal energy equation is given as:

$$\rho_\gamma (c_p)_\gamma \left(\frac{\partial T_\gamma}{\partial t} + \vec{v}_\gamma \cdot \nabla T_\gamma \right) = k_\gamma \nabla^2 T - \nabla \cdot \left(\sum_{i=1}^{i=N} \rho_i \vec{u}_i \bar{h}_i \right) \qquad [9.48]$$

where $(c_p)_\gamma = \sum_{i=1}^{i=N} \frac{\rho_i}{\rho_\gamma} (\bar{c}_p)_i$,

and the partial mass heat capacities and enthalpies $(\bar{c}_p)_i$, $\bar{h}_i$ are again given by the partial molar enthalpy and the partial molar heat capacity divided by the molecular weight of that component.

9.2.2 Boundary conditions

The phase interface boundary conditions derivation must be extensively modified since the assumption of a rigid solid phase with zero velocity is no longer valid. Therefore, expressions describing the boundary conditions for the solid–liquid and solid–vapor interfaces are no longer simple. The conventions and nomenclature for the phase interface boundary conditions are given in Fig. 9.3.

Liquid–gas boundary conditions

The appropriate boundary conditions[1] for the liquid–gas interface are:

$$\rho_\beta h_\beta (\vec{v}_\beta - \vec{w}) \cdot \vec{n}_{\beta\gamma} + \rho_\gamma h_\gamma (\vec{v}_\gamma - \vec{w}) \cdot \vec{n}_{\gamma\beta}$$

$$= -\left\{ \vec{q}_\beta \cdot \vec{n}_{\beta\gamma} + \left[\vec{q}_\gamma + \sum_{i=1}^{i=N} \rho_i \vec{u}_i \bar{h}_i \right] \cdot \vec{n}_{\gamma\beta} \right\} \quad [9.49]$$

and

$$\rho_\beta (\vec{v}_\beta - \vec{w}) \cdot \vec{n}_{\beta\gamma} + \rho_\gamma (\vec{v}_\gamma - \vec{w}) \cdot \vec{n}_{\gamma\beta} = 0 \quad [9.50]$$

Continuous tangent components to the phase interface:

$$\vec{v}_\beta \cdot \vec{\lambda}_{\beta\gamma} = \vec{v}_\gamma \cdot \vec{\lambda}_{\gamma\beta} \quad [9.51]$$

Species jump condition given by:

$$\rho_i (\vec{v}_i - \vec{w}) \cdot \vec{n}_{\gamma\beta} + \rho_\beta (\vec{v}_\beta - \vec{w}) \cdot \vec{n}_{\beta\gamma} = 0, \quad i = 1 \quad [9.52]$$

$$\rho_i (\vec{v}_i - \vec{w}) \cdot \vec{n}_{\gamma\beta} = 0, \quad i = 2, 3, \ldots \quad [9.53]$$

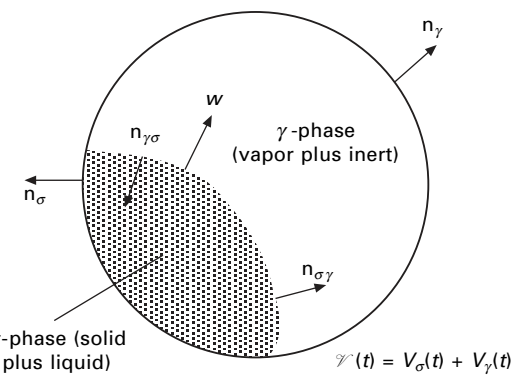

9.3 Typical volume containing a phase interface, with velocities and unit normals indicated. Here, two phases (solid and gas) are shown.

Solid–liquid boundary conditions

The boundary conditions for the solid–liquid interface are in similar form as above except that the phase interface velocity is given by w_2.

$$\rho_\sigma h_\sigma (\vec{v}_\sigma - \vec{w}_2) \cdot \vec{n}_{\sigma\beta} + \rho_\beta h_\beta (\vec{v}_\beta - \vec{w}_2) \cdot \vec{n}_{\beta\sigma} = -\left\{ \vec{q}_\beta \cdot \vec{n}_{\beta\sigma} + \left[\vec{q}_\sigma + \sum_{j=1}^{j=N} \rho_j \vec{u}_j \overline{h}_j \right] \cdot \vec{n}_{\sigma\beta} \right\} \quad [9.54]$$

and

$$\rho_\sigma (\vec{v}_\sigma - \vec{w}_2) \cdot \vec{n}_{\sigma\beta} + \rho_\beta (\vec{v}_\beta - \vec{w}_2) \cdot \vec{n}_{\beta\sigma} = 0 \quad [9.55]$$

Continuous tangent components to the phase interface λ:

$$\vec{v}_\sigma \cdot \vec{\lambda}_{\sigma\beta} = \vec{v}_\beta \cdot \vec{\lambda}_{\beta\sigma} \quad [9.56]$$

Species jump condition given by:

$$\rho_j (\vec{v}_j - \vec{w}_2) \cdot \vec{n}_{\beta\sigma} + \rho_\sigma (\vec{v}_\sigma - \vec{w}_2) \cdot \vec{n}_{\sigma\beta} = 0, \quad J = 1 \quad [9.57]$$

$$\rho_j (\vec{v}_j - \vec{w}_2) \cdot \vec{n}_{\beta\sigma} = 0, \quad j = 2, 3, \ldots \quad [9.58]$$

Solid–gas boundary conditions

The boundary conditions for the solid–liquid interface have different expressions compared to the other interfaces because the interface is between two multi-component phases. The phase interface velocity is given by w_1:

$$\rho_\sigma h_\sigma (\vec{v}_\sigma - \vec{w}_1) \cdot \vec{n}_{\sigma\gamma} + \rho_\gamma h_\gamma (\vec{v}_\gamma - \vec{w}_1) \cdot \vec{n}_{\gamma\sigma} = -\left\{ \left[\vec{q}_\sigma + \sum_{j=1}^{j=N} \rho_j \vec{u}_j \overline{h}_j \right] \cdot \vec{n}_{\sigma\gamma} + \left[\vec{q}_\gamma + \sum_{i=1}^{i=N} \rho_i \vec{u}_i \overline{h}_i \right] \cdot \vec{n}_{\gamma\sigma} \right\} \quad [9.59]$$

and

$$\rho_\sigma (\vec{v}_\sigma - \vec{w}_1) \cdot \vec{n}_{\sigma\gamma} + \rho_\gamma (\vec{v}_\gamma - \vec{w}_1) \cdot \vec{n}_{\gamma\sigma} = 0 \quad [9.61]$$

Continuous tangent components to the phase interface λ:

$$\vec{v}_\sigma \cdot \vec{\lambda}_{\sigma\gamma} = \vec{v}_\gamma \cdot \vec{\lambda}_{\gamma\sigma} \quad [9.61]$$

Species jump condition given by:

$$\rho_j (\vec{v}_j - \vec{w}_1) \cdot \vec{n}_{\sigma\gamma} + \rho_i (\vec{v}_i - \vec{w}_1) \cdot \vec{n}_{\gamma\sigma} = 0, \quad i = 1, \quad j = 1 \quad [9.62]$$

$$\rho_j (\vec{v}_j - \vec{w}_1) \cdot \vec{n}_{\sigma\gamma} = 0, \quad j = 2, 3, \ldots \quad [9.63]$$

$$\rho_j (\vec{v}_j - \vec{w}_1) \cdot \vec{n}_{\sigma\gamma} = 0, \quad i = 2, 3, \ldots \quad [9.64]$$

9.2.3 Volume-averaged equations

The volume-averaging approach outlined by Slattery[4] is applied. In this approach many of the complicated phenomena occurring due to the geometry of the porous material are simplified. Three volume averages are defined. They are:

Spatial average: Average of some function everywhere in the volume:

$$\langle \psi \rangle = \frac{1}{\mathscr{V}} \int_{\mathrm{V}} \psi dV \qquad [9.65]$$

Phase average: Average of some quantity associated solely with each phase:

$$\langle T_\sigma \rangle = \frac{1}{\mathscr{V}} \int_{\mathrm{V}} T_\sigma dV = \frac{1}{\mathscr{V}} \int_{\mathrm{V}_\sigma} T_\sigma dV \qquad [9.66]$$

Intrinsic phase average:

$$\langle T_\sigma \rangle^\sigma = \frac{1}{V_\sigma} \int_{\mathrm{V}} T_\sigma dV = \frac{1}{V_\sigma} \int_{\mathrm{V}_\sigma} T_\sigma dV \qquad [9.67]$$

Volume fractions for the three phases are defined as:

$$\varepsilon_\sigma(t) = \frac{V_\sigma(t)}{\mathrm{V}}, \quad \varepsilon_\beta(t) = \frac{V_\beta(t)}{\mathrm{V}}, \quad \varepsilon_\gamma(t) = \frac{V_\gamma(t)}{\mathrm{V}} \qquad [9.68]$$

The volume and volume fraction of the solid phase changing with time are now changing with time.

It is assumed that the total volume is conserved, or that:

$$\mathrm{V} = V_\sigma(t) + V_\beta(t) + V_\gamma(t) \qquad [9.69]$$

The volume fractions for the three phases are related by:

$$\varepsilon_\sigma(t) + \varepsilon_\beta(t) + \varepsilon_\gamma(t) = 1 \qquad [9.70]$$

and the phase average and the intrinsic phase averages are related as:

$$\varepsilon_\sigma \langle T_\sigma \rangle^\sigma = \langle T_\sigma \rangle \qquad [9.71]$$

Volume average for liquid β*-phase*

We will first examine the volume average for the β-phase. It is complicated because of the three different phase interface velocities which must now be included in the analysis.

The continuity equation for the liquid phase is:

$$\frac{\partial \rho_\beta}{\partial t} + \nabla \cdot (\rho_\beta \vec{v}_\beta) = 0 \qquad [9.72]$$

Integrate over the time-dependent liquid volume within the averaging volume, and divide by the averaging volume to obtain:

$$\frac{1}{\mathrm{V}} \int_{V_{\beta(t)}} \left(\frac{\partial \rho_\beta}{\partial t} \right) dV + \frac{1}{\mathrm{V}} \int_{V_{\beta(t)}} \nabla \cdot (\rho_\beta \vec{v}_\beta) dV = 0 \qquad [9.73]$$

The first term of Equation [9.73] may be taken:

$$\frac{1}{\mathrm{V}} \int_{V_{\beta(t)}} \left(\frac{\partial \rho_\beta}{\partial t} \right) dV \qquad [9.74]$$

and the general transport theorem applied[5]

$$\frac{d}{dt} \int_{V_{(s)}} \psi dV = \int_{V_{(s)}} \frac{\partial \psi}{\partial t} dV + \int_{S_{(s)}} \psi \vec{v}_{(s)} \cdot \vec{n} dS \qquad [9.75]$$

Note that $\Psi = \dfrac{\partial \rho_\beta}{\partial t}$ [9.76]

and using the modified general transport theorem results in:

$$\frac{1}{\mathrm{V}} \int_{V_{\beta(t)}} \left(\frac{\partial \rho_\beta}{\partial t} \right) dV = \frac{d}{dt} \left[\frac{1}{\mathrm{V}} \int_{V_\beta(t)} \rho_\beta dV \right]$$

$$- \frac{1}{\mathrm{V}} \int_{A_{\beta\gamma}} \rho_\beta \vec{w} \cdot \vec{n}_{\beta\gamma} dA - \frac{1}{\mathrm{V}} \int_{A_{\beta\sigma}} \rho_\beta \vec{w}_2 \cdot \vec{n}_{\beta\sigma} dA \qquad [9.77]$$

For the second term,

$$\frac{1}{\mathrm{V}} \int_{V_{\beta(t)}} \nabla \cdot (\rho_\beta \vec{v}_\beta) dV \qquad [9.78]$$

We may use the volume averaging theorem as:

$$\langle \nabla \psi_\beta \rangle = \nabla \langle \psi_\beta \rangle + \frac{1}{\mathrm{V}} \int_{A_{\beta\sigma}} \psi_\beta \vec{n}_{\beta\sigma} dA + \frac{1}{\mathrm{V}} \int_{A_{\beta\gamma}} \psi_\beta \vec{n}_{\beta\gamma} dA \qquad [9.79]$$

to rewrite the term as:

$$\frac{1}{\mathrm{V}} \int_{V_{\beta(t)}} \nabla \cdot (\rho_\beta \vec{v}_\beta) dV = \langle \nabla \cdot (\rho_\beta v_\beta) \rangle = \nabla \cdot \langle \rho_\beta \vec{v}_\beta \rangle$$

$$+ \frac{1}{\mathrm{V}} \int_{A_{\beta\gamma(t)}} \rho_\beta \vec{v}_\beta \cdot \vec{n}_{\beta\gamma} dA + \frac{1}{\mathrm{V}} \int_{A_{\beta\sigma(t)}} \rho_\beta \vec{v}_\beta \cdot \vec{n}_{\beta\sigma} dA \qquad [9.80]$$

noting that:

$$\frac{d}{dt}\left[\frac{1}{\mathrm{V}}\int_{V_\beta(t)}\rho_\beta dV\right] = \frac{d}{dt}\langle\rho_\beta\rangle = \frac{\partial}{\partial t}\langle\rho_\beta\rangle \qquad [9.81]$$

The continuity equation for the liquid phase is rewritten as:

$$\frac{\partial}{\partial t}\langle\rho_\beta\rangle + \nabla\cdot\langle\rho_\beta\vec{v}_\beta\rangle + \frac{1}{\mathrm{V}}\int_{A_{\beta\gamma}}\rho_\beta(\vec{v}_\beta - \vec{w})\cdot\vec{n}_{\beta\gamma}dA$$

$$+\frac{1}{\mathrm{V}}\int_{A_{\beta\sigma}}\rho_\beta(\vec{v}_\beta - \vec{w}_2)\cdot\vec{n}_{\beta\sigma}dA = 0 \qquad [9.82]$$

Liquid density is constant, so that:

$$\langle\rho_\beta\vec{v}_\beta\rangle = \rho_\beta\langle\vec{v}_\beta\rangle \qquad [9.83]$$

$$\langle\rho_\beta\rangle = \varepsilon_\beta\rho_\beta \qquad [9.84]$$

The liquid velocity vector may be used to calculate volumetric flow rates. The flow rate of the liquid phase past a surface area may be expressed by:

$$Q_\beta = \int_A\langle\vec{v}_\beta\rangle\cdot\vec{n}dA \qquad [9.85]$$

The constant-density liquid assumption, Equation [9.84], allows the liquid phase continuity equation to be rewritten as:

$$\frac{\partial\varepsilon_\beta}{\partial t} + \nabla\cdot\langle\vec{v}_\beta\rangle + \frac{1}{\mathrm{V}}\int_{A_{\beta\gamma}}(\vec{v}_\beta - \vec{w})\cdot\vec{n}_{\beta\gamma}dA$$

$$+\frac{1}{\mathrm{V}}\int_{A_{\beta\sigma}}(\vec{v}_\beta - \vec{w}_2)\cdot\vec{n}_{\beta\sigma}dA = 0 \qquad [9.86]$$

The thermal energy equation for the liquid phase was given previously as:

$$\rho_\beta\left(\frac{\partial h_\beta}{\partial t} + \vec{v}_\beta\cdot\nabla h_\beta\right) = -\nabla\cdot\vec{q}_\beta \qquad [9.87]$$

Adding the term $h_\beta\left[\frac{\partial\rho_\beta}{\partial t} + \nabla\cdot(\rho_\beta\vec{v}_\beta)\right]$ to the left hand-side of Equation [9.87] will result in:

$$\frac{\partial}{\partial t}(\rho_\beta h_\beta) + \nabla\cdot(\rho_\beta h_\beta\vec{v}_\beta) = -\nabla\cdot\vec{q}_\beta \qquad [9.88]$$

Following the same procedure used previously for the continuity equation yields the following volume averaged equation:

$$\frac{\partial}{\partial t}(\rho_\beta h_\beta) + \nabla \cdot (\rho_\beta h_\beta \vec{v}_\beta) + \frac{1}{\mathrm{V}} \int_{A_{\beta\gamma}} \rho_\beta h_\beta (\vec{v}_\beta - \vec{w}) \cdot \vec{n}_{\beta\gamma} dA$$

$$+ \frac{1}{\mathrm{V}} \int_{A_{\beta\sigma}} \rho_\beta h_\beta (\vec{v}_\beta - \vec{w}_2) \cdot \vec{n}_{\beta\sigma} dA = -\nabla \cdot \langle \vec{q}_\beta \rangle$$

$$+ \langle \Phi_\beta \rangle - \frac{1}{\mathrm{V}} \int_{A_{\beta\gamma}} \vec{q}_\beta \cdot \vec{n}_{\beta\gamma} dA - \frac{1}{\mathrm{V}} \int_{A_{\beta\sigma}} \vec{q}_\beta \cdot \vec{n}_{\beta\sigma} dA \qquad [9.89]$$

Note that an additional term is present in comparison to Whitaker's equations[1] due to the solid–liquid interface velocity.

The enthalpy of the liquid phase can be expressed as:

$$h_\beta = h_\beta^\circ + (c_p)_\beta (T_\beta - T_\beta^\circ) \qquad [9.90]$$

Accounting for the deviation and dispersion effects from the average properties (marked with a tilde), and writing an expression for the two terms gives:

$$\frac{\partial}{\partial t}\langle \rho_\beta h_\beta \rangle + \nabla \cdot \langle \rho_\beta h_\beta \vec{v}_\beta \rangle = \varepsilon_\beta \rho_\beta (c_p)_\beta \frac{\partial \langle T_\beta \rangle^\beta}{\partial t}$$

$$+ \rho_\beta [h_\beta^\circ + (c_p)_\beta (\langle T_\beta \rangle^\beta - T_\beta^\circ)] \left(\frac{\partial \varepsilon_\beta}{\partial t} + \nabla \cdot \langle \vec{v}_\beta \rangle \right)$$

$$+ \rho_\beta (c_p)_\beta \langle \vec{v}_\beta \rangle \cdot \nabla \langle T_\beta \rangle^\beta + \rho_\beta (c_p)_\beta \nabla \cdot \langle \tilde{T}_\beta \tilde{\vec{v}}_\beta \rangle \qquad [9.91]$$

It is recognized that the term $\left(\frac{\partial \varepsilon_\beta}{\partial t} + \nabla \cdot \langle \vec{v}_\beta \rangle \right)$ is contained in the liquid phase continuity equation, hence:

$$\left(\frac{\partial \varepsilon_\beta}{\partial t} + \nabla \cdot \langle \vec{v}_\beta \rangle \right) + \frac{1}{\mathrm{V}} \int_{A_{\beta\gamma}} (\vec{v}_\beta - \vec{w}) \cdot \vec{n}_{\beta\gamma} dA$$

$$+ \frac{1}{\mathrm{V}} \int_{A_{\beta\sigma}} (\vec{v}_\beta - \vec{w}_2) \cdot \vec{n}_{\beta\sigma} dA = 0 \qquad [9.92]$$

so that:

$$\frac{\partial \varepsilon_\beta}{\partial t} + \nabla \cdot \langle \vec{v}_\beta \rangle$$

$$= -\left\{ \frac{1}{\mathrm{V}} \int_{A_{\beta\gamma}} (\vec{v}_\beta - \vec{w}) \cdot \vec{n}_{\beta\gamma} dA + \frac{1}{\mathrm{V}} \int_{A_{\beta\sigma}} (\vec{v}_\beta - \vec{w}_2) \cdot \vec{n}_{\beta\sigma} dA \right\} \qquad [9.93]$$

The expression for the two terms $\frac{\partial}{\partial t}\langle \rho_\beta h_\beta \rangle + \nabla \cdot \langle \rho_\beta h_\beta \vec{v}_\beta \rangle$ may be written as:

$$\begin{aligned}\frac{\partial}{\partial t}\langle \rho_\beta h_\beta \rangle + \nabla \cdot \langle \rho_\beta h_\beta \vec{v}_\beta \rangle + \rho_\beta (c_p)_\beta \langle \vec{v}_\beta \rangle \cdot \nabla \langle T_\beta \rangle^\beta \\ + \rho_\beta (c_p)_\beta \nabla \cdot \langle \tilde{T}_\beta \tilde{\vec{v}}_\beta \rangle - [h_\beta^\circ + (c_p)_\beta (\langle T_\beta \rangle^\beta - T_\beta^\circ)] \\ \times \left\{ \frac{1}{\mathrm{V}} \int_{A_{\beta\gamma}} \rho_\beta (\vec{v}_\beta - \vec{w}) \cdot \vec{n}_{\beta\gamma} dA \right. \\ \left. + \frac{1}{\mathrm{V}} \int_{A_{\beta\sigma}} \rho_\beta (\vec{v}_\beta - \vec{w}_2) \cdot \vec{n}_{\beta\sigma} dA \right\} \end{aligned} \quad [9.94]$$

Substituting Equation [9.94] back into the thermal energy equation for the liquid phase:

$$\begin{aligned}\varepsilon_\beta \rho_\beta (c_p)_\beta \frac{\partial \langle T_\beta \rangle^\beta}{\partial t} + \rho_\beta (c_p)_\beta \langle \vec{v}_\beta \rangle \cdot \nabla \langle T_\beta \rangle^\beta \\ + \rho_\beta (c_p)_\beta \nabla \cdot \langle \tilde{T}_\beta \tilde{\vec{v}} \rangle \\ + \frac{1}{\mathrm{V}} \int_{A_{\beta\gamma}} \rho_\beta (c_p)_\beta (T_\beta - T_\beta^\circ)(\vec{v}_\beta - \vec{w}) \cdot \vec{n}_{\beta\gamma} dA \\ + \frac{1}{\mathrm{V}} \int_{A_{\beta\sigma}} \rho_\beta (c_p)_\beta (T_\beta - T_\beta^\circ)(\vec{v}_\beta - \vec{w}_2) \cdot \vec{n}_{\beta\sigma} dA \\ - \frac{1}{\mathrm{V}} \int_{A_{\beta\gamma}} \rho_\beta (c_p)_\beta (\langle T_\beta \rangle^\beta - T_\beta^\circ)(\vec{v}_\beta - \vec{w}) \cdot \vec{n}_{\beta\gamma} dA \\ - \frac{1}{\mathrm{V}} \int_{A_{\beta\sigma}} \rho_\beta (c_p)_\beta (\langle T_\beta \rangle^\beta - T_\beta^\circ)(\vec{v}_\beta - \vec{w}_2) \cdot \vec{n}_{\beta\sigma} dA \\ = -\nabla \cdot \langle \vec{q}_\beta \rangle + \langle \Phi_\beta \rangle - \frac{1}{\mathrm{V}} \int_{A_{\beta\gamma}} \vec{q}_\beta \cdot \vec{n}_{\beta\gamma} dA \\ - \frac{1}{\mathrm{V}} \int_{A_{\beta\sigma}} \vec{q}_\beta \cdot \vec{n}_{\beta\sigma} dA \end{aligned} \quad [9.95]$$

Gray's definition of the point functions for a phase property[6] is defined:

$$T_\beta = \langle T_\beta \rangle^\beta + \tilde{T}_\beta \quad [9.96]$$

Therefore, the liquid phase thermal energy equation can be written as:

$$\varepsilon_\beta \rho_\beta (c_p)_\beta \frac{\partial \langle T_\beta \rangle^\beta}{\partial t} + \rho_\beta (c_p)_\beta \langle \vec{v}_\beta \rangle \cdot \nabla \langle T_\beta \rangle^\beta + \rho_\beta (c_p)_\beta \nabla \cdot \langle \tilde{T}_\beta \tilde{\vec{v}} \rangle + \frac{1}{\mathrm{V}} \int_{A_{\beta\gamma}} \rho_\beta (c_p)_\beta \tilde{T}_\beta (\vec{v}_\beta - \vec{w}) \cdot \vec{n}_{\beta\gamma} dA + \frac{1}{\mathrm{V}} \int_{A_{\beta\sigma}} \rho_\beta (c_p)_\beta \tilde{T}_\beta (\vec{v}_\beta - \vec{w}_2) \cdot \vec{n}_{\beta\sigma} dA = -\nabla \cdot \langle \vec{q}_\beta \rangle + \langle \Phi_\beta \rangle - \frac{1}{\mathrm{V}} \int_{A_{\beta\gamma}} \vec{q}_\beta \cdot \vec{n}_{\beta\gamma} dA - \frac{1}{\mathrm{V}} \int_{A_{\beta\sigma}} \vec{q}_\beta \cdot \vec{n}_{\beta\sigma} dA \quad [9.97]$$

Representing the heat flux term $-\nabla \cdot \langle \vec{q}_\beta \rangle$ using Fourier's law ($\vec{q}_\beta = -k_\beta \nabla T_\beta$), and applying the averaging theorem results in:

$$\langle \vec{q}_\beta \rangle = -k_\beta \langle \nabla T_\beta \rangle = -k_\beta \left[\nabla \langle T_\beta \rangle + \frac{1}{\mathrm{V}} \int_{A_{\beta\sigma}} T_\beta \vec{n}_{\beta\sigma} dA + \frac{1}{\mathrm{V}} \int_{A_{\beta\gamma}} T_\beta \vec{n}_{\beta\gamma} dA \right] \quad [9.98]$$

It is relevant to use the intrinsic phase average temperature $\varepsilon_\beta \langle T_\beta \rangle^\beta$ for the temperature field. This leads to:

$$\langle \vec{q}_\beta \rangle = -k_\beta \langle \nabla T_\beta \rangle = -k_\beta \left[\nabla (\varepsilon_\beta \langle T_\beta \rangle^\beta + \frac{1}{\mathrm{V}} \int_{A_{\beta\sigma}} T_\beta \vec{n}_{\beta\sigma} dA + \frac{1}{\mathrm{V}} \int_{A_{\beta\gamma}} T_\beta \vec{n}_{\beta\gamma} dA \right] \quad [9.99]$$

The thermal energy equation for the liquid phase may now be written as:

$$\varepsilon_\beta \rho_\beta (c_p)_\beta \frac{\partial \langle T_\beta \rangle^\beta}{\partial t} + \rho_\beta (c_p)_\beta \langle \vec{v}_\beta \rangle \cdot \nabla \langle T_\beta \rangle^\beta + \rho_\beta (c_p)_\beta \nabla \cdot \langle \tilde{T}_\beta \tilde{\vec{v}}_\beta \rangle + \frac{1}{\mathrm{V}} \int_{A_{\beta\gamma}} \rho_\beta (c_p)_\beta \tilde{T}_\beta (\vec{v}_\beta - \vec{w}) \cdot \vec{n}_{\beta\gamma} dA + \frac{1}{\mathrm{V}} \int_{A_{\beta\gamma}} \rho_\beta (c_p)_\beta \tilde{T}_\beta (\vec{v}_\beta - \vec{w}_2) \cdot \vec{n}_{\beta\sigma} dA = \nabla \cdot \left\{ k_\beta \left[\nabla (\varepsilon_\beta \langle T_\beta \rangle^\beta + \frac{1}{\mathrm{V}} \int_{A_{\beta\sigma}} T_\beta \vec{n}_{\beta\sigma} dA + \frac{1}{\mathrm{V}} \int_{A_{\beta\gamma}} T_\beta \vec{n}_{\beta\gamma} dA \right] \right\} - \frac{1}{\mathrm{V}} \int_{A_{\beta\gamma}} \vec{q}_\beta \cdot \vec{n}_{\beta\gamma} dA - \frac{1}{\mathrm{V}} \int_{A_{\beta\sigma}} \vec{q}_\beta \cdot \vec{n}_{\beta\sigma} dA \quad [9.100]$$

Volume average for gas γ-phase

The gas phase continuity equation is identical, for the most part, to those developed for the solid and liquid phases:

$$\frac{\partial}{\partial t}\langle \rho_\gamma \rangle + \nabla \cdot \langle \rho_\gamma \vec{v}_\gamma \rangle + \frac{1}{\mathrm{V}} \int_{A_{\gamma\beta}} \rho_\gamma (\vec{v}_\gamma - \vec{w}) \cdot \vec{n}_{\gamma\beta} dA$$

$$+ \frac{1}{\mathrm{V}} \int_{A_{\gamma\sigma}} \rho_\gamma (\vec{v}_\gamma - \vec{w}_1) \cdot \vec{n}_{\gamma\sigma} dA = 0 \qquad [9.101]$$

The assumption of constant density for the liquid and solid phases simplified the equations further. However, in the gas phase the density may depend on the temperature and the pressure.

Applying Gray's point functions[6] together with the definition of the intrinsic phase average to the gas phase continuity equation gives:

$$\frac{\partial}{\partial t}(\varepsilon_\gamma \langle \rho_\gamma \rangle^\gamma) + \nabla \cdot (\langle \rho_\gamma \rangle^\gamma \langle \vec{v}_\gamma \rangle) + \nabla \cdot \langle \tilde{\rho}_\gamma \tilde{\vec{v}}_\gamma \rangle$$

$$+ \frac{1}{\mathrm{V}} \int_{A_{\gamma\beta}} \rho_\gamma (\vec{v}_\gamma - \vec{w}) \cdot \vec{n}_{\gamma\beta} dA$$

$$+ \frac{1}{\mathrm{V}} \int_{A_{\gamma\sigma}} \rho_\gamma (\vec{v}_\gamma - \vec{w}_1) \cdot \vec{n}_{\gamma\sigma} dA = 0 \qquad [9.102]$$

The dispersion term in the gas phase can be neglected, hence:

$$\frac{\partial}{\partial t}(\varepsilon_\gamma \langle \rho_\gamma \rangle^\gamma) + \nabla \cdot (\langle \rho_\gamma \rangle^\gamma \langle \vec{v}_\gamma \rangle) + \frac{1}{\mathrm{V}} \int_{A_{\gamma\beta}} \rho_\gamma (\vec{v}_\gamma - \vec{w}) \cdot \vec{n}_{\gamma\beta} dA$$

$$+ \frac{1}{\mathrm{V}} \int_{A_{\gamma\sigma}} \rho_\gamma (\vec{v}_\gamma - \vec{w}_1) \cdot \vec{n}_{\gamma\sigma} dA = 0 \qquad [9.103]$$

Since the gas is a multi-component mixture, in terms of species the continuity equation is:

$$\frac{\partial}{\partial t}\langle \rho_i \rangle + \nabla \cdot \langle \rho_i \vec{v}_i \rangle + \frac{1}{\mathrm{V}} \int_{A_{\gamma\beta}} \rho_i (\vec{v}_i - \vec{w}) \cdot \vec{n}_{\gamma\beta} dA$$

$$+ \frac{1}{\mathrm{V}} \int_{A_{\gamma\sigma}} \rho_i (\vec{v}_i - \vec{w}_1) \cdot \vec{n}_{\gamma\sigma} dA = 0 \quad i = 1, 2, \ldots \qquad [9.104]$$

The final form of the gas phase species continuity equation can be written as:

$$\frac{\partial}{\partial t}(\varepsilon_\gamma \langle \rho_i \rangle^\gamma) + \nabla \cdot (\langle \rho_i \rangle^\gamma \langle \vec{v}_i \rangle)$$

$$+ \frac{1}{\mathrm{V}} \int_{A_{\gamma\beta}} \rho_i (\vec{v}_i - \vec{w}) \cdot \vec{n}_{\gamma\beta} dA + \frac{1}{\mathrm{V}} \int_{A_{\gamma\sigma}} \rho_i (\vec{v}_i - \vec{w}_1) \cdot \vec{n}_{\gamma\sigma} dA \quad [9.105]$$

If only the vapor component (component 1) is considered, the continuity equation can be represented as:

$$\frac{\partial}{\partial t}(\varepsilon_\gamma \langle \rho_1 \rangle^\gamma) + \nabla \cdot (\langle \rho_1 \rangle^\gamma \langle \vec{v}_\gamma \rangle)$$

$$+ \frac{1}{\mathrm{V}} \int_{A_{\gamma\beta}} \rho_1 (\vec{v}_1 - \vec{w}) \cdot \vec{n}_{\gamma\beta} dA = \nabla \cdot \left\{ \langle \rho_\gamma \rangle^\gamma \mathrm{D} \nabla \left(\frac{\rho_1}{\langle \rho_\gamma \rangle^\gamma} \right) \right\} \quad [9.106]$$

The corresponding thermal energy equation for the gas phase may also be written as:

$$\left\{ \sum_{i=1}^{i=N} \langle \rho_p \rangle (c_i)_i \right\} \frac{\partial \langle T_\gamma \rangle^\gamma}{\partial t} + \left\{ \sum_{i=1}^{i=N} (c_p)_i \langle \rho_i \vec{v}_i \rangle \right\} \cdot \nabla \langle T_\gamma \rangle^\gamma$$

$$+ \frac{1}{\mathrm{V}} \int_{A_{\gamma\beta}} \sum_{i=1}^{i=N} \rho_i (c_p)_i \tilde{T}_\gamma (\vec{v}_i - \vec{w}) \cdot \vec{n}_{\gamma\beta} dA$$

$$+ \frac{1}{\mathrm{V}} \int_{A_{\gamma\beta}} \sum_{i=1}^{i=N} \rho_i (c_p)_i \tilde{T}_\gamma (\vec{v}_i - \vec{w}_1) \cdot \vec{n}_{\gamma\sigma} dA$$

$$+ \frac{\partial}{\partial t} \sum_{i=1}^{i=N} (c_p)_i \langle \tilde{\rho}_i \tilde{T}_\gamma \rangle + \nabla \cdot \sum_{i=1}^{i=N} (c_p)_i \langle \tilde{\rho}_i \tilde{\vec{v}}_i \tilde{T}_\gamma \rangle$$

$$= \nabla \cdot \left\{ k_\gamma \left[\nabla (\varepsilon_\gamma \langle T_\gamma \rangle^\gamma) + \frac{1}{\mathrm{V}} \int_{A_{\gamma\alpha}} T_\gamma \vec{n}_{\gamma\sigma} dA \right. \right.$$

$$\left. \left. + \frac{1}{\mathrm{V}} \int_{A_{\gamma\beta}} T_\gamma \vec{n}_{\gamma\beta} dA \right) \right\} - \frac{1}{\mathrm{V}} \int_{A_{\gamma\sigma}} \vec{q}_\gamma \cdot \vec{n}_{\gamma\sigma} dA$$

$$- \frac{1}{\mathrm{V}} \int_{A_{\gamma\beta}} \vec{q}_\gamma \cdot \vec{n}_{\gamma\beta} dA \quad [9.107]$$

Volume average for solid σ-phase

The volume averaging procedure for the liquid phase was made general enough so that the same equations are applicable to the solid phase. The

differences are in the interface velocities; w_2 is for the solid–liquid interface, and w_1 is for the solid–gas interface. Also the species continuity must be accounted for. Since the two components (the liquid and the solid) are assumed to have a constant density, the complications which arose in the gas phase continuity equation will not be encountered here. The appropriate subscripts for the solid phase will be added to the equations.

The solid phase density cannot be assumed constant, since this phase is a mixture of the solid and the liquid components and their proportions can change. However, the expressions are less complicated than the gas phase density since it is assumed that each component's density is constant.

The solid phase continuity equation is:

$$\frac{\partial}{\partial t}\langle \rho_\sigma \rangle + \nabla \cdot \langle \rho_\sigma \vec{v}_\sigma \rangle + \frac{1}{\mathrm{V}} \int_{A_{\sigma\gamma}} (\vec{v}_\sigma - \vec{w}_1) \cdot \vec{n}_{\sigma\gamma}\, dA + \frac{1}{\mathrm{V}} \int_{A_{\sigma\beta}} (\vec{v}_\sigma - \vec{w}_2) \cdot \vec{n}_{\sigma\beta}\, dA = 0 \qquad [9.108]$$

and the species continuity equation is:

$$\frac{\partial}{\partial t}\langle \rho_j \rangle + \nabla \cdot \langle \rho_j \vec{v}_j \rangle + \frac{1}{\mathrm{V}} \int_{A_{\sigma\gamma}} (\vec{v}_j - \vec{w}_1) \cdot \vec{n}_{\sigma\gamma}\, dA + \frac{1}{\mathrm{V}} \int_{A_{\sigma\beta}} (\vec{v}_j - \vec{w}_2) \cdot \vec{n}_{\sigma\beta}\, dA = 0 \quad j = 1, 2, \ldots \qquad [9.109]$$

The same derivation used for the gas phase can be followed, then:

$$\frac{\partial}{\partial t}(\varepsilon_\sigma \langle \rho_\sigma \rangle^\sigma) + \nabla \cdot (\langle \rho_\sigma \rangle^\sigma \langle \vec{v}_\sigma \rangle) + \frac{1}{\mathrm{V}} \int_{A_{\sigma\beta}} \rho_\sigma (\vec{v}_\sigma - \vec{w}_2) \cdot \vec{n}_{\sigma\beta}\, dA + \frac{1}{\mathrm{V}} \int_{A_{\sigma\gamma}} \rho_\sigma (\vec{v}_\sigma - \vec{w}_1) \cdot \vec{n}_{\sigma\gamma}\, dA = 0 \qquad [9.110]$$

and the final form of the solid phase species continuity equation is:

$$\frac{\partial}{\partial t}(\varepsilon_\sigma \langle \rho_j \rangle^\sigma) + \nabla \cdot (\langle \rho_j \rangle^\sigma \langle \vec{v}_j \rangle) + \frac{1}{\mathrm{V}} \int_{A_{\sigma\beta}} \rho_j (\vec{v}_j - \vec{w}_2) \cdot \vec{n}_{\sigma\beta}\, dA + \frac{1}{V} \int_{A_{\sigma\gamma}} \rho_j (\vec{v}_j - \vec{w}_1) \cdot \vec{n}_{\sigma\gamma}\, dA = \nabla \cdot \left\{ \langle \rho_\sigma \rangle^\sigma \mathrm{D}_\sigma \left[\nabla \left(\frac{\rho_j}{\langle \rho_\sigma \rangle^\sigma} \right) \right] - \langle \tilde{\rho}_j \tilde{\vec{v}}_j \rangle \right\} \quad j = 1, 2, \ldots \qquad [9.111]$$

If one needs to track the liquid component (component 1) only, the continuity equation may be expressed as:

$$\frac{\partial}{\partial t}(\varepsilon_\sigma \langle \rho_1 \rangle^\sigma) + \nabla \cdot (\langle \rho_1 \rangle^\sigma \langle \vec{v}_1 \rangle) + \frac{1}{\mathrm{V}} \int_{A_{\sigma\beta}} \rho_j (\vec{v}_j - \vec{w}_2) \cdot \vec{n}_{\sigma\beta} dA$$

$$+ \frac{1}{\mathrm{V}} \int_{A_{\sigma\gamma}} \rho (\vec{v}_1 - \vec{w}_1) \cdot \vec{n}_{\sigma\beta} dA$$

$$= \nabla \cdot \left\{ \langle \rho_\sigma \rangle^\sigma \mathrm{D}_\sigma \nabla \left(\frac{\rho_1}{\langle \rho_\sigma \rangle^\sigma} \right) \right\} \qquad [9.112]$$

Furthermore, if the solid velocity is considered to be zero, the solid phase continuity equation may be presented as:

$$\frac{\partial}{\partial t}(\varepsilon_\sigma \langle \rho_1 \rangle^\sigma) + \frac{1}{\mathrm{V}} \int_{A_{\sigma\beta}} \rho_1 (\vec{v}_1 - \vec{w}_2) \cdot \vec{n}_{\sigma\beta} dA$$

$$+ \frac{1}{\mathrm{V}} \int_{A_{\sigma\gamma}} \rho_1 (\vec{v}_1 - \vec{w}_1) \cdot \vec{n}_{\sigma\gamma} dA = \nabla \cdot \left\{ \langle \rho_\sigma \rangle^\sigma \mathrm{D}_\sigma \nabla \left(\frac{\rho_1}{\langle \rho_\sigma \rangle^\sigma} \right) \right\} \qquad [9.113]$$

The corresponding energy equation for the solid phase can be written as:

$$\left\{ \sum_{j=1}^{j=N} \langle \rho_j \rangle (c_p)_j \right\} \frac{\partial \langle T_\sigma \rangle^\sigma}{\partial t} + \left\{ \sum_{j=1}^{j=N} (c_p)_j \langle \rho_j \vec{v}_j \rangle \right\} \cdot \nabla \langle T_\sigma \rangle^\sigma$$

$$+ \frac{1}{\mathrm{V}} \int_{A_{\sigma\beta}} \sum_{j=1}^{j=N} \rho_j (c_p)_j \tilde{T}_\sigma (\vec{v}_j - \vec{w}_2) \cdot \vec{n}_{\sigma\beta} dA$$

$$+ \frac{1}{\mathrm{V}} \int_{A_{\sigma\gamma}} \sum_{j=1}^{j=N} \rho_j (c_p)_j \tilde{T}_\sigma (\vec{v}_j - \vec{w}_1) \cdot \vec{n}_{\sigma\gamma} dA$$

$$+ \frac{\partial}{\partial t} \sum_{j=1}^{j=N} (c_p)_j \langle \tilde{\rho}_j \tilde{T}_\sigma \rangle + \nabla \cdot \sum_{j=1}^{j=N} (c_p)_j \langle \tilde{\rho}_j \tilde{\vec{v}}_j \tilde{T}_\sigma \rangle$$

$$= \nabla \cdot \left\{ k_\sigma \left[\nabla (\varepsilon_\sigma \langle T_\sigma \rangle^\sigma) + \frac{1}{\mathrm{V}} \int_{A_{\sigma\gamma}} T_\sigma \vec{n}_{\sigma\gamma} dA \right. \right.$$

$$\left. \left. + \frac{1}{\mathrm{V}} \int_{A_{\sigma\beta}} T_\sigma \vec{n}_{\sigma\beta} dA \right] \right\} - \frac{1}{\mathrm{V}} \int_{A_{\sigma\gamma}} \vec{q}_\sigma \cdot \vec{n}_{\sigma\gamma} dA$$

$$- \frac{1}{\mathrm{V}} \int_{A_{\sigma\beta}} \vec{q}_\sigma \cdot \vec{n}_{\sigma\beta} dA \qquad [9.114]$$

The continuity and thermal energy equations have been volume averaged for all three phases. The various continuity equations are given in several forms. They cover conditions such as non-zero solid velocity or tracing only the liquid component.

9.3 Total thermal energy equation

The three phases are assumed to be in local thermal equilibrium so that:

$$\langle T_\sigma \rangle^\sigma = \langle T_\beta \rangle^\beta = \langle T_\gamma \rangle^\gamma = \langle T \rangle \quad [9.115]$$

$$\langle T \rangle \equiv \varepsilon_\sigma \langle T_\sigma \rangle^\sigma + \varepsilon_\beta \langle T_\beta \rangle^\beta + \varepsilon_\gamma \langle T_\gamma \rangle^\gamma = \langle T_\sigma \rangle^\sigma = \langle T_\beta \rangle^\beta = \langle T_\gamma \rangle^\gamma \quad [9.116]$$

Applying the equilibrium condition, the three individual phase equations can be added to present a single energy equation. Except for the addition of extra terms due to the solid–gas and solid–liquid phase interface velocities, this equation is similar to that derived by Whitaker.[1] The equation is written in positive flux terms, i.e. liquid is evaporating into the gas phase, rather than condensing.

$$\left[\varepsilon_\sigma \left\{ \sum_{j=1}^{j=N} \langle \rho_j \rangle (c_p)_j \right\} + \varepsilon_\beta \rho_\beta (c_p)_\beta + \varepsilon_\gamma \left\{ \sum_{i=1}^{i=N} \langle \rho_i \rangle (c_p)_i \right\} \right] \frac{\partial \langle T \rangle}{\partial t}$$

$$+ \left[\sum_{j=1}^{j=N} (c_p)_j \langle \rho_j \vec{v}_j \rangle + \rho_\beta (c_p)_\beta \langle \vec{v}_\beta \rangle + \sum_{i=1}^{j=N} (c_p)_i \langle \rho_i \vec{v} \rangle \right] \cdot \nabla \langle T \rangle$$

$$+ \frac{1}{V} \int_{A_{\sigma\gamma}} \sum_{j=1}^{j=N} \rho_j (c_p)_j \tilde{T}_\sigma (\vec{v}_\sigma - \vec{w}_1) \cdot \vec{n}_{\sigma\gamma} dA$$

$$+ \frac{1}{V} \int_{A_{\gamma\sigma}} \sum_{i=1}^{j=N} \rho_j (c_p)_i \tilde{T}_\gamma (\vec{v}_i - \vec{w}_1) \cdot \vec{n}_{\gamma\sigma} dA$$

$$+ \frac{1}{V} \int_{A_{\sigma\beta}} \sum_{j=1}^{j=N} \rho_j (c_p)_j \tilde{T}_\sigma (\vec{v}_\sigma - \vec{w}_2) \cdot \vec{n}_{\sigma\beta} dA$$

$$+ \frac{1}{V} \int_{A_{\beta\sigma}} \rho_\beta (c_p)_\beta \tilde{T}_\beta (\vec{v}_\beta - \vec{w}_2) \cdot \vec{n}_{\beta\sigma} dA$$

$$+ \frac{1}{V} \int_{A_{\beta\gamma}} \rho_\beta (c_p)_\beta \tilde{T}_\beta (\vec{v}_\beta - \vec{w}) \cdot \vec{n}_{\beta\gamma} dA$$

$$+ \frac{1}{V} \int_{A_{\gamma\beta}} \sum_{i=1}^{i=N} \rho_i (c_p)_i \tilde{T}_\gamma (\vec{v}_i - \vec{w}) \cdot \vec{n}_{\gamma\beta} dA$$

$$= \nabla \cdot \left\{ \begin{array}{l} \nabla[(k_\sigma \varepsilon_\sigma + k_\beta \varepsilon_\beta + k_\gamma \varepsilon_\gamma)\langle T \rangle \\ +(k_\sigma - k_\beta)\frac{1}{\mathrm{V}} \int_{A_{\sigma\beta}} T_\sigma \vec{n}_{\sigma\beta} dA \\ +(k_\beta - k_\gamma)\frac{1}{\mathrm{V}} \int_{A_{\beta\gamma}} T_\beta \vec{n}_{\beta\gamma} dA \\ +(k_\sigma - k_\gamma)\frac{1}{\mathrm{V}} \int_{A_{\sigma\gamma}} T_\gamma \vec{n}_{\sigma\gamma} dA \end{array} \right\}$$

$$- \frac{1}{\mathrm{V}} \int_{A_{\sigma\beta}} \vec{q}_\sigma \cdot \vec{n}_{\sigma\beta} dA - \frac{1}{\mathrm{V}} \int_{A_{\beta\gamma}} \vec{q}_\sigma \cdot \vec{n}_{\beta\gamma} dA$$

$$+ \frac{1}{\mathrm{V}} \int_{A_{\gamma\sigma}} \vec{q}_\gamma \cdot \vec{n}_{\sigma\gamma} dA \qquad [9.117]$$

where the averaged density is obtained from:

$$\langle \rho \rangle = \varepsilon_\sigma \sum_{j=1}^{j=N} \langle \rho_j \rangle^\sigma + \varepsilon_\beta \langle \rho_\beta \rangle^\beta + \varepsilon_\gamma \sum_{i=1}^{i=N} \langle \rho_i \rangle^\gamma \qquad [9.118]$$

and a mass fraction weighted average heat capacity by:

$$C_p = \frac{\varepsilon_\sigma \sum_{j=1}^{j=N} \langle \rho_j \rangle^\sigma (c_p)_j + \varepsilon_\beta \rho_\beta (c_p)_\beta + \varepsilon_\gamma \sum_{i=1}^{i=N} \langle \rho_i \rangle^\gamma (c_p)_i}{\langle \rho \rangle} \qquad [9.119]$$

Equations [9.118] and [9.119] allow the first term in the thermal energy equation to be written as:

$$\left[\varepsilon_\sigma \left[\sum_{j=1}^{j=N} \langle \rho_j \rangle (c_p)_j \right] + \varepsilon_\beta \rho_\beta (c_p)_\beta + \varepsilon_\gamma \left\{ \sum_{i=1}^{i=N} \langle \rho_i \rangle (c_p)_i \right\} \right] \frac{\partial \langle T \rangle}{\partial t}$$

$$= \langle \rho \rangle C_p \frac{\partial \langle T \rangle}{\partial t} \qquad [9.120]$$

Then the interphase flux terms in the total thermal energy equation must be considered. Interphase flux terms must include the exchange of mass between the liquid and the gas, between the liquid and the solid, and between the gas and the solid.

First the derivation for the liquid–gas interface is presented, and then the other two interfaces are treated.

The jump boundary condition for the liquid–gas interface was shown previously to be:

$$\rho_\beta h_\beta (\vec{v}_\beta - \vec{w}) \cdot \vec{n}_{\beta\gamma} + \rho_\gamma h_\gamma (\vec{v}_\gamma - \vec{w}) \cdot \vec{n}_{\gamma\beta}$$

$$= - \left\{ \vec{q}_\beta \cdot \vec{n}_{\beta\gamma} + \left[\vec{q}_\gamma + \sum_{i=1}^{i=N} \rho_i \vec{u}_i \overline{h}_i \right] \cdot \vec{n}_{\gamma\beta} \right\} \qquad [9.121]$$

It may be rewritten as:

$$\rho_\beta h_\beta(\vec{v}_\beta - \vec{w}) \cdot \vec{n}_{\beta\gamma} + \sum_{i=1}^{i=N} \rho_i \overline{h}_i(\vec{v}_i - \vec{w}) \cdot \vec{n}_{\gamma\beta} = -(\vec{q}_\beta - \vec{q}_\gamma) \cdot \vec{n}_{\beta\gamma} \quad [9.122]$$

The jump boundary condition for the solid–gas interface was expressed previously as:

$$\rho_\sigma h_\sigma (\vec{v}_\sigma - \vec{w}_1) \cdot \vec{n}_{\sigma\gamma} + \rho_\gamma h_\gamma (\vec{v}_\gamma - \vec{w}_1) \cdot \vec{n}_{\gamma\sigma}$$

$$= -\left\{ \left[\vec{q}_\sigma + \sum_{j=1}^{j=N} \rho_j \vec{u}_j \overline{h}_j \right] \cdot \vec{n}_{\sigma\gamma} + \left[\vec{q}_\gamma + \sum_{i=1}^{i=N} \rho_i \vec{u}_i \overline{h}_i \right] \cdot \vec{n}_{\gamma\sigma} \right\} \quad [9.123]$$

and this may be represented as:

$$\sum_{j=1}^{j=N} \rho_j \overline{h}_j (\vec{v}_j - \vec{w}_1) \cdot \vec{n}_{\sigma\gamma} + \sum_{i=1}^{i=N} \rho_i \overline{h}_i (\vec{v}_i - \vec{w}_1) \cdot \vec{n}_{\gamma\sigma}$$

$$= -(\vec{q}_\sigma - \vec{q}_\gamma) \cdot \vec{n}_{\sigma\gamma} \quad [1.124]$$

The jump boundary condition for the solid–liquid interface was given previously as:

$$\rho_\sigma h_\sigma (\vec{v}_\sigma - \vec{w}_2) \cdot \vec{n}_{\sigma\beta} + \rho_\beta h_\beta (\vec{v}_\beta - \vec{w}_2) \cdot \vec{n}_{\beta\sigma}$$

$$= -\left\{ \vec{q}_\beta \cdot \vec{n}_{\beta\sigma} + \left[\vec{q}_\sigma + \sum_{j=1}^{j=N} \rho_j \vec{u}_j \overline{h}_j \right] \cdot \vec{n}_{\sigma\beta} \right\} \quad [9.125]$$

and may be rewritten as:

$$\sum_{j=1}^{j=N} \rho_j \overline{h}_j (\vec{v}_j - \vec{w}_2) \cdot \vec{n}_{\sigma\beta} + \rho_\beta h_\beta (\vec{v}_\beta - \vec{w}_2) \cdot \vec{n}_{\beta\sigma}$$

$$= -(\vec{q}_\sigma - \vec{q}_\beta) \cdot \vec{n}_{\sigma\beta} \quad [9.126]$$

Using Equations [9.122], [9.124] and [9.126], we may write the interphase flux terms in the total thermal energy equation as:

$$-\frac{1}{V} \int_{A_{\sigma\beta}} (\vec{q}_\sigma - \vec{q}_\beta) \cdot \vec{n}_{\sigma\beta} dA - \frac{1}{V} \int_{A_{\beta\gamma}} (\vec{q}_\beta - \vec{q}_\gamma) \cdot \vec{n}_{\beta\gamma} dA$$

$$-\frac{1}{V} \int_{A_{\gamma\sigma}} (\vec{q}_\sigma - \vec{q}_\gamma) \cdot \vec{n}_{\sigma\gamma} dA$$

$$= + \frac{1}{\mathrm{V}} \int_{A_{\sigma\beta}} \left[\sum_{j=1}^{j=N} \rho_j \bar{h}_j (\vec{v}_j - \vec{w}_2) \cdot \vec{n}_{\sigma\beta} + \rho_\beta h_\beta (\vec{v}_\beta - \vec{w}_2) \cdot \vec{n}_{\beta\sigma} \right] dA$$

$$+ \frac{1}{\mathrm{V}} \int_{A_{\beta\gamma}} \left[\rho_\beta h_\beta (\vec{v}_\beta - \vec{w}) \cdot \vec{n}_{\beta\gamma} + \sum_{i=1}^{i=N} \rho_i \bar{h}_i (\vec{v}_i - \vec{w}) \cdot \vec{n}_{\gamma\beta} \right] dA$$

$$+ \frac{1}{\mathrm{V}} \int_{A_{\sigma\gamma}} \left[\sum_{j=1}^{j=N} \rho_i \bar{h}_i (\vec{v}_j - \vec{w}_1) \cdot \vec{n}_{\sigma\gamma} + \sum_{i=1}^{i=N} \rho_i \bar{h}_i (\vec{v}_i - \vec{w}_1) \cdot \vec{n}_{\gamma\sigma} \right] dA \qquad [9.127]$$

The total thermal energy equation is now written as:

$$\langle \rho \rangle C_p \frac{\partial \langle T \rangle}{\partial t}$$

$$+ \left[\sum_{j=1}^{j=N} (c_p)_j \langle \rho_j \vec{v}_j \rangle + \rho_\beta (c_p)_\beta \langle \vec{v}_\beta \rangle + \sum_{i=1}^{i=N} (c_p)_i \langle \rho_i \vec{v}_i \rangle \right] \cdot \nabla \langle T \rangle$$

$$- \frac{1}{\mathrm{V}} \int_{A_{\sigma\beta}} \left\{ \begin{array}{l} \sum_{j=1}^{j=N} \rho_j [\bar{h}_j - (c_p)_j \tilde{T}_\sigma] (\vec{v}_j - \vec{w}_2) \cdot \vec{n}_{\sigma\beta} \\ + \rho_\beta [h_\beta - (c_p)_\beta \tilde{T}_\beta] (\vec{v}_\beta - \vec{w}_\beta) \cdot \vec{n}_{\beta\sigma} \end{array} \right\} dA$$

$$- \frac{1}{\mathrm{V}} \int_{A_{\beta\gamma}} \left\{ \begin{array}{l} \rho_\beta [h_\beta - (c_p)_\beta \tilde{T}_\beta] (\vec{v}_\beta - \vec{w}_\beta) \cdot \vec{n}_{\beta\gamma} \\ + \sum_{i=1}^{i=N} \rho_i [\bar{h}_i - (c_p)_i \tilde{T}_\gamma] (\vec{v}_i - \vec{w}) \cdot \vec{n}_{\gamma\beta} \end{array} \right\} dA$$

$$- \frac{1}{\mathrm{V}} \int_{A_{\sigma\gamma}} \left\{ \begin{array}{l} \sum_{j=1}^{j=n} \rho_j [\bar{h}_j - (c_p)_j \tilde{T}_\sigma] (\vec{v}_j - \vec{w}_1) \cdot \vec{n}_{\sigma\gamma} \\ + \sum_{i=1}^{i=N} \rho_i [\bar{h}_i - (c_p)_i \tilde{T}_\gamma] (\vec{v}_i - \vec{w}_1) \cdot \vec{n}_{\gamma\sigma} \end{array} \right\} dA$$

$$= \nabla \cdot \left\{ \begin{array}{l} \nabla [(k_\sigma \varepsilon_\sigma + k_\beta \varepsilon_\beta + k_\gamma \varepsilon_\gamma) \langle T \rangle] \\ + (k_\sigma - k_\beta) \frac{1}{\mathrm{V}} \int_{A_{\sigma\beta}} T_\sigma \vec{n}_{\sigma\beta} dA \\ + (k_\beta - k_\gamma) \frac{1}{\mathrm{V}} \int_{A_{\beta\gamma}} T_\beta \vec{n}_{\beta\gamma} dA \\ + (k_\sigma - k_\gamma) \frac{1}{\mathrm{V}} \int_{A_{\sigma\gamma}} T_\gamma \vec{n}_{\sigma\gamma} dA \end{array} \right\} \qquad [9.128]$$

Next, the phase interface velocities can be expressed in terms of enthalpies of vaporization, sorption, and desorption.

The enthalpies for each phase were previously defined as:

$$\overline{h}_j = h_j^\circ + (c_p)_j (T_\sigma - T_\sigma^\circ) \quad [9.129]$$

$$h_\beta = h_\beta^\circ + (c_p)_\beta (T_\beta - T_\beta^\circ) \quad [9.130]$$

$$\overline{h}_i = h_i^\circ + (c_p)_i (T_\gamma - T_\gamma^\circ) \quad [9.131]$$

The intrinsic phase average temperatures, temperature dispersion, and overall average temperatures are related by:

$$\tilde{T}_\sigma = \langle T_\sigma \rangle^\sigma - T_\sigma \quad [9.132]$$

$$\tilde{T}_\beta = \langle T_\beta \rangle^\beta - T_\beta \quad [9.133]$$

$$\tilde{T}_\gamma = \langle T_\gamma \rangle^\gamma - T_\gamma \quad [9.134]$$

$$\langle T_\sigma \rangle^\sigma = \langle T_\beta \rangle^\beta = \langle T_\gamma \rangle^\gamma = \langle T \rangle \quad [9.135]$$

One can use these relations to rewrite the integrands inside the volume integrals on the left-hand side of the total thermal energy equation. The result for the liquid–gas interface is:

$$-\frac{1}{\mathrm{V}} \int_{A_{\beta\gamma}} \left\{ \rho_\beta [h_\beta - (c_p)_\beta \tilde{T}_\beta] (\vec{v}_\beta - \vec{w}) \cdot \vec{n}_{\beta\gamma} + \sum_{i=1}^{i=N} \rho_i [\overline{h}_i - (c_p)_i \tilde{T}_\gamma] (\vec{v}_i - \vec{w}) \cdot \vec{n}_{\gamma\beta} \right\} dA$$

$$= -\frac{1}{\mathrm{V}} \int_{A_{\beta\gamma}} \left\{ \begin{array}{l} [h_\beta^\circ - (c_p)_\beta (\langle T_\beta \rangle^\beta - T_\beta^\circ)] \rho_\beta (\vec{v}_\beta - \vec{w}) \cdot \vec{n}_{\beta\gamma} \\ + \sum_{i=1}^{i=N} [h_i^\circ - (c_p)_i (\langle T_\gamma \rangle^\gamma - T_\gamma^\circ)] \rho_i (\vec{v}_i - \vec{w}) \cdot \vec{n}_{\gamma\beta} \end{array} \right\} dA \quad [9.136]$$

From the species jump conditions:

$$\rho_i (\vec{v}_i - \vec{w}) \cdot \vec{n}_{\gamma\beta} + \rho_\beta (\vec{v}_\beta - \vec{w}) \cdot \vec{n}_{\beta\gamma} = 0, \; i = 1 \quad [9.137]$$

$$\rho_i (\vec{v}_i - \vec{w}) \cdot \vec{n}_{\gamma\beta} = 0, \; i = 2, 3, \ldots \quad [9.138]$$

Note that the subscript 1 refers to the component (water) which is actually crossing the phase boundary as it goes from a liquid to a vapor.

From the species jump conditions one may write:

$$\rho_1(\vec{v}_1 - \vec{w}_2) \cdot \vec{n}_{\sigma\beta} = -\rho_\beta(\vec{v}_\beta - \vec{w}_2) \cdot \vec{n}_{\beta\sigma} \quad [9.139]$$

Then, the integral may be restated as:

$$-\frac{1}{\mathrm{V}}\int_{A_{\beta\gamma}} \begin{Bmatrix} [h_\beta^\circ - (c_p)_\beta(\langle T\rangle - T_\beta^\circ)]\rho_\beta(\vec{v}_\beta - \vec{w}) \cdot \vec{n}_{\beta\gamma} \\ + [h_{g1}^\circ - (c_1)_1(\langle T\rangle - T_\gamma^\circ)]\rho_1(\vec{v}_1 - \vec{w}) \cdot \vec{n}_{\gamma\beta} \end{Bmatrix} dA$$

$$= -\frac{1}{\mathrm{V}}\int_{A_{\beta\gamma}} \begin{Bmatrix} [h_\beta^\circ - (c_p)_\beta(\langle T\rangle - T_\beta^\circ)]\rho_\beta(\vec{v}_\beta - \vec{w}) \cdot \vec{n}_{\beta\gamma} \\ - [h_{g1}^\circ - (c_1)_1(\langle T\rangle - T_\gamma^\circ)]\rho_1(\vec{v}_1 - \vec{w}) \cdot \vec{n}_{\beta\gamma} \end{Bmatrix} dA$$

$$= \left\{ \begin{bmatrix} h_{g1}^\circ - h_\beta^\circ + (c_p)_1(\langle T\rangle - T_\gamma^\circ) \\ -(c_p)_\beta(\langle T\rangle - T_\beta^\circ) \end{bmatrix} \right\} \frac{1}{\mathrm{V}}\int_{A_{\beta\gamma}} \rho_\beta(\vec{v}_\beta - \vec{w}) \cdot \vec{n}_{\beta\gamma} dA$$

[9.140]

The following definitions can be applied:

$$\Delta h_{\mathrm{vap}} \text{ (at temperature } \langle T\rangle)$$

$$= \{[h_{g1}^\circ - h_\beta^\circ + (c_p)_1(\langle T\rangle - T_\gamma^\circ) - (c_p)_\beta(\langle T\rangle - T_\beta^\circ)]\} \quad [9.141]$$

$$\langle \dot{m}_{lv} \rangle = \frac{1}{\mathrm{V}}\int_{A_{\beta\gamma}} \rho_\beta(\vec{v}_\beta - \vec{w}) \cdot \vec{n}_{\beta\gamma} dA \quad [9.142]$$

to rewrite the integral as:

$$-\frac{1}{\mathrm{V}}\int_{A_{\beta\gamma}} \begin{Bmatrix} \rho_\beta[h_\beta - (c_p)_\beta \tilde{T}_\beta](\vec{v}_\beta - \vec{w}) \cdot \vec{n}_{\beta\gamma} + \\ \sum_{i=1}^{i=N} \rho_i[\overline{h}_i - (c_p)_i \tilde{T}_\gamma](\vec{v}_i - \vec{w}) \cdot \vec{n}_{\gamma\beta} \end{Bmatrix} dA = \Delta h_{\mathrm{vap}} \langle \dot{m}_{lv} \rangle$$

[9.143]

The corresponding terms for the phase interface between the solid and the liquid are identical, except that the quantity Δh_{vap} is no longer used. Instead, the differential enthalpy of sorption[7] is applied, which is given the notation Q_l. The differential heat of sorption is the heat evolved when one gram of water is absorbed by an infinite mass of the solid, when that solid is at a particular equilibrated moisture content. This is very similar to the heat of solution or heat of mixing that occurs when two liquid components are mixed. For textile fibers there is a definite relationship between the equilibrium values of the differential heat of sorption and the water content of the fibers, and those relationships can be used in the thermodynamic equations which will be discussed in a later section.

The solid–liquid interface integral term is thus given as:

$$-\frac{1}{\mathrm{V}}\int_{A_{\sigma\beta}}\left\{\begin{array}{l}\rho_\beta[h_\beta-(c_p)_\beta\tilde{T}_\beta](\vec{v}_\beta-\vec{w}_2)\cdot\vec{n}_{\beta\sigma}\\+\sum_{j=1}^{j=N}\rho_j[\bar{h}_j-(c_p)_j\tilde{T}_\sigma](\vec{v}_j-\vec{w}_2)\cdot\vec{n}_{\sigma\beta}\end{array}\right\}dA \qquad [9.144]$$

From the species jump conditions one may equate:

$$\rho_1(\vec{v}_1-\vec{w}_2)\cdot\vec{n}_{\sigma\beta}=-\rho_\beta(\vec{v}_\beta-\vec{w}_2)\cdot\vec{n}_{\beta\sigma} \qquad [9.145]$$

or rewrite the integral as:

$$-\frac{1}{\mathrm{V}}\int_{A_{\sigma\beta}}\left\{\begin{array}{l}[h_\beta^\circ-(c_p)_\beta(\langle T\rangle-T_\beta^\circ)]\rho_\beta(\vec{v}_\beta-\vec{w}_2)\cdot\vec{n}_{\beta\sigma}\\+[h_{s1}^\circ-(c_p)_1(\langle T\rangle-T_\sigma^\circ)]\rho_1(\vec{v}_1-\vec{w}_2)\cdot\vec{n}_{\sigma\beta}\end{array}\right\}dA$$

$$=-\frac{1}{\mathrm{V}}\int_{A_{\sigma\beta}}\left\{\begin{array}{l}[h_{s1}^\circ-(c_p)_1(\langle T\rangle-T_\sigma^\circ)]\rho_1(\vec{v}_1-\vec{w}_2)\cdot\vec{n}_{\sigma\beta}\\-[h_\beta^\circ-(c_p)_\beta(\langle T\rangle-T_\beta^\circ)]\rho_\beta(\vec{v}_\beta-\vec{w}_2)\cdot\vec{n}_{\beta\sigma}\end{array}\right\}dA$$

$$=\left\{[h_{s1}^\circ-h_\beta^\circ+(c_p)_{s1}(\langle T\rangle-T_\sigma^\circ)-(c_p)_\beta(\langle T\rangle-T_\beta^\circ)]\right\}$$

$$\times\frac{1}{\mathrm{V}}\int_{A_{\sigma\beta}}\rho_\beta(\vec{v}_\beta-\vec{w}_2)\cdot\vec{n}_{\sigma\beta}dA \qquad [9.146]$$

One may use the following definitions:

$$Q_1\ (\text{at temperature}\ \langle T\rangle)=[h_{s1}^\circ-h_\beta^\circ+(c_p)_1(\langle T\rangle-T_\sigma^\circ)-(c_p)_\beta(\langle T\rangle-T_\beta^\circ)] \qquad [9.147]$$

$$\langle\dot{m}_{sl}\rangle=\frac{1}{\mathrm{V}}\int_{A_{\sigma\beta}}\rho_\sigma(\vec{v}_\sigma-\vec{w}_2)\cdot\vec{n}_{\sigma\beta}dA \qquad [9.148]$$

to rewrite the original integral as:

$$-\frac{1}{\mathrm{V}}\int_{A_{\sigma\beta}}\left\{\begin{array}{l}\sum_{j=1}^{j=N}\rho_j[\bar{h}_j-(c_p)_j\tilde{T}_\sigma](\vec{v}_j-\vec{w}_2)\cdot\vec{n}_{\sigma\beta}\\+\rho_\beta[h_\beta-(c_p)_\beta\tilde{T}_\beta](\vec{v}_\beta-\vec{w}_2)\cdot\vec{n}_{\beta\sigma}\end{array}\right\}dA=Q_l\langle\dot{m}_{sl}\rangle \qquad [9.149]$$

For the gas–solid interface, the heat of desorption for the vapor is equal to the energy required to desorb the liquid plus the enthalpy of vaporization, as:

$$Q_{sv}=Q_l+\Delta h_{\mathrm{vap}} \qquad [9.150]$$

The derivation is exactly the same as for the other two interfaces, where the only component crossing the phase interface is component 1 (water) and hence, the integral is:

$$-\frac{1}{\mathrm{V}}\int_{A_{\sigma\gamma}}\left\{\sum_{j=1}^{j=N}\rho_j[\bar{h}_j-(c_p)_j\tilde{T}_\sigma](\vec{v}_j-\vec{w}_1)\cdot\vec{n}_{\sigma\gamma}\right.$$
$$\left.+\sum_{i=1}^{i=N}\rho_i[\bar{h}_i-(c_p)_i\tilde{T}_\gamma](\vec{v}_i-\vec{w}_1)\cdot\vec{n}_i-\vec{w}_1)\cdot\vec{n}_{\gamma\sigma}\right\}dA$$
$$=(Q_l+\Delta h_{\mathrm{vap}})\langle\dot{m}_{sv}\rangle \qquad [9.151]$$

where $\langle\dot{m}_{sl}\rangle$ is the mass flux desorbing from the solid to the liquid phase, $\langle\dot{m}_{sv}\rangle$ is the mass flux desorbing from the solid into the gas phase, and $\langle\dot{m}_{lv}\rangle$ is the mass flux evaporating from the liquid phase to the gas phase.

The total thermal energy equation now becomes:

$$\langle\rho\rangle C_p\frac{\partial\langle T\rangle}{\partial t}$$
$$+\left[\sum_{j=1}^{j=N}(c_p)_j\langle\rho_j\vec{v}_j\rangle+\rho_\beta(c_p)_\beta\langle\vec{v}_\beta\rangle+\sum_{i=1}^{i=N}(c_p)_i\langle\rho_i\vec{v}_i\rangle\right]\cdot\nabla\langle T\rangle$$
$$+\Delta h_{\mathrm{vap}}\langle\dot{m}_{lv}\rangle+Q_l\langle\dot{m}_{sl}\rangle+(Q_l+\Delta h_{\mathrm{vap}})\langle\dot{m}_{sv}\rangle$$
$$=\nabla\cdot\left\{\begin{array}{l}\nabla[k_\sigma\varepsilon_\sigma+k_\beta\varepsilon_\beta+k_\gamma\varepsilon_\gamma)\langle T\rangle]\\+(k_\sigma-k_\beta)\frac{1}{\mathrm{V}}\int_{A_{\sigma\beta}}T_\sigma\vec{n}_{\sigma\beta}dA\\+(k_\beta-k_\gamma)\frac{1}{\mathrm{V}}\int_{A_{\beta\gamma}}T_\beta\vec{n}_{\beta\gamma}dA\\+(k_\sigma-k_\gamma)\frac{1}{\mathrm{V}}\int_{A_{\sigma\gamma}}T_\gamma\vec{n}_{\sigma\gamma}dA\end{array}\right\} \qquad [9.152]$$

One may simplify the total thermal energy equation based on an effective thermal conductivity, and present the total thermal energy equation in a much shorter form as:

$$\langle\rho\rangle C_p\frac{\partial\langle T\rangle}{\partial t}$$
$$+\left[\sum_{j=1}^{j=N}(c_p)_j\langle\rho_j\vec{v}_j\rangle+\rho_\beta(c_p)_\beta\langle\vec{v}_\beta\rangle+\sum_{i=1}^{i=N}(c_p)_i\langle\rho_i\vec{v}_i\rangle\right]\cdot\nabla\langle T\rangle$$
$$+\Delta h_{\mathrm{vap}}\langle\dot{m}_{lv}\rangle+Q_l\langle\dot{m}_{sl}\rangle+(Q_l+\Delta h_{\mathrm{vap}})\langle\dot{m}_{sv}\rangle$$
$$=\nabla\cdot(K^T_{\mathrm{eff}}\cdot\nabla\langle T\rangle) \qquad [9.153]$$

The effective thermal conductivity can be expressed in a variety of ways,[1]

depending on the assumptions made with respect to the isotropy of the porous medium, the importance of the dispersion terms, etc. The effective thermal conductivity is also an appropriate place to include radiative heat transfer, by adding an apparent radiative component of thermal conductivity to the effective thermal conductivity to account for radiation heat transfer.

9.4 Thermodynamic relations

The gas phase is assumed to be ideal, which gives the intrinsic phase partial pressures as:

$$\langle p_i \rangle^\gamma = \langle \rho_i \rangle^\gamma R_i \langle T \rangle \quad i = 1, 2, ... \qquad [9.154]$$

Noting that component 1 is water, and component 2 is air, one can present:

$$\langle \rho_\gamma \rangle^\gamma = \langle \rho_1 \rangle^\gamma + \langle \rho_2 \rangle^\gamma \qquad [9.155]$$

$$\langle p_\gamma \rangle^\gamma = \langle p_1 \rangle^\gamma + \langle p_2 \rangle^\gamma \qquad [9.156]$$

The differential heat of sorption, Q_l, and the concentration of water in the solid phase must now be connected. An example[8] of a general form for Q_l (in J/kg), as illustrated in Fig. 9.4, can be expressed as a function of the relative humidity ϕ:

$$Q_l\,(\text{J/kg}) = 1.95 \times 10^5 (1 - \phi)\left(\frac{1}{0.2 + \phi)} + \frac{1}{1.05 - \phi}\right),$$

$$\phi = \frac{p_v}{p_s} = \frac{\langle p_1 \rangle^\gamma}{p_s} \qquad [9.157]$$

The differential heat of sorption and the actual equilibrium water content in the solid phase can then be connected further. For the two-component mixture

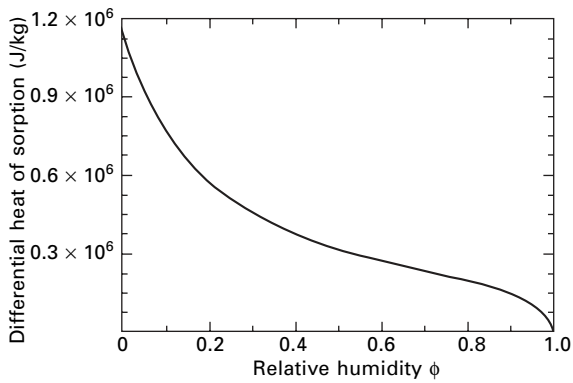

9.4 Generic differential heat of sorption for textile fibers (sorption hysteresis neglected).

of solid (component 2) plus bound water (component 1) in the solid phase, the density is given by:

$$\langle \rho_\sigma \rangle^\sigma = \langle \rho_1 \rangle^\sigma + \langle \rho_2 \rangle^\sigma \qquad [9.158]$$

One could make the assumption that mass transport in the textile fiber is so rapid that the fiber is always in equilibrium with the partial pressure of the gas phase, or is saturated if any liquid phase is present. This would eliminate the need to account for the transport through the solid phase. There are a variety of sorption isotherm relationships that could be used, including the experimentally determined relationships for a specific fiber type, but a convenient one[8] is given by:

$$\text{Regain } (R) = R_f(0.55\phi)\left[\frac{1}{(0.25 + \phi)} + \frac{1}{(1.25 - \phi)}\right] \qquad [9.159]$$

R_f is the standard textile measurement of grams of water absorbed per 100 grams of fiber, measured at 65% relative humidity. One may rewrite this in terms of the intrinsic phase averages for both phases as:

$$R = \frac{\langle \rho_1 \rangle^\sigma}{100\langle \rho_2 \rangle^2}$$

$$= R_f\left(55\frac{\langle p_1 \rangle^\gamma}{p_s}\right)\left[\frac{1}{\left(0.25 + \dfrac{\langle p_1 \rangle^\gamma}{p_s}\right)} + \frac{1}{\left(1.25 - \dfrac{\langle p_1 \rangle^\gamma}{p_s}\right)}\right] \qquad [9.160]$$

If the assumption is that the solid phase is not always in equilibrium, one may use relations available between the rate of change of concentration of the solid phase and the relative humidity of the gas phase, an example of which is given by Norden and David.[9]

The vapor pressure–temperature relation for the vaporizing β-phase can be given as:

$$\langle p_1 \rangle^\gamma = p_1^\circ \exp\left\{-\left[\left(\frac{2\sigma_{\beta\gamma}}{r\rho_\beta R_1 \langle T \rangle}\right) + \frac{\Delta h_{\text{vap}}}{R_1}\left(\frac{1}{\langle T \rangle} - \frac{1}{T_\circ}\right)\right]\right\} \qquad [9.161]$$

This relation gives the reduction or increase in vapor pressure from a curved liquid surface resulting from a liquid droplet influenced by the surface interaction between the solid and the liquid, usually in a very small capillary.

In many cases, the Clausius–Clapeyron equation will be sufficiently accurate for the vaporizing species, and the gas phase vapor pressure may be found from:

$$\langle p_1 \rangle^{\gamma} = p_1^{\circ} \exp\left\{-\left[\frac{\Delta h_{\text{vap}}}{R_1}\left(\frac{1}{\langle T \rangle} - \frac{1}{T_{\circ}}\right)\right]\right\} \quad [9.162]$$

This vapor pressure–temperature relation is only good if the liquid phase is present in the averaging volume. However, one may encounter situations where only the solid phase and the gas phase are present. To get the vapor pressure in the gas phase in this situation, one can use the sorption isotherm and assume that the gas phase is in equilibrium with the sorbed water content of the solid phase.

One can use any isotherm relation where the solid's water content is known as a function of relative humidity. The equation given previously is one example:

$$\frac{\langle \rho_1 \rangle^{\sigma}}{\langle \rho_2 \rangle^{\sigma}} = \frac{\varepsilon_{\sigma l} \rho_l}{(1 - \varepsilon_{\sigma l})\rho_s}$$

$$= R_f \left(0.55 \frac{\langle p_1 \rangle^{\gamma}}{p_s}\right) \left[\frac{1}{\left(0.25 + \dfrac{\langle p_1 \rangle^{\gamma}}{p_s}\right)} + \frac{1}{\left(1.25 - \dfrac{\langle p_{11} \rangle^{\gamma}}{p_s}\right)}\right] \quad [9.163]$$

9.5 Mass transport in the gas phase

The volume average form of the gas phase continuity equation was found to be:

$$\frac{\partial}{\partial t}(\varepsilon_{\gamma} \langle \rho_{\gamma} \rangle^{\gamma}) + \nabla \cdot (\langle \vec{\rho}_{\gamma} \rangle^{\gamma} \langle \vec{v}_{\gamma} \rangle) + \frac{1}{\mathrm{V}} \int_{A_{\gamma\beta}} \rho_{\gamma} (\vec{v}_{\gamma} - \vec{w}) \cdot \vec{n}_{\gamma\beta} dA$$

$$+ \frac{1}{\mathrm{V}} \int_{A_{\gamma\sigma}} \rho_{\gamma} (\vec{v}_{\gamma} - \vec{w}_1) \cdot \vec{n}_{\gamma\sigma} dA = 0 \quad [9.164]$$

and the species continuity equation was given as:

$$\frac{\partial}{\partial t}(\varepsilon_{\gamma} \langle \rho_1 \rangle^{\gamma}) + \nabla \cdot (\langle \rho_1 \rangle^{\gamma} \langle \vec{v}_1 \rangle) + \frac{1}{\mathrm{V}} \int_{A_{\gamma\beta}} \rho_1 (\vec{v}_1 - \vec{w}) \cdot \vec{n}_{\gamma\beta} dA$$

$$= \nabla \cdot \left\{ \langle \rho_{\gamma} \rangle^{\gamma} \mathrm{D} \nabla \left(\frac{\langle \rho_i \rangle^{\gamma}}{\langle \rho_{\gamma} \rangle^{\gamma}} \right) \right\} \quad [9.165]$$

where the dispersion and source terms were omitted from the equation.

If the mass flux from one phase to another is defined as:

$$\langle \dot{m}_{lv} \rangle = \frac{1}{\forall} \int_{A_{\beta\gamma}} \rho_\beta (\vec{v}_\beta - \vec{w}) \cdot \vec{n}_{\beta\gamma} dA \qquad [9.166]$$

or

$$\langle \dot{m}_{lv} \rangle = -\frac{1}{\forall} \int_{A_{\beta\gamma}} \rho_\gamma (\vec{v}_\gamma - \vec{w}) \cdot \vec{n}_{\gamma\beta} dA \qquad [9.167]$$

the expression for $\langle \dot{m}_{sv} \rangle$ is similar. The gas phase continuity equation may now be rewritten as:

$$\frac{\partial}{\partial t}(\varepsilon_\gamma \langle \rho_\gamma \rangle^\gamma) + \nabla \cdot (\langle \rho_\gamma \rangle^\gamma \langle \vec{v}_\gamma \rangle) = \langle \dot{m}_{lv} \rangle + \langle \dot{m}_{sv} \rangle \qquad [9.168]$$

For the two species (1 – water, and 2 – air), the species continuity equations are presented as:

$$\frac{\partial}{\partial t}(\varepsilon_\gamma \langle \rho_1 \rangle^\gamma) + \nabla \cdot (\langle \rho_1 \rangle^\gamma \langle \vec{v}_\gamma \rangle) - \langle \dot{m}_{lv} \rangle + \langle \dot{m}_{sv} \rangle$$

$$= \nabla \cdot \left\{ \langle \rho_\gamma \rangle^\gamma D \nabla \left(\frac{\langle \rho_1 \rangle^\gamma}{\langle \rho_\gamma \rangle^\gamma} \right) \right\} \qquad [9.169]$$

$$\frac{\partial}{\partial t}(\varepsilon_\gamma \langle \rho_2 \rangle^\gamma) + \nabla \cdot (\langle \rho_2 \rangle^\gamma \langle \vec{v}_\gamma \rangle) = \nabla \cdot \left\{ \langle \rho_\gamma \rangle^\gamma D \nabla \left(\frac{\langle \rho_2 \rangle^\gamma}{\langle \rho_\gamma \rangle^\gamma} \right) \right\} \qquad [9.170]$$

If the effects of the dispersion terms in the diffusion equations are neglected, one may incorporate an effective diffusivity into the species continuity equations, which are now given as:

$$\frac{\partial}{\partial t}(\varepsilon_\gamma \langle \rho_1 \rangle^\gamma) + \nabla \cdot (\langle \rho_1 \rangle^\gamma \langle \vec{v}_\gamma \rangle) - \langle \dot{m}_{lv} \rangle - \langle \dot{m}_{sv} \rangle$$

$$= \nabla \cdot \left\{ \langle \rho_\gamma \rangle^\gamma D_{\text{eff}} \nabla \left(\frac{\langle \rho_1 \rangle^\gamma}{\langle \rho_\gamma \rangle^\gamma} \right) \right\} \qquad [9.171]$$

$$\frac{\partial}{\partial t}(\varepsilon_\gamma \langle \rho_2 \rangle^\gamma) + \nabla \cdot (\langle \rho_2 \rangle^\gamma \langle \vec{v}_\gamma \rangle) = \nabla \cdot \left\{ \langle \rho_\gamma \rangle^\gamma D_{\text{eff}} \nabla \left(\frac{\langle \rho_2 \rangle^\gamma}{\langle \rho_\gamma \rangle^\gamma} \right) \right\} \qquad [9.172]$$

The effective diffusivity will be dependent on the gas phase volume ε_γ; as the solid volume and the liquid volume fractions increase, there will be less

space available in the gas phase for the diffusion to take place. One may define the effective diffusivity as:

$$D_{\text{eff}} = \frac{D_{12}\varepsilon_\gamma}{\tau} = \frac{D_a\varepsilon_\gamma}{\tau} \qquad [9.173]$$

where the effective diffusivity D_{eff} is related to the diffusion coefficient of water vapor in air (D_{12} or D_a) divided by the effective tortuosity factor τ.

A good relation for the binary diffusion coefficient of water vapor in air is given by Stanish *et al.*[10] as:

$$D_{12} = \left(\frac{2.23}{\langle p_1\rangle^\gamma + \langle p_2\rangle^\gamma}\right)\left(\frac{T}{273.15}\right)^{1.75} \text{(m K s units)} \qquad [9.174]$$

To simplify, one could assume the tortuosity factor is constant, and let the variation in the gas phase volume take care of the changes in the effective diffusion coefficient.

Another simplification is to account only for the water vapor movement, and hence the continuity equation becomes:

$$\frac{\partial}{\partial t}(\varepsilon_\gamma\langle\rho_1\rangle^\gamma) + \nabla\cdot(\langle\rho_1\rangle^\gamma\langle\vec{v}_\gamma\rangle) - \langle\dot{m}_{lv}\rangle - \langle\dot{m}_{sv}\rangle$$

$$= \nabla\cdot\left\{\langle\rho_\gamma\rangle^\gamma\frac{D_{12}}{\tau}\nabla\left(\frac{\langle\rho_1\rangle^\gamma}{\langle\rho_\gamma\rangle^\gamma}\right)\right\} \qquad [9.175]$$

9.6 Gas phase convective transport

It is often necessary to include forced convection through porous media – it is an important part of the transport process of mass and energy through porous materials. If gravity is neglected, the gas phase velocity is expressed as:[1]

$$\langle\vec{v}_\gamma\rangle = -\frac{1}{\mu_\gamma}K_\gamma\cdot\{\varepsilon_\gamma[\nabla\langle\rho_\gamma - \rho_0\rangle^\gamma]\} \qquad [9.176]$$

where the permeability tensor K_γ is a transport coefficient. Equation [9.176] is the general Darcy relation.[11]

There are other relations which pertain to gas flow through a porous material. For example, the modified form of Darcy's law:

$$\nabla P + \frac{\mu}{K}\vec{v}_\gamma = 0 \qquad [9.177]$$

The permeability coefficient K can be obtained experimentally. The permeability may be modified to account for the decrease in gas phase volume as the solid swells and/or the liquid phase accumulates. One can

account for the variation of K as a function of the gas phase volume – the approach used by Stanish *et al.*[10]

$$K_\gamma = K_{dry}^{\gamma}\left(\frac{\varepsilon_\gamma}{\varepsilon_{\gamma dry}}\right) \qquad [9.178]$$

Relation [9.178] is a very simple model, and may be improved upon. Dullien[11] presents a variety of relationships for the dependency of K on porosity; some of his relations may be more realistic in the case of fibrous layers. It is also possible to relate the change in the material permeability to the effective tortuosity function τ. This is useful, because τ is affected by the same factors related to the decrease in gas phase volume, and change in physical geometry, that are needed to account for the Darcy's law relations defining convective gas flow.

9.7 Liquid phase convective transport

Whitaker's derivation[1] for the convection transport of the liquid phase is one of the most complicated parts of his general theory. He accounts for the capillary liquid transport, which is greatly influenced by the geometry of the solid phase, and the changeover from a continuous to a discontinuous liquid phase. His eventual transport equation, which gives an expression for the liquid phase average velocity is quite complicated, and depends on several hard-to-obtain transport coefficients. His final equation is given as:

$$\langle \vec{v}_\beta \rangle = -\left(\frac{\varepsilon_\beta \xi \mathrm{K}_\beta}{\mu_\beta}\right) \cdot [k_\varepsilon \nabla \varepsilon_\beta + k_{\langle T \rangle} \nabla \langle T \rangle - (\rho_\beta - \rho_\gamma)] \qquad [9.179]$$

One advantage of Whitaker's derivation is that it is almost completely independent of the other transport equation derivations. This means that one may use another expression for the liquid phase velocity if one can substitute a relation that is more amenable to experimental measurement and verification.

One such relation is given by Stanish *et al.*[10] The velocity is assumed proportional to the gradient in pressure within the liquid. The pressure in the liquid phase is assumed to be the sum of the gas pressure within the averaging volume minus the capillary pressure (P_c):

$$\langle \vec{v}_\beta \rangle = -\left(\frac{k_\beta}{\mu_\beta}\right) \nabla (\langle p_1 \rangle^\gamma + \langle p_2 \rangle^\gamma - P_c) \qquad [9.180]$$

To use this type of relation, it is necessary to obtain an expression for the capillary pressure as a function of saturation condition. It is also necessary to determine when the liquid phase becomes discontinuous; where, at that point, liquid movement ceases. These types of relations can be identified

experimentally for materials of interest, or they may be found in the literature for a wide variety of materials.

Capillary pressure P_c is often a function of the fraction of the void space occupied by the liquid. Liquid present in a porous material may be either in a pendular state, or in a continuous state. If the liquid is in a pendular state, it is in discrete drops or regions that are unconnected to other regions of liquid. If liquid is in the pendular state, there is no liquid flow, since the liquid does not form a continuous phase. There may be significant capillary pressure present, but until the volume fraction of liquid rises to a critical level to form a continuous phase, there will be no liquid flow. This implies that there is a critical saturation level, which we can think of as the relative proportion of liquid volume within the gas phase volume that must be reached before liquid movement may begin.

Experimentally measured liquid capillary curves often show significant hysteresis, depending on whether liquid is advancing (imbibition) or receding (drainage) through the porous material. A typical capillary pressure curve is shown in Fig. 9.5.

We may take a definition for liquid saturation as:

$$S = \frac{V_\beta}{V_\gamma + V_\beta} = \frac{\varepsilon_\beta}{\varepsilon_\beta + \varepsilon_\gamma} \qquad [9.181]$$

The point at which the liquid phase becomes discontinuous is often called the irreducible saturation (s_{ir}).[12] When the irreducible saturation is reached, the flow is discontinuous, which implies that liquid flow ceases when:

$$\varepsilon_b < s_{ir}[1 - (\varepsilon_{ds} + \varepsilon_{bw})] \qquad [9.182]$$

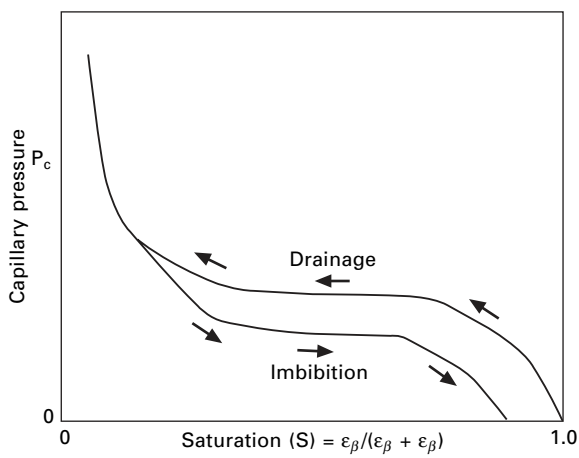

9.5 Typical appearance of capillary pressure curves as a function of liquid saturation for porous materials.

An empirical equation given by Stanish *et al.*[10] suggests a form for the equation for capillary pressure as a function of the fraction of void space occupied by liquid:

$$P_c = a\left(\frac{k_\beta}{\mu_\gamma}\right)^{-b}, \text{ where } a \text{ and } b \text{ are empirical constants} \qquad [9.183]$$

For liquid permeability as a function of saturation:[10]

$$K_\beta = \begin{cases} 0; & (\varepsilon_\beta/\varepsilon_\gamma) < s_{ir} \\ K_\beta^s \left\{1 - \cos\left[\frac{\pi}{2}\frac{(\varepsilon_\beta/\varepsilon_\gamma) - s_{ir}}{(1 - s_{ir})}\right]\right\}; & (\varepsilon_\beta/\varepsilon_\gamma) \geq s_{ir} \end{cases} \qquad [9.184]$$

where K_β^s is the liquid phase Darcy permeability when fully saturated.

Another way to construct a liquid phase transport equation is to consider the moisture distribution throughout the porous material as akin to a diffusion process. By combining the conservation of mass and Darcy's equation, a differential equation for the local saturation S may be written as:[13]

$$\frac{\partial S}{\partial t} = \frac{\partial}{\partial y}\left[F(s)\frac{\partial S}{\partial y}\right] \qquad [9.185]$$

where the 'moisture diffusivity' is given by:

$$F(s) = \frac{\left(\frac{K_\beta}{\mu_\beta}\right)\left(\frac{dP_c}{dS}\right)}{(\varepsilon_\beta + \varepsilon_\gamma)} \qquad [9.186]$$

If we rewrite the saturation variable S in terms of its original definition:

$$S = \frac{V_\beta}{V_\gamma + V_\beta} = \frac{\varepsilon_\beta}{\varepsilon_\beta + \varepsilon_\gamma} \qquad [9.187]$$

the differential equation for liquid migration under the influence of capillary pressure may be written as:

$$\frac{\partial}{\partial t}\left(\frac{\varepsilon_\beta}{(\varepsilon_\beta + \varepsilon_\gamma)}\right) = \frac{\partial}{\partial y}\left[\frac{\left(\frac{K_\beta}{\mu_\beta}\right)\left(\frac{dP_c}{dS}\right)}{(\varepsilon_\beta + \varepsilon_\gamma)}\frac{\partial}{\partial y}\left(\frac{\varepsilon_\beta}{(\varepsilon_\beta + \varepsilon_\gamma)}\right)\right] \qquad [9.188]$$

Although we have these relations for the capillary pressures and permeability as a function of saturation and irreducible saturation, it is often difficult to obtain permeabilities for many fibrous materials. Wicking studies on fabrics

are usually carried out parallel to the plane of the fabric by cutting a strip, dipping one end in water, and studying liquid motion as it wicks up the strip.[14,15] However, wicking through fibrous materials often takes place perpendicular to the plane of the fabric, where the transport properties are quite different due to the highly anisotropic properties of oriented fibrous materials such as fabrics.

The usefulness of the relations contained in Equations [9.181]–[9.188] are that they allow one to model the drying behavior of porous materials by accounting for both a constant drying rate period and a falling rate period. In the constant drying rate period, evaporation takes place at the surface of the porous material, and capillary forces bring the liquid to the surface. When irreducible saturation is reached in regions of the porous solid, drying becomes limited by the necessity for diffusion to take place through the porous structure of the material, which is responsible for the 'falling rate' period of drying. These effects are most important for materials that are thick, or of low porosity. For materials of the porosity and thickness typical of woven fabrics, almost all drying processes are in the constant rate regime, which suggests that many of the complicating factors which are important for thicker materials can be safely ignored. Studies on the drying rates of fabrics[16–19] suggest that simply assuming drying times proportional to the original liquid water content are a good predictor of the drying behavior of both hygroscopic and non-hygroscopic fabrics. Wicking processes perpendicular to the plane of the fabric take place very quickly, and the falling rate period is very short once most of the liquid has evaporated from the interior portions of fabrics.

9.8 Summary of modified transport equations

The set of modified equations which describe the coupled transfer of heat and mass transfer through hygroscopic porous materials are summarized below.

Total thermal energy equation:

$$\langle\rho\rangle C_p \frac{\partial\langle T\rangle}{\partial t} + \begin{bmatrix} \sum_{j=1}^{j=N} (c_p)_j \langle\rho_j \vec{v}_j\rangle \\ + \rho_\beta (c_p)_\beta \langle\vec{v}_\beta\rangle \\ + \sum_{i=1}^{i=N} (c_p)_i \langle\rho_i \vec{v}_i\rangle \end{bmatrix} \cdot \nabla\langle T\rangle + \Delta h_{vap} \langle\dot{m}_{lv}\rangle$$

$$+ Q_1 \langle\dot{m}_{sl}\rangle + (Q_l + \Delta h_{vap})\langle\dot{m}_{sv}\rangle$$

$$= \nabla \cdot (K_{eff}^T \cdot \nabla\langle T\rangle) \qquad [9.189]$$

Liquid phase equation of motion:

$$\langle \vec{v}_\beta \rangle = -\left(\frac{k_\beta}{\mu_\beta} \right) \nabla (\langle p_1 \rangle^\gamma + \langle p_1 \rangle^\gamma - P_c) \quad [9.190]$$

Liquid phase continuity equation:

$$\frac{\partial \varepsilon_\beta}{\partial t} + \nabla \cdot \langle \vec{v}_\beta \rangle + \frac{1}{V} \int_{A_{\beta\gamma}} (\vec{v}_\beta - \vec{w}) \cdot \vec{n}_{\beta\gamma} \, dA + \frac{1}{V} \int_{A_{\beta\sigma}} (\vec{v}_\beta - \vec{w}_2) \cdot \vec{n}_{\beta\sigma} \, dA = 0 \quad [9.191]$$

which can be rewritten as:

$$\frac{\partial \varepsilon_\beta}{\partial t} + \nabla \cdot \langle \vec{v}_\beta \rangle + \frac{(\langle \dot{m}_{lv} \rangle - \langle \dot{m}_{sv} \rangle)}{\rho_\beta} = 0 \quad [9.192]$$

Gas phase equation of motion:

$$\langle \vec{v}_\gamma \rangle = -\left(\frac{k_\gamma}{\mu_\gamma} \right) \nabla (\langle p_1 \rangle^\gamma + \langle p_2 \rangle^\gamma) \quad [9.193]$$

Gas phase continuity equation:

$$\frac{\partial}{\partial t} (\varepsilon_\gamma \langle \rho_\gamma \rangle^\gamma) + \nabla \cdot (\langle \rho_\gamma \rangle^\gamma \langle \vec{v}_\gamma \rangle) = \langle \dot{m}_{lv} \rangle + \langle \dot{m}_{sv} \rangle \quad [9.194]$$

Gas phase diffusion equations:

$$\frac{\partial}{\partial t} (\varepsilon_\gamma \langle \rho_1 \rangle^\gamma) + \nabla \cdot (\langle \rho_1 \rangle^\gamma \langle \vec{v}_\gamma \rangle) - \langle \dot{m}_{lv} \rangle - \langle \dot{m}_{sv} \rangle = \nabla \cdot \left\{ \langle \rho_\gamma \rangle^\gamma \, \mathrm{D}_{eff} \nabla \left(\frac{\langle \rho_1 \rangle^\gamma}{\langle \rho_\gamma \rangle^\gamma} \right) \right\} \quad [9.195]$$

$$\frac{\partial}{\partial t} (\varepsilon_\gamma \langle \rho_2 \rangle^\gamma) + \nabla \cdot (\langle \rho_2 \rangle^\gamma \langle \vec{v}_\gamma \rangle) = \nabla \cdot \left\{ \langle \rho_\gamma \rangle^\gamma \, \mathrm{D}_{eff} \nabla \left(\frac{\langle \rho_1 \rangle^\gamma}{\langle \rho_\gamma \rangle^\gamma} \right) \right\} \quad [9.196]$$

Solid phase density relations:

$$\langle \rho_\sigma \rangle^\sigma = \langle \rho_1 \rangle^\sigma + \langle \rho_2 \rangle^\sigma \quad [9.197]$$

$$\boldsymbol{\rho}_1 = \varepsilon_{\sigma L} \rho_L \quad [9.198]$$

$$\rho_2 = (1 - \varepsilon_{\sigma L}) \rho_S \quad [9.199]$$

$$\varepsilon_{sS} + \varepsilon_{\sigma L} = 1 \quad [9.200]$$

Solid phase continuity equation:

$$\frac{\partial}{\partial t} (\varepsilon_\sigma \langle \rho_\sigma \rangle^\sigma) + \nabla \cdot (\langle \rho_\sigma \rangle^\sigma \langle \vec{v}_\sigma \rangle) + \langle \dot{m}_{sl} \rangle + \langle \dot{m}_{sv} \rangle = 0 \quad [9.201]$$

Solid phase equation of motion (for one-dimensional geometry):

$$\langle v_\sigma \rangle^\sigma = \frac{1}{\langle \rho \rangle^\sigma \xi^{n-1}} \int_0^\xi \frac{\partial}{\partial t} \langle \rho_\sigma \rangle d\xi \qquad [9.202]$$

Solid phase diffusion equation (for vaporizing component):

$$\frac{\partial}{\partial t}(\varepsilon_\sigma \langle \rho_1 \rangle^\sigma) + \nabla \cdot (\langle \rho_1 \rangle^\sigma \langle \vec{v}_1 \rangle) + \langle \dot{m}_{sl} \rangle + \langle \dot{m}_{sv} \rangle$$

$$= \nabla \cdot \left\{ \langle \rho_\sigma \rangle^\sigma \, \mathrm{D}_\sigma \nabla \left(\frac{\langle \rho_1 \rangle^\sigma}{\langle \rho_\sigma \rangle^\sigma} \right) \right\} \qquad [9.203]$$

Volume constraint:

$$\varepsilon_\sigma(t) + \varepsilon_\beta(t) + \varepsilon_\gamma(t) = 1 \qquad [9.204]$$

Thermodynamic relations:

$$\langle \rho_1 \rangle^\gamma = \langle \rho_1 \rangle^\gamma R_1 \langle T \rangle \qquad [9.205]$$

$$\langle \rho_2 \rangle^\gamma = \langle \rho_2 \rangle^\gamma R_2 \langle T \rangle \qquad [9.206]$$

$$\langle \rho_\gamma \rangle^\gamma = \langle \rho_1 \rangle^\gamma + \langle \rho_2 \rangle^\gamma \qquad [9.207]$$

$$\langle \rho_\gamma \rangle^\gamma = \langle \rho_1 \rangle^\gamma + \langle \rho_2 \rangle^\gamma \qquad [9.208]$$

If liquid phase is present, vapor pressure is given by:

$$\langle \rho_1 \rangle^\gamma = p_1^\circ \exp\left\{ -\left[\left(\frac{2\sigma_{\beta\gamma}}{r\rho_\beta R_1 \langle T \rangle} \right) + \frac{\Delta h_{vap}}{R_1} \left(\frac{1}{\langle T \rangle} - \frac{1}{T_\circ} \right) \right] \right\} \qquad [9.209]$$

or

$$\langle \rho_1 \rangle^\gamma = p_1^\circ \exp\left\{ -\left[\frac{\Delta h_{vap}}{R_1} \left(\frac{1}{\langle T \rangle} - \frac{1}{T_\circ} \right) \right] \right\} \qquad [9.210]$$

If the liquid phase does not exist, but the liquid component is desorbing from the solid, the reduced vapor pressure in equilibrium with the solid phase must be used. This relation may be determined directly from the sorption isotherm for the solid:

$$\langle p_1 \rangle^\gamma = f(p_s, \rho_l, \rho_s, \varepsilon_{\sigma L}) \text{ at the temperature } \langle T \rangle, \text{ only } \varepsilon_{\sigma L} \text{ is unknown} \qquad [9.211]$$

Sorption relations (volume average solid equilibrium):

$$Q_l \,(\mathrm{J/kg}) = 0.195 \left(1 - \frac{\langle p_1 \rangle^\gamma}{p_s} \right) \left(\frac{1}{\left(0.2 + \frac{\langle p_1 \rangle^\gamma}{p_s} \right)} + \frac{1}{\left(1.05 - \frac{\langle p_1 \rangle^\gamma}{p_s} \right)} \right) \qquad [9.212]$$

$$\frac{\langle \rho_1 \rangle^{\sigma}}{\langle \rho_2 \rangle^{\sigma}} = \frac{\varepsilon_{\sigma l} \rho_l}{(1 - \varepsilon_{\sigma l}) \rho_s}$$

$$= R_f \left(0.55 \frac{\langle p_1 \rangle^{\gamma}}{p_s} \right) \left(\frac{1}{\left(0.25 + \frac{\langle p_1 \rangle^{\gamma}}{p_s} \right)} + \frac{1}{\left(1.25 - \frac{\langle p_1 \rangle^{\gamma}}{p_s} \right)} \right) \qquad [9.213]$$

The preceding list contains a total of 20 equations and 20 unknown variables, which allow for the solution of the set of equations using numerical methods. The 20 unknown variables are:

$$\varepsilon_{\sigma}, \varepsilon_{\beta}, \varepsilon_{\gamma}, \langle \vec{v}_{\sigma} \rangle, \langle \vec{v}_{\beta} \rangle, \langle \vec{v}_{\gamma} \rangle, \langle T \rangle,$$
$$\langle \dot{m}_{sl} \rangle, \langle \dot{m}_{sv} \rangle, \langle \dot{m}_{lv} \rangle, Q_{sl}$$
$$\langle p_{\gamma} \rangle^{\gamma}, \langle p_1 \rangle^{\gamma}, \langle p_2 \rangle^{\gamma}, \langle \rho_{\gamma} \rangle^{\gamma}, \langle \rho_1 \rangle^{\gamma}, \langle \rho_2 \rangle^{\gamma}$$
$$\langle p_{\gamma} \rangle^{\sigma}, \langle p_1 \rangle^{\sigma}, \langle p_2 \rangle^{\sigma}$$

Note that the aforementioned set of equations is accompanied with the appropriate initial and boundary conditions.

9.9 Comparison with previously derived equations

The simplified system of partial differential equations given in the previous section contains many equations with a large number of unknown variables. Even for the simplified case of vapor diffusion, the system of equations is quite confusing, and it is difficult to verify their accuracy other than by checking for dimensional consistency. One way of checking their validity is to see if they simplify down to more well-known diffusion equations for the transport of water vapor in air through a porous hygroscopic solid. Such a system of equations has been well documented by Henry,[20] Norden and David,[9] and Li and Holcombe,[21] who have used them to describe the diffusion of water vapor through a hygroscopic porous material.

The same assumptions used by those previous workers will be made here to transform the system of equations for the case of vapor diffusion (no liquid or gas phase convection) to their system of equations. For clarity of comparison, the same variables, notations, and units will be used.

The major simplifying assumptions are: (i) there is no liquid or gas phase convection, (ii) there is no liquid phase present, (iii) the heat capacity of the gas phase can be neglected, (iv) the volume of the solid remains constant and does not swell, (v) the solid and gas phase volume fractions are both constant, (vi) the thermal conductivity is expressed as a constant scalar thermal conductivity coefficient, (vii) the gas phase diffusion coefficient is constant, (viii) the transport is one-dimensional (e.g. x-direction).

The total thermal energy equation becomes:

$$\langle\rho\rangle C_p \frac{\partial\langle T\rangle}{\partial t} + (Q_l + \Delta h_{vap})\langle\dot{m}_{sv}\rangle = \nabla\cdot(K_{eff}^T\cdot\nabla\langle T\rangle) \qquad [9.214]$$

and can be replaced by

$$\langle\rho\rangle C_p \frac{\partial\langle T\rangle}{\partial t} + (Q_l + \Delta h_{vap})\langle\dot{m}_{sv}\rangle = k_{eff}\frac{\partial^2\langle T\rangle}{\partial x^2} \qquad [9.215]$$

The gas phase continuity equation becomes:

$$\varepsilon_\gamma \frac{\partial}{\partial t}(\langle p_\gamma\rangle^\gamma) = \langle\dot{m}_{sv}\rangle \qquad [9.216]$$

The gas phase diffusion equation (component 1 – water vapor):

$$\varepsilon_\gamma \frac{\partial}{\partial t}(\langle p_1\rangle^\gamma) - \langle\dot{m}_{sv}\rangle = \nabla\cdot\left\{\langle\rho_\gamma\rangle^\gamma \mathrm{D}_{eff}\nabla\left(\frac{\langle\rho_1\rangle^\gamma}{\langle\rho_\gamma\rangle^\gamma}\right)\right\} \qquad [9.217]$$

simplified to:

$$\varepsilon_\gamma \frac{\partial}{\partial t}(\langle p_1\rangle^\gamma) - \langle\dot{m}_{sv}\rangle = \mathrm{D}_{eff}\frac{\partial^2\langle\rho_1\rangle^\gamma}{\partial x^2} \qquad [9.218]$$

The solid phase continuity equation (component 1 – water):

$$\varepsilon_\sigma \frac{\partial}{\partial t}(\langle p_1\rangle^\sigma) + \langle\dot{m}_{sv}\rangle = 0 \qquad [9.219]$$

For the solid phase diffusion equation (component 1 – water), it is assumed that the diffusional transport through the solid phase is insignificant compared with the diffusion through the gas phase. This is a reasonable assumption since the diffusion coefficient for water in a solid is always much less than the diffusion coefficient of water vapor in air. Therefore, the diffusion equation reduces to the continuity equation:

$$\varepsilon_\sigma \frac{\partial}{\partial t}(\langle\rho_1\rangle^\sigma) + \langle\dot{m}_{sv}\rangle = \nabla\cdot\left\{\langle\rho_\sigma\rangle^\sigma \mathrm{D}_\sigma\nabla\left(\frac{\rho_1}{\langle\rho_\sigma\rangle^\sigma}\right)\right\} = 0 \qquad [9.220]$$

Volume fraction constraint:

$$\varepsilon_\gamma + \varepsilon_\sigma = 1;\ \varepsilon_\sigma = 1 - \varepsilon_\gamma \qquad [9.221]$$

Thermodynamic relations:

$$\langle p_1\rangle^\gamma = \langle p_1\rangle^\gamma R_1\langle T\rangle \qquad [9.222]$$

$$\langle p_2\rangle^\gamma = \langle\rho_2\rangle^\gamma R_2\langle T\rangle \qquad [9.223]$$

$$\langle\rho_\gamma\rangle^\gamma = \langle\rho_1\rangle^\gamma + \langle\rho_2\rangle^\gamma \qquad [9.224]$$

$$\langle p_\gamma\rangle^\gamma = \langle p_1\rangle^\gamma + \langle p_2\rangle^\gamma \qquad [9.225]$$

One can add Equations [9.218] and [9.219] together to obtain a single continuity equation for water (component 1):

$$\left[\varepsilon_\sigma \frac{\partial}{\partial t}(\langle \rho_1 \rangle^\sigma) + \langle \dot{m}_{sv} \rangle\right] + \left[\varepsilon_\gamma \frac{\partial}{\partial t}(\langle p_1 \rangle^\gamma) - \langle \dot{m}_{sv} \rangle\right]$$

$$= \mathrm{D}_{eff} \frac{\partial^2 \langle \rho_1 \rangle^\gamma}{\partial x^2} \qquad [9.226]$$

which can be represented in terms of the gas phase volume fraction as:

$$(1 - \varepsilon_r) \frac{\partial}{\partial t}(\langle \rho_1 \rangle^\sigma) + \varepsilon_\gamma \frac{\partial}{\partial t}(\langle \rho_1 \rangle^\gamma) = \mathrm{D}_{eff} \frac{\partial^2 \langle \rho_1 \rangle^\gamma}{\partial x^2} \qquad [9.227]$$

Application of the above assumptions reduces the large equation set down to two main equations for the energy balance and the mass balance:

$$\langle \rho \rangle C_p \frac{\partial \langle T \rangle}{\partial t} + (Q_l + \Delta h_{vap}) \langle \dot{m}_{sv} \rangle = k_{eff} \frac{\partial^2 \langle T \rangle}{\partial x^2} \qquad [9.228]$$

$$(1 - \varepsilon_\gamma) \frac{\partial}{\partial t}(\langle \rho_1 \rangle^\sigma) + \varepsilon_\gamma \frac{\partial}{\partial t}(\langle \rho_1 \rangle^\gamma) = \mathrm{D}_{eff} \frac{\partial^2 \langle \rho_1 \rangle^\gamma}{\partial x^2} \qquad [9.229]$$

To make the comparison easier with the existing equations of Henry,[20] Norden and David,[9] and Li and Holcombe,[21] one can rewrite the intrinsic phase averaged equations in terms of the concentration variables – for water in the solid (C_F), and for water vapor in the gas (C):

$$C_F = \frac{\text{mass of water in solid phase}}{\text{solid phase volume}} = \frac{m_{1\sigma}}{V_\sigma} = \rho_{1\sigma} \qquad [9.230]$$

$$C = \frac{\text{mass of water in gas phase}}{\text{gas phase volume}} = \frac{m_{1\gamma}}{V_\gamma} = \rho_{1\gamma} \qquad [9.231]$$

Since the definition of intrinsic phase average gives the same quantity as the true point value, one may use the relations:

$$\langle \rho_1 \rangle^\sigma = \langle C_F \rangle^\sigma = C_F \qquad [9.232]$$

$$\langle \rho_1 \rangle^\gamma = \langle C \rangle^\gamma = C \qquad [9.233]$$

to rewrite the mass balance equation as:

$$(1 - \varepsilon_\gamma) \frac{\partial C_F}{\partial t} + \varepsilon_\gamma \frac{\partial C}{\partial t} = \mathrm{D}_{eff} \frac{\partial^2 C}{\partial x^2} \qquad [9.234]$$

The diffusion coefficient for water vapor in air modified by the gas volume fraction and the tortuosity are used to obtain the effective diffusion coefficient as:

$$(1 - \varepsilon_\gamma)\frac{\partial C_F}{\partial t} + \varepsilon_\gamma \frac{\partial C}{\partial t} = \frac{D_a \varepsilon_\gamma}{\tau} \frac{\partial^2 C}{\partial x^2} \quad [9.235]$$

The thermal energy equation is:

$$\langle \rho \rangle C_p \frac{\partial \langle T \rangle}{\partial t} + (Q_l + \Delta h_{vap})\langle \dot{m}_{sv} \rangle = k_{eff} \frac{\partial^2 \langle T \rangle}{\partial x^2} \quad [9.236]$$

The energy equation may be modified by recognizing that the mass flux term is contained in the solid phase continuity equation, such as:

$$\varepsilon_\sigma \frac{\partial}{\partial t}(\langle \rho_1 \rangle^\sigma) + \langle \dot{m}_{sv} \rangle = 0 \Rightarrow \langle \dot{m}_{sv} \rangle = -\varepsilon_\sigma \frac{\partial C_F}{\partial t} \quad [9.237]$$

so that the thermal energy equation may now be rewritten as:

$$\langle \rho \rangle C_p \frac{\partial \langle T \rangle}{\partial t} - (Q_l + \Delta h_{vap})\varepsilon_\sigma \frac{\partial C_F}{\partial t} = k_{eff} \frac{\partial^2 \langle T \rangle}{\partial x^2} \quad [9.238]$$

Referring to the mass fraction weighted average heat capacity, Equation [9.119],

$$C_p = \frac{\varepsilon_\sigma \sum_{j=1}^{j=N} \langle \rho_j \rangle^\sigma (c_p)_j + \varepsilon_\gamma \sum_{i=1}^{i=N} \langle \rho_j \rangle^\gamma (c_p)_i}{\langle p \rangle}$$

and spatial average density, Equation [9.118],

$$\langle \rho \rangle = \varepsilon_\sigma \sum_{j=1}^{j=N} \langle \rho_j \rangle^\sigma + \varepsilon_\gamma \sum_{i=1}^{i=N} \langle \rho_i \rangle^\gamma$$

the thermal energy equation may be expressed as:

$$\{\varepsilon_\sigma[\langle \rho_1 \rangle^\sigma (c_p)_1 + \langle \rho_2 \rangle^\sigma (c_p)_2] + \varepsilon_\gamma[\langle \rho_1 \rangle^\gamma (c_p)_1 + \langle \rho_2 \rangle^\gamma (c_p)_2]\} \frac{\partial \langle T \rangle}{\partial t}$$

$$-(Q_l + \Delta h_{vap})\varepsilon_\sigma \frac{\partial C_F}{\partial t} = k_{eff} \frac{\partial^2 \langle T \rangle}{\partial x^2} \quad [9.239]$$

If it is assumed that the heat capacity of the gas phase is negligible, then the thermal energy equation becomes:

$$\{\varepsilon_\sigma[\langle \rho_1 \rangle^\sigma (c_p)_1 + \langle \rho_2 \rangle^\sigma (c_p)_2]\} \frac{\partial \langle T \rangle}{\partial t}$$

$$-(Q_l + \Delta h_{vap})\varepsilon_\sigma \frac{\partial C_F}{\partial t} = k_{eff} \frac{\partial^2 \langle T \rangle}{\partial x^2} \quad [9.240]$$

Dividing the previous equations by the solid volume fraction yields.

$$[\langle \rho_1 \rangle^{\sigma} (c_p)_1 + \langle \rho_2 \rangle^{\sigma} (c_p)_2] \frac{\partial \langle T \rangle}{\partial t}$$

$$- (Q_l + \Delta h_{vap}) \varepsilon_{\sigma} \frac{\partial C_F}{\partial t} = \frac{k_{eff}}{\varepsilon_{\sigma}} \frac{\partial^2 \langle T \rangle}{\partial x^2} \quad [9.241]$$

To be consistent with the notation of Li and Holcombe,[21] ($k_{eff}/\varepsilon_{\sigma}$) is replaced by K.

A volumetric heat capacity C_v is defined as:

$$C_v = \langle \rho_1 \rangle^{\sigma} (c_p)_1 + \langle \rho_2 \rangle^{\sigma} (c_p)_2 \quad [9.242]$$

Note: Units for $\langle \rho_j \rangle^{\sigma} (c_p)_j$ are $\left(\frac{\text{kg}}{\text{m}^3}\right)\left(\frac{\text{J}}{\text{kg} \cdot \text{K}}\right) \Rightarrow \left(\frac{\text{kg}}{\text{m}^3 \cdot \text{K}}\right)$

The final thermal energy equation reduces to:

$$C_v \frac{\partial \langle T \rangle}{\partial t} - (Q_l + \Delta h_{vap}) \frac{\partial C_F}{\partial t} = K \frac{\partial^2 \langle T \rangle}{\partial x^2} \quad [9.243]$$

The two simplified equations for the mass and energy balance are thus:

$$(1 - \varepsilon_{\gamma}) \frac{\partial C_F}{\partial t} + \varepsilon_{\gamma} \frac{\partial C}{\partial t} = \frac{D_a \varepsilon_{\gamma}}{\tau} \frac{\partial^2 C}{\partial x^2} \quad [9.244]$$

$$C_v \frac{\partial \langle T \rangle}{\partial t} - (Q_l + \Delta h_{vap}) \frac{\partial C_F}{\partial t} = K \frac{\partial^2 \langle T \rangle}{\partial x^2} \quad [9.245]$$

As shown above, the general equations given in Section 9.9, with proper assumptions, can be reduced to the equations derived by Henry,[20] Norden and David,[9] and Li and Holcombe,[21] for describing the diffusion of water vapor through a hygroscopic porous material.

9.10 Conclusions

Whitaker's theory of coupled heat and mass transfer through porous media was modified to include hygroscopic porous materials which can absorb liquid into the solid matrix. The system of equations described in this chapter make it possible to evaluate the time-dependent transport properties of hygroscopic and non-hygroscopic clothing materials by including many important factors which are usually ignored in the analysis of heat and mass transfer through textile materials. The equations allow for the unsteady capillary wicking of sweat through fabric structure, condensation and evaporation of sweat within various layers of the clothing system, forced gas phase convection through the porous structure of a textile layer, and the swelling and shrinkage of fibers and yarns.

The simplified set of equations for heat and mass transfer, where mass transport occurs due to diffusion within the air spaces of the porous solid, was shown to reduce to the well-known coupled heat and mass transfer models for hygroscopic fabrics, as exemplified by the work of Li and Holcombe.[21]

9.11 Nomenclature

A area [m^2]

$a_{\sigma\beta}$ $A_{\sigma\beta}/\mathscr{V}$ surface of the σ–β interface per unit volume [m^{-1}]

$A_m(t)$ material surface [m^2]

c_p constant pressure heat capacity [J/kg · K]

C_p mass fraction weighted average constant pressure heat capacity [J/kg · K]

C_F concentration of water in a fiber [kg/m^3]

C_s concentration of liquid in the solid phase [kg/m^3]

C_V volumetric heat capacity [$kg/m^3 \cdot K$]

D gas phase molecular diffusivity [m^2/sec]

D_{eff} effective gas phase molecular diffusivity [m^2/sec]

D diffusion coefficient [m^2/sec]

D_a diffusion coefficient of water vapor [m^2/sec]

$D_{L\sigma}$ diffusion coefficient of liquid in the solid phase [m^2/sec]

$\vec{g}$ gravity vector [m/sec^2]

h enthalpy per unit mass [J/kg]

$h°$ reference enthalpy [J/kg]

$\bar{h}_i$ partial mass enthalpy for the ith species [J/kg]

$h_{\sigma\beta}$ heat transfer coefficient for the σ–β interface [J/sec · m^2 · K]

Δh_{vap} enthalpy of vaporization per unit mass [J/kg]

k thermal conductivity [J/sec · m · K]

k_ε $\partial\langle P_c\rangle/\partial\varepsilon_\beta$ [N/m^2]

$k_{\langle T\rangle}$ $\partial\langle P_c\rangle/\partial\langle T\rangle$ [$N/m^2 \cdot K$]

K permeability coefficient [m^2]

K_β Darcy permeability for liquid phase [m^2]

K_β liquid phase permeability tensor [m^2/sec]

K_γ gas phase permeability tensor [m^2/sec]

L total half-thickness of body model system [0.056 m]

m mass [kg]

$\langle \dot{m}_{sl} \rangle$ mass rate of desorption from solid phase to liquid phase per unit volume [kg/sec-m^3] $\langle \dot{m}_{sl} \rangle = \frac{1}{\mathrm{V}} \int_{A_{\sigma\beta}} \rho_\sigma (\vec{v}_\sigma - \vec{w}_2) \cdot \vec{n}_{\sigma\beta} dA$

$\langle \dot{m}_{sv} \rangle$ mass rate of desorption from solid phase to vapor phase per unit volume [kg/sec · m^3]

$\langle \dot{m}_{lv} \rangle$ mass rate of evaporation per unit volume [kg/sec·m^3]
$\vec{n}$ outwardly directed unit normal
p pressure [N/m^2]
p_γ total gas pressure [N/m^2]
p_a partial pressure of air [N/m^2]
p_v partial pressure of water vapor [N/m^2]
p_s saturation vapor pressure (function of T only) [N/m^2]
P_c $p_\gamma - p_\beta$, capillary pressure [N/m^2]
p_0 reference pressure [N/m^2]
p_1° reference vapor pressure for component 1 [N/m^2]
Q volumetric flow rate [m^3/sec]
Q_1 differential enthalpy of sorption from solid phase to liquid phase per unit mass [J/kg]
Q_{sv} enthalpy of vaporization from liquid bound in solid phase to gas phase per unit mass [J/kg]
$\vec{q}$ heat flux vector [J/sec·m^2]
$\vec{r}$ position vector [m]
r characteristic length of a porous media [m]
R_i gas constant for the ith species [N·m/kg·K]
R universal gas constant [8314.5 N·m/(kg·K)]
R_f textile measurement (@ $\phi = 0.65$), grams of water absorbed per 100 grams of fiber [fraction]
S saturation, fraction of void space occupied by liquid [fraction]
s_{ir} irreducible saturation; saturation level at which liquid phase is discontinuous
T temperature [K]
T_0 reference temperature [K]
T total stress tensor [N/m^2]
t time [sec]
$\vec{u}_i$ diffusion velocity of the ith species [m/s]
$\vec{v}$ mass average velocity [m/s]
$\vec{v}_i$ velocity of the ith species [m/s]
$\langle \vec{v}_\beta \rangle$ volume average liquid velocity [m/s]
$V_\sigma(t)$ volume of the solid phase contained within the averaging volume [m^3]
$V_\beta(t)$ volume of the liquid phase contained within the averaging volume [m^3]
$V_\gamma(t)$ volume of the gas phase contained within the averaging volume [m^3]
$\mathscr{V}$ averaging volume [m^3]
$\mathscr{V}_m(t)$ material volume [m^3]
$\vec{w}$ velocity of the β–γ interface [m/sec]
$\vec{w}_1$ velocity of the σ–γ interface [m/sec]

$\vec{w}_2$ velocity of the σ–β interface [m/sec]

Greek symbols

$\varepsilon_\sigma(t)$ $V_\sigma/\mathscr{V}$, volume fraction of the solid phase
$\varepsilon_\beta(t)$ $V_\beta/\mathscr{V}$, volume fraction of the liquid phase
$\varepsilon_\gamma(t)$ V_γ/v, volume fraction of the gas phase
$\varepsilon_{\sigma L}$ V_L/V_σ, volume fraction of the liquid in the solid phase
$\varepsilon_{\sigma S}$ V_S/V_σ, volume fraction of the liquid in the solid phase
ε_{ds} $V_{ds}/\mathscr{V}$, volume fraction of the dry solid (constant)
$\varepsilon_{bw}(t)$ $V_{bw}/\mathscr{V}$, volume fraction of the water dissolved in the solid phase
Φ rate of heat generation [J/sec·m^3]
ϕ p_v/p_s, relative humidity
$\vec{\lambda}$ unit tangent vector
μ shear coefficient of viscosity [N·sec/m^2]
μ_β viscosity of the liquid phase [for water, 9.8×10^{-4} kg/m·s at 20 °C]
μ_γ viscosity of the gas phase [kg/m·s]
ρ density [kg/m^3]
ρ_β density of liquid phase [kg/m^3]
ρ_i density of the ith species [kg/m^3]
ρ_{ds} density of dry solid [for polymers typically 900 to 1300 kg/m^3]
ρ_w density of liquid water [approximately 1000 kg/m^3]
ρ_γ density of gas phase (mixture of air and water vapor) [kg/m^3]
ρ_v density of water vapor in the gas volume (equivalent to mass concentration) [kg/m^3]
ρ_a density of the inert air component in the gas volume (equivalent to mass of air/total gas volume) [kg/m^3]
τ viscous stress tensor [N/m^3]
τ tortuosity factor
$\vec{\xi}$ thermal dispersion vector [J/sec·m^3]
ξ dummy integration variable
ξ a function of the topology of the liquid phase

Subscripts and superscripts

o denotes a reference state
i designates the ith species in the gas phase
l, L liquid
s, S solid
σ designates a property of the solid phase
β designates a property of the liquid phase
γ designates a property of the gas phase
$\sigma\beta$ designates a property of the σ–β interface

$\sigma\gamma$ designates a property of the σ–γ interface
$\beta\gamma$ designates a property of the β–γ interface

Mathematical symbols

d/dt total time derivative
D/Dt material time derivative
$\partial/\partial t$ partial time derivative
$\langle\psi\rangle$ spatial average of a function ψ which is defined everywhere in space
$\langle\psi_\beta\rangle$ phase average of a function ψ_β which represents a property of the β phase
$\langle\psi_\beta\rangle^\beta$ intrinsic phase average of a function ψ_β which represents a property of the β phase
$\tilde{\psi}_\beta$ denotes dispersion/deviation from the average for that phase or quantity

9.12 References

1. Whitaker, S. A., 'Theory of Drying in Porous Media', in *Advances in Heat Transfer* **13**, New York, Academic Press, 1977, 119–203.
2. Jomaa, W., Puiggali, J, 'Drying of Shrinking Materials: Modellings with Shrinkage Velocity', *Drying Technology* 1991, **9** (5), 1271–1293.
3. Crapiste, G., Rostein, E. and Whitaker, S., 'Drying Cellular Material. I: Mass Transfer Theory', *Chem Eng Sci*, 1988 **43**, 2919–2928; 'II: Experimental and Numerical Results', *Chem Eng Sci*, 1988 **43**, 2929–2936.
4. Slattery, J., *Momentum, Energy, and Mass Transfer in Continua*, McGraw-Hill, New York, 1972.
5. Slattery, J., *Momentum, Energy, and Mass Transfer in Continua*, McGraw-Hill, New York, 1972, 19.
6. Gray, W., 'A Derivation of the Equations for Multi-phase Transport', *Chemical Engineering Science*, 1975 **30**, 229–233.
7. Morton, W. and Hearle, J., *Physical Properties of Textile Fibres*, John Wiley & Sons, New York, 1975, 178.
8. Lotens, W., *Heat Transfer from Humans Wearing Clothing*, Doctoral Thesis, published by TNO Institute for Perception, Soesterberg, The Netherlands, 1993, 34–37.
9. Nordon, P. and David, H. G., 'Coupled Diffusion of Moisture and Heat in Hygroscopic Textile Materials', *Int J Heat Mass Transfer*, 1967 **10** 853–866.
10. Stanish, M., Schajer, G. and Kayihan, F., 'A Mathematical Model of Drying for Hygroscopic Porous Media', *AIChE Journal*, 1986 **32** (8) 1301–1311.
11. Dullien, F., *Porous Media: Fluid Transport and Pore Structure*, Academic Press, London, 1979, Chapters 4 and 6.
12. Kaviany, M., *Principles of Heat Transfer in Porous Media*, Springer-Verlag, New York, 1991, 428–431.
14. Chatterjee, P., *Absorbency*, Elsevier Science Publishing Co., Inc., New York, 1985, 46–47.
15. Ghali, K., Jones, B. and Tracy, J., 'Modeling heat and mass transfer in fabrics', *Int J Heat and Mass Transfer*, 1995 **38** (1) 13–21.

16. Gahli, K., Jones, B. and Tracy, J., Modeling Moisture Transfer in Fabrics, *Experimental Thermal and Fluid Science*, 1994 **9** 330–336.
17. Crow, R. and Moisture, 'Liquid and Textiles – A Critical Review', Defense Research Establishment Ottowa, *DREO Report No. 970*, June 1987.
18. Crow, R. and Osczevski, R., 'The Effect of Fibre and Fabric Properties on Fabric Drying Times', Defense Research Establishment Ottowa, *DREO Report No. 1182*, August, 1993.
19. Crow, R. and Dewar, M., 'The Vertical and Horizontal Wicking of Water in Fabrics', Defense Research Establishment Ottowa, *DREO Report No. 1180*, July, 1993.
20. Henry, P., 'Diffusion in absorbing media', *Proceeding of the Royal Society of London*, 1939 **171A** 215–241.
21. Li, Y. and Holcombe, B., 'A Two-Stage Sorption Model of the Coupled Diffusion of Moisture and Heat in Wool Fabrics', *Textile Research Journal*, 1992 **62** (4) 211–217.

10

The cellular automata lattice gas approach for fluid flows in porous media

D. LUKAS and L. OCHERETNA, Technical University of Liberec, Czech Republic

10.1 Introduction

It is appropriate to recollect the meaning of the word 'automaton', initially, for a better understanding of the concept of cellular automata. The word 'automaton' (plural – 'automata') is derived from the Greek word 'automatos' meaning 'acting of one's own will, self-moving'. In ancient Egypt, the term automaton was utilised for toys to demonstrate basic scientific principles. During the period of the Italian renaissance, automaton was the term used for mechanical devices, which were usually powered by wind or by moving water. The concept of modern automata started with the invention of automated animals (birds in a cage, mechanical ducks, etc.) and humanoids (robots). Therefore, in general, automaton suggests self-operation of activities or functions of an object in the absence of any permanent external governing factor.

One of the most popular modern automata, which can be found at any workplace, is a computer, forming an inseparable part of our life. However, this chapter will be mainly focused on a new type of automata, the 'cellular automata', which have received a lot of attention recently in the area of modelling and simulation.

According to one of the definitions provided by encyclopaedia, a 'cellular automaton' is a discrete model studied in computability theory and mathematics. Another definition states that it is a simplified mathematical model of spatial interactions in which each site, i.e. each cell or node of a two-dimensional plane, is assigned with a particular state at every instance of time and it changes stepwise automatically according to specific rules conditioned by its own state and by the states of its neighbouring sites. In Section 10.1.1, the ways by which cellular automata are used for modelling of physical phenomena and for reincarnation of some other models will be discussed. A more detailed definition of cellular automata and the difference between finite and cellular automata will be given in Section 10.1.2. Physical principles of lattice gas cellular automata will be described in Section 10.2. In the next Section, 10.3,

the reader will be introduced to various lattice gas models based on cellular automata: models of Hardy, de Pazzis and Pomeau (HPP) and Frisch, Hasslacher and Pomeau (FHP), along with their variations. Examples of computer simulations based on the Frisch, Hasslacher and Pomeau models will be presented in the Section 10.4, where physical phenomena such as fluid flow in an empty canal and in a canal with porous fiber-like material will be investigated. Lastly, Section 10.5 contains some suggestions and further information.

10.1.1 Historical overview

Cellular automata have been invented independently many times and, as indicated previously (Wolfram, 1983), have been used for different purposes and under different names, viz. 'tessellation automata', 'homogeneous structures', 'cellular structures', 'tessellation structures' and 'iterative arrays'. Some submit that cellular automata were introduced by John von Neumann under the name 'cellular space' at the end of 1940s. Others say that cellular automata were introduced by John von Neumann with his co-worker Stanislaw Ulam (Toffoli, 1991; Wolf-Gladrow, 2000). Original and pioneering work in this area was also done by Konrad Zuse around this time.

It is mentioned in literature that mainly two journeys took place during the development of cellular automata. The first of them built up cellular automata, originally perceived merely as 'toy' tools, into serious systems of biological investigation and monitoring. Based on von Neumann's works about self-reproducing systems (von Neumann, 1963, 1966), these studies have been developed in Lindenmayer, (1968), Herman, (1969), Ulam, (1974), Kitagawa, (1974) and Rosen (1981), for example. The last one streamed into computer problems (Sarkar, 2000). An excellent instance of the application of cellular automata in biology is the game of 'Life', invented by John Conway (Gardner, 1970). Examples of cell patterns obtained by Conway's game 'Life' are shown in Fig. 10.1. A system evolution after 80 time steps or time units (t.u.) from an initial state has been considered there. It has been shown that simple update rules may lead to the formation of complex cellular patterns similar to living cell colonies, and plant and animal tissues. Several theoretical studies and analyses, related to the properties of cellular automata, augured their occurrence in modelling physical problems, especially in the simulation of hydrodynamic phenomena. It has already been noted that, in spite of simple update rules, cellular automata can display complex behaviour, which makes this suitable for use as a simulation tool for the description of many-particle or collective physical phenomena. The fully discrete model of hydrodynamics, based on the cellular automata concept, was first introduced by Hardy, de Pazzis and Pomeau (Hardy *et al.*, 1973), nowadays known as the HPP model. This model led to many interesting results, but it has had

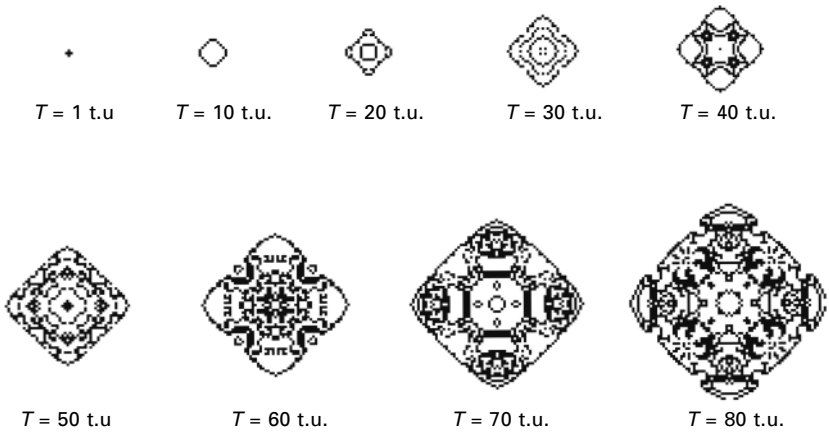

10.1 Sets of patterns obtained in Conway's game of 'Life' for various time evolution steps T (courtesy of Jakub Hrůza).

limited application because of its anisotropic behaviour. It was not refined until 1986, when Frisch, Hasslacher and Pomeau designed their own 'FHP' model, based on a triangular lattice. Since then, application of the FHP model in modelling hydrodynamic problems has led to the design of derivative models. In the next sections, examples of such models and their usage in transport phenomena through porous materials will be discussed.

10.1.2 Finite automata, cellular automata, and cellular automata lattice gases

The phrase 'cellular automaton' usually indicates an infinite set of finite automata, which are interrelated in a specific manner. A lattice gas cellular automaton is a special case of cellular automaton. What do the terms finite automaton, cellular automata, and lattice gas cellular automata mean in general and in the realm of cellular automata? Definitions of these terms are provided below.

Finite automata. 'Finite automata' refers, in general, to a class of mathematical models of processors, or a special class of programming languages, that are characterised by having a finite number of states (Lawson, 2003), which evolve in time and produce outputs according to rules depending on inputs (Rivet and Boon, 2001). Similar definitions of finite automata can be found in literature sources, which refer to principles of simulation, modelling and programming. Taking this viewpoint, a finite automaton model consists of a finite set of internal states $Q = \{q_0, q_1, \ldots, q_n\}$, where q_0 is an initial state, of a finite set of possible input signals $A = \{a_1, a_2, \ldots, a_m\}$, and of a finite set

of possible output signals $B = \{b_1, b_2, \ldots, b_p\}$ (Kudryavtsev, originally Кудрявцев, 1985). Elements of the aforementioned set Q indicate a state space of the automaton, while sets A and B are the so-called alphabets (Chytil, 1984). It is assumed that the finite automaton works at discrete time moments, i.e. at discrete time steps t, $t + 1$, $t + 2$, etc. There exist two functions that drive the work of the finite automaton with respect to time, which are called transition functions. The first of them, denoted as φ, determines the state $q(t + 1)$ of a finite automaton at an instant $t + 1$ if the previous automaton's state $q(t)$ and actual input signals $a(t)$ are known. Then $q(t + 1) = \varphi(q(t), a(t))$. The last-mentioned function ψ designates output signals $b(t)$, where $b(t) = \psi(q(t), a(t))$. An output signal of a finite automaton can be used as an input signal for another automaton. Three possible methods of finite automata representation are shown in Fig. 10.2. The term 'individual automaton' is used instead of 'finite automaton' in the realm of lattice gas cellular automata models (Rivet, 2001). This notation will be followed hereafter.

Cellular automata. According to Wolfram (1986), 'cellular automaton' is a set of identical cells located in a regular and uniform lattice. A single cell is considered to be an individual automaton. The main characteristics of a finite automaton, mentioned above, relate to a cell of a cellular automaton. Therefore, a cellular automaton can be represented by a set of synchronized identical finite automata, which exchange their input and output signals with predefined neighbourhoods in accordance to a connection rule, which is the same for all finite automata in a particular model (Rivet, 2001). Purposely, this definition does not contain any reference to the geometrical structure of the lattice, as it is not important to know the distances or angles between neighbours. However, it may be noted that all finite automata in a cellular automaton are identical and frame a homogeneous structure having a uniform internal structure and obeying the same evolution and connection rules. An example of a two-dimensional cellular automaton is presented in Fig. 10.3. Evolution rules are carried out in this case for the concrete transition function.

Lattice gas cellular automata. As mentioned earlier (Frisch *et al*., 1986), the points of view from which a fluid can be described are molecular, kinetic, and macroscopic. The detailed behaviour of a fluid in a continuum at macroscopic level is provided by partial differential equations, e.g. Navier–Stokes equations for the flow of an incompressible fluid. Some other numerical techniques, such as finite-difference and finite-element methods, are used for transforming a continuum system into a discrete one (Chen *et al*., 1994). The lattice gas models based on cellular automata are newer compared to the numerical methods mentioned above. These models make it possible to describe the behaviour of fluid systems at a molecular level under various microscopic conditions. They are based on detailed information about individual particles,

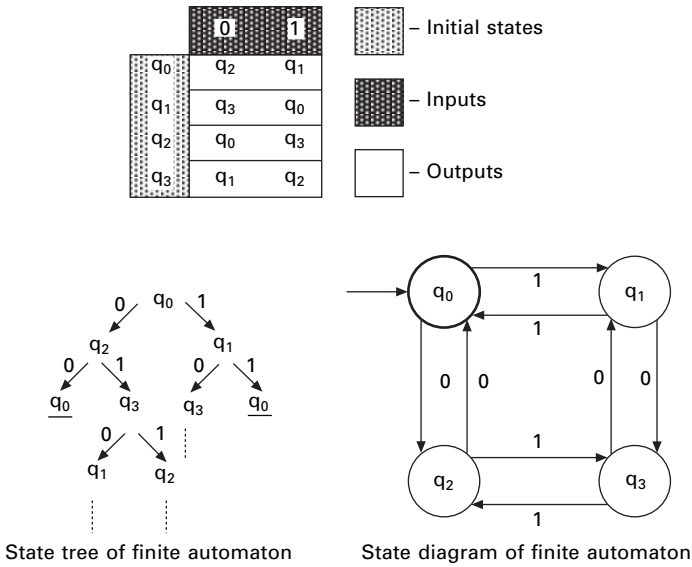

10.2 Classical method of finite automata represented with state tree, state diagram and an input–output table. The table of states determines an initial state q_0, final states and a transition function φ. For instance, from the second table line it is evident that, with the instant state $q(t) = q_1$ and the momentary input signal $a(t) = 0$, the subsequent output state is $q(t + 1) = \varphi\,(q(t), a(t)) = q_3$. The original root of the state tree arises from the initial state q_0. The number of links that come out from each cusp of the tree is equal to the total number of input and output signals. Successors of each state are created according to the input signals, using the transition functions. Cusps of the state diagram agree with the states of automaton. Links indicate the possible transitions between all possible states.

such as their positions, masses, and velocities and they provide output in terms of molecular dynamics. Thus, lattice gas models entered into the history as an alternative for modelling fluid systems.

It is a well-known fact from the molecular theory developed in the last century that, in the equilibrium state, individual molecules in crystals fluctuate around their average locations and that only occasionally do they jump out to other locations; these are considered as fluctuations. These jumps occur due to the molecule's interaction with other molecules, when the system is shifted from its equilibrium state by some agent. A remarkable idea was to consider that a fluid has a structure similar to a crystal and that every liquid molecule sits at some fixed point, having the same number of neighbouring sites at a definite distance. These sites are either empty or occupied by a molecule (Boublík, 1996). These spatially organized patterns of molecules are in accordance with the term 'lattice gas model'. Different types of lattice gas models were proposed for a description of simple liquid behaviour.

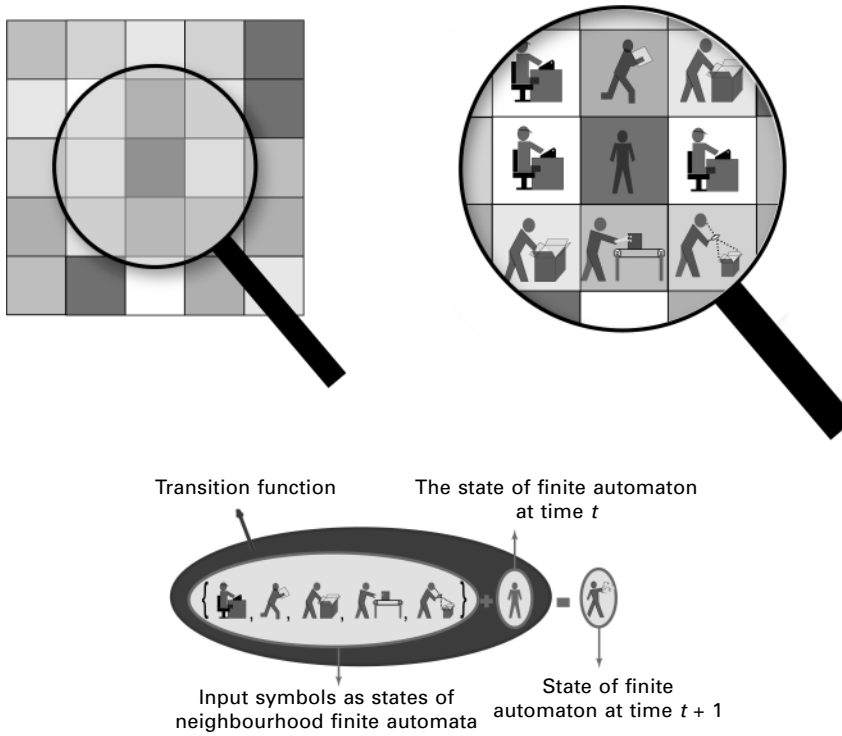

10.3 Graphical interpretation of a cellular automaton: general appearance of a lattice of cells, detailed configuration providing status of neighbourhood cells of a reference cell, and application of a transition function on input symbols (represented by all the states of the neighbourhood) and an instantaneous state of the cell in question at times t and $t + 1$.

There are two distinct basic lattice gas models mentioned in the literature: non-interacting and interacting. The non-interacting lattice gas is mentioned in Kittel's book (Kittel, 1977). This model is represented by a set of N non-interacting atoms distributed over N_0 lattice cells. Each cell is either occupied or empty. This system does not have any kinetic energy or any energy due to interaction. In spite of that, it found its application in statistical physics because the non-interacting lattice gas model provides the correct shape of the ideal gas state equation where the pressure is obtained as a partial volume derivation of the system entropy. The interference of non-interacting lattice gas models and models based on cellular automata possibly helped towards a creation of interacting lattice gas models. Models, partly discrete with respect to time and space, were well known from the point of view of biological applications of cellular automata since the end of the 1960s. The first so-

called classical lattice gases appeared as theoretical models for liquid–gas transition around the late sixties and beginning of seventies (Stanley, 1971). A moment-conserving lattice gas model started to be an object of interest in hydrodynamics and statistical mechanics when Kadanoff and Swift proposed their first discrete-velocity model (Kadanoff and Swift, 1968). They created a version of the Ising model in which positive spins acted as particles with momentum in one of the four directions on a square lattice, while negative spins acted as holes. Particles were then allowed to collide each with other or to exchange their positions with holes satisfying the conservation of energy and momentum (Rothman and Zaleski, 1994). Thus, the first interacting lattice gas models appeared at the beginning of the 1970s. The previously mentioned HPP model (Section 10.1.1) was the first well-known interacting lattice gas model, which reflected inception of current lattice gas models.

Lattice gas cellular automata belong to the general class of cellular automata, thus sharing features characteristic to that class:

(i) Being one of the cellular automata, lattice gas cellular automata consist of identical individual automata which are tied geometrically to the nodes of a Bravais lattice, situated in a Euclidean space of dimension D. Individual automata are also called 'nodes' in the purview of cellular automata lattice gases.

(ii) The instantaneous state of lattice gas cellular automata depends on the states of all individual automata. Each individual automaton can inherit any one of the 2^B states. The quantity B represents the number of channels that correspond to the geometry of a lattice. These links play a role of 'communication channels' between neighbouring lattice nodes. Each channel may either be occupied by a fictitious particle or remain empty, and so it has two possible states of existence. Consequently, information about the channel's occupation corresponds to signals fed to individual automata.

(iii) The elementary evolution process of lattice gas cellular automata takes place in regular discrete time steps and consists of two distinct phases of evolution. The first of them is the collision phase. During this phase, each individual automaton takes the new post-collision state depending on input signals and transition rules. New states of individual automata generate output signals for the next evolution step. During the propagation phase, output signals of one automaton are conveyed to its neighbouring nodes, i.e. neighbouring individual automata, along the channels, thus, becoming a part of the input signals for its neighbours during the next time step. We should emphasise that all the changes in each of the individual automata of the lattice gas cellular automata, transmit output signals simultaneously. The transition rules are the same for all individual automata and do not depend on their position.

In Fig. 10.4 is sketched the two-dimensional lattice gas cellular automata model based on the triangular Bravais lattice and the state of one individual automaton in a pre-collision phase. Detailed description of the principles and the terms related to the lattice gas cellular automata are furnished in the sections of this chapter to follow.

10.2 Discrete molecular dynamics

At a microscopic level, physical fluids consist of discrete particles. The particles of various fluids have variant shapes, masses, degrees of freedom, chemical structure etc., as shown in Fig. 10.5. That is why the very microscopic guise of collision events between and among them is quite likely to be different. The structure of the individual molecules of physical fluids influences the fluid density and formulates the concrete fashion of molecular interactions, which can affect fluid viscosity. On the other hand, as is well known from previous experiments, the general macroscopic behaviour of a fluid hardly depends on the nature of the individual particles constituting that fluid. From a theoretical point of view, significant variations of the molecular forms do not alter the basic nature of the macroscopic equations governing fluid dynamics. Those universal equations, such as the Navier–Stokes equation describing fluid dynamics or the equation of continuity, are, in fact, quite insensitive to microscopic details (Wolfram, 1986).

The next underlying property of fluids is based on the spatial scale relationship between the mean free path of a particle after and before the

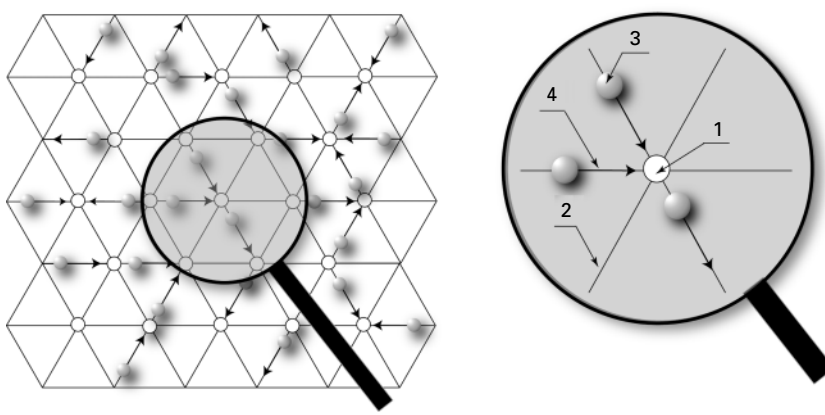

10.4 Two-dimensional lattice gas cellular automata with a selected individual automaton highlighted will all details. The numbers assigned to the highlighted automaton indicate: 1 – the central node; 2 – a link/channel that connects the central node and one of the neighbouring nodes of the individual automaton; 3 – a moving particle; 4 – an arrow representing the particle velocity vector.

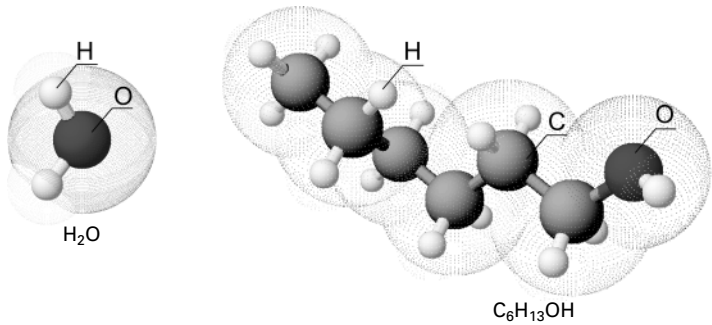

10.5 Water and hexanol molecules have different structures.

succeeding collision and the areas in which collision events occur. As mentioned before (Succi, 2001), in a common collection of gas and liquid molecules, the average inter-particle separation is much greater than the typical size of an individual molecule, as is estimated by the 'de Broglie length'; $\lambda = h/p$, where h is the Planck constant and p is a particle momentum. So the molecules may be treated as point-like particles. Moreover, these point-like particles/molecules interact via short-range potentials and the effective ranges of interaction potentials are much smaller than the mean inter-particle separation.

The universality of fluid dynamics leads one to attempt to extend the universality of the hydrodynamic to model fluids with even simpler microscopic dynamics, molecular structure, and inter-molecular interactions than any real fluid has. The gap between space scales of particles' free movements and particles' interactions, i.e. collision events, opens up the possibility of restricting the particle collisions strictly as localized events and of building up this concept as a lattice model, aiming at drastic simplification of classic Newtonian mechanics. From this, one can envisage a splendid fluid model with few assumptions to accomplish it, such as, considering that the particles travel only along the links in regular lattices, and that the inter-particulate collisions occur only at lattice nodes. This super simplification brings about a fully discrete model of hydrodynamics (Rothman and Zaleski, 1994), where the discreteness concerns space, time, particle velocities and any other microscopic observable physical quantities. Lattice gas cellular automata, as these models are generally called, are, in fact, drastically simplified versions of molecular dynamics. The cornerstone for this research has been laid by Frisch *et al*. (1986) and Hardy *et al*. (1973).

It has been shown that lattice gas cellular automata, having continuity on a large scale, can be described by the partial differential equations of hydrodynamics. The Navier–Stokes system of equations (Landau and Lifschitz, 1987) is introduced below, in Equations [10.1] and [10.2]. The system of continuity equation will be started with the law of mass conservation.

$$\frac{\partial \rho}{\partial t} + \vec{\nabla}(\rho \vec{v}) = 0 \qquad [10.1]$$

where t is time, $\vec{v} = \vec{v}(x, y, z, t)$ is the local and momentary liquid velocity vector close to a point having positional coordinate (x, y, z) in a rectangular Cartesian system, and ρ denotes the fluid's density derived from its mass. The symbol $\vec{\nabla}$ denotes the vector of differential operations $(\vec{i}\partial/\partial x, \vec{j}\partial/\partial y, \vec{k}\partial/\partial z)$ containing unitary vectors $\vec{i}$, $\vec{j}$, and $\vec{k}$, oriented along x, y and z axes respectively.

The intrinsic Navier–Stokes equation relates the fluid's elementary changes in velocity at particular spatial locations with external forces, such as a force field, a pressure drop, and viscous drag being their origin. Based on Newtonian mechanics, this equation has to reflect conservation laws of momentum and energy. For a non-compressive liquid, the equation takes the form:

$$\frac{\partial \vec{v}}{\partial t} + (\vec{\nabla} \times \vec{v}) \times \vec{v} + \frac{1}{2}\vec{\nabla}(v^2) = -\frac{\vec{\nabla} p}{\rho} - \vec{\nabla} U + \frac{\eta}{\rho}\Delta \vec{v} \qquad [10.2]$$

where p is the pressure, η is the dynamic viscosity, and U represents the scalar potential due to an external field. Finally, Δ is the scalar product of $\vec{\nabla}$ and $\vec{\nabla}$ i.e. $\Delta = \vec{\nabla} \cdot \vec{\nabla}$.

Ultimately, to comment briefly on the idea of a creation of a beneficial lattice model of physical fluids with respect to the content of Chapter 14, where formally similar lattice structures of fluids interacting with fibrous materials, so-called 'auto-models', are introduced. Auto-models reflect the universal behaviour of liquids with respect to equilibrium thermodynamic laws, where the leading parameter is the surface tension and the underlying microscopic phenomena are attractive and repulsive forces, primarily considered as interaction energies between neighbouring molecules. This universality also leads to the lattice models in Chapter 14.

10.2.1 Lattice as a discrete space

The advantages of quite a simple model of hydrodynamics, which has been discussed above, will now be introduced. The spatial structure and the geometry of the fluid model's discrete space will be introduced at first. Lattices are realised in various dimensions. Here, only one- and especially two-dimensional lattices will be considered. A lattice consists of links, which will be referred to as 'channels' henceforth, to evoke traffic paths for particle movements. It also consists of nodes, where particles can collide. The channels connect the neighbouring 'nodes'. As a rule, several channels meet in one node and the total number of channels that meet in a node is denoted by B, known as the 'connectivity'. A node in a cellular automaton represents an individual

automaton, where inputs and outputs are realised through channels with jumping particles. Nodes will be represented by their radius vectors $\vec{x}_i$ in a desirably chosen coordinate system. The structure of a channel network predescribes the set of allowed particle velocities. Nodes connected directly by a channel are neighbours and the set of all neighbouring nodes of the one in question is called its 'neighbourhood'. From the above it follows that the set of all possible particle velocity directions destines the system of its neighbourhoods since these directions link the neighbours. The distance between nearest neighbours is denoted Δl, and this length is called the 'lattice unit', expressed in units of l.u. The channel vector $\vec{e}_i$ is the unitary vector connecting neighbouring nodes through the channel i. In brief, the site at the centre is connected to its B neighbours by channels corresponding to the unity vectors $\vec{e}_i$ through $\vec{e}_B$.

It is essential that such lattices be homogeneous and symmetric, as will be explained in detail later on. Additionally, the issue of symmetry of the concerned lattices is the major obstacle standing between the super-simplified discrete lattice gas cellular automata and continuum hydrodynamics, thus drawing one's attention momentarily towards it.

Previous works with lattice models of hydrodynamics, introduced by Hardy, de Pazzis, and Pomeau (Hardy, 1973, 1976), dealt with issues related to problems of statistical mechanics, such as ergodicity and time correlations. Unfortunately, they have only limited application because this class of lattice gas models is limited to anisotropic hydrodynamics. Their anisotropic behaviour will be briefly dealt with in Section 10.2.4, describing the collisions of a lattice gas stream with a straight wall. The anisotropic properties of the HPP model were the direct consequence of the choice of a square lattice. It seems quite surprising that it took one decade to realise the direct consequences of underlying lattice symmetry on the hydrodynamics of lattice models. Fortunately, a very simple extension of the lattice shape to a triangular one with hexagonal symmetry suffices to inspire a discrete model to describe the macroscopic isotropic behaviour of hydrodynamics. The triangular lattice for lattice gas cellular automata was first introduced by Frisch, Hasslacher and Pomeau (Frisch, 1986). The lattice gas cellular automata based on square or on triangular lattices will be explained in detail in Section 10.3.

Another necessity originating from the nature of cellular automata pertaining to the discrete fluid models is the structural homogeneity of the underlying lattices with respect to the neighbourhood of each node, which has to be identical. Figure 10.6 depicts two regular and square lattices partly covering a plane. One of these lattices has each of its odd rows shifted by a distance equal to half the length of its elementary side, i.e. half of the lattice unit (l.u.). A lattice without such a shift has identical neighbourhoods. This is the reason behind the fact that only the lattice without any shift fulfils the homogeneity conditions. The homogeneity conditions within a family of

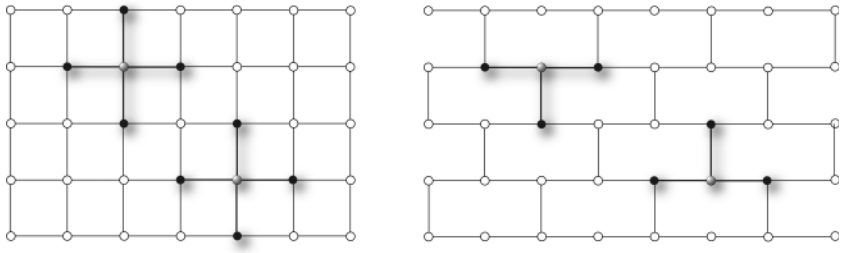

10.6 Illustration of two rectangular lattices with unlike neighbourhoods: The square lattice on the left-hand side is homogeneous, having identical neighbourhoods surrounding it. The neighbourhoods of the right-hand side rectangular lattice consist of three nodes appearing in two configurations, as highlighted.

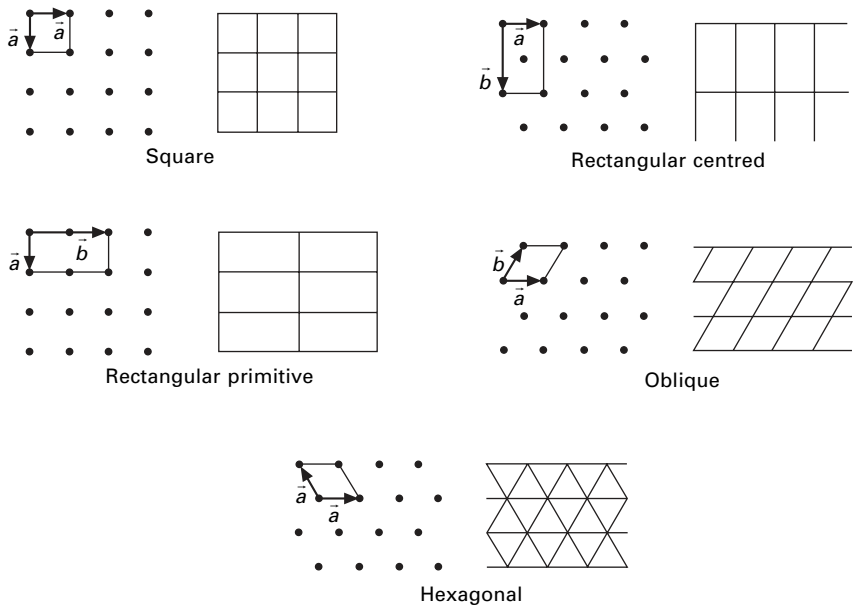

10.7 All possible two-dimensional configurations of Bravais lattices.

regular lattices may be verified from the definition of Bravais lattices (Ashcroft and Mermin, 1976). The complete set of two-dimensional Bravais lattices is introduced in Fig. 10.7.

As is mentioned by Rivet (2001), the Bravais lattice is essentially an infinite one. For a lattice gas cellular automaton, it is considered that the lattice is only a subset of the relevant Bravais lattice. The reason behind it is quite simple: the memories of our computers have finite capacities and hence, in practical applications, this lattice subset contains only a finite number of lattice nodes.

10.2.2 Discrete time

It makes sense to speak about time intervals of lattice gases. The aspect of time dependence of lattice gases makes comparison of collective motions in lattice gases with space- and time- dependent local flows in real fluids possible. Time, as well as space of lattice gas cellular automata, is made discrete. The particles jump from their starting nodes to their destination nodes coherently. This synchronisation of jump of all particles constitutes the next step for the fluid model simplification. Each of the pairs of starting and destination nodes is connected by a channel colinear with the velocity vector of the jumping particle. Briefly speaking, in the synchronised time-cycle, particles hop to the nearest neighbour by the corresponding discrete vector $\vec{v}_i$.

The way to introduce a time unit into the lattice gas cellular automata model is the next problem. According to Rivet (2001), the basic element of a cellular automaton, an individual automaton forming the mathematical model of a processor with a finite number of possible internal states, evolves and produces output data according to a rule depending on input symbols belonging to a finite set of the alphabet. The above definition directs one towards a deterministic evolution rule for the internal state of an individual automaton. Since the internal state of an individual automaton can change, the automaton undergoes some kind of evolution and therefore the underlying notion of the 'past' and a 'future' is derived. However, these primitive notions do not necessarily imply a temporal structure for the automaton, since the concept of a time interval between events and the evolutionary behaviour of a cellular automaton as a whole is not included in the definition. That is why it is imperative to discuss the consequence of local automata synchronisation in a cellular automaton.

Synchronisation of a cellular automata model with respect to time makes time the global parameter for all the nodes simultaneously. Therefore, there must be a single clock for all nodes, which justifies the unified time run for a lattice gas cellular automaton as a whole. The elementary synchronised particle jumps in a lattice gas cellular automaton are repeated at regularly spaced discrete time intervals. The time increment Δt between successive jumps is called the 'time step', which is equivalent to a time unit abbreviated as 1 t.u. For the time step, the relationship $\Delta l = v\Delta t$ holds true. This relationship expresses the fact that a particle with velocity $\vec{v}_i$ present in the ith channel at the node $\vec{x}$ goes to the neighbouring node $\vec{x} + \vec{v}_i\Delta t$ in 1 t.u. The collision phase is considered as an instantaneous one without any consumption of time. It means the time between succeeding collisions is Δt.

The elementary evolution process of a lattice gas cellular automaton, which occurs at each time step, is a sequence of two distinct phases: the collision phase and the propagation phase. The order of these two phases is immaterial regarding time evolution of the cellular automaton. The aspect

that is of great importance is the transition between the phases. Section 10.4.2 is devoted to a deeper description of the propagation and collision phases.

10.2.3 Discrete observables

Observables, i.e. the basic physical quantities of a lattice gas cellular automaton, may be scalars, vectors or more generally tensors of arbitrary order. Basic observables of lattice gas cellular automata are connected to a channel of an index i and so they will be called 'channel observables' henceforth. A typical channel observable is the number of particles $n_i(\vec{x})$ at a channel i of the node $\vec{x}$. The 'value of the observable measured at node $\vec{x}$' is the total amount of the observable quantity present at node $\vec{x}$. It is called the 'microscopic density per node' or simply its 'microscopic density' if the observable is a scalar. If the observable is a vector, the value measured at a node is called a 'microscopic flux'.

The essential observable of a lattice gas is the number of particles, namely the number of particles $n_i(\vec{x})$ at a channel i, i.e. the channel particle density, and the total number of particles at a node $\sum_{i=1}^{B} n_i(\vec{x})$, which is the microscopic particle density at that spot. Commonly, a constraint called the 'exclusion principle' is imposed, which resembles Pauli's exclusion principle in quantum mechanics. The 'exclusion principle' of lattice gases says: No two particles sitting at the same node can move along the same direction of the channel at the same time. The existence or non-existence of a particle at a channel i creates a two-bit 'channel configuration space' composed of two 'channel states'. The distribution of a set of particles on various channels of the particular node defines the 'local configuration space'. Regarding the exclusion principle, the local configuration space consists of 2^B various 'local states', where B is the number of channels growing from a node.

The next scalar observable is the individual mass of a particle. The mass assigned to any particle in a channel i at the node $\vec{x}$ is denoted as $m_i(\vec{x}_i)$. The total mass $m(\vec{x})$ at the node $\vec{x}$, i.e. microscopic mass density, is given by the following formula:

$$m(\vec{x}) = \sum_{i=1}^{B} m_i(\vec{x}) n_i(\vec{x}) \qquad [10.3]$$

Symbol $\vec{v}_i$ is used to denote 'velocity vectors' of particles at a channel i. The velocity vectors must have the same local symmetries as the lattice has; that means the set of velocity vectors includes individual particle velocities that are determined by the structure of the underlying lattice. This set of velocity vectors remains globally invariant for all nodes in the lattice. The number of channels outgoing from a node determines the maximal number of various

velocity vectors. Moreover, some particles can rest in a node with zero velocity. If the evolution rule involves exchanges of particles only with all the nearest neighbours and if all the velocity vectors are non-zero, then the model is said to be 'homokinetic', all velocity vectors having the same modulus $v = |\vec{v}|$. Two homokinetic models HPP and FHP-1 will be introduced shortly in Section 10.3. Assuming a unit time step, the velocity vector of each particle in a homokinetic model is given simply by the vector, $\vec{v}_i = \vec{e}_i \Delta l / \Delta t$.

From the above-mentioned observables, one can easily derive the rest of the scalar and vector observables. To start with the scalars, the total kinetic energy $E(\vec{x})$ at the node $\vec{x}$, i.e. the microscopic density of kinetic energy, is obtained from the following formula:

$$E(\vec{x}) = \frac{1}{2} \sum_{i=1}^{B} m_i(\vec{x}) v^2(\vec{x}) \qquad [10.4]$$

The microscopic density of potential energy $W(\vec{x})$ at a node $\vec{x}$ holds the following relation:

$$W(\vec{x}) = U(x) \sum_{i=1}^{B} n_i(\vec{x}) \qquad [10.5]$$

where $U(x)$ is a scalar potential.

Among the vector observables, particle momentum $\vec{p}_i$ at the channel i is given by:

$$\vec{p}_i(\vec{x}) = m_i(\vec{x}) n_i(\vec{x}) \vec{v}_i(\vec{x}) \qquad [10.6]$$

Component 'α' of momentum of a particle at the channel i is $p_{i\alpha}(\vec{x})$. The total 'α' component of momentum at the node $\vec{x}$ is then determined by the formula [10.7]:

$$p_\alpha(\vec{x}) = \sum_{i=1}^{B} p_{i\alpha}(\vec{x}) = \sum_{i=1}^{B} m_i(\vec{x}) n_i(\vec{x}) v_{i\alpha}(\vec{x}) \qquad [10.7]$$

The microscopic momentum flux $\vec{p}(\vec{x})$ is written as

$$\vec{p}(\vec{x}) = \sum_{i=1}^{B} \vec{p}_i(\vec{x}) = \sum_{i=1}^{B} m_i(\vec{x}) n_i(\vec{x}) \vec{v}_i(\vec{x}) \qquad [10.8]$$

Besides the channel and microscopic observables, there are space-averaged quantities. The space averaging is carried out on a connected subset of the underlying lattice. The set of all nodes in this subset is denoted as ϕ. After that, the space-averaged mass density $m(\phi)$ is defined using the formula

$$m(\phi) = \frac{1}{N(\phi)} \sum_{\vec{x} \in \phi} m(\vec{x}) \qquad [10.9]$$

where, $N(\phi)$ is the total number of nodes in the lattice subset ϕ. Finally, it should be noted that macroscopic densities and macroscopic fluxes that are space- or time–averaged are physically relevant.

The basic notions, definitions and fundamental visage of a lattice cellular automata serve as equipment sufficient to continue with a description of their kinetics or dynamics.

10.2.4 Propagation, conservation laws, and collision rules

The dynamics of lattice gas cellular automata consists of two essential phases: propagation and collision. The propagation phase will be considered first, as it is conceptually much easier to understand. Before the collision phase is dealt with, the basic concept of lattice gas conservation laws will be adopted. As will be shown hereafter, these conservation laws govern the discrete dynamics of lattice gas cellular automata.

Propagation phase. During the propagation phase, a particle is shifted from one node to another, i.e. if a particle is present at any moment t in a node $\vec{x}$, it is shifted to the neighbouring node in time $t + \Delta t$. It is notable here that the neighbourhood is pre-described by all practicable velocity vectors $\vec{v}_i$, according to a node-independent rule that covers the whole lattice. In practice, the particle at the channel i is transferred during the propagation phase from the node $\vec{x}$ to the node $\vec{x} + \vec{v}_i \Delta t$. Consequently, the state of the channel i remains the same, but the node changes from $\vec{x}$ to $\vec{x} + \vec{e}_i$ after the propagation. In other words, the propagation phase carries the particle from channel i of the node $\vec{x}$ to the channel i of the node $\vec{x} + \vec{e}_i$.

The above description of the propagation phase raises the problem of finite size Bravais lattice subsets that are used for lattice gas cellular automata (as mentioned in Section 10.2.1). Indeed, if the lattice under the consideration is finite, the node $\vec{x} + \vec{e}_i$ may be outside this finite lattice, even if the node $\vec{x}$ from which the particle departs is inside. There are various strategies to solve this problem. One of the solutions is to introduce 'periodic boundary conditions'. More precisely, the part of the lattice on which the cellular automaton for the lattice gas is implemented has to be a finite sub-region of the underlying Bravais lattice, whose opposite sides can be connected to form a loop. This wrapping of opposite sides of a finite lattice leads to a periodic motion of the individual particles. The escaping particles return to the finite lattice on the opposite sides of its boundaries. Periodic boundary conditions influence the propagation phase only. Figure 10.8 gives more details about it.

Another solution of the conflict between the theoretically infinite lattices of cellular automata and limited memories of computers that confines one to finite ones is to use 'reflective boundary conditions'. Reflective boundary

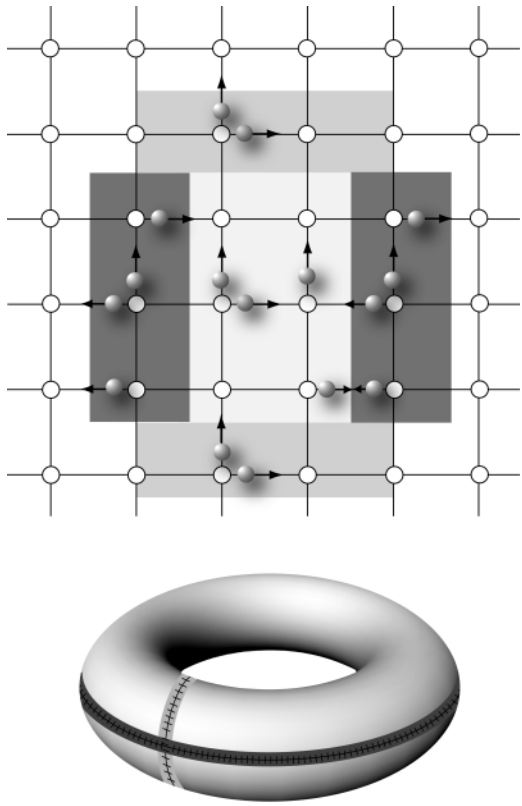

10.8 Periodic boundary conditions for two-dimensional square lattice gas cellular automaton, as used for the HPP model, result in identical collision and propagation occurring at the boundaries opposite each other. A system with periodical boundary conditions may be represented using fine-drawn joins. These joins transform the originally plan or lattice of nodes into a 3-D body on which surface the originally opposite boundaries of the lattice are joined together.

conditions are based on various types of particle collisions with walls that constitute impenetrable boundaries of the finite subset of Bravais lattice or with obstacles that represent the material of a porous or fibrous media. Since these boundary conditions are collision based, it has been decided to describe them in further detail in the subsection under the heading 'Collision rules'. It can be summarised that reflective boundary conditions constitute bouncing of a particle from a wall back to the finite Bravais sub-lattice. The wall remains fixed all the time. It absorbs some of the portion of the colliding particle's momentum, while the particle, after the collision, keeps its original velocity modulus v.

The crucial feature of all the introduced boundary conditions is that they keep all the particles in the game. It means that none of the particles in the

vicinity of the boundary of a finite Bravais sub-lattice may escape; they either reappear on the opposite side in the case of periodic boundary conditions, or bounce back as a result of a collision with a wall satisfying the reflective boundary conditions.

Conservation laws. The propagation phase, except for the boundary conditions, is the shapeless part of the lattice gas cellular automaton's lifetime. Particles move coherently towards their neighbouring nodes through the channels with constant velocities. This phase is purely kinetic. Particle motion is steady and linear during the abrupt and coherent jump. All the physical quantities of the particles, except those depending on the positions of the individual particles, are conserved. The lattice gas time during this phase, as the time step is defined as $\Delta t = \Delta l/v$. As the particle motion inside the channels has no relevance concerning the channels' state of cellular lattice gas automata, the time flux is discrete.

The next phase is very thrilling, when particles collide in an infinitely small time instant. To obtain the reasonable lattice equivalent of a real fluid dynamic, the conservation of particle numbers and conservation of their momentum are considered. Both these laws are described further for local collisions, i.e. inter-particle collisions at individual nodes. The results of such local collisions are unaffected by any events occurring in other nodes. For the conservation of the local particle number n and mass m in a node $\vec{x}$, the following relations hold true:

$$\sum_{i=1}^{B} {}^{n}n_i(\vec{x}) = \sum_{i=1}^{B} n_i(\vec{x}), \sum_{i=1}^{B} {}^{n}m_i(\vec{x})\,{}^{n}n_i(\vec{x}) = \sum_{i=1}^{B} m_i(\vec{x})n_i(\vec{x}) \quad [10.10]$$

The initial distribution of the colliding particles in the node $\vec{x}$ at individual channels i's is represented by $n_i(\vec{x})$, while their post-collision state in the same node and channel is given by 'new' ${}^{n}n_i(\vec{x})$ values. A collision of the particles in a node causes their redistribution possibly at all channels connecting the node in question with its neighbours.

The local momentum conservation during the collision phase may be expressed using its components ${}^{n}p_\alpha(\vec{x})$ and $p_\alpha(\vec{x})$ as:

$$\sum_{i=1}^{B} {}^{n}m_i(\vec{x})\ {}^{n}n_i(\vec{x})v_{i\alpha}(\vec{x}) = \sum_{i=1}^{B} m_i(\vec{x})n_i(\vec{x})\,v_{i\alpha}(\vec{x}) \quad [10.11]$$

Therefore, the redistribution of particles in an individual node obeys the rule of keeping the total momentum in this node constant. Rules governing particulate collision depend on the chosen model of the cellular lattice gas. Three such models will be introduced in Section 10.3.

Collision phase and collision rules. Particle-conserving and momentum-conserving local collision rules safeguard the correspondence of lattice gas

cellular automata models with Navier–Stokes systems (Landau and Lifschitz, 1987). Their concrete form is elucidated here using the original idea of the first and the simplest lattice gas cellular automaton introduced by Hardy, de Pazzis and Pomeau (Hardy and Pomeau, 1972). The model's title is also abbreviated to HPP (Frisch *et al*., 1986; Rivet and Boon, 2001), as has been mentioned earlier. This model is based on the two-dimensional regular square lattice. All the particles have the same unitary modulus of velocity v and they obey the exclusion principle. So the number of particles in a node spans from zero to four. The full set of collision rules for the HPP model can be reconstructed from the reduced set of two collision representatives with the application of lattice symmetry and superposition of the particle distribution obeying the exclusion principle. The representative collision events are depicted in Fig. 10.9.

The collision process is said to be 'microreversible' (Rivet, 2001) if any collision has the same probability as the reverse one, and this kind of collision symmetry is called 'detailed balance'. An original collision and the one assigned reverse to it are depicted in Fig. 10.9 as (A) and (C).

The next vital notion to be discussed is that of 'transitional probability'. Transitional probability denotes the probability of an occurrence of a certain post-collision state in the node as the consequence of a particular initial node configuration. As a rule, the symmetric collisions, matching with the lattice symmetry, have equal probabilities. The efficiency of lattice gas models to scatter particles through their mutual collisions is evaluated in terms of 'effective collision'. A collision is said to be an 'effective collision' when a

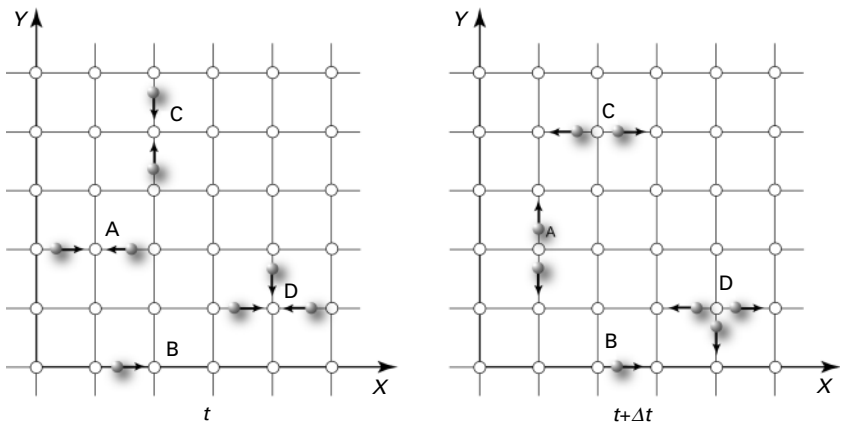

10.9 Schematic representation of collision events as applicable for the HPP model: Effective collisions (A) and (C) are microreversible. Collisions involving one (B) and three particles (D) do not change the velocity distribution of particles. The instantaneous positions of the particles, at time t and at a subsequent moment $t + \Delta t$ after one time step, are shown.

post-collision configuration at a node differs from its pre-collision configuration at the same node (Rivet, 2001). To make this notion more lucid, some of the non-effective collisions are also sketched in Fig. 10.9.

As has been mentioned in the beginning of this subsection, the symmetry of lattice cellular gas models is a vital issue, as it ensures its resemblance with continuum dynamics. Now, the anisotropic properties of a square, two-dimensional, lattice gas automaton may be briefly illustrated using the effect of a particle's collision with a solid impermeable wall, as shown in Fig. 10.10. To start with, various reflection behaviours of particles colliding with an impermeable obstacle will be introduced. Rivet (2001) introduced three different kinds of reflective boundary conditions. There are called 'no-slip', 'free-slip', and 'diffusive' boundary conditions.

No-slip boundary conditions, on a microscopic level, represent a bounce-back reflection of a particle colliding with a wall, i.e. with a wall particle. When a particle reaches the wall, its momentum as a vector is changed with central symmetry. In the centre of the symmetry is located a node where the collision occurs. In other words, the gas particle velocity vector goes round the half circle. Such a bounce-back collision conserves particle number and particle kinetic energy, and results in zero average velocity on a slip of a fluid flux in the vicinity of a wall, as each velocity vector at a time t belongs to the same particle velocity vector but with the opposite orientation at a succeeding time step $t + \Delta t$.

Free-slip boundary conditions are realised by 'specular reflection'. Microscopically, the specular reflection refers to the mirror reflection of a particle on a wall. The vector component of particle momentum, parallel to the wall surface, is conserved during such a collision, while the normal component of it is reversed. As a consequence, the cellular or lattice liquid freely moves along the wall without any change of its velocity component parallel to the wall. A point may be noted here, that it is quite troublesome to find a reflective flat surface on a rugged wall and the reader is referred to the work of Rivet (2001) for more details.

The diffusive boundary conditions are stochastic or statistical combinations of bounce-back and specular reflections occurring with chosen probabilities. All previously mentioned boundary conditions with respective types of reflections, i.e. collisions with walls and obstacles, are depicted in Fig. 10.10.

Going back to the lattice and lattice hydrodynamics isotropy, non-slip boundary collisions, realised by the bounce-back collision rule, are selected to demonstrate the anisotropic behaviour of a square lattice gas flowing along a flat wall in two-dimensional space. Two cases may be well distinguished. The wall inside the implicit square lattice of the HPP model may be either oriented along the channels in the lattice or inclined to this direction by an angle of 45°. In the first instance, a particle has no chance to slow down the bulk flow because every time, a particle from the gas bulk

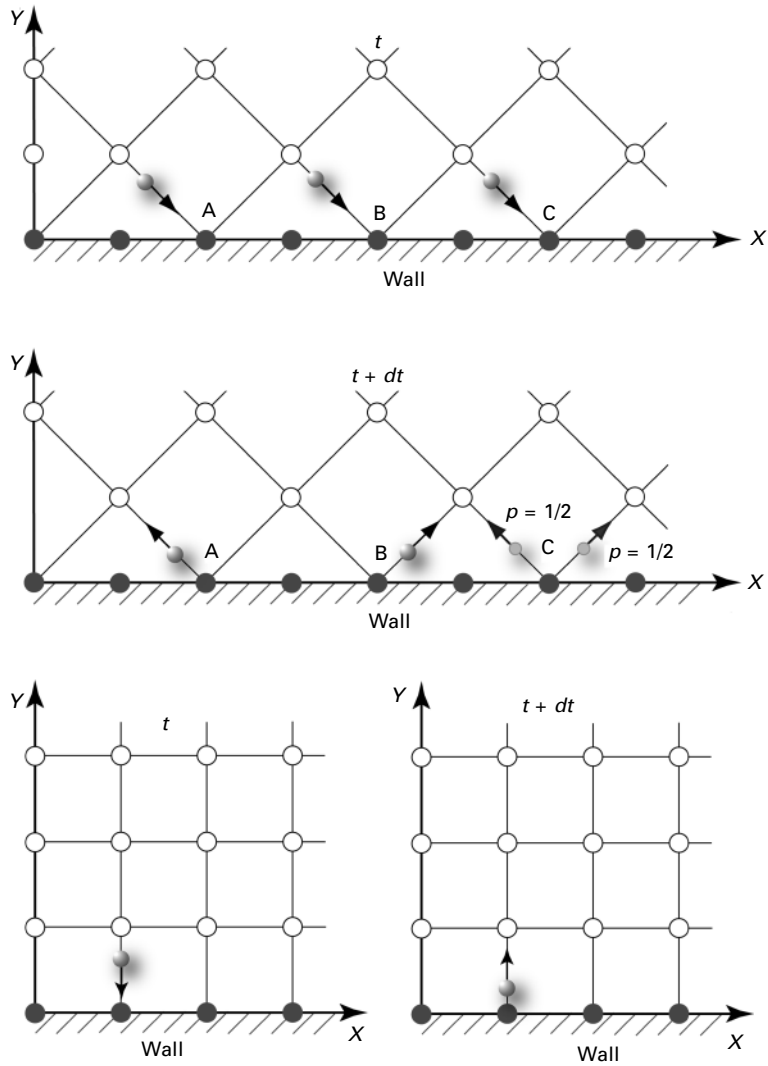

10.10 The upper and middle part of this figure constitutes impermeable walls, angled at 45° from the channel direction of the square lattice of the HPP model. Three various reflective boundary conditions that can appear are: (A) bounce-back reflection, (B) specular reflection, and (C) diffusive reflection. An HPP model with the wall parallel to a system of square lattice channels is depicted at the bottom. All previously mentioned types of reflections are indistinguishable with respect to the orientation of the impermeable wall. Due to the perpendicular direction of the velocity of particles colliding with the wall, there is no change in the particle momentum parallel to the wall before and after collision. Hence, the orientation of such a wall with respect to the lattice channels does not hinder the fluid flux. The initial and subsequent states of the automata are denoted with assigned time moments t and $t + dt$.

flying to the wall, attacks the wall perpendicularly. These colliding particles have zero component of velocity parallel to the wall surface. As a consequence, the wall does not get any chance to break or encumber the adjacent tangential flow. That is why a parabolic velocity profile typical to the laminar fluxes of Newtonian fluids near the walls will not be achieved. It is noticeable that, for the mutual orientation between the wall and the square lattice, the bounce-back reflection is identical to the specular reflection, and also identical to the diffusive reflections. This situation is depicted in Fig. 10.10. The same HPP lattice gas with underlying square lattice behaves in a different way when a wall is at 45° with one of the directions of the lattice channels. Falling particles on the wall carry both perpendicular and parallel momentum components with respect to the wall plane. During a bounce-back collision, a particle reverses its parallel momentum component. In other words, the wall will hinder a lattice gas flux caused by a prevailing movement of particles along the wall. It is now time to organise the parabolic velocity profile. The above-described behaviour of the HPP model is evidence of unsymmetrical properties of lattice gases living on square lattices. It is intuitively felt that such strict differences among various directions in triangular lattices with hexagonal symmetry do not exist. Therefore, the more advanced lattice gas cellular automata models have been developed on these triangular lattices. Two of them, FHP-1 and FHP-2, are described in the next section and additional details about them are mentioned in the Section 10.4.

10.3 Typical lattice gas automata

This section will introduce three classic lattice gas cellular automata models. The last of them will be used further (in Section 10.4) to demonstrate its utility for computer simulation of fibrous masses. Historically, the first lattice model was introduced in the early 1970s by Hardy, de Pazzis and Pomeau. They focused mainly on aspects of statistical physics. This model was based on a two-dimensional square lattice (Hardy *et al*., 1973) and had its roots in the earlier work of Hardy and Pomeau (1972). The same research group introduced fifteen years later (Frisch *et al*., 1986) a lattice gas cellular automata model, FHP-1, based on a triangular lattice with hexagonal symmetry. This was the simplest structure producing proper large-scale dynamics that could mimic the behaviour of a fluid. The last model that will be introduced in this section, abbreviated FHP-2 model, is a variant of the foregoing one. Unlike FHP-1, where all the particles were thought to move with velocities of unitary modulus, FHP-2 model included a possibility of one particle at rest in a node. The common feature of all previously mentioned lattice gas cellular automata models is the choice of basic channel observable values. If mass, velocity, momentum, energy, and time step are non-zero, they are all considered as unitary in their respective units.

10.3.1 Hardy, de Pazzis and Pomeau model

Let a two-dimensional square lattice having four channels at each node be envisaged. Then, the connectivity B is equal to 4, as shown in Fig. 10.9. Thus, each node has four neighbours. The distance Δl between neighbouring nodes is uniform and equal to 1 l.u. All the particles in the model have the same velocity modulus v of 1 (l.u./t.u). The masses m_i of the particles are equal and their value is taken as one unit mass (1 m.u). The model evolves in two phases – propagation and collision. A particle streams from its original node $\vec{x}$ to its neighbouring one $\vec{x} + \vec{v}_i \Delta t$ in the direction in which its velocity $\vec{v}_i$ is directed during the propagation phase. During the collision phase, the frontal collisions, i.e. the collisions of particles with opposite velocities, result in a rotation of both the particles by 90°, as illustrated particularly with examples (A) and (C) in Fig. 10.9. Briefly speaking, the horizontal motion of the particles arriving towards each other is changed to a vertical one when they depart from each other after their mutual frontal collisions. These rotations occur with probability one. It is to be noted that all other local states, denoted as (B) and (D) in the same figure, remain unchanged due to the constraint of momentum conservation. There are 2^4 different local configuration states of this model and only two of them are effective, i.e. two of them lead to the transition of the original state to the next local configuration state. One time-step of the Hardy, de Pazzis and Pomeau model is depicted in Fig. 10.9.

The degree of crystallographic isotropy of the model is not sufficient to produce large-scale isotropic dynamics that have been represented above with the Navier–Stokes equations for physical fluids. The shortcomings of this model are highlighted by the atelier of its designers with the following words (Frisch *et al*., 1986): 'When density and momentum are varied in space and time, micro-dynamic equations emerge differently, understood for HPP model and from the nonlinear Navier–Stokes equations in three respects. These discrepancies may be classified as (i) lack of Galilean invariance, (ii) lack of isotropy, and (iii) a crossover dimension problem.' That is why more advanced models had to be sought. Rivet (2001) glosses this historical development as, 'About ten years after the introduction of the HPP model, the "anisotropy disease" has been cured by models based on the triangular lattice.' Some of the advanced models, developed initially, are discussed in the next subsection.

10.3.2 Two of the Frisch, Hasslacher and Pomeau models

The first member of this group of models with isotropy, producing proper large-scale lattice fluid dynamics, was introduced by Frisch *et al*. (1986). Several versions of the Frisch, Hasslacher and Pomeau model have been successively developed with the same geometrical lattice structure, but with

different collision rules. Two of them will be described further, viz. the FHP-1 and FHP-2 models.

The simplest model of this group, denoted the FHP-1 model, is based on a triangular lattice structure with hexagonal symmetry, having unitary distance Δl between the neighbouring nodes, and unitary modulus of particle velocities v. Particles obey the exclusion principle. Hence, the maximum number of particles in a node is six, equalling the number of neighbours, i.e. to the connectivity $B = 6$. This limited number of simultaneous appearances of particles in one node safeguards the implementation of the exclusion principle on the model. The masses m_i of all particles at each channel i are equal 1 m.u.

The propagation phase in the FHP-1 model proceeds in exactly the same way as for the HPP model. A particle sitting originally in a node $\vec{x}_i$ with a velocity $\vec{v}_i$ is moved along the channel i to the neighbouring node $\vec{x}_i + \vec{v}_i \Delta t$. A substantial difference with the HPP model appears in the collision phase. In FHP-1, two particles coming from opposite directions undergo a binary collision with an output state rotated by +60° or –60°, with equal probabilities. Another remarkable aspect of the FHP-1 model, compared with HPP, is the inclusion of three-particle collisions. When three particles meet simultaneously in one node, having their mutual velocity vectors at an initial angular disposition of 120°, a collision takes place with a rotatory deflection of the velocity vectors by 60°. The rotation by –60° leads to an identical local state transition. There are 2^6 (= b) possible various local states of the FHP-1 model and five of them, viz. three two-particle and two three-particle collisions, are effective. Hence, the collision efficiency of the model is 7.81%, as is obvious from Fig. 10.11.

FHP-2 is a modification of the model FHP-1. As opposed to HPP and FHP-1, this model includes the possibility of one rest particle at each node. The propagation phase is the same as for the FHP-1 model and it has no

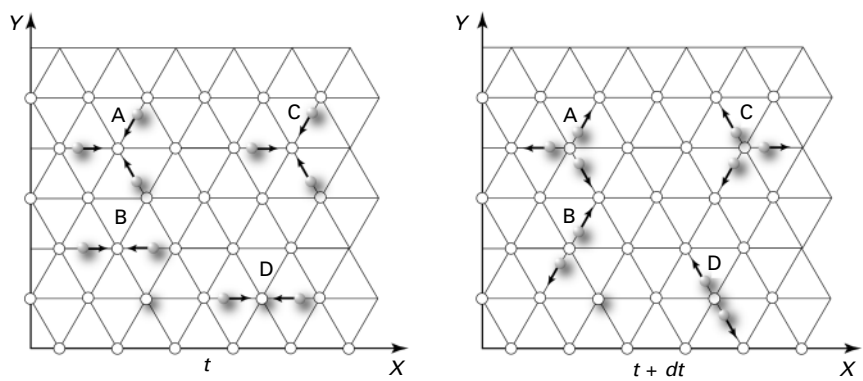

10.11 Typical two- and three-particle collisions in FHP-1 model.

influence on particles at rest. Particles at rest have zero values of velocity, momentum, and energy. These particles do not belong to any channel and so the exclusion principle is valid for this model too.

The collision rules of the FHP-2 model are similar to that of FHP-1 model with the only difference that two additional events are considered in the FHP-2. A moving particle arriving at a node with a rest particle produces a pair of moving particles at angles +60° and –60°, measured from the direction of the incoming particle. The last additional collision event is the reverse to the former. Two colliding particles in a node with their velocity vectors at 120° angle result in one resting particle and in one moving particle moving in the direction of their original pre-collision momentum vector.

There exist $2^7 (= b)$ various local states in the FHP-2 model out of which only 22 are effective, as given in Fig. 10.12. Thus, the collision efficiency of the model is 17.19%. Thanks to the effective collisions with resting particles, FHP-2 does not conserve any kinetic energy. It is assumed that either the energy is exchanged with an adjacent thermodynamic reservoir or the resting particles vibrate with a vibrational energy equalling their original kinetic one.

10.4 Computer simulation of fluid flows through porous materials

In this section, the application of FHP-1 and FHP-2 lattice gas cellular automata models to simulate fluid flows in porous media is introduced. The section is divided into three subsections. To start with, a description of a lattice gas algorithm for general-purpose computers is considered. The text

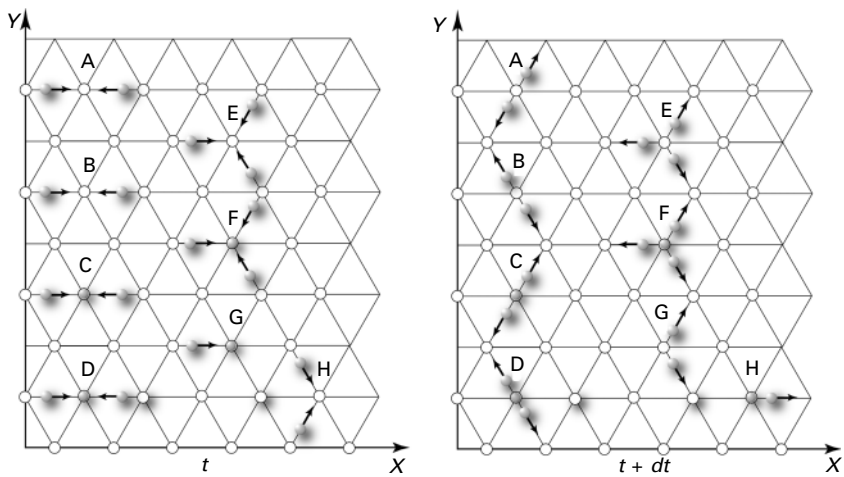

10.12 Typical two- and three-particle collisions in FHP-2 model.

then follows with two examples of computer simulations based on the FHP-1 lattice gas model. The first of them is devoted to the study of two-dimensional flow in an empty channel, the next one to fluid flow through a porous medium that mimics a fibrous material forced by a certain pressure gradient. Output data are compared with Darcy's law relating values of flow rate and pressure gradient. The final computer simulation is focussed on the FHP-2 lattice gas model to study a fluid flow in a channel under the influence of outward vibrations transmitted to the fluid environment.

Fluid flow through a porous media, and especially through fibrous materials, is a subject of wide interest. The textile industry encounters this phenomenon during many production and finishing processes. In these circumstances, permeability is the physical parameter of prime interest. Moreover, the permeability measurement is one of the most important ways that enables an evaluation of final products, as it provides concrete information about the usability of a material for an application. For example, permeability is a critical parameter for the application of fibrous materials such as filters, barrier materials and sportive clothing. The invention of *Gore-Tex* materials was based on an idea of combining various layers with different permeabilities to reach optimal comfort with respect to the diffusion of water vapour outwards and exclusion of external liquid droplets.

Modelling the generation and propagation of sound wave hangs together with the study of acoustic properties of fibrous materials. New trends are, for instance, looking for ultrasound applications in textile technology to enhance traditional processes (Moholkar, 2002). Newly developing technologies are: (i) application of ultrasound in textile pre-treatment and finishing processes aiming to accelerate diffusion of liquids and gases into fibrous materials; (ii) ultrasound treatment used for reducing the viscosity and surface tension of resin systems involved in the production of fibre reinforced composites; (iii) application of ultrasound for impregnation of fibrous nanomaterials, produced by electrospinning, with highly viscous liquids (Ocheretna and Kostakova, 2005a).

10.4.1 Lattice gas algorithm

A large variety of computers ranging from personal computers to powerful parallel processing supercomputers and a wide range of programming languages explain the existence of the quanta of lattice gas algorithms that have been implemented since 1985. The algorithm used in the present work is designed for a general-purpose computer. It includes an unchangeable part that can be used as a basis for each new algorithm, independent of the concrete choice of a lattice gas model.

Each node of a lattice in the algorithm is conceived as a box with two main sections. The first of them is intended for registration of an instantaneous

state. The second one serves as a bin for information about the new state of the cellular automaton in the next time step. When the new state of the system is accepted and becomes the new instantaneous state, data from the second sections are removed to the first ones so that the algorithm is ready for the next evolution step. Each of the sections is divided further into several shelves, where various prices of information about the node, related to the chosen time step, are collected, such as information about the channel occupation by particles, total number of particles in the node, and x- and y-components of velocities for all particles in the node. This set of information makes it possible to make all propagation and collision changes 'simultaneously' and to have comprehensive information about the system at any moment.

The lattice gas algorithm starts with the occupation of chosen lattice nodes with solid stationary particles, which represent walls of a cavity or a channel. They can also in personate the material of a porous medium, particularly a fibrous material. Creation of fluid particles takes place on resting free parts of a lattice, where no solid non-moving particles are present. Each channel in each node takes either the value 1 or 0 at random, with pre-described probability. The value 1 means the occupation of a channel with a fluid particle, while the value 0 marks empty channels. Thereafter, the number of fluid particles and x- and y-components of their total velocity in each node are calculated. This information is stored in different arrays.

The main part of the lattice gas algorithm consists of collision and propagation phases that repeat, subsequently. The algorithm starts with the collision phase, which is carried out uniformly and practically simultaneously in each lattice node s, excepting those occupied by a solid non-moving particle. The collision phase consists of the following steps:

(i) Selecting the lattice node s_0;
(ii) Detecting the input information about the number of particles n_0 in the node s_0. If $n_0 = 0$ return to the Step 1. For the opposite case, detecting the x-component v_x and the y-component v_y of the total particle velocity $\vec{v}$ in the node s_0;
(iii) Keeping the new value of the particle number ${}^n n_0$ in the node equal to the input value n_0;
(iv) Choosing a channel $i (i = 1, \ldots, B)$ of the node s_0 at random;
(v) If the channel is empty, then, occupying the selected channel i of the node s_0 with a particle, i.e. with the value 1, and reducing the parameter ${}^n n_0$ by 1. In case the channel i is settled by a particle, going back to Step 4;
(vi) Repeating Steps 4 and 5 till the parameter ${}^n n_0$ equals zero;
(vii) Calculating the x-component of the total particle velocity ${}^n v_x$ of the newly created configuration in the node s_0. If the ${}^n v_x$ in the node s_0 is not equal to the original input value v_x, going back to Step 2;

(viii) Calculating the y-component of the total particle velocity ${}^{n}v_y$ of the newly-proposed configuration in s_0. If the ${}^{n}v_y$ in this node is not equal to the original input value v_y, going back to the Step 2;
(ix) Registering the new information, i.e. the new configuration parameters' the occupation of individual channels, ${}^{n}n_{0,i}$, ${}^{n}v_{x,i}$, and ${}^{n}v_{y,i}$, in the node s_0, into information fields. The newly obtained configuration conserves the particle number and momentum components and thus can really be considered as a new configuration for the node s_0;
(x) Repeating the previous steps for all the lattice nodes.

The propagation phase comes after the collision phase and consists of the following points in succession:

(i) Selecting a lattice node s_0 and detecting the input information of this node. Of particular interest now is the channel occupation;
(ii) Scanning through the channels of the node s_0 subsequently, and looking for the first occupied channel denoted here as i. If all channels are empty, returning to Step 1;
(iii) If the channel i is occupied, then detecting the state of the neighbouring node s_i, which communicates with the node s_0 through the channel i.
(iv) If the node s_i is not occupied by a solid, stationary particle, relocating the particle in the channel i from the node s_0 to the neighbouring node s_i so that the new particle number value ${}^{n}n_i$ in the node s_i extends by 1. New values of the x-component ${}^{n}v_{xi}$ and the y-component ${}^{n}v_{yi}$ of velocity in the node s_i are extended by v_{xi} and v_{yi}. If the node s_i is occupied by a solid, unmoving particle, implementing reflection depending on the chosen type of boundary conditions;
(v) Repeating the previous steps for all the other lattice nodes in a chosen sequence.

Thus, the basic skeleton of the lattice gas algorithm for a general-purpose computer, which has been used for further introduced simulation experiments, has been detailed. There are also so-called 'mobile parts' of the algorithm apart from the previously described skeleton of the algorithm. These mobile parts have not been involved in those aforementioned steps. Each particular simulation experiment includes, for instance, subroutines for the generation of extra conditions. These subroutines provide, for example, pressure gradient, gravity and vibration waves. Subroutines also ensure the formation of special output data files.

10.4.2 Computer simulation of two-dimensional fluid flow in porous materials

As mentioned in Section 10.1, the lattice gas cellular automata can describe complex hydrodynamic phenomena in that they can substitute for Navier–

Stokes equations. It is, then, quite natural to verify if the simulation model fulfils the basic fluid-flow laws, for instance, Darcy's law. This law was named after the French engineer Henri Darcy (Rothman, 1988), who established it empirically during the middle of the nineteenth century. He found that the flow rate through a porous medium, including a fibrous one, is linearly proportional to the applied pressure gradient. This law is valid for laminar flows, where the Reynolds number is relatively small. In other words, the law is valid for steady Poiseuille flows with parabolic velocity profiles in free channels.

An elementary example of a fluid flow satisfying Darcy's law is the three-dimensional flow between two parallel plates. It is a simple model for the flow through a single pore, the channel, which can be reduced to a two-dimensional case due to its cross-sectional symmetry. Many researchers have dealt with this problem. For example, Rothman in his work (Rothman, 1988) studied two-dimensional Poiseuille flow as a function of the channel width for various pressure gradients. The same dependence was of Chen's interest (Chen *et al*., 1991) for three-dimensional channel flows. Interesting problems were solved by Yang a few years ago (Yang *et al.*, 2000), based on the Lattice–Boltzmann model, where the influence of various interactions between the fluid and the channel walls was considered. In particular, one part of the channel surface was wetted by a liquid while other parts repelled it. The first simulation experiments of the present work are aimed at studying two-dimensional fluid flows under the influence of various pressure gradients and under conditions where the laminar character of the flow transits to a turbulent one.

Fluid flow in a free two-dimensional channel. The concrete implementation of the lattice gas cellular automata that is used here is based on the FHP-1 model. The following values of channel parameters were chosen: the length L of the channel was chosen to be 550 lattice units (l.u.). In principle, the channel was infinitely long, thanks to the periodic boundary conditions applied on its left and right sides. The width d of the channel was $160\sqrt{3/2}$ l.u. Top and bottom channel ends were composed of solid walls to restrict the flow. The bounce-back reflections were pre-set for the fluid particle collisions with solid wall particles. Fluid particles were generated in the free space between the walls. The mass of each particle was one mass unit (m.u.). The average microscopic mass density $m(\vec{x})$ was chosen to be 3.5 particles per node.

Subsequently, the pressure gradient was varied to study the flow rate versus pressure gradient relationship. A similar method, as used later in this chapter, was exploited previously McNamara and Zanetti (1986) and Rothman (1988), for the creation of a pressure gradient. The pressure gradient in that work was created in terms of reversing particle momentum vectors with the

chosen probability f_x at all nodes of a vertical line of nodes, the length of which was equal to the channel width d, located on the left side of the horizontal channel. In fact, the parameter f_x expressed the average change in the x-component of the particle momentum at a particular node during one time step or time unit (t.u.). This flipping mechanism acted merely on particles with negative x-components of velocity pointing leftwards. The 'total force' applied on the line of nodes was, then, nf_x, where n represented the number of nodes in the line that spanned across the channel width. So the pressure P applied at the left-hand channel side was accordingly (Rothman, 1988; Lukas and Kilianova, 1996) expressed as $P = nf_x/d$. That is why, dimensionally, f_x had to have the dimension derived from dimensions of pressure and length, say, m.u. ∗ l.u./t.u.^{2} The value of the pressure gradient was obtained as the quotient of the 'total force' nf_x and the product of the channel length and the channel width $L * d$.

During the study, the system was allowed to relax, i.e. to evolve to a steady state flow, after the start of each simulation. The steady flow rate was achieved after about 10 000 t.u. for parameter f_x values ranging between 0.005-0.06 m.u. ∗ l.u./t.u.^{2}. The smaller the probability value f_x, the longer was the time period needed for achievement of a steady state flow. For example, for $f_x = 0.005 – 0.012$ m.u. ∗ l.u./t.u.^{2} it took more than 13 000 t.u., as is evident from Fig. 10.13. The x-component of velocity was averaged over the whole channel length L for each horizontal node layer over 5000 time steps in the steady-state region to obtain velocity profiles for various pressure gradients. These computer-simulated outputs are presented in Fig. 10.14, exhibiting parabolic velocity profiles typical for Poiseuille flows.

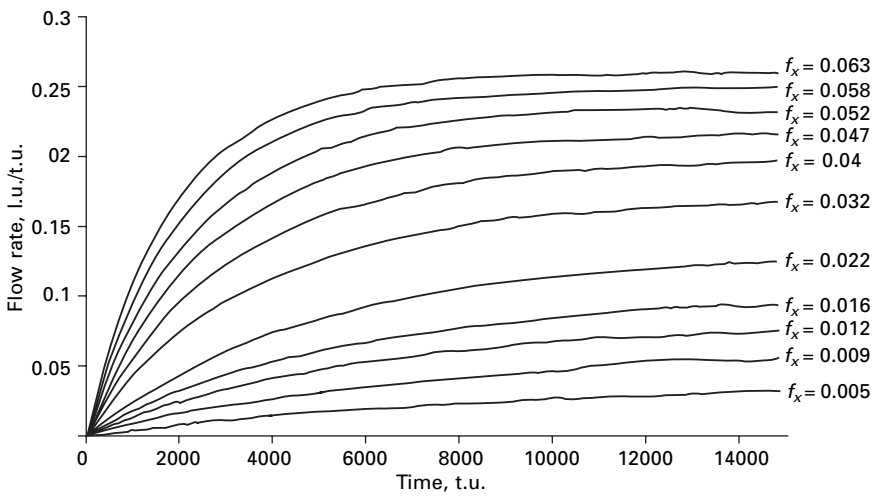

10.13 Volumetric flow rate of the channel flow as a function of time, with various values of the parameter f_x.

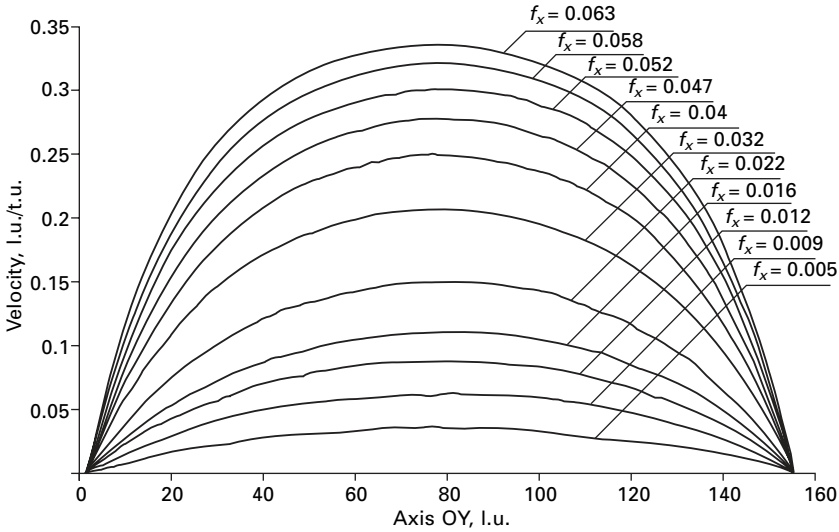

10.14 Velocity profiles for various values of the parameter f_x in the free two-dimensional channel.

Twelve independent experiments were carried out, for which the parameter f_x varied from 0 to 0.06 m.u. $*$ l.u./t.u.^{2}. The pressure gradients corresponding to these f_x values were between 0 and $4.6 * 10^{-4}$ m.u./(t.u.^{2} $*$ l.u.). This span of pressure gradients provided flow rates within the interval 0-0.25 l.u./t.u. The flow rate q was considered as a volumetric flow rate and could be easily detected as $q = \vec{v}_x$, where $\vec{v}_x$ is the average x component of velocity per particle space, averaged over the entire lattice. The area where Darcy's law was valid for the investigated systems is shown in Fig. 10.15. It can be seen that the linear dependence between flow rate and pressure gradient held for low flow rates up to 0.1 l.u./t.u For this region, Darcy's law was valid. When the flow rate exceeded the value 0.15 l.u./t.u., the laminar flow probably changed into a turbulent one which led to the deviation from the linear relationship. This limit point depends, of course, on the channel width. The wider the channel is, the smaller the pressure gradient value limit for linear behaviour.

Fluid flow through two-dimensional fibrous materials. Two-dimensional fluid flow through a porous medium that mimics a fibrous material, represented by a set of parallel pores, was studied in this experiment. The porous material was placed at the middle of a channel of length $L = 450$ l.u. and of width $d = 250\sqrt{3/2}$ l.u. The thickness of the model of the fibrous material was 90 l.u. and so it covered approximately one-fifth of the channel length. The width of pores inside the porous material was chosen as 10 l.u., and the distance between these equidistant and parallel pores was 18 l.u. The fluid

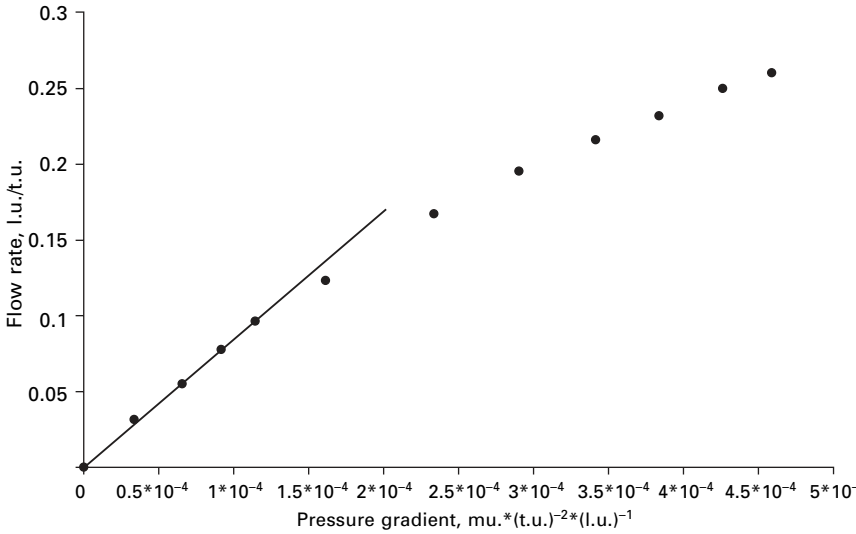

10.15 The extent of linearity of the flow rate's dependency on the pressure gradient delimits the region of Darcy's law validity.

flow in the channel was confined by solid walls, i.e. fibre surfaces, with the same boundary conditions as were used in previous computer simulations. The bounce-back reflections were exerted for fluid particle collisions with the fibers of the porous material. The fluid particles were generated again with a density of 3.5 particles per node. A pressure gradient was created in the same way as described previously, with periodic boundary conditions on the left and right sides of the channel. In the first series of computer simulations, the model of the fibrous material was located in a vertical direction, i.e. perpendicular to the direction of the fluid flow and the channel axis. In the final group of experiments, porous material crossed the channel axis at an angle 45°. Pores in the two-dimensional models of a fibrous material pointed, in both the cases, to the natural directions of the underlying triangular Bravais lattice, for more details see Figs. 10.21 and 10.22. They were horizontal in the first case, while they were inclined at 60° in the final one. The two previously mentioned orientations of fibrous materials in channels enabled variation of the inlet area of the fibrous material, keeping its internal geometrical characteristics intact. Several interesting features of the flow through these porous materials were exhibited during the computer simulations.

At the beginning of the simulations, the steady fluid flow states were required for the next investigations. From Fig. 10.16, it is evident that the system with vertical orientation of the porous membrane reached its steady state just after 1000 t.u. The time requirement was more than 2000 t.u. when the two-dimensional model of the fibrous material was orientated as shown in Fig. 10.17. The development of temporal peaks of flow rate, which appeared

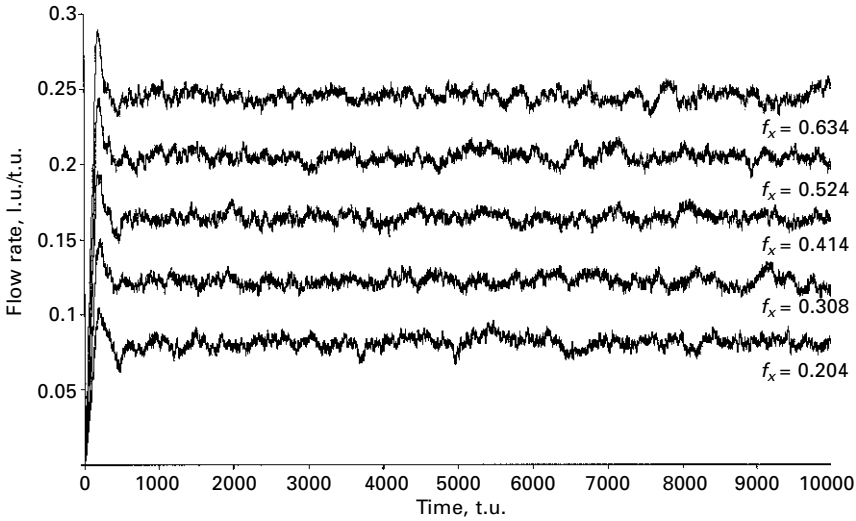

10.16 Particle flow rate as a function of time for various values of the parameter f_x concerned with the fluid flow through a vertical two-dimensional model of a fibrous material with horizontal pores.

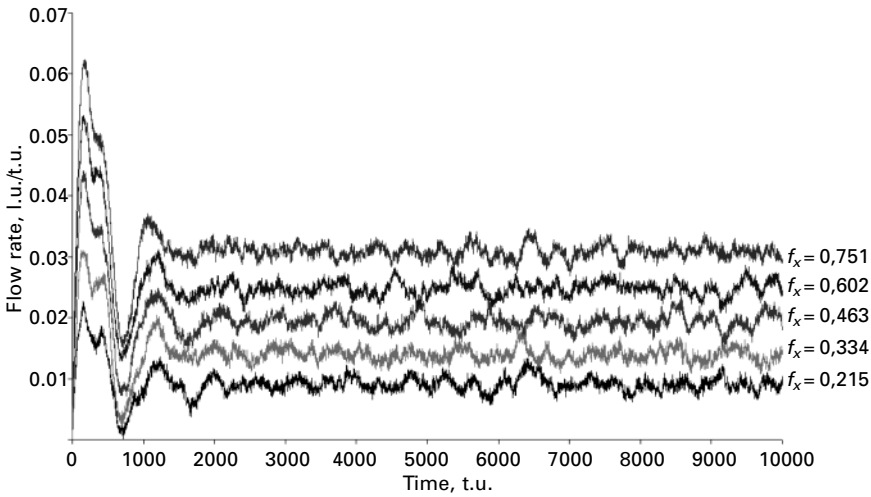

10.17 Particle flow rate as a function of time for various values of parameter f_x related to the fluid flow through a declined model of a fibrous material.

for low time values, was notable. They came into being as a consequence of the first strike of a group of fluid particles with the fibrous material, when the x-components of momentum had been reversed on the left-hand side of the channel with the probability f_x. The flight was not hindered by any porous medium other than the channel walls, which represented a gigantic

pore, until they reached the inlet side of the fibrous material. These peaks were higher for simulations with a declined porous membrane.

The same method as described for the computer experiments with a free channel was used for both the arrangements of porous membranes to obtain the velocity profiles. Interesting behaviour in the case of vertical as well as declined orientations of the fibrous layer, as demonstrated by computer simulation outputs, can be seen in Figs 10.18 and 10.19. Evidently, the flow was faster for the vertically orientated porous membranes than that for the declined ones, under the same pressure gradient values. As a result, the first case acquired the turbulent character at smaller pressure gradient values. It may also be noted that the local average velocity maxima corresponded to the positions of pores in the porous membrane. This effect is typical for fluids that do not wet pore walls (Yang *et al.*, 2000). In Fig. 10.19, the velocity profiles of the system with the declined membrane may be noted too. The two lower curves predicated a laminar flow since their shapes resembled parabolic profiles. However, with increasing pressure gradient, the fluid flow probably became turbulent. The deformation of the upper curves could be explained quite simply. The declined layer of the fibrous material was in contact with the channel walls on its top and bottom edges. Two blind porous areas arose there. Particles that had been caught inside those areas could not come out easily.

Both of those systems behaved in accordance with Darcy's law, as was confirmed by the computer simulation outputs presented in Fig. 10.20. A

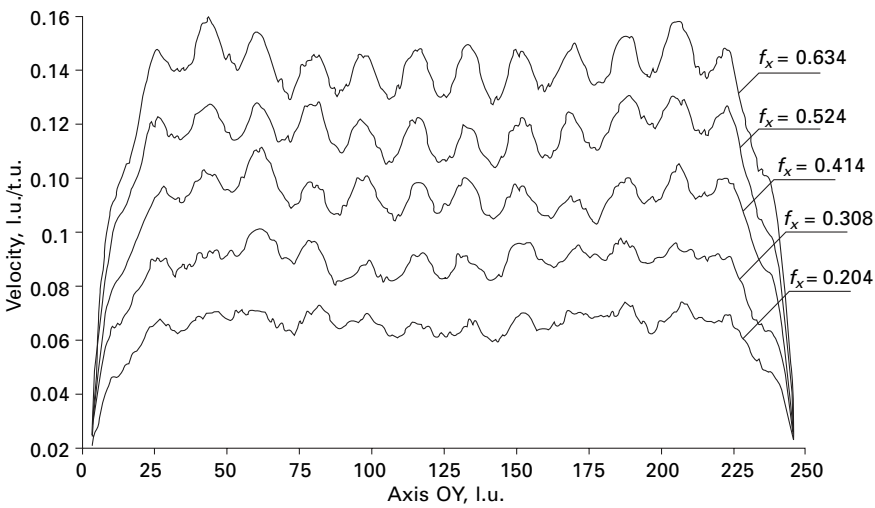

10.18 Velocity profiles for various values of the parameter f_x associated with the fluid flow through a vertical porous material. The horizontal axis represents the position across the channel from the axis *y*.

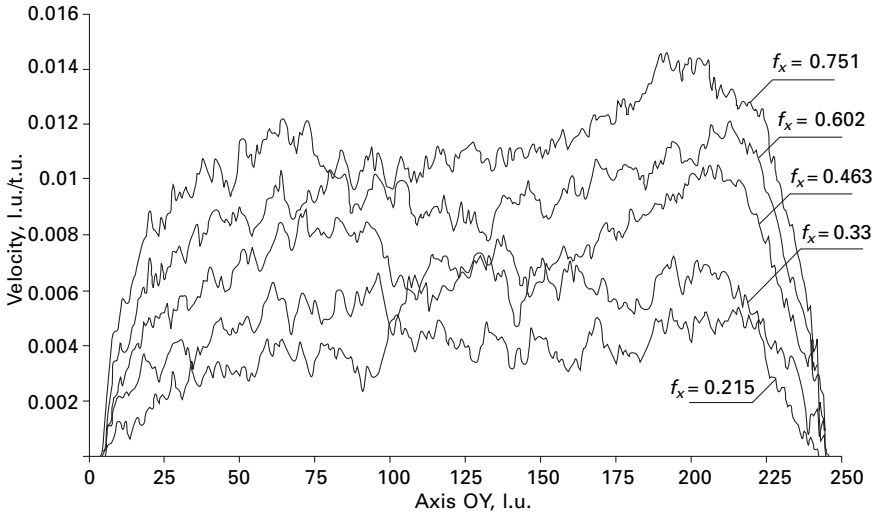

10.19 Velocity profiles for various values of parameter f_x regarding fluid flow through declined layer of fibrous material.

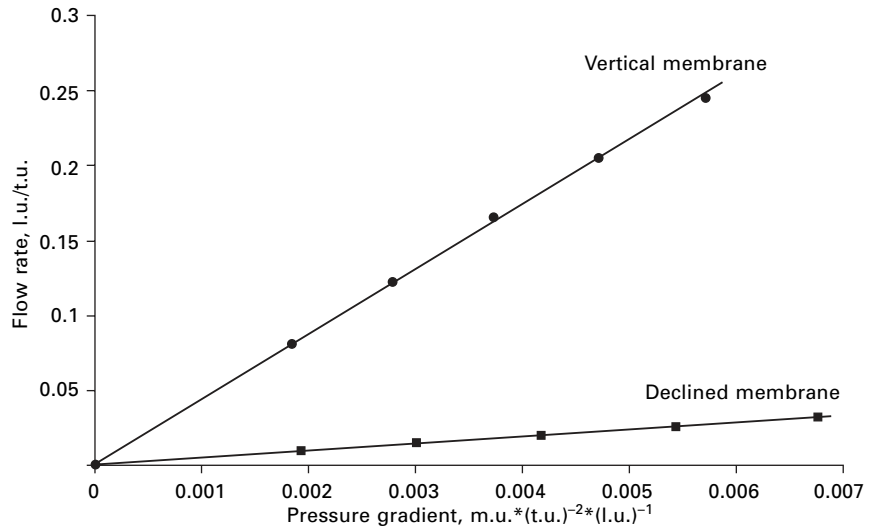

10.20 Linearity of flow rate versus pressure gradient relationships validates Darcy's law for fluid flows through vertical and declined porous materials within the limits of the gradient values used for the present purpose.

nearly perfect linear dependence between the flow rate and the pressure gradient was found in both cases. It seems to be reasonable that the flow rate was higher when the inlet area of a porous medium was smaller, because lower resistance of porous medium was experienced and the flow was not so

tortuous. The velocity fields were monitored and expressed graphically for both the systems for better understanding of these phenomena. Particle velocities were space-averaged inside 5 l.u. × 5 l.u. squares and, simultaneously, these space-averaged velocities were time-averaged over 5000 t.u. inside steady-state regions of flows. Velocity vector arrays were obtained for maximal pressure gradients used for both systems. Local fluid flows were nearly parallel to the channel walls at the middle of the channel, as is evident from Fig. 10.21. In the interface between the free channel area and the porous membrane appeared a reorganization of fluid velocity directions, because the flow impacted on the solid parts of the fibrous material and the fluid particles tried to stream to the pores inside the fibrous layer. The reorganization of flow directions was even more evident in the regions of contact between the channel walls and fibrous material than close to the channel axis. An interesting situation appeared in the system with the declined membrane, as is visible from Fig. 10.22. Flow was distorted in this case through a greater part of the channel. The distortions took place on the upper as well as the bottom channel areas, in front of, and behind, the fibrous material layer as well, explained by previously described blind pores. On account of the appearance of tortuous flow, the flow rate decreased compared to the system where the membrane was placed along the vertical direction. It is also evident from Fig. 10.22 that the local fluid flow in blind pores close to channel walls was zero.

It has been mentioned in the introduction of this section that the investigation is focused here mainly on the fluid flows through fibrous materials in order to carry out a permeability study. Some interesting problems will be discussed

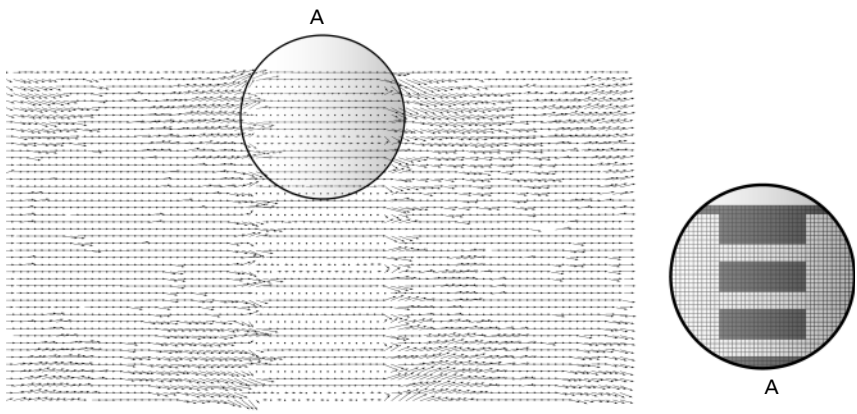

10.21 The field of velocity vectors for a fluid flow through a vertical fibrous layer. The length of each vector corresponds to the space and the time-averaged speed of the moving particles in a node at the vicinity. The horizontal side of the rectangular figure is parallel to the *x*-axis, while the vertical one has its direction identical to the *y*-axis.

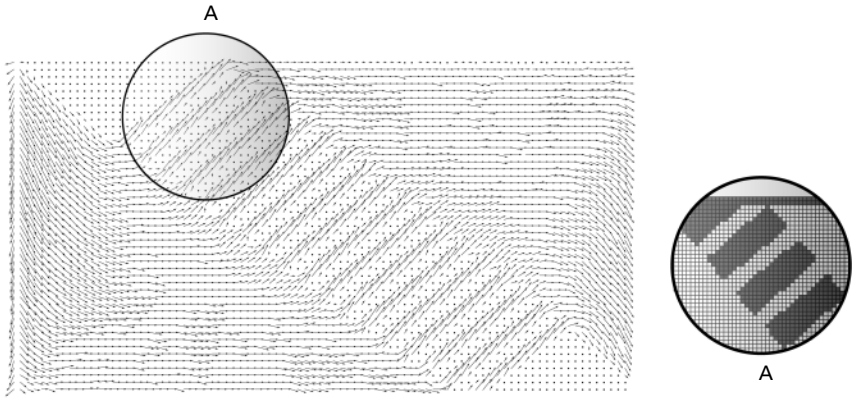

10.22 The field of velocity vectors for a fluid flow through a declined layer of fibrous material. The horizontal side of the rectangular figure is parallel to the *x*-axis while the vertical one is directed towards the *y*-axis.

in the next part of this section, such as the sound wave motion through the fibrous materials and porous media in general and its attenuation.

10.4.3 Computer simulation of fluid flow through fibrous materials affected by sound vibrations

In this subsection, the results of computer simulations for fluid behaviour in a free channel with a porous medium under the influence of vibrations will be presented. Here, an algorithm based on the FHP-2 lattice gas cellular automata model was used. A more detailed description of this model has been given in the Section 10.3.2. The specificity of the algorithm used has been described earlier (Ocheretna, 2005b). This algorithm created sound excitations as harmonic plane waves that travelled through the fluid along the channel and created variations as pressure waves. The pressure is, as a rule, proportional to the particle density in the FHP-2 lattice gas cellular automata model (Rothman, 1988).

Firstly, let the focus be on the transmission of a sound wave through a fluid and on detection of attenuation of the sound wave in a free channel with respect to various periods of vibration and densities of the fluid. The free channel was created on a lattice with length L = 350 l.u. and width $d = 250\sqrt{3/2}$ l.u. The two-dimensional channel was confined within solid walls at its top and bottom sides. Between the walls, liquid particles were generated. Computer simulation trials were performed for particle densities 1.2 and 3.5 particles per node. Specular reflections of fluid particles from solid boundaries were used. A fictitious transmitter of harmonic signals was located on the left-hand side of the channel. These computer experiments

were carried out for five different periods T of sound waves: 10, 15, 30, 45 and 60 t.u. The simulation program included the action of a fictitious sound transducer that was exerted at each time step based on an equation of harmonic vibrations. The action of the transducer was converted into the probability of deflections of fluid particles from their original positions within the transducer area. Fluid particles were considered to bounce in the positive direction of the x-axis if the value of the transducer displacements were positive, and were similarly related for the negative values. The bouncing probability f_x inside the transducer area is, in fact, time dependent, and so, the bouncing probability in the x-component of a particle's momentum at a node during one time step at time t is $f_x(t) = f_{x,\max} \sin(2\pi t/T)$. As a consequence of the discrete time of lattice gas cellular automata, probabilities $f_x(t)$ were coarse-grained. Periodic boundary conditions on the left- and right-hand sides of the channel were used.

Information about particle density in each node after the transducer was obtained as an output of the computer simulation. In order to quantify the attenuation coefficient and attenuation in general, the value of particle density obtained for each column of nodes was traced as a function of distance from the transducer (Ocheretna and Lukas, 2005c). Then the attenuation of the pressure wave was clearly visible and the attenuation coefficient was measurable, as shown in Fig. 10.23 (a) and (b). Firstly, maximal deflections of the particle density about their average values were detected, as shown in Fig. 10.23 (a). Then a regression curve was interlarded through the dots obtained from the density profile, and the equation of the regression was found, as shown in Fig. 10.23 (b). The attenuation coefficient k was taken from the regression equation and, in the same way, was found for other

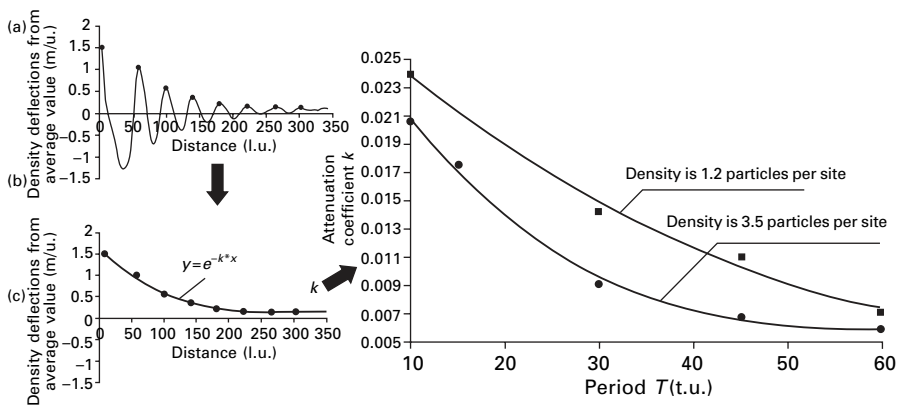

10.23 Comparison of attenuation coefficients in the free channel with various values of time period T of waves for two different particle densities.

waves generated with different periods T. Relationships between the attenuation of sound (pressure) waves and the transducer operational period T, which is a reciprocal of the transducer frequency, are shown for two different fluid densities in Fig. 10.23 (c). It can be seen that the sound waves of different T's were attenuated quickly in the system with high particle density. It is also evident that waves of smaller period values T have the highest attenuation coefficient, which means a more rapid extinction compared to those with higher values of T.

The same channel size and boundary conditions were used for the other computer simulations. Two-dimensional models of fibrous materials, with regular internal structures, were placed adjacent to the transducer area. The residual free part of the cavity was filled up with fluid particles at a density of 3.5 particles per node. Having knowledge of the previous results, it was decided to increase the period T up to 200 t.u. to prolong the life of a wave before it was quenched. Figure 10.24 shows the density profiles of waves which propagated through the regular chessboard-like fibrous material layers of equal thickness but of various porosities: 0.678, 0.736, 0.795, and 0.833. Density profiles of waves that travelled through the porous materials of various thicknesses: 10, 30, 50, and 70 l.u., having the same porosity of 0.678, are presented in Fig. 10.25. It is quite clear that the absorption of a wave depended on the structure and pore size of porous media. The attenuation of a sound wave increased with decreasing porosity or with increasing thickness of a porous material.

The concept used here could be used for an investigation into the behaviour of real porous media, including fibrous materials. However, digital images of real fibrous materials have to be carefully analyzed to exactly mimic their internal morphology.

10.5 Sources of further information and advice

Interesting facts about cellular automata creation can be found in Hyötyniemi (2004). More generalised information regarding the lattice gas cellular automata may be obtained from some recently published monographs (Rothman and Zaleski, 1997; Chopard and Droz, 1998) and review articles (Chen *et al.*, 1991; Boon, 1992). In this chapter, three basic models of lattice gas cellular automata have been dealt with, but there exist many more. For instance, the FHP-3 model is a further variant of the FHP-2 model (Rivet, 2001), where the collision rules are designed to include as many collisions as possible to achieve a collision efficiency of 59.4 %. The FHP-3 model was later modified (Bernadin, 1990; McNamara, 1990; Hanon and Boon, 1997) in order to study diffusion phenomena. The modifications involved consideration of mixtures of two species of particles that were chemically inert to each other and had identical mechanical properties. The model was called the 'coloured

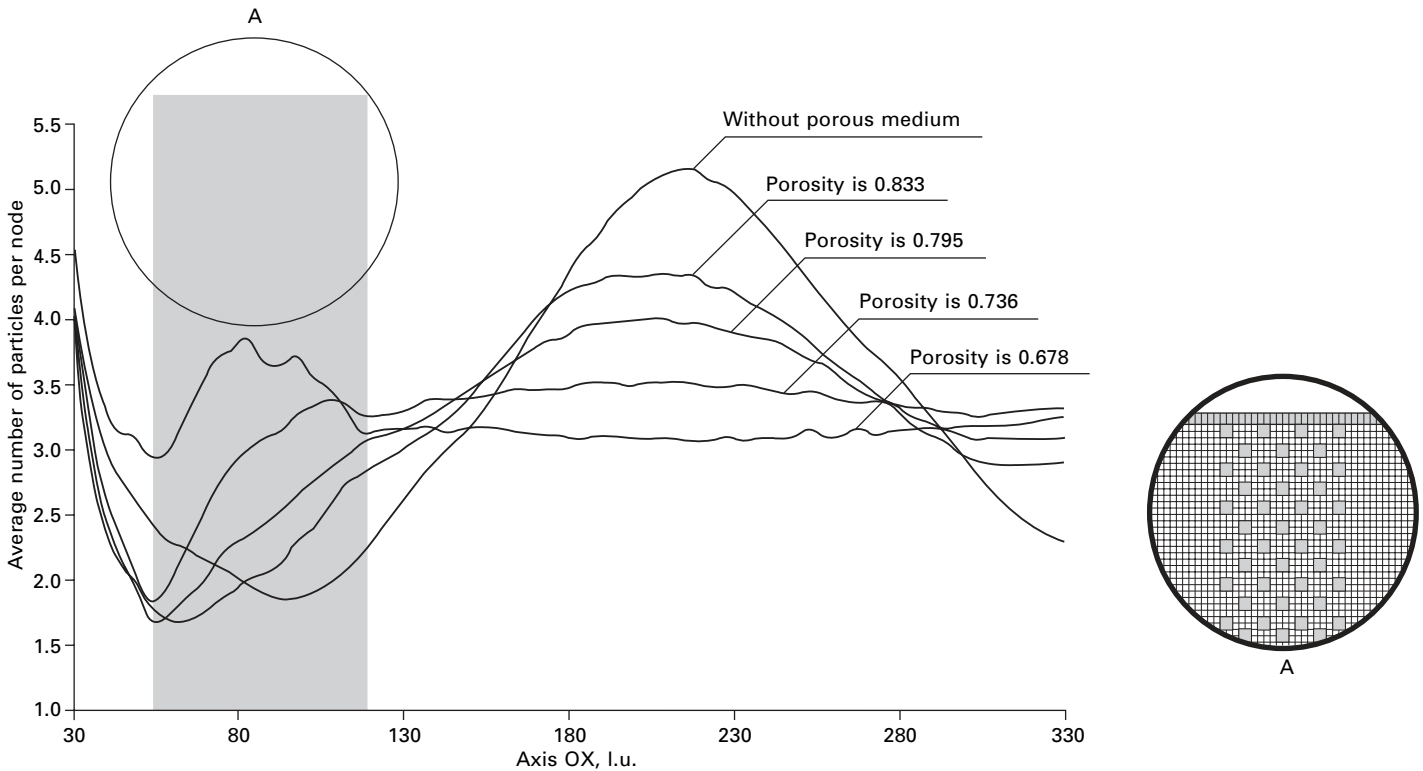

10.24 Snapshots of particle density in waves that propagate down the *x*-axis through media of various porosities. The grey rectangle represents the localization of porous media in the channel. The transducer operates in an area just before the channel region is filled up by the model of the fibrous material.

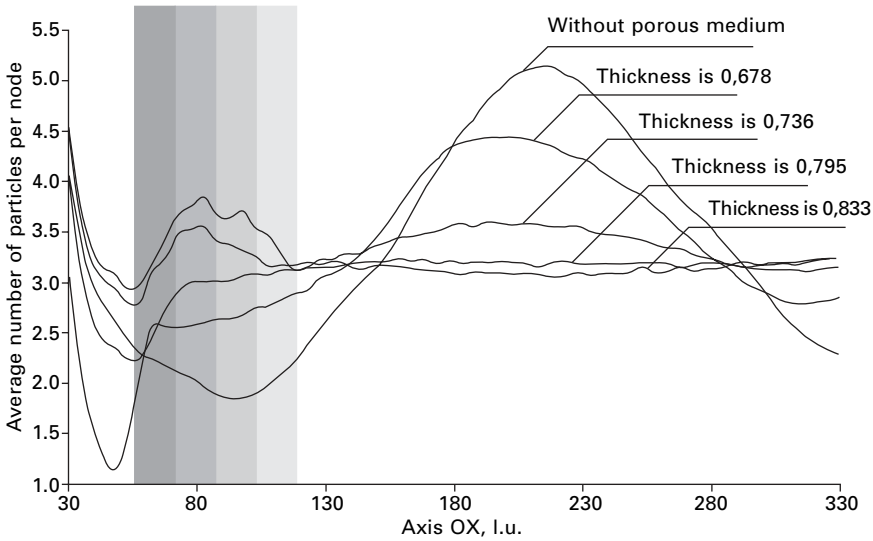

10.25 Instantaneous particle densities in waves propagating through porous media of various thicknesses. Different degrees of grey shades represent the gradual growth of the thickness of the model of fibrous material. The transducer operates in an area just before the channel region is filled up by the porous medium.

FHP' model (i.e. CFHP). Grosfils, Boon and Lallemand (in Boon, 1992) introduced in the beginning of the 1990s a lattice gas cellular automata model with non-trivial thermodynamics that contained thermal effects. The model was abbreviated as GBL following the initials of its developers. All previously mentioned lattice gas cellular automata models were built up on underlying two-dimensional lattices. The next evolution aimed at three dimensions.

The frequently used three-dimensional lattice gas cellular automata model with correct isotropy is the 'face-centred-hyper-cubic' model, FCHC. More information is provided in papers by Henon (1987, 1989, 1992).

One of the main drawbacks of lattice gas cellular automata is their statistical noise, hence, 'lattice Boltzmann' models have been developed to quench this noise. The first lattice Boltzmann model was proposed by McNamara and Zanetti (1988) and almost at the same time it was also introduced by Higuera and Jimenz (1989). Some general books on lattice Boltzmann models were written later (Wolf-Gladrow, 1999; Succi, 2001).

The most significant application of lattice gas cellular automata is on the flow of heat and mass through porous media. Basic articles in this area have been written by Rothman (1988, 1990) followed by Kohring (1991), Chen *et al*. (1991a), and Lutsko *et al*. (1992). The first lattice Boltzmann simulation

of porous media was performed on a cubic lattice (Foti *et al.*, 1989). Generally speaking, lattice gas cellular automata and lattice Boltzmann models are considered to be the most suitable for simulating microhydrodynamic flows through porous media (Koponen *et al.*, 1998) and hence through fibrous materials too.

Finally, let the two seemingly similar models in this book, viz. the lattice gas cellular automata and the auto-models from Chapter 14, entitled, 'Computer simulations', be compared. Lattice gas cellular automata are, in many respects, akin to Markov random field models, especially in those cases where collision rules are governed by transition probabilities (Rivet, 2001). Intuitively, a lattice gas automaton with probabilistic transitions in the collision phase is a spatial stochastic scheme, where the local configuration of a node is influenced by that of its neighbouring nodes. The random variable of lattice gas automata is a numeric integral code representing a local configuration, i.e. the local distribution of particle velocity vector of the node in question. Both the models have nearly identical geometry and formal descriptions of basic notions (Lukas and Chaloupek, 1998) but the construction of their temporal evolution is quite different. In other words, the great difference between the lattice gas cellular automata and the auto-models appears in the rules governing their dynamics. The auto-model dynamics are driven by subsequent alternations of variable values in restricted number of cells/nodes. Generally, the dynamics of auto-models that are used frequently allow only subsequent local changes of a variable in an isolated cell/node or these variable values can be subsequently exchanged in a couple of cells/nodes only. On the other hand, the collision laws of lattice gas cellular automata, reflecting chosen conservation laws, can be run in all lattice nodes simultaneously. The differences between the two aforementioned discrete models reflect discontinuity in recently developed theoretical tools describing equilibrium thermodynamics, such as the above mentioned auto-models, and non-equilibrium thermodynamics, such as the lattice gas cellular automata. Both the models could be used, obviously, for the description of a system in an equilibrium state. Auto-models reflect naturally inter-particle energy exchanges while lattice gas cellular automata mimic conservation laws of chosen scalar as well as vector observables. A more detailed discussion about the mutual relationship between the auto-models, represented by the popularly known Ising model, and the cellular automata, in general, can be found in Vichniac's work (Vichniac, 1984). Lastly, the auto-models and the lattice gas cellular automata may be pointed out to be different from the point of view, purely formal, that the basic element of a cellular automaton is known as a 'node', while the term 'cell' is used in the realm of the auto-model, as presented in Chapter 14.

10.6 References

Ashcroft N W and Mermin N D (1976), *Solid State Physics*, Holt-Saunders, Philadelphia.

Bernardin D and Sero-Guillaume O E (1990), 'Lattice gas mixture models for mass diffusion', *Eur. J. Mech. B*, **9**, 21.

Boon J P (editor) (1992), 'Lattice gas automata theory, implementation, and simulation', Special issue of *J. Stat. Phys*., **68**(3/4).

Boublík T (1996), *Statistická termodynamika*, Academia, Praha

Chen S, Doolen G D and Matthaeus W H (1991), 'Lattice gas automata for simple and complex fluids', *J. Stat. Phys*., **64**(5/6), 1133–1162.

Chen S, Diemer K, Doolen G, Eggert K, Fu C, Gutman S and Travis B J (1991a), 'Lattice gas automata for flow through porous media', *Physica D*, **47**(1/2), 72–84.

Chen S, Doolen G D and Eggert K G (1994), 'Lattice-Boltzmann fluid dynamics', *Los Alamos Science*, **22**, 100–109.

Chopard B and Droz M (1998), *Cellular Automata Modeling of Physical Systems*, Cambridge, Cambridge University Press.

Chytil M (1984), *Automaty a Gramatiky*, Praha, SNTL.

Dieter A, Wolf-Gladrow D (2000), *Lattice Gas Cellular Automata and Lattice Boltzmann Models*, Berlin, Springer.

Foti E, Succi S and Higuera F (1989), 'Thee-dimensional flows in complex geometries with the lattice Boltzmann method', *Europhys. Lett*., **10**(5), 433.

Frisch U, Hasslacher B and Pomeau Y (1986), 'Lattice-Gas Automata for the Navier–Stokes Equation', *Physical Review Letters*, **56**(14), 1505–1508.

Gardner M (1970), 'The fantastic combinations of John Horton Conway's new solitary game of "life"', *Scientific American*, **223**(4), 120–123.

Hanon D and Boon J P (1997), 'Diffusion and correlations in a lattice gas automata', *Phys. Rev. E*, **48**, 2655–2668.

Hardy J and Pomeau Y (1972), 'Thermodynamics and hydrodynamics for a model fluid', *J. Math. Phys*., **13**, 1042–1051.

Hardy J, Pomeau Y and de Pazzis O (1973), 'Time evolution of a two-dimensional model system. I. Invariant states and time correlation functions', *J. Math. Phys*., **14**, 1746–1759.

Hardy J, de Pazzis O and Pomeau Y (1976), 'Molecular dynamics of classical lattice gas, transport properties and time correlation function', *Phys. Rev. A*, **13**, 1949–1961.

Henon M (1987), 'Isometric collision rules for the 4-D FCHC lattice gas', *Complex Systems*, **1**, 475–494.

Henon M (1989), 'Optimization of collision rules in the FCHC lattice gas and addition of rest particles', *Discrete Kinetic Theory, Lattice Gas Dynamics and Foundations of Hydrodynamics*, Singapore, World Scientific.

Henon M (1992), 'Implementation of the FCHC lattice gas model on the connection machine', *Proceedings of the NATO advanced research workshop on lattice gas automata theory, implementation, and simulation*, Nice (France).

Herman G (1969), 'Computing ability of a developmental model for filamentous organisms', *J. Theoret. Biol*., **25**, 421.

Higuera F and Jimenz J (1989), 'Boltzmann approach to lattice gas simulations', *Europhys. Lett*., 9, 663.

Hyötyniemi H (2004), *Complex Systems – Science on the Edge of Chaos*, Helsinki University of Technology, Control Engineering Laboratory, Report 145.

Kadanoff K and Swift J (1968), 'Transport coefficient near the critical point: a master-equation approach', *Phys. Rev*., **165**, 310–322.

Kitagawa T (1974), 'Cell space approaches in biomathematics', *Math. Biosci*., **19**, 27.
Kittel Ch (1980), *Thermal Physics,* John Wiley & Sons Inc., New York.
Kohring G A (1991), 'Calculation of the permeability of porous media using hydrodynamic cellular automata', *J. Stat. Phys*., **63**(1/2), 411–418.
Koponen A, Kandhai D, Hellen E, Alava M, Hoekstra A, Kataja K, Niskasen K and Sloot P (1998), 'Permeability of three-dimensional random fiber webs', *Phys. Rev. Lett*., **80**(4), 716.
Kudryavtsev V B, Aleshin C V, Podkolzin A S (1985), *Introduction to the automata theory*, Moscow, Nauka.
Landau L D and Lifschitz E M (1987), *A Course of Theoretical Physics, Fluid Mechanics*, 2nd edition, Pergamon Press, Oxford.
Lawson M (2003), *Finite Automata*, Chapman & Hall/CRC Press.
Lindenmayer A (1968), 'Mathematical models for cellular interactions in development', *J. Theoret. Biol*., **18**, 280.
Lukas D and Kilianova M (1996), 'Modelovani proudeni pomoci bunecnych automatu', 12th *Conference of Czech and Slovak Physicists*, Ostrava (Czech Republic), Vol. 2, 729–732.
Lukas D and Chaloupek J (1998), 'Interakcni energie a hybnosti v mrizovych modelech tekutin', *STRUTEX Struktura a strukturni mechanika textilii*, Liberec (Czech Republic), 34–38.
Lutsko J L, Boon J P and Somers J A (1992), 'Lattice gas automata simulations of viscous fingering in porous media', *Lecture Notes in Physics*, **398**, 124–135, Berlin, Springer-Verlag.
McNamara G and Zanetti G (1986), 'Direct measure of viscosity in a lattice gas model', *Cellular Automata '86* (abstract), MIT Lab. for Comp.
McNamara G and Zanetti G (1988), 'Use of the Boltzmann equation to simulate lattice gas automata', *Phys. Rev. Lett*., **61**, 2332.
McNamara G R (1990), 'Diffusion in a lattice gas automaton', *Europhys. Lett*., **12**, 329.
Moholkar V S (2002), *Intensification of Textile Treatments; Sonoprocesses Engineering*, Enschede, Twente University Press.
Ocheretna L and Košťáková E (2005a), 'Ultrasound and Textile Technology – Cellular Automata Simulation and Experiments', *Proceedings of ForumAcusticum*, Budapest, Hungary, 29 Aug–2 Sep, 2843–2848.
Ocheretna L (2005b), 'Modeling of generation and propagation of harmonic waves based on a FHP lattice gas model', *Proceedings of 8th International Conference Information Systems Implementation and Modelling*, Ostrava (Czech Republic), 313–318.
Ocheretna L and Lukas D (2005c), 'Modeling of ultrasound wave motion by means of FHP lattice gas model', *5th World Textile Conference AUTEX 2005, Proceedings*, Book 2, University of Maribor, 634–639.
Rivet J-P and Boon J P (2001), *Lattice Gas Hydrodynamics*, Cambridge, Cambridge University Press.
Rosen R (1981), 'Pattern generation in networks', *Prog. Theor. Biol*., **6**, 161.
Rothman D G (1988), 'Cellular automaton fluids: a model for flow in porous media', *Geophysics*, **53**, 509–518.
Rothman D H (1990), 'Macroscopic laws for immiscible two-phase flow in porous media: results from numerical experiments', *J. Geophys. Res*., **95**, 8663–8674.
Rothman D H and Zaleski S (1994), 'Lattice-gas models of phase separation: interfaces, phase transitions, and multiphase flows', *Reviews of Modern Physics*, **66**, 1417–1479.

Rothman D and Zaleski S (1997), *Lattice Gas Cellular Automata: Simple Models of Complex Hydrodynamics*, Cambridge, Cambridge University Press.

Sarkar P (2000), 'A brief history of cellular automata', *ACM Computing Surveys*, **32**(1), 80–107.

Stanley H (1971), *Introduction to Phase Transitions and Critical Phenomena*, New York, Dover.

Succi S (2001), *The Lattice Boltzmann Equation for Fluid Dynamics and Beyond*, Oxford, Clarendon Press.

Toffoli T and Margolus N (1991), *Cellular automata machines*, Moscow, Mir.

Ulam S (1974), 'Some ideas and prospects in biomathematics', *Ann. Rev. Biol*., **255**.

Vichniac G Y (1984), 'Simulating physics with cellular automata', *Physica D*, **96**, 96–116.

von Neumann J (1963), 'The general and logical theory of automata', in *John von Neumann, Collected Works*, edited by Taub A H, Vol. Design of Computers, Theory of Automata and Numerical Analysis, Pergamon Press, New York, 288–329.

von Neumann J (1966), *The theory of self-reproducing automata*, edited by Burks A W, Urbana, University of Illinois Press.

Wolf-Gladrow D (1999), *An Introduction to Lattice-Gas Cellular Automata and Lattice Boltzmann Models*, Berlin, Springer-Verlag.

Wolfram S (1983), 'Statistical mechanics of cellular automata', *Reviews of Modern Physics*, **55**(3), 601–644.

Wolfram S (1986), 'Cellular automaton fluids 1: Basic theory', *Journal of Statistical Physics*, **45**, 471–526.

Yang Z L, Dinh T N, Nourgaliev R R and Sehgal B R (2000), 'Evaluation of the Darcy's law performance for two-fluid flow hydrodynamics in a particle debris bed using a lattice-Boltzmann model', *Heat and Mass Transfer*, **36**, 295–304.

11

Phase change in fabrics

K. GHALI, Beirut Arab University, Lebanon
N. GHADDAR, American University of Beirut, Lebanon
B. JONES, Kansas State University, USA

11.1 Introduction

Phase change in fabrics can result from moisture sorption/de-sorption processes in the fiber, from moisture condensation/evaporation in the fabric air void volume, and from the presence of micro-encapsulated phase-change paraffin inside textile fabrics with melting and crystallization points set at temperatures close to comfort values.

The structure of a fabric system consists of a solid fiber and entrapped air. The ability of the fabric to transport dry heat is largely influenced by the amount of entrapped air while the ability to transport water vapor is influenced by the volume of the solid fiber and its arrangement. The solid fiber represents an obstacle to the moving water vapor molecule, and tends to increase the evaporative resistance of the fabric. In addition, the solid fiber serves to absorb or de-absorb moisture, depending on the relative humidity of the entrapped air in the microclimate and on the type of the solid fiber. For example, wool fiber can take up to 38% of moisture relative to its own dry weight. The moisture sorption/de-sorption capability of the fabric influences the heat and moisture transport across the fabric and its dry and the evaporative resistance. When fibers absorb moisture, they generate heat. The released heat raises the temperature of the fiber, which results in an increase of dry heat flow and a decrease in latent heat flow across the fabric. The opposite effect takes place in the case of water vapor de-sorption. When thermal conditions change at the fabric boundaries, the hygroscopic fabric experiences a delayed effect on heat and moisture transport.

The water content of the fabric does not only include the absorbed water in the solid fiber and the water vapor in the entrapped microclimate, but also includes the liquid water that can be present in the void space. This liquid water can originate from a moist source in which the liquid water is wicked or it can result from condensation in the case where water vapor continues to diffuse through a fully-saturated solid fiber. Similar to the sorption/de-sorption of moisture, liquid condensation and evaporation influence the flow of heat

and moisture across the fabric by acting as a heat source or sink in the heat transfer process. In addition, condensation has a significant effect on thermal comfort because of the uncomfortable sensation of wetness by humans.

With the advancement of technology, phase change occurrence in fabrics is no longer limited to moisture sorption/de-sorption in the solid fiber and moisture condensation/evaporation in the void space of the fabric, but it also occurs by incorporating micro-encapsulated phase change materials (PCM) inside textile fabrics. The introduction of PCM technology in clothing was developed and patented in 1987 for the purpose of improving the thermal performance of textile materials during changes in environmental temperature conditions (Bryant and Colvin, 1992). PCMs improve the thermal performance of clothing when subjected to heating or cooling by absorbing or releasing heat during a phase change at their melting and crystallization points.

Since adsorption/de-sorption is addressed in Chapter 12 of this book, this chapter will mainly take into consideration the effect of condensation and the effect of using PCM in fabrics on the transport of heat and moisture through fibrous medium, and their impacts on clothing properties and comfort.

11.1.1 Mechanism of moisture condensation/evaporation

For condensation to take place in a fibrous medium, a temperature gradient should exist across the medium such that one side of the fibrous system is directly exposed to a moist hot air environment or is being sprayed with liquid water, while the other side of the fabric is subject to a low temperature. In addition, the fibrous system should have a low water vapor permeability to achieve condensation. This situation is common in the case of human clothing systems, where clothing can be sandwiched between a hot humid human skin and an outer lining fibrous layer of low water vapor permeability exposed to a cold air stream.

When a dry hygroscopic fibrous layer is suddenly exposed to the above-mentioned conditions, the water vapor originating at the hot side will diffuse into the fibrous medium. First, there will be a rapid moisture uptake by the dry solid fiber. The heat released as a result of adsorption by the fiber will raise the temperature of the fibers and increase their water vapor pressure. As a result, the vapor pressure gradient between the absorbed water and the microclimate water vapor will be reduced, causing a slow down in the rate of adsorption. The increase in the fiber diameter (swelling) due to moisture uptake will lower the permeability of the fabric system to water vapor (see Chapter 9 for discussion of sorption kinetics). The fabric will remain dry if the water vapor pressure of the microclimate is greater than the water vapor pressure of the bound water, and if the vapor concentration in the microclimate is less than the saturation vapor concentration at the fabric local temperature. When equilibrium between the absorbed water in the solid fiber and the

microclimate is established, the diffused water vapor from the humid side will be transferred to the environment without the occurrence of condensation. In this case, the transient effect of absorption ends, but the dry and latent heat transport from the hot humid source continues and the fibrous medium does not become wet. If the vapor concentration is increased to a level such that somewhere within the fibrous system moisture saturation is reached, condensation will occur. The condition of saturation could be attained by increasing the concentration of the water vapor in the microclimate, which can be achieved by either increasing the water vapor concentration at the warm side of the system or by lowering the permeability of the fabric to water vapor. In addition, increasing the temperature gradient across the fabric by lowering the temperature of the colder side will cause the condition of saturation in the microclimate to occur at lower microclimate water vapor concentration.

Condensation is a phenomenon that is more likely to take place when the fibrous medium is exposed to large temperature differences and to a high humid source that causes the local relative humidity of the microclimate to reach 100%. Once the microclimate of the fibrous system attains saturation while there is still extra moisture diffusing into it, condensation continues to occur. Therefore, unlike the absorption process, which is transient in nature, the condensation process is continuous.

Since condensation takes time, a state of transitory super-saturation may exist in the microclimate causing the relative humidity to exceed 100%. Yet this state of super-saturation does not last, and given enough time, the excess moisture will condense, thus reducing the relative humidity to 100% (Jones, 1992). The condensation process will release the heat of condensation, affecting both temperature and concentration gradients across the fabric. Condensation in a fibrous medium can occur anywhere within the fibrous medium when the local vapor pressure rises above the saturation vapor pressure at that location temperature. The location of the condensation can be predicted by utilizing the saturation vapor line and water vapor pressure line (Keighley, 1985; Ruckman, 1997). Figure 11.1 shows a schematic of water vapor pressure variation against temperature of the fibrous medium (curve A) and the corresponding saturation vapor pressure (curve B). Saturation line curve B shows the water vapor pressure corresponding to 100% relative humidity at a specific temperature. If the microclimate water pressure at that temperature exceeds the saturation temperature, condensation will occur at that location. There is a linear relation between saturated water vapor pressure and temperature. At high temperatures, saturation vapor pressure is already high, and for condensation to occur, the local water vapor pressure should be greater than the saturation pressure. For that reason, condensation is more likely to occur close to the colder boundary of the fibrous system.

Contrary to the case for condensation, evaporation of liquid water occurs

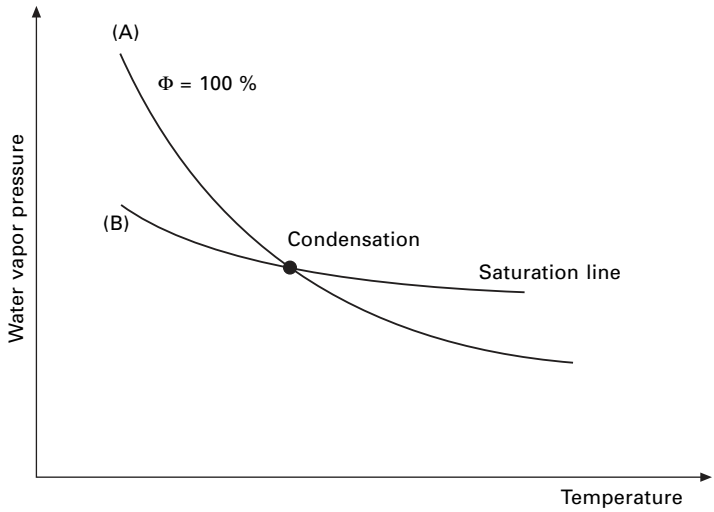

11.1 Schematic of the water vapor pressure distribution in a fibrous medium against its temperature variation (curve A) and the corresponding saturation vapor pressure distribution (curve B).

when the relative humidity of the surrounding microclimate in the void space is less than 100%. When liquid water exists in the fabric void space, a saturated boundary layer is formed at the interface between the liquid and the microclimate air. If the vapor pressure of this boundary is greater than the vapor pressure of the microclimate air, then evaporation occurs. In this case, the rate of moisture leaving the fibrous system is greater than the rate of moisture going into the system. Evaporation of moisture in a fibrous system usually moves from the warm moist boundary of the fibrous medium across the gas-filled void space where it may condense or diffuse out of the fibrous system, depending on the coupled moisture and temperature distributions.

11.1.2 Effect of condensation on clothing heat transfer and comfort

Clothing is a crucial factor in determining human thermal comfort. The purpose of clothing is to maintain a uniform body temperature under different body activity levels and different environment temperatures. In addition, clothing keeps the human body skin dry by preventing the accumulation of sweat on the human skin and by allowing the perspired body water to flow to the outside environment. In most comfortable environmental conditions at low activity levels, the perspired sweat from the skin escapes through clothing without the incidence of condensation since the rate of perspiration is low. At higher activity levels, the perspiration increases to a level that may cause

condensation to occur within the clothing system. The occurrence of sweat in the clothing system is generally affected by the vapor permeability of the different fabric layers constituting the clothing ensemble, the skin vapor concentration, and the environment temperature.

Comfortable clothing should not only provide human thermal comfort sensation, but should also give the wearer a minimum awareness of this comfort, as was suggested by Keighley (1985). The condensation of sweat on the clothing layers affects both the human sensation of comfort and the attentiveness of the wearer to the clothing ensemble. When condensation occurs in clothing, the moisture permeability of the fabric decreases, allowing more sweat to accumulate on the skin, thus affecting the human thermal sensation of comfort. In addition, the pressure of the garment on the human skin increases because of its increased weight. As a result, the awareness of the clothing wearer increases and the clothing system will be considered uncomfortable.

The condensation process liberates heat of condensation causing the local clothing temperature to increase at the condensation location, thus changing the temperature gradient across the clothing that existed prior to the condensation process. In most cases, the temperature gradient across the clothing system uniformly increases from the human skin to the outside environment. As condensation occurs, the temperature gradient from the skin to the location of condensation decreases and the temperature gradient from the spot of condensation to the outside environment increases (Lotens, 1993). Since the heat of condensation at the human skin does not leave the human clothing system because of the perspired moisture, it may be suggested that the sweating process is thermally ineffective in providing the necessary heat loss from the human body. But as was explained by Lotens (Lotens, 1993), the heat has already left the human skin and passed a good distance in the clothing system away from the human skin, causing an increase in the temperature of the outer clothing layer where condensation is more likely to take place. The increase in temperature of the outer layer causes an increase in the dry heat transport from clothing, which may compensate for the decrease in the latent heat transport from the clothing system. However, in this case, the clothing will be wet and will be considered uncomfortable.

11.1.3 Mechanism of phase change in PCM fabrics

Unlike the phase change mechanism in the condensation/evaporation process, which depends on the moisture and temperature gradient across the fabric, the mechanism of the phase change process in PCM fabrics is a temperature-driven process. It mainly depends on the temperature and the type of the PCM that is encapsulated in a protective wrapping or microcapsules of a few microns in diameter. The microcapsules are incorporated into the fibers of

the fabric by the wet spinning process or coated onto the surface of the fabric substrate (Pause, 1995). Microcapsules protect the PCM and prevent its leakage during its liquid phase. PCMs are combinations of different types of paraffin (octadecane, nonadecane, hexadecane, etc…), each with a different melting and crystallization point. Changing the proportionate amounts of each paraffin type can yield the desired physical properties (melting and crystallization). When the encapsulated PCM is subject to heating, it absorbs heat energy and undergoes a phase change as it goes from solid to liquid. This phase change produces a temporary cooling effect. Similarly, when a PCM fabric is subject to a cold environment where the temperature is below the crystallization point, the micro-capsulated liquid PCM will change back to the solid phase producing a temporary warming effect.

11.2 Modeling condensation/evaporation in thin clothing layers

The theoretical modeling of the coupled heat and moisture transfer with phase change in a clothing fibrous medium relies on extensive studies performed by many researchers on the heat and mass transfer process in porous media. Coupled heat and mass transfer with condensation/evaporation is of a special importance to the building insulation industry and to the research studies on energy conservation (Vafai and Sarkar, 1986; Vafai and Whitaker, 1986). Condensation can lead to an increase in the thermal conductivity of the insulating material, since the thermal conductivity of water is approximately 24 times that of the conductivity of the air. As a result, the insulating material loses its basic role in the reduction of heat transfer and in conserving energy. In addition, condensation usually results in corrosion and deterioration of the quality of the insulating material. Most research on modeling heat and mass transfer with phase change in porous media is applicable to highly porous thin textile materials. The approach to modeling the condensation/evaporation process in clothing was based on the fundamental studies of Henry (1948) and the subsequent models that were developed by Farnwoth (1986) and by Lotens *et al*. (1995) for highly porous media.

11.2.1 Farnworth model

Theoretical modeling of the combined heat and water vapor transport through clothing with sorption and condensation started with the model of Farnworth (1986). This model is a simplified expression of Henry's model with restrictive assumptions limiting the model applicability to a multi-layered clothing system where each layer is characterized by a uniform temperature and moisture content. The assumptions made by Farnworth were as follows.

(i) There is no convective airflow and/or convective transport of liquid.

(ii) The mass of absorbed water is proportional to the relative humidity of the microclimate with a restrictive upper limit of absorbed water vapor. This assumption is important to limit the vapor pressure of the absorbed water to its upper limit, which is the saturation water vapor pressure.
(iii) Clothing radiation can be neglected.

Based on the above assumptions, Farnworth derived the following conservation equations for mass and heat transport, respectively:

$$\frac{\partial M_i}{\partial t} = \frac{P_{i-1} - P_i}{R_{e,i-1}} - \frac{P_i - P_{i+1}}{R_{e,i}} \quad [11.1]$$

$$C_i = \frac{\partial T_i}{\partial t} = \frac{T_{i-1} - T_i}{R_{d,i-1}} - \frac{T_i - T_{i+1}}{R_{d,i}} + Q_{ci} \quad [11.2]$$

where M_i (kg) is the total moisture in the clothing layer which is the summation of the liquid water present in the void space of the fabric layer and the absorbed water vapor bound to the solid fiber of the fabric layer, C_i (J/kg · K) is the heat capacity per unit area of the clothing layer, T_i (°C) and P_i (kPa) are the temperature and water vapor pressure of the clothing layer respectively, $R_{d,i}$ (m^2 · °C/W) and $R_{e,i}$ (m^2 · kPa/W) are the dry and evaporative resistances characteristic of each clothing layer, Q_{ci} (W/m^2) is the quantity of heat per unit area which is released in the layer because of moisture adsorption and condensation, and i represents the layer index.

The model of Farnworth is easy to use but it is too simplistic to be applied to the whole clothing system. The assumption of linear regain increase with relative humidity presents a serious deficiency in the model. Moisture regain at low and high relative humidity is far from being linear (Chapter 12). If the empirical equilibrium relation between regain and relative humidity is used, the model will still remain limited due to the lumped moisture content and temperature value for each fabric layer. When condensation/ evaporation is taking place, the Farnworth model cannot be used for studying the temperature and moisture distribution inside a fibrous system.

11.2.2 Lotens model

The Lotens model is similar to the Farnworth model in its applicability to a clothing ensemble system and in its ability to integrate the clothing model with a nude human model (Lotens, 1993). However, the Lotens model presents a simple physical condensation theory with its associated effects on moisture distribution, temperature, and total heat transfer from the clothing ensemble. The Lotens model can predict the thermal performance of permeable and impermeable garments in cold and hot environmental conditions (Lotens *et al*., 1995).

Unlike the absorption phenomenon, which is a transient process lasting for a limited time depending on the fabric hygroscopicity property, condensation is a continuous process. According to Lotens (1993), this continuing nature of condensation can actually simplify the modeling of the condensation process and allow the incorporation of condensation in clothed human body modeling. Lotens' model divides the clothing system into: (i) an inner underclothing layer; (ii) an outer clothing layer; and (iii) an outer air layer, as shown in Fig. 11.2. The outer layer is characterized by a lower permeability compared to the inner, underclothing layer, to allow condensation to occur.

Based on the mass and heat balance between the clothing layers and the outer environmental air layer, the mass and heat transfer resistance network is constructed, neglecting the ventilation mass and heat resistance and the radiative heat transfer resistance.

$$\frac{P_s - P_1}{R_{e1}} + \Psi = \frac{P_1 - P_a}{R_{e2} + R_{e3}} \qquad [11.3]$$

$$\frac{T_s - T_1}{R_{d1}} + \Psi\, h_{fg} = \frac{T_1 - T_a}{R_{d2} + R_{d3}} \qquad [11.4]$$

where R_e is the evaporative heat resistance $m^2 \cdot kPa/W$, R_d is the dry heat transfer resistance $m^2 \cdot K/W$, h_{fg} is the heat of condensation and Ψ is the condensation rate $kg/m^2 \cdot s$. When condensation occurs, $P_1 = P_{sat}(T_1)$, and the three unknowns in the above equations, Ψ, P_1 and T_1 can be calculated.

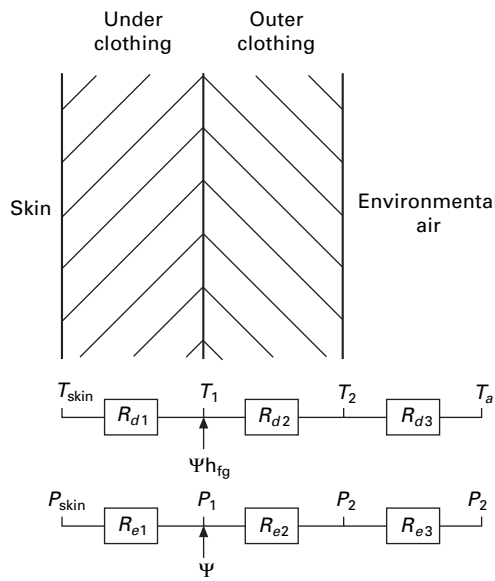

11.2 Lotens clothing system model.

The above simple clothing ensemble model is integrated with the human nude model by Lotens after taking into account the area increase because of the clothing and the ventilation of the inner surface of the outer layer (Lotens, 1993).

The simple clothing model developed by Lotens explains the effect of the condensation process on the dry and evaporative resistances of clothing. Dry and evaporative heat transfer leaving the skin, (Q_d, Q_e), are not the same as the heat dissipated to the outside environment during moisture condensation. During the occurrence of condensation, the rate of moisture leaving the skin is not equal to the moisture leaving the human clothing system, and thus there will be an increase in the temperature of the clothing ensemble at the spot of condensation. Consequently, the dry heat that is dissipated from the human skin is not the same as the dry heat reaching the outside environment. As a result of condensation, the apparent dry and evaporative resistances (R_{dt}, R_{et}) can be calculated as follows:

$$R_{dt} = \frac{T_s - T_a}{Q_d + \Psi h_{fg}} \qquad [11.5]$$

$$R_{et} = \frac{P_s - P_a}{Q_e - \Psi h_{fg}} \qquad [11.6]$$

where R_{dt} is the apparent clothing ensemble dry heat transfer resistance $m^2 \cdot °C/W$, and R_{et} is the apparent clothing ensemble evaporative heat resistance $m^2 \cdot kPa/W$.

Because of condensation, the dry resistance becomes smaller and the evaporative resistance becomes larger. In reality, condensation represents a link between the dry and latent heat that leaves the human skin. Condensation balances the decrease in the latent heat transfer by an increase in dry heat transfer.

Experimental verification of Lotens condensation theory. The condensation theory has been validated by the experimental findings of Lotens and other co-authors. Lotens' aim was to experimentally determine the effect of condensation on the latent and dry heat flows through different clothing ensembles and the resulting effect on the apparent dry and evaporative heat resistances. In the experiment of Van de Linde and Lotens (1983), the condensation effect was tested on human subjects wearing impermeable garments while exercising on a treadmill in the presence and absence of sweat from the skin. The absence of sweat was achieved by wrapping the subjects with plastic foil. Experimental findings showed that, in the absence of sweat, the impermeable garments showed higher dry resistance. The lower resistance of the garment in the presence of sweat is attributed to the presence of sweat condensation. The condensation theory has also been checked by

the experimental study of Havenith and Lotens (1984). In this study, impermeable garments were compared to semi-permeable garments in terms of their heat transport ability from human subjects exercising on a bicycle ergo meter in an environment of 14 °C temperature and 90% relative humidity. The experiments showed that the impermeable garments transport more dry heat compared to the semi permeable garments and that their outer surface temperature is higher due to sweat condensation. Van De Linde (1987) tested the condensation theory on the ability of impermeable garments to transport the body-generated heat for different exercise rates and ambient temperature. While exercising in cool environmental conditions at 16 °C, the condensation of sweat generated by the increased human subject work rate was reported to increase the outer garment temperature and to reduce its dry resistance. The same phenomenon was also observed at a higher environmental temperature of 26 °C (Van De Linde, 1987).

Lotens (1995) performed numerical simulations to compare the accuracy of his model with the experimental results and to determine the important parameters that evoke condensation. He found that the skin vapor concentration, the vapor resistance of the outer layer, and the air temperature are the important parameters that evoke condensation.

11.3 Modeling condensation/evaporation in a fibrous medium

From the simplified lumped models, it is clear that the effect of condensation on the heat and moisture transfer is captured. These simple models are able to describe the heat and mass transfer with condensation in the clothing ensemble and can be easily integrated with the human thermal model. However, they incorporate only the diffusion of heat and the diffusion of water vapor within the clothing system, and they ignore convection of air and liquid wicking. In addition, the lumped modeling approach relies on the physical dry and evaporative resistance properties of the fabric, which may change when condensation occurs. In the following section, a more accurate mathematical modeling of condensation within fibrous medium is presented.

11.3.1 Mathematical modeling of condensation

Figure 11.3 is a schematic of a fibrous porous system model consisting of the following: solid fiber, absorbed water vapor to the solid fiber, gaseous mixture of water vapor and air, and liquid water in the void space. To correctly model condensation/evaporation with sorption in a clothing system, the model should include the following features:

- The ability to simulate heat and moisture in space and time without lumping for the heat and concentration parameters.

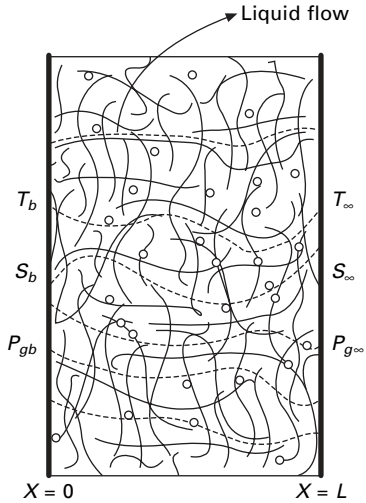

11.3 The fibrous medium system model consisting of the solid fiber, the water vapor absorbed by the solid fiber, the gaseous mixture of water vapor and air, and liquid water in the void space.

- A mechanism of the moisture water vapor movement that could take place due to gradients in the partial water vapor and the convective airflow due to pressure gradients across the clothing system. In situations when there is no total pressure gradient, during sedentary human activity, water vapor diffuses in a clothing ensemble by the driving force of the partial water vapor pressure gradient between the human skin and the outside environment. In movement conditions, pressure gradients can be induced across the fabric leading to bulk moisture movement.
- Water liquid transport is driven by capillary forces and surface tension. The inclusion of liquid transport is important for modeling coupled heat and the moisture transfer process with condensation because liquid moisture will affect the pore moisture content and the condition of saturation. In addition, the transport of liquid moisture across textiles increases their thermal conductivity, and thus affects the transport of heat across the clothing system.
- The transport of energy that can occur by conduction, as well as convection of the phases that are able to move, i.e. liquid water, water vapor and dry air. The sorption/de-sorption of the hygroscopic fibers with their associated heat of sorption should not be neglected because most textile fibers have a certain degree of moisture absorption ability. The fiber absorption characteristic significantly influences the heat and moisture transfer processes.

The above-mentioned inclusions can simultaneously be incorporated with

the theoretical development of the coupled heat and moisture processes and condensation, after applying the following simplifying assumptions:

(i) The porous system is assumed to be in local thermal equilibrium. Local thermodynamic equilibrium exists if the pore dimension of the fibrous medium is very small;
(ii) the volume changes of the fibers due to changes in moisture content, and therefore the porosity, is constant; and
(iii) the fibrous media is homogenous and isotropic.

With these assumptions, the governing equations of heat and moisture transport with condensation/evaporation can be developed using the considerable research work carried out in the literature by Gibson and Charmachi (1997), Zhongxuan *et al*. (2004), and Xiaoyin and Jintu (2004). The formulation adapted from Zhongxuan *et al*. (2004) will be presented in this section.

The water vapor conservation distribution is governed by the following equation:

$$\varepsilon \frac{\partial[(1-S)\rho_v]}{\partial t} + (1-\varepsilon)\frac{\partial C_f}{\partial t} - W = -\frac{\partial J_{vD}}{\partial x} - \frac{\partial J_{vC}}{\partial x} \qquad [11.7]$$

where S is the liquid water volumetric saturation (liquid volume/pore volume), ε is the porosity of the fabric, ρ_v is the density of water vapor, W is the evaporation or condensation flux of water in the void space (kg/m^3 · s), C_f is the moisture concentration in the fiber (kg/m^3), J_{vD} is the mass flux of water vapor by diffusion (kg/m^2 · s), J_{vC} is the mass flux of water vapor by bulk flow (kg/m^2 · s). The first term on the left-hand side of Equation [11.7] is the storage term of the water vapor in the void space, the second term is the absorbed water vapor stored in the solid fiber, and the third term, W, is the evaporation/condensation term. The right-hand side of Equation [11.7] represents the net diffusive and convective flows of water vapor. The moisture absorbed in the solid fiber can be calculated by using the Fickian law of diffusion as follows:

$$\frac{\partial C_f}{\partial t} = \frac{1}{r}\frac{\partial}{\partial r}\left[rD_f \frac{\partial C_f}{\partial r} \right] \qquad [11.8]$$

where D_f is the fiber diffusion coefficient and r is the radial coordinate. The fiber diffusion coefficient primarily depends on the stage of absorption, the rapid stage of moisture uptake, and the slower stage of absorption. The moisture boundary condition at the fiber surface is determined by assuming instantaneous moisture equilibrium with the microclimate air. Thus, the moisture content at the fiber surface can be determined by the relative humidity of the microclimate air and temperature. It can be obtained directly from the moisture sorption isotherm of the fiber.

The diffusion of water vapor flux in the voids is described by Stefen's law (Shuye and Guanyu, 1997) and can be represented by the following expression after substituting for the diffusion coefficient of the water vapor in terms of temperature and gaseous pressure:

$$J_{vD} = -1.952\, x10^{-7}\, \varepsilon(1 - S)\frac{T^{0.8}}{P_a}\frac{\partial P_v}{\partial x} \qquad [11.9]$$

where P_a is the partial pressure of dry air and P_v is the partial pressure of water vapor. The convective water vapor flux in the fibrous medium is

$$J_{vC} = \rho_v u \qquad [11.10]$$

Since Darcy's law holds in the pore of the inter fiber, the convective velocity, u, can be written as

$$u = -\frac{kk_{rg}}{\mu_g}\frac{\partial P_g}{\partial x} \qquad [11.11]$$

where k is the intrinsic permeability of the fibrous media, k_{rg} is the relative permeability of the gas, μ_g is the dynamic viscosity of the water vapor, and $P_g = P_a + P_v$ is the gaseous pressure. The condensation/evaporation term W of Equation [11.7] is given by Qing-Yong (2000) as

$$W = \varepsilon(1 - S)S_f h_w \frac{M_w}{RT} P_s(T) - P_v) \qquad [11.12]$$

where S_f is the specific area of the fabric, h_w is the mass transfer coefficient, M_w is the molecular mass of water vapor, R is the universal gas constant, and $P_s(T)$ is the saturation water vapor.

The liquid moisture mass conservation equation is given by

$$\varepsilon\rho_w \frac{\partial(S)}{\partial t} + W = -\frac{\partial J_l}{\partial x} \qquad [11.13]$$

where ρ_w is the density of liquid moisture. The first term in Equation [11.13] represents the storage of liquid water in the void, and the second term represents the condensation/evaporation flux. The right-hand side of Equation [11.13] represents the net capillary flow of liquid water and can be written (Nasrallah and Perre, 1988) as

$$J_l = -\rho_w \frac{kk_{rw}}{\mu_w}\frac{\partial}{\partial x}(P_g - P_c) \qquad [11.14]$$

where K_{rw} is the relative permeability of the liquid water, μ_w is the dynamic viscosity of the water, and P_c is the capillary pressure of the fabric function of saturation and surface tension.

The dry air mass conservation equation is:

$$\varepsilon \frac{\partial[(1 - S\rho_a]}{\partial t} = -\frac{\partial J_{aD}}{\partial x} - \frac{\partial J_{aC}}{\partial x} \quad [11.15]$$

The first term in Equation [11.15] represents the dry air storage in the void space, and the right-hand side first and second terms represent the diffusive dry air mass flux and the convective dry air mass flux, respectively. The dry air mass flux J_{aD} is equal in magnitude to the water vapor diffusive mass flux given by

$$J_{aD} = -J_{vD} \quad [11.16]$$

and the convective air mass flux J_{aC} can be expressed as

$$J_{aC} = -\rho_a \frac{kk_{rg}}{\mu_g} \frac{\partial P_g}{\partial x} \quad (11.17)$$

where k_{rg} is the relative permeability of the gas and μ_g is the dynamic viscosity of the gaseous phase.

The energy equation is represented by the following:

$$C_v \frac{\partial T}{\partial t} - \lambda(1 - \varepsilon)\frac{\partial C_f}{\partial t} + Q_c = \frac{\partial}{\partial x}\left(K_c \frac{\partial T}{\partial x}\right) \quad [11.18]$$

where C_v is the volumetric heat capacity of the fabric (J/m^3·K), K_c thermal conductivity of the fabric (W/m·K), λ heat of sorption (J/kg), and Q_c is the heat flux of condensation or evaporation (J/m^3·s). The first term in the energy equation represents the heat storage term in the fabric, the second term represents energy released by sorption, the third term represents the heat released by condensation, and the right-hand side represents the net conducted heat flow.

To solve the conservation Equations [11.7] through [11.18] of liquid moisture, water vapor, dry air, and energy, initial and boundary conditions need to be specified. The initial values of temperature, water vapor concentration, degree of saturation, absorbed moisture in the solid fiber, and the gaseous pressure in the fibrous medium should be known. In most practical cases, the initial conditions are uniform throughout the medium. The boundary conditions can be a constant temperature, saturation, and gaseous pressure or can be a convective air flow condition. Uniform initial conditions for a 1-D system can be expressed as

$$T(x, t = 0) = T_o,\ \rho_v(x, t = 0) = \rho_{vo},\ S(x, t = 0) = S_o$$

$$P_g(x, t = 0) = p_{go},\ C_f(x, t = 0) = f(\rho_{vo}, T_o) \quad [11.19]$$

while boundary conditions can be written as

$$T(x=0,t)=T_b,\ S(x=0,t)=S_b,\ P_g(x=0,t)=p_{gb},\ J_l|_{x=l}=0$$
$$-k\left.\frac{\partial T}{\partial x}\right|_{x=l}=h_c(T|_{x=l}-T_\infty),\ J_{vD}|_{x=l}+J_{vc}|_{x=l}=h_m(\rho_v|_{x=l}-\rho_{v\infty})$$

[11.20]

Other boundary conditions can be used depending on the physical system under consideration.

11.4 Effect of fabric physical properties on the condensation/evaporation process

11.4.1 Effect of vapor hydraulic permeability

The hydraulic conductivity of the fabric defines the ease with which water vapor passes in the voids of the fibrous media. This factor is determined by the permeability of the fabric to air flow when subject to a pressure difference. The type of yarn count, twist, and weave affect the permeability and thus the hydraulic conductivity of the fibrous media. For very small values of vapor permeability, the moisture movement within the fibrous media is only by diffusion. In such a case, it was found by Xiaoyin and Jintu (2004) that moisture distribution for a fibrous media sandwiched between a hot moist boundary and a cold boundary is close to a convex shape, with a relatively small variation in moisture content. Increasing the vapor permeability will lead to an increase in the amount of condensed water since more water will be transported across the fibrous media. However, with larger values of vapor permeability, the moisture content close to the warm boundary decreases while the moisture content close to the cold boundary increases, resulting in the occurrence of moisture condensation closer to the cold boundary. Fabrics characterized by high porosity are more advantageous for thermal comfort and heat loss than impermeable fabrics, because high porosity makes the wet region of the fibrous media occur away from the skin while minimizing the heat loss from the skin, since no condensation occurs in the fibrous media adjacent to the skin.

11.4.2 Effect of liquid water permeability

The transport mechanism of liquid water in a fibrous media is governed by its capillarity and by the liquid permeability of the fibrous medium. The capillarity represents the driving force for the liquid movement, whereas the permeability describes the ease with which water moves through the fibrous medium. For a fibrous medium with zero permeability, the condensate liquid moisture will be immobile. For higher liquid permeability values, the condensate moisture will be mobile and the condensates will move from the region of

higher moisture content towards the region of lower water content. The findings of Xiaoyin and Jintu (2004) showed that, with the increase of liquid moisture mobility, the moisture distribution of a fibrous media bounded by the extreme boundary conditions of warm moist and cold dry conditions will shift from concave to almost even. The mobility of the liquid moisture will definitely affect both thermal comfort and heat loss from the skin or warm boundary.

11.4.3 Effect of material hygroscopicity

As the hygroscopicity of the fabric increases, its moisture content will increase, mainly due to the water absorbed into the solid fiber. In steady-state conditions, this increase in moisture content leads to a decrease in the insulation value of the fibrous material, and thus more heat loss is observed from the fibrous medium (Xiaoyin and Jintu, 2004). However, during transient conditions, hygroscopic wool battings have shown less condensation when compared to non-hygroscopic battings of polypropylene (Jintu *et al*., 2004). For the same boundary conditions across the battings assembly, Jintu *et al*. (2004) showed that condensation starts after a short time for the propylene battings whereas condensation starts to appear in the wool battings after 4 hours. Furthermore, in transient conditions, the hygroscopicity of the fibrous medium decreases the heat loss from the human skin because of the heat liberated by the moisture absorption. Therefore, it is suggested that hygroscopic fabrics can be advantageous for cold protective clothing in transient conditions.

11.4.4 Effect of pressure difference across the fibrous medium

During exercise, the human limbs move back and forth forcing the renewal of the microclimate air existing between the skin and the clothing layers. The renewal of the microclimate air is driven by the pressure difference between the microclimate environment and the outside atmospheric motion. The pressure difference alternates between a positive value forcing the microclimate air to be discharged out of the clothing system and a negative value allowing atmospheric air to fill the space between the skin and the human clothing ensemble. The atmospheric pressure gradient developed during the limb motion will definitely affect the fibrous water vapor distribution and to a lesser extent the liquid moisture distribution. The liquid water movement is due to gradients in capillarity and to atmospheric pressures. Fengzhi *et al*. (2004) found that water vapor concentration in the void space is largely affected by the pressure difference and that the concentration of water vapor was high at the location of the lower pressure. Fengzhi *et al*. (2004) also found that the liquid water distribution was not significantly affected by

atmospheric pressure, as was the case with water vapor when the atmospheric pressure was increased from 1.0135×10^5 Pa to 2.0135×10^5 Pa.

11.5 Modeling heating and moisture transfer in PCM fabrics

The effect of the phase change that takes place in PCM fabrics is transitory. This transitory property is similar to sorption/de-sorption and different from condensation/evaporation phenomena. It lasts for a finite time, determined by the quantity of encapsulated paraffin and the thermal load impending on the PCM fabric. When a PCM fabric is exposed to heating from the sun or a hot environment, it will absorb this transient heat as it changes phase from solid to liquid, and it will prevent the temperature of the fabric from rising by keeping it constant at the melting point temperature of the PCM. Once the PCM has completely melted, its transient effect will cease and the temperature of the fabric will rise. In a similar manner, when a PCM fabric is subject to a cold environment, where the temperature is below the crystallization temperature, it will interrupt the cooling effect of the fabric structure by changing from liquid to solid, and the temperature of the fabric will stay constant at the crystallization temperature. Once all the PCM has crystallized, the fabric temperature will drop, and the PCM will have no effect on the fabric's thermal performance. Thus, the thermal performance of a PCM depends on the phase temperature, the amount of PCM that is encapsulated, and the amount of energy it absorbs or releases during a phase change.

Research studies on quantifying the effect of PCMs in clothing on heat flow from the body during sensible temperature transients were conducted by Shim (1999) and Shim *et al*. (2001). Shim *et al*. (2001) measured the effect of one and two layers of PCM clothing materials on reducing the heat loss or gain from a thermal manikin as it moved from a warm chamber to a cold chamber and back again. Their results indicated that the heating and cooling effects lasted approximately 15 min and that the heat release by the PCM in a cold environment decreased the heat loss by 6.5W for the one layer PCM clothing and 13.5W for the two-layer PCM clothing, compared to non-PCM suits. Shim and McCullough (2000) experimentally studied the effects of PCM-ski ensembles on the comfort of human subjects during exercise, and they found no appreciable effect of PCM material on comfort compared to non-PCM-ski clothing. The study of Shim and McCullough (2000) on the effect of PCM-ski ensembles on exercise was done after conditioning the human subjects inside cold environmental chambers.

The transport processes of heat and moisture from the human body are enhanced by the ventilating motion of air through the fabric initiated by the relative motion of the human with respect to the environment. Periodic renewal of the air adjacent to the skin by air coming from the environment has a

significant effect on the heat loss from the body and on comfort sensations. When sudden changes in the environmental air take place, it is desirable to delay the adjacent air temperature swings to reduce sudden heat loss or gain from the body. During exercise in cold environments, there is a periodic ventilation of the skin adjacent layer. Cold environmental air is pumped inside the clothing ensemble, while warm air heated by the human skin is forced to move out. During the air passage into and out of the clothing system, the moving air is intercepted by the PCM fabrics. It is questionable whether the PCM fabric is actually able to regenerate itself during exercise at steady-state environmental conditions, and whether the PCM fabric can act as a heat exchanger between the incoming cold air and the leaving warm air. The study of Ghali *et al*. (2004) addressed this question by performing experiments to investigate the effect of PCMs on clothing during periodic ventilation. The study of Ghali *et al*. (2004) also included a model and a numerical investigation of the transient effect of the phase change material during the sinusoidal motion pattern of the fabric induced by body movement upon exercise. In their work, PCMs were incorporated in a numerical three-node model (Chapter 8), for the purpose of studying their transient effect on body heat loss during exercise when subjected to sudden environmental conditions from warm indoor air to cold outdoor air. In deriving the energy balance for the fabric, the following assumptions were made: (i) the PCM is homogeneous and isotropic; (ii) the thermophysical properties of the PCM are constant in each phase; (iii) the phase change occurs at a single temperature; and (iv) the difference in density between solid and liquid phases is negligible.

The study findings of Ghali *et al*. (2004) indicated that the heating effect lasts approximately 12.5 minutes, depending on the PCM percentage and cold outdoor conditions. The heat released by PCMs decreased the clothed-body heat loss by an average of 40–55 W/m^2 depending on the ventilation frequency and the crystallization temperature of the PCM. A typical PCM percentage of the total mass of the fabric is about 20%. It is not recommended by the textile industry to increase the percentage of PCM because it will increase the cost of the fabric as well as its weight. The 20% is actually representative of what is used by industrial manufacturers.

The sensitivity of the PCM fabric performance to the amount of the PCM present in the fabric was also considered in the work of Ghali *et al*. (2004). The PCM percentage, α, was found to affect the length of time of the period during which the phase change process takes place but had negligible effect on the sensible heat loss from the skin when compared to non-PCM fabric. The reported durations of the phase change effect corresponding to $\alpha = 0$, 20%, 30% and 40% PCM are 0, 8.23 min, 12.26 min and 16.6 min, respectively, due to a change from an indoor environment at 26 °C and relative humidity of 50% to an outdoor environment at 2 °C and relative humidity of 80%. The experimental results of Ghali *at al*. (2004) revealed that, under steady-state

environmental conditions, the oscillating PCM fabric has no effect on the dry fabric resistance, even though the measured sensible heat loss increases with the decreasing air temperature of the environmental chamber. When a sudden change in ambient temperature occurs, the PCM fabric delays the transient response and decreases body heat loss. PCM has no effect on thermal performance of the fabric during exercise in steady-state environmental conditions.

11.6 Conclusions

Phase change is a phenomenon that occurs in a fibrous medium as a result of sorption/de-sorption of fiber moisture, condensation/evaporation of moisture in the void place, and melting/solidification of PCM when incorporated into the fabric structure. Both melting/solidification of PCM and sorption/de-sorption of fiber moisture processes are transitory in nature. Both are important in the study of transient thermal sensations of human subjects in changing environmental conditions. Their effect on the thermal performance of the fabric primarily depends on the hygroscopicity of the fabric, the amount of encapsulated PCM, and other environmental factors. Modeling the heat and moisture transfer for the sorption/de-sorption phenomena should include the diffusion process of moisture into the fiber, the diffusion of moisture in the void space, and the convective flow of moisture. Other complications are important in modeling sorption/de-sorption and include the change of the fabric permeability due to moisture sorption (Gibson, 1996) and the need to consider different temperatures for the different phases that constitute the fabric structure.

The condensation/evaporation phase change process is different from the other phase change phenomena by its steady-state nature. Evaporation and/or condensation take place depending on the temperature and moisture distribution. The condensation process continues provided that there is a supply of moisture and that the void water vapor pressure exceeds saturation. The condensation phenomenon is relevant to the study of thermal comfort since it leads to the loss of the main role of clothing in keeping the human body dry. It also affects the thermal performance of fabrics by decreasing the dry resistance of the fabric and increasing the fabric's evaporative resistance. Modeling condensation/evaporation is more complicated than modeling sorption/de-sorption. In addition to including diffusive and convective moisture vapor, modeling condensation should also include the liquid flow of moisture. Current research models describing condensation account for all complicated factors such as hygroscopic sorption, convective and diffusion of moisture, capillary flow of liquid moisture, and coupled diffusion of heat and mass flow. However, efforts to incorporate such a detailed condensation clothing fibrous model with the human thermal model have relied on simple human

thermal physiology models (Gibson, 1996) while the detailed human thermal physiology models that are integrated with condensation clothing models have relied on simple clothing condensation models (Lotens, 1993).

11.7 Nomenclature

C_f	moisture concentration in the fiber (kg/m^3)
C_i	heat capacity per unit area of the clothing layer (J/kg · K)
C_v	volumetric heat capacity of the fabric (J/m^3 · K)
D_f	fiber diffusion coefficient (m^3/s)
h_{fg}	heat of vaporization (J/kg)
h_w	mass transfer coefficient (m/s)
J_{aC}	convective dry air mass flux (kg/m^2 · s)
J_{aD}	diffusive dry air mass flux (kg/m^2 · s)
J_l	net capillary liquid moisture flow (kg/m^2 · s)
J_{vC}	mass flux of water vapor by bulk flow (kg/m^2 · s)
J_{vD}	mass flux of water vapor by diffusion (kg/m^2 · s)
k	intrinsic permeability (m^2)
K_c	thermal conductivity of the fabric (W/m · K)
k_{rg}	relative permeability of the gas
K_{rw}	relative permeability of the liquid water
M_i	total moisture in the clothing layer i (kg)
P_a	partial pressure of dry air (kPa)
P_c	capillary pressure (kg/m · s^2)
P_i	water vapor pressure of clothing layer i (kPa)
Ps	skin vapor pressure (kPa)
P_{sat}	saturation pressure (kPa)
P_v	partial pressure of water vapor (kPa)
Q_c	heat flux of condensation or evaporation (J/m^3 · s)
Q_{ci}	condensation/absorption heat release (W/m^2)
Q_d	dry heat transfer (W/m^2)
Q_e	evaporative heat transfer (W/m^2)
$R_{d,i}$	fabric dry resistance of clothing layer i (m^2 · °C/W)
R_{dt}	apparent fabric dry resistance (m^2 · °C/W)
$R_{e,i}$	fabric evaporative resistance of clothing layer i (m^2 kPa/W)
R_{et}	apparent fabric evaporative resistance (m^2 · kPa/W)
S	liquid water volumetric saturation (liquid volume/pore volume)
S_f	specific area (1/m)
T_i	temperature of the clothing layer (°C)
W	evaporation or condensation flux of water in the void space (kg/m^3 · s)

Greek symbols

α	PCM percentage of total fabric mass (%)
Ψ	condensation rate (kg/m$^2 \cdot$s)
ε	porosity of the fabric.
μ_g	dynamic viscosity (kg/m$\cdot$s)
μ_w	dynamic viscosity of water (kg/m$\cdot$s)
λ	heat of sorption (J/kg)
ρ_v	water vapor density (kg/m^3)
ρ_w	water liquid density (kg/m^3)

11.8 References

Bryant Y G and Colvin D P (1992), 'Fibers with enhanced, reversible thermal energy storage properties', *Techtextil-Symposium*, 1–8.

Farnworth B (1986), 'A numerical model of the combined diffusion of heat and water vapor through clothing', *Tex. Res. J.*, **56**, 653–665.

Fengzhi L, Yi L, Yingxi L and Zhongxuan L (2004), 'Numerical simulation of coupled heat and mass transfer in hygroscopic porous materials considering the influence of atmospheric pressure', *Numerical Heat Transfer, Part B*, **45**, 249–262.

Ghali K, Ghaddar N and Harathani J (2004), 'Experimental and numerical investigation of the effect of phase change materials on clothing during periodic ventilation', *Textile Res. J.*, **74**(3), 205–214.

Gibson P (1996), 'Multiphase heat and mass transfer through hygroscopic porous media with applications to clothing materials', Natick/TR–97/005.

Gibson P and Charmachi M (1997), 'Modeling convection/diffusion processes in porous textiles with inclusion of humidity dependent air permeability', *Int. Comm. Heat Mass Transfer*, **24** (5), 709–724.

Havenith G and Lotens W (1984), *What, actually is the advantage of semipermeable over impermeable rain wear*?, Report, TNO Institute for Perception, Soesterberg, IZF, 1984–6.

Henry P S H (1948), 'Diffusion of moisture and heat through textiles, *Discuss. Faraday Soc.*, **3**, 243–257.

Jintu F, Xiaoyin C, Xinhuo W and Weiwei S (2004), 'An improved model of heat and moisture transfer with phase change and mobile condensates in fibrous insulation and comparison with experimental results', *Int. J. of Heat and Mass Transfer*, **47**, 2343–2352.

Jones F E (1992), *Evaporation of Water with Emphasis on Application and Measurement*, Lewis Publishers, MI, USA, 25–43.

Keighley J H (1985), 'Breathable fabrics and comfort in clothing', *J. Coated Fabrics*, **15** (10), 89–104.

Lotens W (1993), *Heat Transfer from Humans Wearing Clothing*, Doctoral Thesis, The Royal Institute of Technology, Stockholm, Sweden.

Lotens W, Van De Linde F J G and Havenith G (1995), 'Effects of condensation in clothing on heat transfer', *J. Ergonomics*, **38**(6), 1114–1131

Nasrallah S B and Perre P (1988), 'Detailed study of a model of heat and mass transfer during convective drying of porous media', *Int. J. Heat Mass Transfer*, **31**(5), 957–967.

Pause B H (1995), 'Membranes for building', *Textile Asia*, **26** (11), 81–83.
Qing-Yong Z (2000), 'A numerical simulation of drying process in wool fabrics', *Int. Conf. on Applied Fluid Dynamics*', Beijing, China, 621–626.
Ruckman J E (1997), 'An analysis of simultaneous heat and water vapor transfer through waterproof breathable fabrics', *J. Coated Fabrics*, **26** (4), 293–307.
Shim H (1999), *The Use of Phase Change Materials in Clothing*, Doctoral research dissertation, Kansas State University, Manhattan, Kansas.
Shim H and McCullough E A (2000), 'The effectiveness of phase change materials in outdoor clothing' *Proceedings of the International Conference on Safety and Protective Fabrics'*, Industrial Fabrics Association International, Roseville, MN, April, 26–28, 2000.
Shim H, McCullough E A and Jones B W (2001), 'Using phase change materials in clothing', *Textile Res J*, **71**(6), 495–502.
Shuye L and Guanyu Z (1997), 'Numerical simulation of heat and mass transfer in wet unsaturated porous media', (in Chinese), *J. Tsinghua Univ.*, **37**, 86–90.
Vafai K and Sarkar S (1986), 'Condensation effects in a fibrous insulation slab', *J. Heat Transfer*, **108**, 667–675.
Vafai K and Whitaker S (1986), 'Heat and mass transfer accompanied by phase change in porous insulations', *J. Heat Transfer*, **108**, 132–140.
Van De, Linde F J G and Lotens W (1983), 'Sweat cooling in impermeable clothing', *Proceedings of an International Conference on Medical Biophysics, Aspects of Protective clothing*, Lyon, 260–267.
Van De Linde F J G (1987), *Work in Impermeable Clothing: Criteria for Maximal Strain*, Report, TNO Institute for Perception, Soesterberg, IZF, 1987–24.
Xiaoyin C and Jintu F (2004), 'Simulation of heat and moisture transfer with phase change and mobile condensates in fibrous insulation', *Int. J. of Thermal Sciences*, **43**, 665–676.
Zhongxuan L, Fengzhi L, Yingxi L and Yi L (2004), 'Effect of the environmental atmosphere on heat, water and gas transfer within hygroscopic fabrics', *J. of Computational and Applied Mathematics*, **163**, 199–210.

12

Heat–moisture interactions and phase change in fibrous material

B. JONES, Kansas State University, USA
K. GHALI, Beirut Arab University, Lebanon
N. GHADDAR, American University of Beirut, Lebanon

This chapter focuses on phase-change phenomena associated with the adsorption of moisture into fibers, the condensation of moisture onto fibers, and the release or absorption of heat associated with this change of phase. First, a set of mathematical relationships is developed that describes these interactions. These relationships may be somewhat simplified compared to the relationships developed in other chapters so that it is easier to focus on the heat and moisture interactions. However, every effort is made to point out any limitations associated with this simplification. The equations are also developed so that they are based on variables, properties, and other parameters that are readily measured or readily obtained. These equations are then presented in a finite difference form that has been proven effective in modeling heat and moisture interactions in clothing systems.

12.1 Introduction

Each fiber in a fibrous media continually exchanges heat and moisture with the air in the microclimate immediately surrounding it, as shown in Fig. 12.1. In addition, there will be radiation heat exchanges with other fibers and other surfaces. These radiation exchanges are not addressed in the present chapter but may be important in certain situations, especially in fibrous media with a low fiber density or with high temperature gradients. The heat and moisture exchanges between the fiber and the surrounding environment are the focus of this chapter.

When there is a temperature difference between a fiber and the air in the surrounding microclimate, a net heat flow results; this exchange is generally well understood, at least in principle. Similarly, if there is difference between the water vapor pressure at the fiber surface and the water vapor pressure in the air in the surrounding microclimate, there will be a net exchange of moisture. For a given fibrous material, the vapor pressure at the surface depends upon the amount of moisture adsorbed onto that surface and the

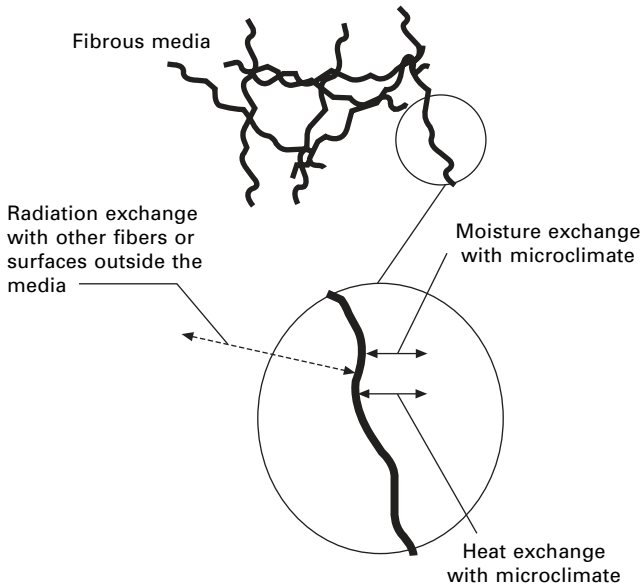

12.1 Heat and moisture between a fiber and its microclimate.

temperature of the fiber. The amount of moisture on the fiber is not limited by adsorption, however. When the fiber becomes saturated with respect to the adsorption state, i.e. it has adsorbed as much moisture as it can, additional moisture may condense as a liquid onto the surface of the fiber. Depending on the nature of the fibrous media, large amounts of water condensate may be held on the surface of the fiber.

The liquid on the surface may be relatively immobile and trapped in place, or may be transported within the fibrous media by capillary pressure. This capillary pressure transport is not addressed in the present chapter but is addressed in other chapters. Generally, the moisture adsorbed onto a fiber is considered to be immobile and can only move by exchange with the air in the surrounding microclimate. While not well understood or documented, it is possible that the adsorbed moisture becomes mobile when the fiber is nearly saturated with adsorbed moisture. There could then be some transport along the fiber in this situation.

There is sometimes confusion with respect to the use of the term ‘saturated’ with regard to moisture in a fibrous media. When a fiber has all of the moisture adsorbed that it can hold in the adsorbed state, it is said to be saturated. Similarly, when a fibrous media is fully wetted with liquid, it is said to be saturated. In the present chapter, both forms may be used with the context making it clear what which form is intended.

12.2 Moisture regain and equilibrium relationships

It is customary to refer to the adsorbed moisture content of fibrous material as 'moisture regain'. The moisture regain is defined as the mass of moisture adsorbed by a fiber divided by the dry mass of the fiber. The dry mass of the fiber is the mass of fiber when it is in equilibrium with completely dry air, even though some fibers may contain a residual amount of moisture in this state. The mass of moisture adsorbed does not include this residual moisture in the dry state (Morton and Hearle, 1993). Mathematically, the regain (R) is defined as

$$R = \frac{\text{Mass at given condition} - \text{Mass at dry condition}}{\text{Mass dry condition}}$$

It is customary to express regain as a percentage.

The equilibrium moisture regain of most fibrous material depends primarily on the relative humidity of the air in the ambient microclimate surrounding a fiber. That is, the equilibrium regain will be nearly the same at different temperatures if the ambient relative humidity is the same. Ambient temperature and atmospheric pressure can have a small impact independent of relative humidity. However, relative humidity is clearly the dominant variable for most terrestrial applications at common indoor and outdoor environmental temperatures. At more extreme conditions, such as might occur in manufacturing processes, the relationship between relative humidity and regain may not hold.

Figure 12.2 presents standardized relationships for moisture regain for a number of common fibers (Morton and Hearle, 1993). In general, natural fibers tend to have higher regains than manufactured fibers, with some of the latter fibers having nearly negligible regain. The regains shown in Fig. 12.2 are for raw fibers. A variety of surface finishes and other treatments are often applied to raw fibers to impart desired properties. While generally not applied for the purpose of changing moisture regain characteristics, some treatments can impact the moisture regain curve and care must be used in applying the equilibrium relationships in Fig. 12.2, especially for fibers that have very low regains in the raw state.

The curves in Fig. 12.2 stop at 100% relative humidity, as the regain is defined in terms of adsorbed moisture. Once the ambient microclimate relative humidity reaches 100%, liquid water may condense on the fiber. In terms of actual moisture present on a real fiber, the curves do not terminate at the values shown in Fig. 12.2. Rather, the curves actually become vertical and can extend to very large values, depending on the nature of the fibrous media. For individual fibers, it is difficult to define an upper limit. For fibers in a fibrous media, the upper limit is controlled by a number of factors including the porosity of the media and its structure.

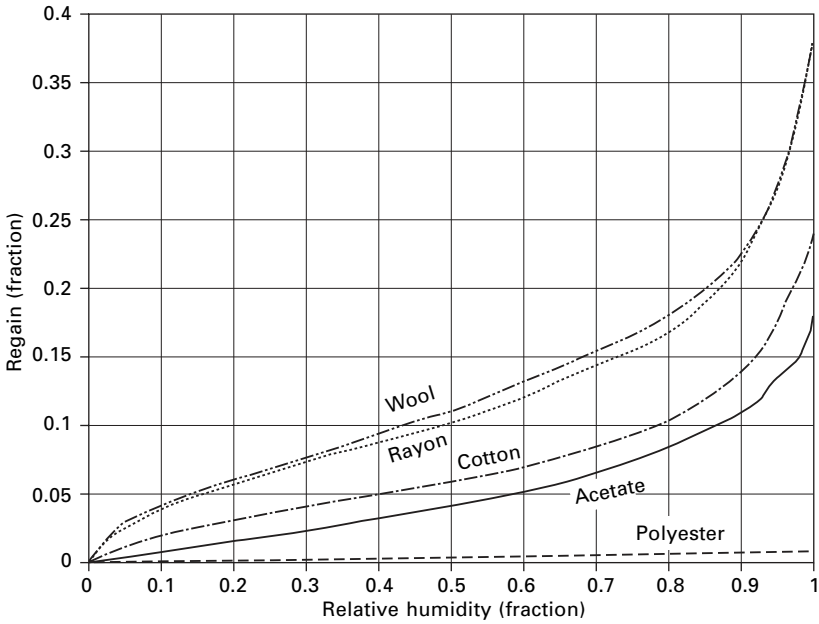

12.2 Equilibrium regain for typical fibers (based on data from Morton and Hearle, 1993).

12.3 Sorption and condensation

The heat of adsorption describes the amount of energy that is released when water vapor in the air is adsorbed onto the fiber surface. Similarly, this same amount of energy must be added when moisture is desorbed from the fiber. The heat of adsorption is not a constant, even for a given fiber, but depends on the environmental conditions under which the adsorption or desorption occurs. The primary factor affecting the heat of adsorption is the microclimate relative humidity and, for most applications at normal environmental temperatures and pressures, heat of adsorption can be treated as a function of humidity alone.

Figure 12.3 shows the heat of adsorption for several fibers. It is seen that, as the microclimate relative humidity becomes high, the heat of adsorption becomes equal to the heat of vaporization. The heat of sorption is often divided into two components: the heat of vaporization and the 'heat of wetting'. The heat of wetting is the added heat that is released above and beyond the heat release that would occur if the vapor simply condensed. Or viewed differently, it is the heat that is released if liquid water is added to a fiber. In Fig. 12.3, it is the distance between the heat of adsorption curve and the heat of vaporization line. It is often more convenient to present data in terms of the heat of wetting as it allows the large heat of vaporization, which is the same for all fibers, to be subtracted.

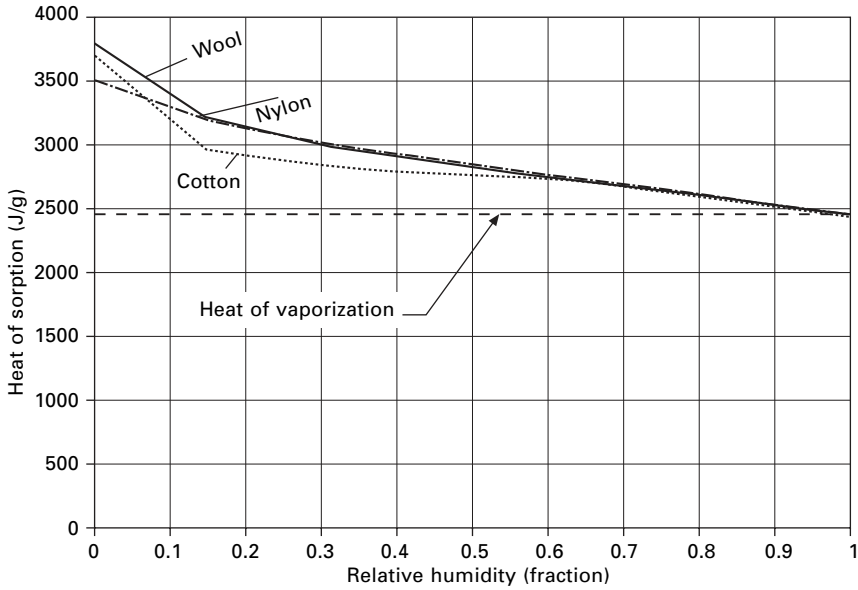

12.3 Heat of adsorption for typical fibers (based on data from Morton and Hearle, 1993).

As can be seen from Fig. 12.3, the heat of sorption for a given relative humidity does not vary greatly from fiber to fiber, especially when one considers the large heat of vaporization component that is common. Given the inaccuracies associated with many fibrous media heat and mass transport calculations, it is often adequate to simply use a common heat of sorption curve for all fibers.

12.4 Mass and heat transport processes

For steady-state conditions where any moisture on the fiber is immobile, there will be no net moisture exchange between the fiber and the air in the surrounding void space in the media. In this steady-state condition, there is no need to address heat–moisture interactions associated with moisture phase change. However, there are many situations where there is a net exchange of moisture between the fiber and the void space and it is necessary to develop mathematical descriptions of these processes. While relationships describing the heat and moisture transport between the fiber and the immediate void space can be developed, these processes are generally not the limiting factors in the transport phenomena. The high surface area associated with the fiber–microclimate interface results in minimal restriction to moisture and heat transport, and local equilibrium between the fiber and the surrounding microclimate is achieved over the time-scale of most applications for fibrous

media; or it is at least an acceptable approximation. The factors limiting the heat and moisture interchanges are the restrictions of heat and vapor transport in the bulk fibrous media.

A transient, one-dimensional moisture balance gives the following relationship at any location in the media:

$$\frac{\partial R}{\partial t}\rho = -\frac{\partial m}{\partial x} \qquad [12.1]$$

where R is the regain (kg H_2O per kg of dry fabric), ρ is the bulk density of the dry porous media (kg/m^3), m is the vapor moisture flux through the media (kg/s m^2), t is time (s), and x is distance along the dimension of interest (m).

This formulation ignores the water vapor in the air in the void space in the media. Normally, the amount of moisture stored in this phase is small compared with the regain. Additionally, it does not play an important role in the heat and moisture interactions and thus is ignored in the equations developed in this chapter.

The vapor moisture flux is proportional to the vapor partial pressure flux for most fibrous media and the relationship can be written as

$$m = -\varphi\frac{\partial P}{\partial x} \qquad [12.2]$$

where P is the vapor pressure (kPa), and φ is the vapor permeability of the media (kg/s m kPa)

While it is customary to use concentration gradients rather than vapor pressure gradients as the driving force for vapor diffusion, the vapor pressure gradients are equally valid and are more convenient for this application (Fu, 1995). The vapor permeability, φ, is an empirical parameter that describes the overall ability of vapor phase moisture to be transported through the media and is equal to the inverse of the vapor resistance per unit thickness (ASTM, 2005a).

Equations [12.1] and [12.2] combine to give a moisture balance in terms of partial pressure:

$$\frac{\partial R}{\partial t}\rho = \varphi\frac{\partial^2 P}{\partial x^2} \qquad [12.3]$$

The right-hand term expands directly to three dimensions, but the one-dimensional form is retained here for simplicity.

A one-dimension, transient energy balance can be written in similar fashion

$$\frac{\partial T}{\partial t}c\rho = -\frac{\partial q}{\partial x} - Q_S\frac{\partial m}{\partial x} \qquad [12.4]$$

where T is the temperature (°C), c is the heat capacitance of the bulk fibrous media (kJ/kg °C), q is the heat flux through the media (kW/m^2), and Q_S is the heat of adsorption (kJ/kg).

Several terms in the transient energy balance that are normally negligible have been omitted in Equation [12.4] to yield a relatively simple expression. Equation [12.4] should be acceptably accurate as long as there are no extreme temperature gradients in the porous media.

The heat flux through the fibrous media is proportional to the temperature gradient and the relationship can be written as

$$q = -k\frac{\partial T}{\partial x} \qquad [12.5]$$

where k is the thermal conductivity of the fibrous media (W/mK).

It should be noted that the thermal conductivity, above, is for the air–fiber combination that makes up the fibrous media and can be determined experimentally (ASTM, 2005b). Equations [12.5] and [12.2] combined with Equation [12.4] allow the energy balance to be expressed in terms of the temperature gradient and the vapor pressure gradient:

$$\frac{\partial T}{\partial t} c\rho = k\frac{\partial^2 T}{\partial x^2} + Q_S \varphi \frac{\partial^2 P}{\partial x^2} \qquad [12.6]$$

Equations [12.3] and [12.6] then describe the transient energy and mass balances at a location within a fibrous media. These equations also describe the transport of heat and vapor through the media. These equations are coupled in that there is a relationship between P, T, and R. Using the approximation that fiber is in moisture and thermal equilibrium with the immediately surrounding void space, this relationship is defined by the curve for the particular fiber in question in Fig. 12.2. Note that relative humidity is a unique function of P and T. Similarly, there is also a relationship between Q_S and P and T, with that relationship being defined by the appropriate heat of adsorption curve such as is shown in Fig. 12.3.

In order to solve Equations [12.3] and [12.6], appropriate boundary conditions, empirical relationships for equilibrium regain, and empirical relationships for heat of adsorption are required. In addition, the values of the bulk density, heat capacitance, thermal conductivity, and vapor permeability must be known. The thermal conductivity and the vapor permeability generally must be determined experimentally for the fibrous media of interest. One way to measure these parameters is to use a sweating hotplate (ASTM, 2005a; ISO, 1995). The bulk density can be measured experimentally (ASTM, 2005b). Thermal capacitance of the media can estimated with reasonable accuracy if the fiber content is known:

$$c = c_F + Rc_L \qquad [12.7]$$

where c_F is the thermal capacitance of the fiber (kJ/kg K), and c_L is the thermal capacitance of liquid water (kJ/kg K).

The air in the void space in the media is again ignored in Equation [12.7] and the equation is valid as long as the bulk density of the media is much greater than the density of air, which is true for nearly all applications. It should also be noted that the liquid term is based on the approximation that the thermal capacitance of a fiber increases with adsorbed moisture as if the adsorbed moisture is in the liquid state. This approximation is sufficiently accurate for all but the most precise calculations.

12.5 Modeling of coupled heat and moisture transport

Modeling the coupled heat flow requires appropriate boundary conditions to be established and Equations [12.3] and [12.6] to be solved. Fortunately, the equations are generally well bounded and well behaved, and the simplest of numerical methods may be used to solve the equations with acceptable accuracy. For modeling purposes, these equations can be written in finite difference form:

$$\Delta R_i \rho = \varphi \frac{P(\phi_{i-1}, T_{i-1}) + P(\phi_{i+1}, T_{i+1}) - 2P(\phi_i, T_i)}{\Delta x^2} \Delta t \qquad [12.8]$$

$$\Delta T_i c_i \rho = Q_s(\phi_i) \Delta R_i \rho + k \frac{T_{i-1} + T_{i+1} - 2T_i}{\Delta x^2} \Delta t \qquad [12.9]$$

where Δt is the integration time step (s), Δx is the distance step in the x-direction (m), ϕ_i is the local relative humidity (fraction), i refers to a specific discrete location in the x direction, $P(\phi, T)$ is the equilibrium vapor pressure for the fibrous media at the local relative humidity and temperature (kPa), and $Q_s(\phi)$ is the heat of sorption for the fibrous media at the local relative humidity, (kJ/kg).

The local relative humidity, ϕ_i is determined from the adsorption equilibrium curve for the media, such as in Fig. 12.2, corresponding to the local regain. This relative humidity value is then used to determine the equilibrium pressure from

$$P(\phi, T) = \phi(R)\, P_s(T) \qquad [12.10]$$

where $\phi(R)$ is the relative humidity corresponding to the local regain R from the equilibrium relationship (fraction) and $P_s(T)$ is the saturation pressure of water at local temperature T (kPa).

This same value of relative humidity is also used to determine the heat of sorption from the heat of sorption curve for the media, such as in Fig. 12.3.

Given initial conditions of temperature and regain, T and R, throughout

the media, appropriate boundary conditions, the equilibrium relationships such as in Fig. 12.2, and the heat of sorption information such as in Fig. 12.3, Equations [12.8]–[12.10] can be used to step through time and model the media response fully representing the interactions between heat and moisture. Time steps as small as 0.1 second or less may be required for clothing applications when boundary conditions change rapidly. However, the simplicity of the time-based solution puts little demand on computational capability, and transient solutions for complex systems can be readily solved. For thin fabric layers, it is often sufficient to use only a single increment in the x-direction. For thick fabric layers or fiber fillings, only a small number of increments in the x-direction is generally quite sufficient to obtain solutions of acceptable accuracy; generally, less than ten increments is adequate.

Equations [12.8] and [12.9] can be readily expanded to three dimensions. The single dimension form is presented here for simplicity. For many clothing applications, the radial direction from the body is usually the dominant direction for heat and moisture fluxes and local, one-dimensional representations are usually acceptable as long as the local variations in clothing and boundary conditions are addressed.

Equation [12.3] and [12.6] and, consequently, Equations [12.8] and [12.9] apply only when the moisture adsorbed or condensed onto the fiber is immobile. This limitation prevents these equations from being considered general representations of mass transport in fibrous media. Once the media contains sufficient moisture for this condensed moisture to become mobile and be transported in significant amounts by capillary pressure gradients, the air in the microclimate surrounding the fiber is saturated, $\phi = 1$, and the heat and moisture interaction phenomenon becomes one of condensation or evaporation.

Establishing the necessary boundary conditions is often the most difficult aspect of modeling heat and moisture interactions with fibrous media. Without proper boundary conditions, the equations described previously are of limited value. Each application is unique and it is not feasible to address all boundary condition situations that might be encountered with fibrous media. The following discussion addresses boundary conditions in a layered, cylindrical system which is typical of clothing applications and is depicted in Fig. 12.4.

The nomenclature for Fig. 12.4 follows:

q_c is the conduction or convection heat transfer to/from a surface (W/m^2),
q_r is the radiation between two surfaces or between a surface and the surrounding environment (W/m^2),
m is the vapor flux to/from a surface ($kg/s\ m^2$),
r is the characteristic radius of the respective layer (m),
the i subscript refers to the inner surface of a layer,
the o subscript refers to the outer surface of a layer,
the s subscript refers to the body surface, and
the e subscript refers to the surrounding environment.

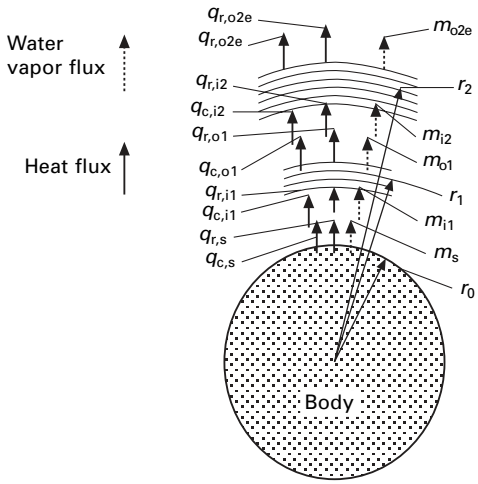

12.4 Depiction of boundary conditions for a two-layer radial system.

Each layer of porous media (e.g. fabric) is shown divided into a number of sub-layers that could correspond to Δx in the finite difference solution. The radius of each layer is characterized by a single value. This simplification is acceptable as long as the layer thickness is less than about one-fourth of the radius. The intervening air layers may present substantial resistance to heat and moisture transport and, consequently, are important in the overall modeling of the system. They do not normally contribute appreciably to the storage of heat or moisture and, thus, simplified modeling is usually acceptable even for transient applications. Figure 12.4 shows all of the boundary conditions for heat and mass transport in a two-layer system. These boundaries can be represented in several ways for finite difference solutions. Figure 12.5 shows one form that is compatible with Equations [12.8] and [12.9].

In the simplest representation, the air can be treated as a single lumped resistance to heat or water vapor transport. For this situation, the boundary conditions shown in Fig. 12.5 take the following form:

$$q_{o1}\frac{r_1}{r_0} = q_{i2}\frac{r_2}{r_0} = \frac{T_{1,n} - T_{2,1}}{\dfrac{r_0}{h_{c,1-2}\dfrac{r_1 + r_2}{2}} + \dfrac{r_0}{h_{r,1-2}\dfrac{r_1 + r_2}{2}} + \dfrac{\Delta x_1 r_0}{2k_1 r_1} + \dfrac{\Delta x_2 r_0}{2k_2 r_2}} \quad [12.11]$$

$$m_{01}\frac{r_1}{r_0} = m_{i2}\frac{r_2}{r_0} = \frac{P_{1,n} - P_{2,1}}{\dfrac{r_0}{h_{m,1-2}\dfrac{r_1 + r_2}{2}} + \dfrac{\Delta x_1 r_0}{2\varphi_1 r_1} + \dfrac{\Delta x_2 r_0}{2\varphi_2 r_2}} \quad [12.12]$$

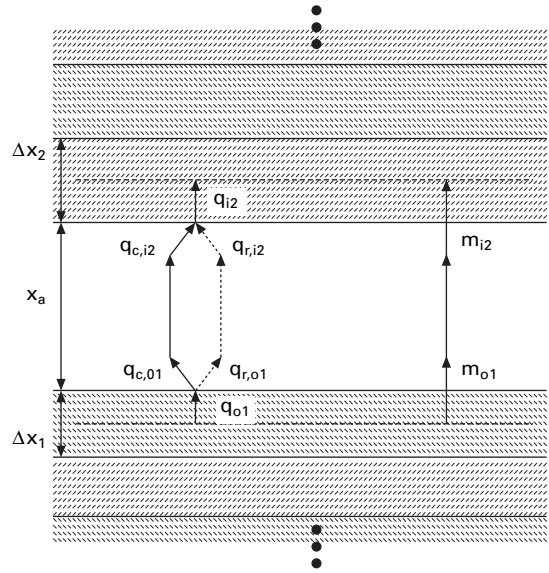

12.5 Boundary condition detail between layers 1 and 2.

where q_{o1} is the total heat flux from the outer surface of layer 1 (W/m^2), q_{i2} is the total heat flux to the inner surface of layer 2 (W/m^2), $h_{c,1\text{-}2}$ is the overall heat conduction/convection heat transfer coefficient for the air layer (K/W m^2), $h_{r,1\text{-}2}$ is the linearized radiation heat transfer coefficient for the air layer (K/W m^2) (see ASHRAE, 2005), m_{o1} is the vapor mass flux from the outer surface of layer 1 (kg/s m^2), m_{i2} is the vapor mass flux from the inner surface of layer 2 (kg/s m^2), and $h_{m,1\text{-}2}$ is the mass transfer coefficient for the air layer (kPa m^2 s/kg).

Note that the r/r_0 terms are included to account for the increasing area at increasing distances in the radial direction. Equations [12.8]–[12.10] plus Equations [12.11] and [12.12] for each air layer along with time-dependent values for temperature and vapor pressure for the body surface and the environment allow calculation of the time-dependent heat and vapor flows in the porous media system, fully accounting for the heat and moisture phase change interactions.

12.6 Consequences of interactions between heat and moisture

Equations [12.8] and [12.9] show a clear coupling between moisture and heat in porous media. In particular, Equation [12.9] shows that any increase in regain results in an increase in temperature and vice versa. The heat of sorption is large and, consequently, only small changes in regain can result

in large temperature changes. Since heat flows are driven by the temperature gradients, the adsorption and desorbtion of moisture by the media has a large impact on the heat fluxes through the media as well.

It has been know for many years that moisture sorption and desorption can impact body heat loss and affect perceptions of the thermal environment (Rodwell *et. al*. 1965). This effect has been modeled for clothing systems using the above equations and has been measured experimentally as well (deDear *et. al*., 1989; Jones and Ogawa, 1992). The effect is so large that a person dressed in clothing made of highly adsorptive fibers such as wool or cotton can experience a short-term change in heat loss from the body of the order of 50 W/m^2 when going from a dry environment (e.g. 25% rh) to a humid environment (e.g. 75% rh), even when the temperatures of both environments are identical. This effect is relatively short-lived and may only last for 5–10 minutes but is sufficient to elicit a strong change in thermal sensation and plays a large role in the perceived effect of humidity on comfort in many situations. A lesser, but still important, effect can persist for 30 minutes to an hour for some moderately heavy indoor clothing made of highly adsorptive fibers.

This interaction is particularly important for the drying of porous media. The transport of adsorbed moisture from a porous media is driven by the vapor pressure gradient. A negative vapor pressure gradient from the media to the surroundings will result in transport of water vapor from the media to the surroundings. The source of this water vapor is moisture adsorbed on the fibers. As the moisture is released and the regain decreases, there is a cooling effect on the media, as quantified by Equations [12.8] and [12.9]. Only a very small decrease in regain results in a large cooling effect. This small decrease in regain has minimal impact on the local equilibrium relative humidity (refer to Fig. 12.2). However, the large change in temperature has a big impact on the saturation pressure. The net result is a big decrease in local vapor pressure (refer to Equation [12.10]). The end result is that the cooling effect nearly eliminates the partial pressure gradient that is driving the moisture removal and, in the absence of a heat source, drying proceeds at a very low rate. The drying of a porous media is almost always limited by heat transfer and this effect is why thick media can take hours of even days to dry.

For fibers such as polypropylene or polyethylene that adsorb very little moisture, the interaction of heat and moisture is very minimal unless the conditions are such that condensation occurs. In the case where condensed moisture is present, but still relatively immobile, the equations presented in this chapter still apply and the strong interaction between heat and moisture will be present.

12.7 References

ASHRAE (2005), *Handbook of Fundamentals*, Chapter 8, American Society of Heating, Refrigerating and Air-conditioning Engineers, Atlanta, US.

ASTM (2005a), 'ASTM 1868-02, Standard Test Method for Thermal and Evaporative Resistance of Clothing Materials Using a Sweating Hot Plate,' *2005 Annual Book of ASTM Standards*, *Vol. 11.03,* American Society for Testing and Materials, West Conshohocken, PA, US.

ASTM (2005b), 'ASTM D 1518–85(2003), Standard Test Method for Thermal Transmittance of Textile Materials,' *2005 Annual Book of ASTM Standards, Vol. 7.01*, American Society for Testing and Materials, West Conshohocken, PA, US.

deDear R.J., Knudsen H.N., and Fanger P.O. (1989) 'Impact of Air Humidity on Thermal Comfort during Step Changes,' *ASHRAE Transactions*, Vol. 95, Part 2.

Fu G. (1995), '*A Transient, 3-D Mathematical Thermal Model for the Clothed Human*,' Ph.D. Dissertation, Department of Mechanical Engineering, Kansas State University, Manhattan, US.

ISO (1995), '*ISO 11092, Textiles – Physiological Effects – Measurement of Thermal and Water Vapour Resistance Under steady-State Conditions (Sweating Guarded Hotplate Test)*, International Organization for Standardization, Geneva, Switzerland.

Jones B.W., and Ogawa Y. (1992), 'Transient Interaction Between the Human Body and the Thermal Environment', *ASHRAE Transactions*, Vol. 98, Part. 1.

Morton W.E., and Hearle J.W.S. (1993), *Physical Properties of Textile Fibres, 3rd Edition*, The Textile Institute, Manchester, UK.

Rodwell E.C., Rebourn E.T., Greenland J., and Kenchington K.W.L. (1965) 'An Investigation of the physiological Value of Sorption Heat in Clothing Assemblies,' *Journal of the Textile Institute*, Vol. 56, No. 11.